Pretreatments for Metal-to-Metal Bonding

By:

G.W.Critchlow

A Doctoral Thesis submitted in partial fulfilment of the requirements for the award of the degree of Doctor of Philosophy of Loughborough University

September 1997

Department of Physics

Supervisor: Dr D.M.Brewis
Institute of Surface Science & Technology
Loughborough University, Loughborough,
Leicestershire, LE11 3TU.

Director of Research: Prof. K.R.A.Ziebeck
Physics Department
Loughborough University, Loughborough,
Leicestershire, LE11 3TU.

ABSTRACT

It is well-established that, with aluminium alloy adherends, a degree of surface treatment is required to optimise adhesive bond durability. A number of key surface physicochemical parameters have been identified as required to provide this optimisation, particularly in demanding exposure conditions, namely: macro- and micro-roughness, wettability, freedom from contamination, desirable chemistry, and hydration resistance.

In the present study, a range of treatments have been studied to determine how they modify the metal surface and what impact such changes have on bond durability. The surface treatments were either pre-existing and used for reference purposes or novel ones deemed worthy of study for environmental reasons. The following aluminium treatments were studied: acetone degreasing, grit-blasting, Bonderite 705 chromate-phosphate conversion coating, Bonderite 777 a zirconia-based conversion coating, EP2472 a mixed-phase conversion coating, CO_2-laser ablation, chromic acid etching and phosphoric acid anodising.

Preliminary studies were carried out to establish protocols for joint preparation and testing.

From a combination of surface analytical and bond test data, surface macro-roughness was demonstrated to have a small but significant effect on the durability of single lap shear joints exposed to deionised water at 60°C; surfaces, with roughness, R_a, values of approximately 3 μm, performed worse than those with, R_a, values of 1μm. This result was attributed to incomplete wetting of the grit-blasted adherends by the adhesive an effect caused by residual organic contamination.

CO_2-laser treatment was shown by Auger electron spectroscopy, scanning electron microscopy and contact angles to provide an atomically-clean surface which, with

aluminium adherends and a 120°C curing adhesive, gives times-to-failure in stressed single lap shear tests at 1 kN applied load and 60°C of approximately 500 hours. This time-to-failure is similar to grit-blasting and Bonderite 705 treatment and a factor of x25 greater than simply degreasing. The laser treatment had a larger interaction with mild steel adherends but a less favourable influence on bond durability. A mechanism of laser-surface interaction has been proposed which involves the formation of a near-surface plasma which radiates in the ultra-violet regime to clean and heat the substrate. Differences in reflection coefficients, to the 10.6 μm radiation produced by the CO_2-laser, between aluminium and steel account for the observed difference in laser-surface interactions.

Auger electron spectroscopy was used to provide information on the growth rate and chemistry of the Bonderite 705 conversion coating on aluminium 5251 and 5083 alloys. With treatment times up to 60 seconds the growth rate was constant at 86 $nm.min^{-1}$; this value is comparable to that measured for a similar film from ellipsometry. Scanning electron microscopy was used to demonstrate that over-treatment occurs with time leading to problems associated with water loss from the thick conversion coated film. In particular, impact test results indicated that the 1 μm thick film produced after 1000 seconds was cohesively weak leading to poor bond test results.

The chromate-free conversion coatings performed similarly to the optimised chromic acid etch in stressed single lap shear trials at 60°C with the EP2472 performing slightly better than the Bonderite 777 at all applied loads. In these tests, the phosphoric acid anodise treated adherends performed best of all. These results were accounted for by reference to surface analysis data using both Auger and X-ray photoelectron spectroscopies, scanning electron microscopy and complementary techniques. The interphase produced by the phosphoric acid anodise was thought to account for its excellent performance. A similar, though less extensive, interphase is potentially produced by the EP2472 process, whereas the Bonderite 777 and optimised chromic acid etch processes are similar to each other and highly

micro-rough.

All of the conversion coated surfaces would be expected to be hydration resistant. A high valency state phosphorous compound was identified as present within the conversion coatings from the Auger electron spectroscopy studies. The presence of this component is expected to be significant in terms of the long-term durability performance of these treatments.

Studies have also been conducted which show that the presence of high levels of magnesium in the surface region of aluminium alloys does not have a seriously detrimental effect on joints exposed to deionised water at 60°C; this is in contrast with some published work.

A combination of the above-mentioned studies enables a greater understanding of how the aforementioned surface physicochemical properties inter-relate to influence metal-metal adhesive joint durability when exposed to accelerated degradation conditions.

ACKNOWLEDGEMENTS

The author would like to acknowledge the contribution made by the following friends, colleagues and organisations towards this project:

Dr D.M.Brewis for his continued support and technical assistance throughout this project;

Mr M.F.Page and Mr J.S.Bates, Electron Microscopy Unit, IPTME, Loughborough University for providing the electron micrographs used in this work;

Mr C.A.Cottam, Physics Department, Loughborough University for carrying out the CO_2-laser ablation treatment and the XRD analysis. In addition, I would like to thank Chris for his helpful discussions in understanding the mechanisms of laser-surface interactions;

Dr A.Maddison, Stoke Golding Applied Research for the treatment of coupons and the impact test results presented in Section 3.3.3;

The management of Brent (Europe) Ltd, for help with the treatment of conversion coated aluminium coupons and financial support in respect of the durability data presented in Section 3.3.4;

The Department of Trade and Industry, UK, under the MTS programme. The literature search upon which this work was based was carried out under Project 4 which covers the *Characterisation of Surface Condition for Adhesive Bonding*. In addition, some of the bond strength data presented in Section 3.3.2.3 were obtained under this programme.

CONTENTS

CHAPTER 1 - LITERATURE REVIEW

1.1 BACKGROUND INFORMATION

Adhesive bonding is the joining of two materials via their interaction with a third medium, ie. the adhesive. The present study is concerned exclusively with the adhesive bonding of metals. In particular, the majority of work has been carried out using aluminium alloy whilst mild steel adherends have been used to a limited extent. These materials being two of the most widely-studied and industrially-useful metallic adherends.

There exists a vast literature on the topic of metal-to-metal bonding. Many studies have focused on the influence of surface treatments and the factors which influence the durability, or permanence, of metal-to-metal bonds; this is one such study. The majority of reported work originates from academia and representatives of the aerospace, transport, defence and general engineering industries or their materials suppliers.

The advantages that adhesive bonding offers over other fastening or joining techniques include: greater uniformity of stress distributions, permitting the use of thinner and lighter materials; the avoidance of holes in the structure thereby improving fatigue life; the flexibility of the adhesive permitting a degree of differential thermal expansion enabling different adherends to be used, and; the ability to design joints with smooth external surfaces to facilitate an improved cosmetic appearance and provide more efficient aerodynamics. These, and other advantages offered by adhesive bonding have recently been highlighted by Kinloch[1] and make it a key enabling technology in all of the aforementioned industries.

The first reported use of metal-to-metal bonding of aluminium was in 1946; with the De Havilland Dove aircraft assembled using Redux 775 adhesive (vinyl fomaldehyde-phenolic)[2]. By 1955 all-aluminium sandwich panels were used by

Martin and Hexcel in the Martin flying boat, the Seamster[3]. Since this time, increased confidence in adhesive bonding of aluminium brought about by such programmes as the Primary Adhesively Bonded Structures Technology (PABST) project in the 1970s has led to its widespread use, particularly in the aerospace industry[3-5]. For example, in an overview article produced in 1979 it was stated that VFW-Fokker consider "a high percentage of contemporary and future projects would be inconceivable both technically and economically without the bonding technique". On the Airbus A 300 a large number of components including skin panels measuring up to 8m long and 2m wide were reported as being bonded. In addition to the Airbus project VFW-Fokker used bonded assemblies in such applications as space probes, wing spars, helicopter rotor blades and engine covers[6].

Many examples of the use of bonded aluminium are given in the literature[1-6].

The attainment of "satisfactory" initial bonds is easily achieved with a minimum of surface preparation. However, there are many examples in the literature where joints which perform well initially do not provide good durability. In the present study, the relationship between joint durability, rather than initial joint strengths, and metal pretreatment has been considered of key importance.

It is well established that in order to optimise joint durability with metallic adherends some modification is required to the mill-finished material[7,8]. The minimum treatment might involve the removal of oils or other loosely-bound material by means of a simple degrease. The more successful treatments yield surfaces which have a number of key features, being: macro- and micro-rough, to provide the potential for mechanical interlocking and an increased area over which interactions can occur; hydration resistant, to reduce the influence of water at the bondline; free from contamination, to facilitate wetting and to prevent the formation of weak boundary layers and the masking of important topography, and; wettable, to enable complete spreading of a subsequently applied adhesive. Establishing the physicochemical changes introduced to surfaces as a function of different treatments

has been a major part of the present study. Surface analytical techniques such as Auger electron spectroscopy (AES), X-ray photoelectron spectroscopy (XPS) and electron microscopy (EM) have been widely used by other workers to obtain this information[9]. Additional techniques such as X-ray diffraction (XRD) and differential scanning calorimetry (DSC) can be used to provide complementary information. These techniques have been employed throughout the present study.

Joint durability is a difficult parameter to fully evaluate. Although, notable work has been carried out on aluminium, for example, by Minford[3] and others[10,11]. However, predicting the lifetime of adhesive joints remains something of a "Holy Grail" to adhesion scientists. There are a large number of joint test configurations mentioned in the literature, some of which have become the subject of standards documents[12,13]. The single lap shear configuration whether unperforated or perforated, unstressed or stressed has been used throughout the present work. This configuration is convenient to assemble with a good degree of control over the overlap length and the bondline thickness, and, in addition, it replicates a configuration which is commonly found in industry.

1.2 THEORIES OF ADHESION

There have been a number of theories proposed to explain the phenomenon of adhesion. A number of comprehensive reviews on adhesion mechanisms are given in the references[14-17]. The most widely accepted of these are detailed below:

1.2.1 MECHANICAL THEORY

This is, at least in part, an intuitive explanation whereby the surface features ie. asperities and pores, when fully wetted by an adhesive produce a degree of micro-mechanical interlocking.

In support of this theory is the work by Venables *et al* who used electron microscopy (both SEM and TEM) to identify the presence of sub-micron sized features on CAE, CAA and PAA treated aluminium[18]. This theory suggests that such features produce a "micro-composite interphase" with the adhesive resulting in improved joint strengths.

It has been shown by Chen *et al* that once such features have been removed from a previously micro-rough surface there is a resultant decrease in joint strengths[19]. In this case, aluminium 2024-T3 alloy was treated by the standard FPL (CAE) etch to produce sub-micron sized fibrils on the surface. The addition of low levels, up to 100ppm, of F^- ions to the etchant bath or rinse water was shown to remove the micro-fibrils from the surface. This resulted in a reduction in CDP test values by a factor of x20 compared with uncontaminated controls. A similar result was been demonstrated by other workers when the CAE surface was either masked by a contaminating overlayer, or, the beneficial topography was removed by mechanical damage[20].

Further evidence is given by the work of Bishopp *et al*[21] who also used TEM to demonstrate complete pore penetration of the PAA oxide on aluminium but little penetration following CAA treatment. The differences in treatment and degrees of pore penetration was reflected in durability results whereby the PAA outperformed

the CAA.

It is possible that, by engineering a micro-rough surface, the increase in joint performance is attributable to a much increased surface area over which interactions between the adhesive and adherend can occur.

1.2.2 ADSORPTION THEORY

This theory encompasses the range of inter-atomic and inter-molecular interactions which might exist between the adhesive and the adherend. Such interactions include both physisorption, and, when chemical bonding is permitted, chemisorption. A compilation of these forces along with their energies and equilibrium bond lengths are given in Table 1[14].

Table 1 - A Summary of Inter-atomic and Inter-molecular Forces (after ref.14).

Bond type	Bond energy ($kJ.mol^{-1}$)	Equilibrium length (nm)
Primary:		
ionic	600 - 1200	0.2 - 0.4
covalent	60 - 800	0.07 - 0.3
Secondary:		
hydrogen	~50	0.3
dipole interaction	~20	0.4
London dispersion (van der Waals)	~40	<1

It is clear from Table 1 that these forces act only over short distances. For this reason good wetting of the adherend by the adhesive is important. To produce optimum adhesion primary bonding, whether this be by ionic or covalent bonds, is required. Such primary bonding has proved difficult to directly observe. Techniques such as infra-red spectroscopy and static secondary ion mass spectrometry (SSIMS) have been employed to achieve this. In one study, Kinloch *et al* used SSIMS to explain the interaction of a silane coupling agent on steel by

identifying the presence of Fe-O-Si^+ fragments in the SSIMS spectrum[16].

The London dispersion (otherwise known as van der Waals) forces are the summation of the instantaneous dipole moments acting between the adherend and adhesive atoms in close proximity. Given this condition, such interactions always occur. The other forces are only present when there is a chemical reaction between adherend and adhesive.

1.2.3 ELECTROSTATIC THEORY

According to the electrostatic theory, as advocated by Derjaguin et al, electron transfer occurs between an adhesive and an adherend having different electronic structures. This effect leads to a double-layer of electronic charge at the interface. The work of adhesion required to separate adhesive and adherend is then related to the energy stored in a capacitor-type system. The limitation of this theory is that it does not account for the energy dissipated in the deformation of the adherends. Good agreement has, however, been demonstrated between this theory and some experimental results. Furthermore, in some instances adhesion cannot be explained without invoking this theory. It has been suggested that, given intimate contact between the adhesive and the adherend, the electrostatic component of adhesion is relatively small in relation to other forces (eg. inter-atomic or inter-molecular). However, because the electrostatic force is independent of separation distance (unlike other forces) it becomes more significant at larger distances.

1.2.4 DIFFUSION THEORY

This involves the mutual diffusion of polymer molecules across an interface, thereby, eliminating it. This theory is applied only to polymer-to-polymer adhesion and is generally considered inapplicable to metal-to-metal bonding.

1.3 ANALYTICAL TECHNIQUES

A recent survey of the literature by Critchlow and Brewis has identified over thirty different analytical techniques which have been applied to adhesion studies with aluminium alloy adherends[8]. These range from simple optical inspection to more complicated ultra high vacuum based techniques, such as AES and XPS. In the present study, a range of techniques was used for surface characterisation, failure analysis, and, to provide additional information about the systems under investigation. A summary of the techniques used most extensively in this study is provided in the following section.

It is important to note that no single surface analytical technique can provide all of the information required when studying a bonded system in detail. A recent review of the use of surface analysis in adhesion studies by Brewis and Critchlow[9] highlights this point. Each analytical technique has its limitations as well as its capabilities. Table 2 provides a summary of these for the most commonly used surface analytical techniques applied to adhesion studies, namely; AES, XPS and secondary ion mass spectrometry (SIMS). Comparative data are also given in Table 2 for energy dispersive X-ray analysis (EDXA) and laser microprobe mass spectrometry (LAMMS or LIMA), these being complementary techniques. In all cases, surface analytical techniques can be used to provide sub-surface information to a depth of many microns by the use of ion-erosion or mechanical sectioning techniques[22].

Table 2 - A Comparison of Analytical Techniques.

Parameter	Technique				
	AES	XPS	SIMS	EDXA	LAMMS
Excitation source	electrons	X-rays	ions	electrons	photons
Species detected	electrons	electrons	ions	X-rays	ions
Spatial resolution	100nm	100μm 10μm (imaging)	1μm (SSIMS) 20nm (imaging)	$\geq$1μm	0.25μm
Sampling depth	2-5nm	2-5nm	0.1nm (SSIMS)	1μm	0.25μm
Depth profiling	yes	yes	yes	yes	yes
Quantitative	yes	yes	yes[1]	yes	no
Compound information	limited	yes	yes	no	yes
Sensitivity	>0.1%	>0.1%	0.1% (SSIMS) ppm (DSIMS)	0.2-0.3%	ppm
Elemental range	Li - U	Li - U	H - U	Na - U[2] B - U[3]	H - U
Sample types	metals, ceramics, flat glasses, limited data from polymers	all solids	all solids	all solids	all solids[4]

Key: DSIMS - Dynamic secondary ion mass spectrometry, SSIMS - Static secondary ion mass spectrometry
[1] - with similar standards
[2] - with a Be window on the detector
[3] - with a windowless detector
[4] - with a few exceptions

Table 2 gives details of the excitation sources used and the species detected with the various techniques; a more detailed description of each is given in the references[23-28]. However, a brief outline of the working principles behind AES, XPS and EM follows:

1.3.1 AUGER ELECTRON SPECTROSCOPY

In AES, the sample is irradiated by a focused, monoenergetic electron beam with an incident energy typically in the range 1keV to 10keV. If sufficiently energetic, such an electron will create a vacancy in a core level electron shell by the emission of a secondary electron from within an atom in the sample surface. One method by which the now excited atom can relax is via the Auger process; see Figure 1a. The Auger process leads to the emission of a second electron, the Auger electron, from the surface. The electrons emitted from the surface are then detected using an electron energy analyser to provide an electron energy distribution (or spectrum) containing secondary and elastically backscattered electrons along with the Auger electrons. Typically, a concentric hemispherical analyser (CHA) or a cylindrical mirror analyser (CMA) combined with a suitable electron detector are used to produce the spectrum.

The energy of a particular Auger electron depends upon the energy levels of the atom from which it was emitted according to the following equation (for the interaction illustrated in Figure 1a).

$$E_{KL1L2,3} = E_K - E_{L1} - E_{L2,3*}$$

Where $E_{KL1,L2,3}$ is the energy of the Auger electron emitted in Figure 1a, E_K and E_{L1} are the binding energies of the respective atomic levels and $E_{L2,3*}$ is the binding energy of an electron in the L2,3 shell given a vacancy in the L1 shell. The individual values of the energy levels are principally a function of the nuclear charge on a particular atom and as such the energy of the Auger electron is also dependent on this value.

By measuring the energy at which a particular Auger the line occurs it is thereby possible to determine the atom from which it originates. This can be deduced from first principles or, as is most commonly carried out, from data compilations. By considering all of the peaks in the spectrum it is thereby possible to identify, qualitatively, all of the elements present in the surface with the exception of H and He. This technique cannot detect H or He since these elements do not have sufficient electrons to undergo the Auger process.

Quantification may be achieved from first principles. However, relative sensitivity factors (RSFs) based upon known reference materials are most commonly used to quantify AES data. The Auger electrons have energies mostly in the range 40 to ~2500eV. Electrons of this energy have an attenuation length (ie. the distance which the electron travels before undergoing either elastic or inelastic collisions and thereby losing energy to form part of the background in the spectrum rather than forming part of the Auger peak) of the order of a few atomic layers. This limits the sampling depth of the technique.

In some instances, rather than just elemental information, additional compound information is available from AES data[23]. Peak shifts, which might be of the order of 10 to 15eV, enable different oxidation states of an element to be identified. For example, metallic aluminium has a low energy (LVV) Auger peak at 68eV, whilst aluminium in the form of alumina has its (LVV) peak at 51eV[29].

There are, however, limitations in the range of materials suitable for AES analysis. For example, insulating materials, such as polymers, can suffer sample charging as a consequence of their interaction with the incident electron beam used in AES. Although flat glasses and ceramics can be successfully analysed, only limited information can generally be available from non-smooth, insulating materials such as adhesively-bonded fracture surfaces. In such cases, the experimental conditions need to be optimised to minimise charging problems, invariably, this is at the expense of limiting elemental range or sensitivity.

In-depth information can be obtained by combining AES with inert ion-bombardment. This method is commonly used to probe the topmost 1 to 2 microns of a sample, for example, in determining the composition of thin films produced by different metal treatments.

Depth scale calibration can be achieved by using either empirically derived etch rates or theoretically derived ones based upon the following equation[30]:

$$Z_a = (M_a \times S_a \times j_a) / (D_a \times Na \times e)$$

Where for material a, Z_a is the etch rate ($m.s^{-1}$), M_a is the mole mass ($kg.mol^{-1}$), S_a is the sputter yield[31] ($atoms.ion^{-1}$), j_a is the primary ion current density ($A.m^{-2}$), D_a is the density ($kg.m^{-3}$), Na is Avogadro's number and e is the charge on an electron. In general, the density term, D_a, will not be known precisely and consequently the use of experimentally derived etch rates leads to more accurate depth scale calibration. A combination of empirically- and theoretically-derived etch rates have been used in the present study.

In summary, AES can provide both qualitative and quantitative chemical information from a solid surface with good lateral and depth resolution. Under normal circumstances, the elemental range is from Li to U with detection limits of 0.1 to 1 atom% depending upon the matrix elements. Limited information can be obtained from rough, insulating samples. Depth profiling can be carried out to depths of tens of microns.

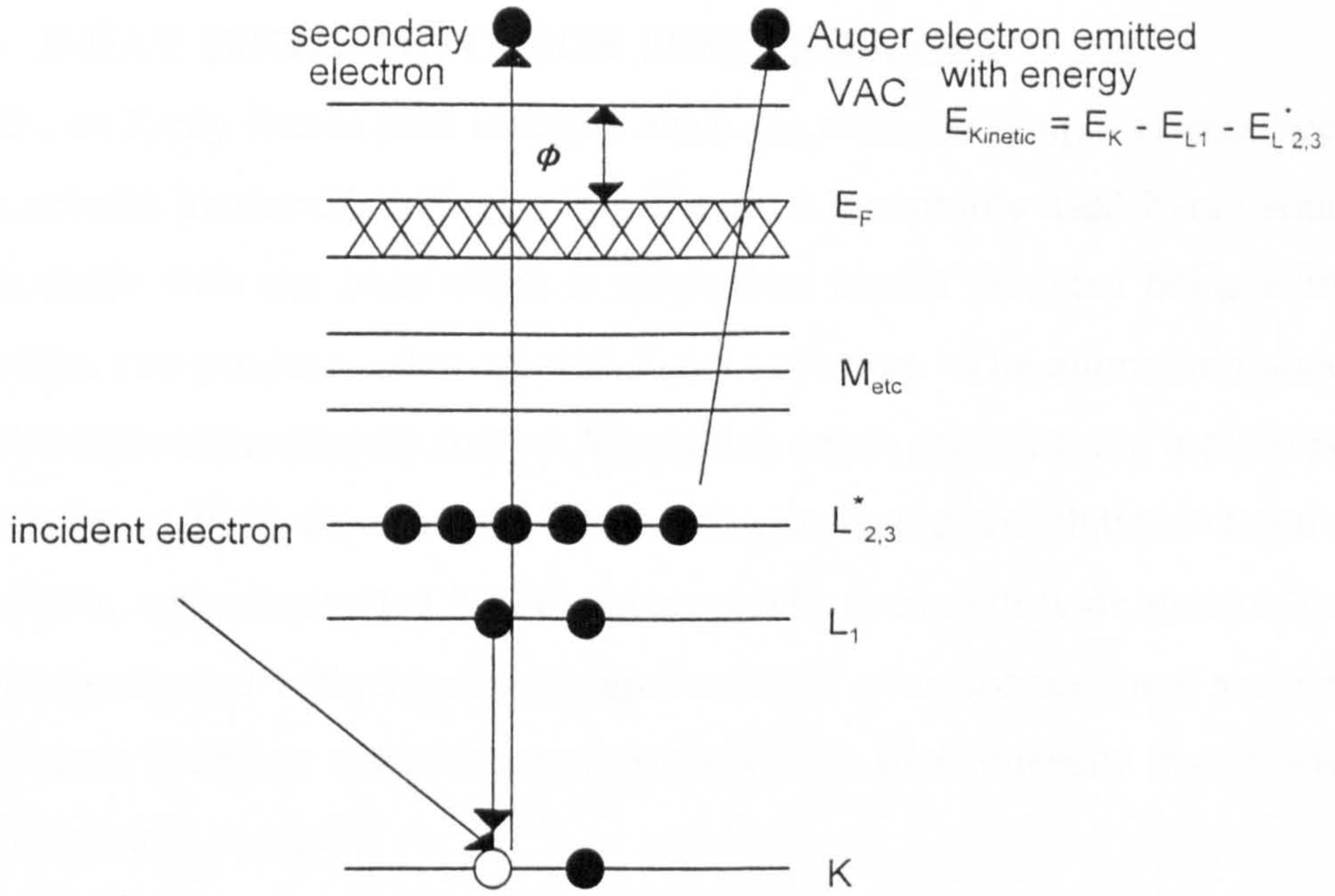

X-ray photoelectron emitted with energy

$E_{Kinetic} = h\nu - \phi - E_b$

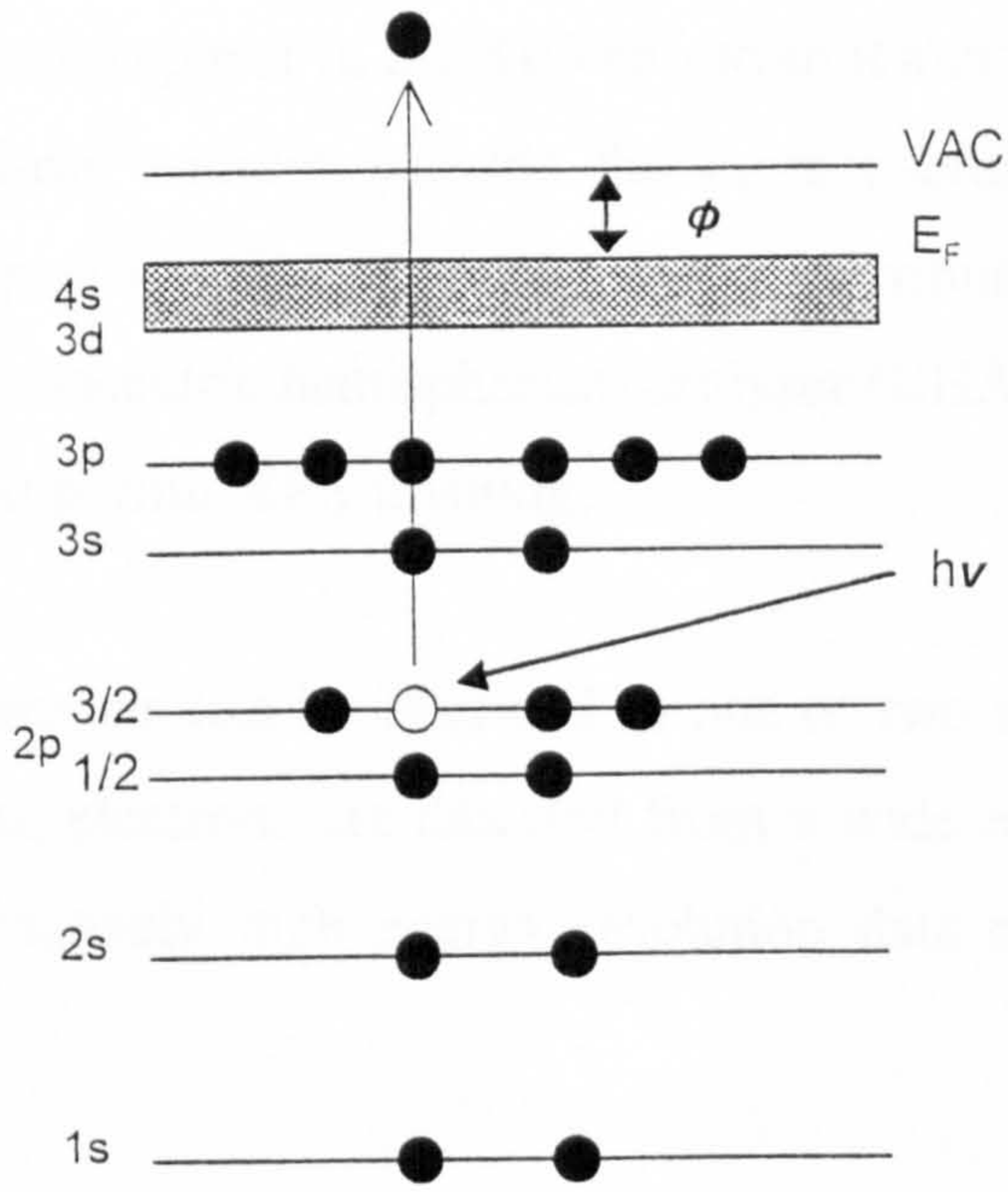

Figure 1 - To show the processes by which a. a KL1L2,3 Auger electron, and b. a $2p_{2/3}$ photoelectron are generated.

1.3.2 X-RAY PHOTOELECTRON SPECTROSCOPY

In XPS, an X-ray flux is used to excite electrons from the sample surface according to the scheme illustrated in Figure 1b. The most commonly used X-ray source has a twin anode with one facet which is magnesium coated the other being aluminium and which can produce either type of X-ray radiation. The aluminium anode was used throughout the present study. Alternative anode materials are used to perform non-routine analysis, for example, where enhanced energy resolution is required[32,33]. In addition, monochromated X-ray sources can be used to provide spectra free from satellite peaks and with improved signal-to-noise over conventional sources; also synchrotron radiation might be used to provide a high intensity X-ray source of variable photon energy[23].

If a non-monochromated source is used, as in the present work, the X-ray induced spectrum contains a contribution to the background from the Bremmstrahlung radiation and minor peaks from secondary X-ray lines emitted from the source. These features do not appear in the XPS spectrum if a monochromated X-ray source is used. All X-ray sources provide the more useful photoelectron and X-ray induced Auger peaks. The electron energy distribution is, in most instances, obtained using a concentric hemispherical analyser (CHA). More advanced electron optics are used to permit XPS imaging.

Generally, instruments can be operated in one of two modes: in a broad scan (or survey) spectrum, electrons are detected from a wide energy range, typically 0 to ~1250eV; alternatively high energy resolution data can be obtained as will be discussed later.

The broad scan spectrum provides surface elemental identification. All elements in the range Li to U have at least one XPS peak within the energy range detailed above. It is worth noting that the X-ray induced electrons have similar energy to those observed in AES, for this reason both techniques have similar sampling depths.

X-ray induced photoelectrons from element a. have kinetic energy E_{aKE}, determined by the following equation:

$$E_{aKE} = h\nu - E_B - e\phi$$

Where $h\nu$, the energy of the incident photons is known, (the aluminium X-ray source emits photons of energy 1486.6eV), E_B is the binding energy of the electron in its orbital and $e\phi$ is a constant term being the work function of the spectrometer. In practice, the data acquisition system will give either the kinetic energy or the binding energy of the peaks present in the spectrum. E_B is the usual diagnostic parameter allowing elemental identification to be made by reference to data compilations in the literature[23,34].

Quantification is achieved by the use of relative sensitivity factors appropriate to the instrument being used. These may be theoretically or experimentally derived and allow surface compositions to be determined, usually expressed in atom percent terms. The detection limits for most elements in XPS are in the range ~0.1 to 1%, a value comparable to that of AES.

The precise value of E_B for any given element is also dependent upon its chemical environment. More intimate chemical information can be determined by accurately measuring the discrete chemical shifts caused by localised electron-electron interactions[35] this high-resolution mode is, therefore, the other method of operating the XPS spectrometer.

To obtain this information the energy resolution of the spectrometer is increased by decreasing the pass energy of the CHA. Curve fitting or peak deconvolution are commonly carried out on high energy resolved data to identify the relative amounts of different components of an elemental peak; these procedures have not been used in the present study. The Auger parameter can be used to provide specific chemical information in those instances when the precise value of E_B is difficult to establish,

for example when analysing insulating materials[23,27,28].

Additional information can be obtained from XPS such as imaging, non-destructive depth profiling (for shallow depths), valence band and photoelectron diffraction data[23]. XPS can be used, in conjunction with taper sectioning or inert-ion bombardment, in the same way as is commonly-used in AES, to obtain in-depth information. These features were either not available or not used on the instrument available to the present study.

In summary, XPS shares many of the features of AES in terms of its surface sensitivity and detection limits. It does not, in general, posses the same degree of lateral resolution as AES, but does have a number of advantages. Firstly, the experimental databases exist to be able to make reliable assignments of chemical shift data. Secondly, additional information can be obtained in the XPS spectrum. Thirdly, the range of materials which can be analysed by XPS is more extensive than that which is possible with AES. Finally, the effects of beam damage are generally less severe with XPS than with AES.

1.3.3 X-RAY DIFFRACTION

XRD can be used to provide both elemental and compound information from crystalline phases within a solid[36].

The Bragg equation, given below, defines the angle (θ) at which constructive interference of waves (of wavelength λ) occur when scattered from a crystalline surface:

$$2\,d\sin\theta = n\lambda$$

Where n is an integer and d is the crystal spacing.

With the diffractometer used, the value of λ was a known constant and the angle θ was varied to provide spectra containing peaks with measurable values of d. By

1.3.5 CONTACT ANGLE MEASUREMENT

The contact angle made by a liquid in contact with a solid surface is defined as "the angle between the liquid / vapour interface and the liquid / solid interface from the point of three phase contact at equilibrium"[39,40]. This is illustrated schematically in Figure 2.

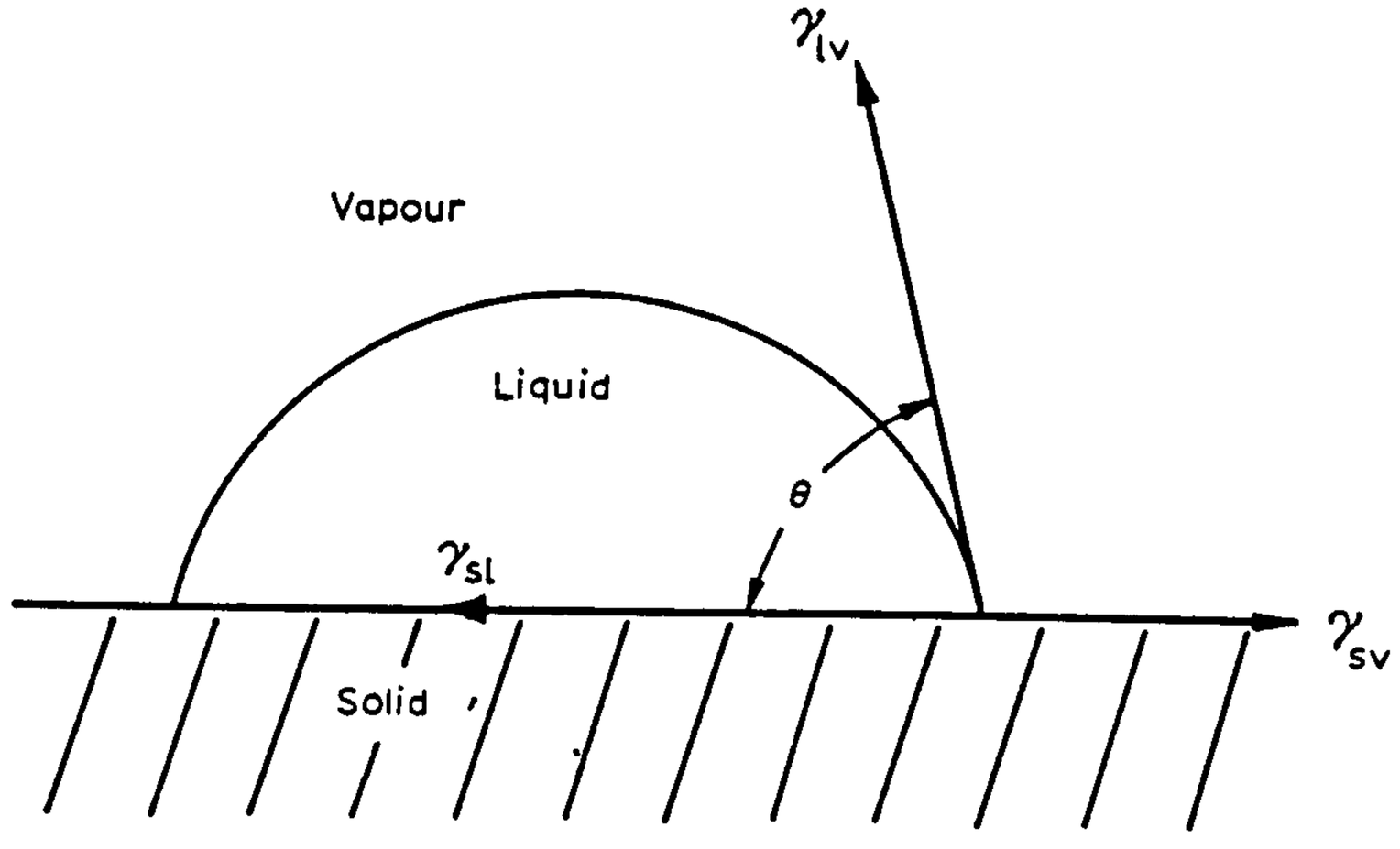

Figure 2 - To show the contact angle, θ, at the three-phase point between a droplet on a solid surface in a gaseous atmosphere (after ref.16, pg 20).

The measured value of angle θ, produced by any solid surface, is a function of its topography and chemistry. A detailed consideration of the influence of surface roughness is outside of the scope of this work since, in the present study, contact angles were used only to provide a measure of surface cleanliness.

1.3.6 DIFFERENTIAL SCANNING CALORIMETRY

Thermal analysis techniques such as DSC are used to provide information relating to chemical reaction kinetics[40,41]. In the present work, DSC has been used to determine the activation energy for the formation of polymer-polymer bonds with Araldite 2007, the adhesive used in the main durability programme. The procedure for this has been detailed by Ozawa[43] and Zukas *et al*[44]. In addition, DSC has been used to determine the glass transition temperature, T_g for the same polymer[41].

In power compensated DSC the sample under investigation and a reference material are maintained at the same temperature throughout a (temperature) scan using independent power supplies. In the present study, adhesive samples were studied; these were contained in aluminium pans with spacers and lids. Duplicate pans, spacers and lids were used as the reference material.

Any difference in the energy supplied to the sample (polymer+pan+lid+spacer) and reference material (pan+lid+spacer) in order to maintain this condition can then be attributed to a thermal event within the polymer. The thermal event might be identified as either exothermic or endothermic depending upon the direction of deviation from the DSC baseline[41].

1.4 PRETREATMENTS FOR ALUMINIUM

1.4.1 TREATMENTS IDENTIFIED

There exists a large number of treatments for aluminium to enhance bond durability. Particular attention is drawn to the books by Minford[3] and by Thrall and Shannon[4] and a number of review articles[45-47] which provide good overviews of most of these. Such diversity reflects a number of factors including the ongoing requirement for better performing treatments for structural applications, and, for environmentally-friendly methods.

Any particular surface treatment may be combined with an appropriate chemical "add-on" prior to application of the adhesive. Whilst acknowledging the usefulness of primers, hydration inhibitors and coupling agents an in-depth discussion of their merits, or otherwise, is beyond the scope of this work. In the present work, particular emphasis is made on the modification of the metal (oxide) surface.

The different treatments identified, from the available literature are, are listed in Table 3 together with their reference sources. Details of multi-stage pretreatments are given in the references.

The treatments listed in Table 3 can be considered in terms of both their ability to modify the aluminium surface, and, their performance in comparative durability studies. These aspects will be addressed in the following sections.

Table 3 - A Summary of Surface Treatments Identified for Aluminium Bonding.

Surface treatment	Reference Source
A.c. phosphoric and sulphuric acid anodise	48-50
Acid paste treatment	51, 52
Alcohol-phosphoric acid etch	52, 53
Ammonium tartrate anodise	54
Belt-sand abrasion	52,55
Boric acid anodise	56
Chromate conversion coating	52, 55, 57-61
Chromate-phosphate conversion coating	59, 62, 63
Chromic acid etch - including the FPL, optimised FPL, chromic-sulphuric and potassium dichromate-sulphuric acid etches	45, 46, 51, 52, 53, 55, 56, 58, 60, 64-119
Chromic acid anodise plus phosphoric acid dip	110
Chromic acid anodise	45, 46, 53, 56, 76, 79, 82, 86, 87, 90, 91, 93, 96, 98, 107, 109, 111, 116-118, 120-127
Corona discharge	128
Degrease plus deoxidize	55, 129
Degrease plus alkaline clean	50, 109
Grit-blasting or sandblasting.	51, 52, 55, 58, 73, 83, 97, 109, 117, 122, 130-132
Hydrofluoric-nitric acid etch	133
Liquid or vapour degrease	52, 53, 55, 58, 73, 83, 87, 97, 122, 128, 129, 134
Machine surface plus immersion in 10°C distilled or tap water	135
Machine surface plus polish plus immersion in 10°C distilled or tap water	135
Nitric acid-sodium sulphate etch	73, 81
Oxalic acid anodise	89
Phosphoric acid anodise	45, 46, 48, 53, 54, 56, 59, 70, 72, 79, 80, 82, 83, 86-91, 93, 94, 97, 98, 101, 102, 104, 107-111, 113, 116-118, 123, 125, 127, 131, 134, 136-142
Phosphoric acid anodise plus phosphoric acid dip	119
Phosphoric acid etch	60
Plasma-spray	142
Primed-only	55, 116, 143
Scotchbrite abrasion	117, 140
Sealed chromic acid anodise	67, 78, 103, 120
Sealed sulphuric acid anodise	52, 53, 120, 136
Silicate alkaline etch	60
Sodium hydroxide based etch	144
STAB 1, 2 and 3	102
Sulphuric acid etch	133
Sulphuric acid anodise	52-54, 56, 66, 90, 98, 109, 116, 120, 125, 136, 141
Sulphuric acid anodise plus phosphoric acid dip	110, 115, 116
Sulphuric acid-ferric sulphate based etch	95, 104, 119
Sulphuric acid-ferric sulphate based etch plus anodise	119
Sulphuric acid-ferric sulphate based etch plus anodise plus phosphoric acid dip	119
Tartaric acid anodise	56
Wire-wool abrasion	107
Zirconium conversion coating	60

1.4.2 SURFACE MODIFICATION AND ITS INFLUENCE ON BOND DURABILITY

The degree of modification of a mill-finished aluminium surface by a particular treatment has been considered, wherever details are available, in terms of the following parameters: surface wettability; surface macro- and micro-roughness; mechanical and chemical stability of the oxide; and the degree of contamination. These parameters have also been studied for both the existing and novel treatments studied in the following Chapters.

The treatments identified can be grouped into three main classifications: mechanical, chemical or electrochemical.

1.4.2.1 Mechanical treatments

Grit-blasting or sandblasting usually with graded alumina or silica may be combined with degreasing to produce a highly macro-rough surface providing the possibility of mechanical interlocking. Grit-blasting gives variable durability results. In one example, after exposure to a sea-coast environment, it has been shown to provide more durable bonds than a variety of chemical treatments[52]. In other studies, grit-blasting has shown to be either superior or inferior to the FPL etch in high humidity and high temperature environments[53,55,83,109,117]. There is little information in the literature to correlate durability results with, for example, grit-size or blasting conditions. Interesting results are obtained by the subsequent application of γ-glicidoxytrimethoxysilane, where subsequent bonds fail cohesively within the adhesive after immersion in water at 23°C this is reflected in improved durability results[130].

Mechanical abrasion by Scotchbrite, belt-sand or wire wool has been used, usually followed by a rinse or degrease stage. Scotchbrite has also been used as an initial stage in a PAA treatment[140]. As with grit-blasting, mechanical abrasion has been demonstrated to provide a highly rough surface for bonding. However, possible

residual debris and mechanical damage to the adherend are considered to be detrimental to bonding[117]. Scotchbrite treated surfaces have been observed to have poor wettability with subsequently poor bond durability. In one study, Scotchbrite treated surfaces performed worse than FPL or grit-blasted surfaces after 30 days exposure to 85% RH at 70°C[117]. Belt-sand treated surfaces performed satisfactorily across a wide range of environments[55]. No systematic study to optimise the mechanical abrasion treatment has been identified in this survey.

Machining the surface, with or without polishing followed by immersion in either distilled or tap water at 10°C has been shown produce variable bond durability depending on which treatment is used. This result is attributable to variations in oxide composition and stability. There are no durability comparisons between these treatment methods and industrial standards[135].

Liquid and vapour degreasing are most commonly used to remove oils and other organic contaminants from a mill-finished surface, usually as the first stage in the wide variety of multi-stage treatments. Methods include: rinse or wipe with acetone, methyl ethyl ketone or carbon tetrachloride, or; vapour degrease in perchloroethylene, trichloroethylene or 1,1,1-trichloroethane. It should be noted that chlorinated solvents can attack aluminium with the formation of toxic fumes. Good initial bond strengths have been obtained with degreased-only surfaces[53,87]. However, after exposure to most aggressive environments, degreased-only surfaces consistently show poor bond durability[83,87,122].

Corona discharge treatment has been shown to markedly increase surface energy. However, this treatment does not enhance durability when compared with an abraded surface. The formation of a weakly-bound oxide after treatment is postulated as the cause of poor durability[128].

Plasma-spray coating of 99.5% pure alumina powder onto a mechanically roughened aluminium surface has been shown to facilitate good adhesion in glass reinforced epoxide composite-to-aluminium joints. Wedge test results with plasma-sprayed adherends show less crack growth than with BAC 5555 treated controls[142]. No long-term durability results utilising plasma-sprayed adherends are available.

1.4.2.2 Chemical treatments

Degrease plus alkaline cleaning is commonly used as the initial stage in multi-stage treatments. The degrease stage has previously been covered in this review. Few processing details are given in the literature on the deoxidizing or cleaning agents, mainly trade names, for example; ICI Deoxidiser No. 1, Oakite NST or Isoprep 44 are mentioned. Treatment times and temperatures are variable. The function of the alkaline cleaning stage is to remove the existing oxide. However, there is no conclusive information on the surface modification caused by these treatments. Durability results are consistently poor, with degreased and deoxidised or degreased and alkaline cleaned surfaces performing worse than FPL etched surfaces[55,109].

There is no information given regarding the surface modification induced by the reported *acid paste treatment*. Exposure to adverse environments shows acid paste treated joints to be susceptible to attack by moisture to a much greater extent than with FPL-type etched adherends[51,52].

A range of *chromic acid etches* (CAE) exists. The most commonly used etch solution being sodium dichromate-sulphuric acid based, the FPL (Forest Products Laboratory) etch; a term which is sometimes used erroneously to cover all chromic acid etches.

The FPL etch in its standard, modified or optimised form is the most extensively studied of all treatments. It is used either as a stand-alone treatment prior to bonding[69], or as a pretreatment prior to anodising[94]. The structure produced is reported to be highly rough with a well defined matrix of ~5nm diameter fibrils

extending ~40nm from the surface, but with a relatively thin barrier oxide layer of the order of 5nm beneath this structure[86]. There is disagreement concerning the oxidation state of the surface after FPL etching. There is, however, agreement that on 2000 series alloys, the magnesium-rich oxide on the mill-finished surface is removed in the FPL etch[74,84]. The structure and composition of the oxide is highly dependent upon processing conditions. For example, small changes in bath composition by the addition of aluminium and copper compounds produces the optimised FPL etch[100]. Garnish[143] described an electrochemical study in which small quantities of various metals were added to a chromic acid bath. Copper, among other metals, considerably increased the etch rate, the porosity of the surface and the resultant peel strengths. Pocius studied the electrochemistry of the CAE treatment of aluminium alloys[144]. In this work, he gave a detailed account of the various aspects of the pretreatment including the removal of mill-scale, the effect of copper and the formation of oxide during the rinse stage. A wide variety of processing parameters is given in the "References" section[69,104,111,113,114,129]; these include a variety of degrease and alkaline clean options and variations to the actual FPL bath parameters and rinse conditions.

Final rinse and drying conditions markedly affect the nature and thickness of the oxide and therefore performance in adhesive joints. McCarvill and Bell[135] compared the strengths of unetched aluminium-epoxide butt joints after immersion in distilled and tap water at 10°C. In distilled water, a maximum strength occurred after about 1h immersion whereas with tap water a maximum value occurred after about 12h immersion. The maximum joint strength observed with tap water was significantly higher than that with distilled water. The difference was attributed to a thicker and less perfect bayerite layer in the case of distilled water. McGarel et al[111] found that with CAE, CAA and PAA treatments a tap water rinse resulted in much better durability than when using distilled water with SLS joints. However, with wedge tests no clear pattern emerged and in a CDP test, only in one case (FPL, 60°C rinse) was there a significant difference between the rinses with a distilled water rinse being highly deleterious. McNamara et al[105] reported that if the pH of the

rinse water following an FPL etch was less than 3 then a reduction in peel strength can occur. In addition, Wegman[145] reported much higher joint strengths with CAE treated aluminium which had been rinsed in tap water rather than either distilled or deionised water. As previously mentioned, Chen et al[85] found that if the rinse water was contaminated with F^- ions then the durability, as assessed in a CDP test, was much diminished.

The FPL etched surface has been shown to be extremely susceptible to modification by contamination[19] or hydration[64,70,77] and to mechanical damage by handling[20]. For these reasons, a short surface exposure time prior to priming or bonding[71,100] and a minimum of handling should be employed. If stored in a "contamination-free" environment, the FPL etched surface is expected to retain its bondability indefinitely[77]. In many durability studies, FPL etched surfaces are consistently out-performed by anodised equivalents[72,76,80,90,110]. Boeing maintain that FPL etching gives inconsistent results, making it an unsuitable stand-alone treatment for the bonding of primary structures[88]. There are also environmental problems concerned with the handling and disposal of chromium compounds from the etch bath[102,146].

Other chromic acid based etch treatments have been studied, though to a lesser extent than the FPL etch[51,58,64,87,90,98,99,107,109,125]. These are usually combined with a sequence of degrease and rinse procedures. Chromic-sulphuric acid etching has been identified as a good pretreatment for subsequent chromic acid anodising[120]. Chromic-sulphuric acid etch treatment for longer than 10 minutes has been reported to produce a surface oxide comparable to the FPL etch[99]. The presence of relatively low levels of magnesium in the oxide after chromic acid etching has been observed. CAE treated joints exposed to water vapour do deteriorate markedly, indicating that they are not water-stable. In a number of durability studies it is shown that chromic acid etching does not compare favourably with phosphoric or chromic acid anodising[96,98,107].

The P2 etch is a patented, chromate-free, sulphuric acid-ferric sulphate based treatment[95]. SEM has shown the P2 etched surface to have comparable surface topography to that which had been FPL etched[119]. The P2 treated surface comprises Al(oxide), C, O, S and Fe with the surface oxide a few tens of nanometres in thickness[119]. Russell and Garnis used wedge tests at 60°C and 100% RH to compare the P2 treatment with the FPL etch[147]. The durability with 6061-T6 alloy was superior in the case of the P2 etch. In the study by Digby and Packham[119], the P2 etch was compared to the FPL etch both as a stand-alone treatment, and, as an initial stage in a full PAA process. Although as a stand-alone treatment the P2 did not perform as well as the FPL etch in wedge tests, it did produce comparable data to the FPL etch when used as part of the PAA process. The latter conclusion was previously drawn in the work by Russell[81]. In addition, Quick concluded that the P2 etch provides broadly comparable results to PAA and optimised FPL treatments in both tensile lap shear and peel tests[104].

No information relating surface parameters to durability has been identified using *other etches* to those previously mentioned. Limited studies suggest that the order of increasing bond durability on a number of etches can be ranked as follows: hydrofluoric-nitric acid etch < alcohol-phosphoric acid etch = phosphoric acid etch < silicate alkali etch = sodium hydroxide based etch. No durability data have been presented for the nitric acid-sodium sulphate and sulphuric acid etches. The FPL treatment is generally regarded as superior to the aforementioned etches.

The processing route for *conversion coating* normally includes a degrease plus an alkaline cleaning stage prior to coating[59]. Zirconium-based coatings have been tried and were found to give durability results comparable to the FPL etch[60]. However, most studies have concentrated on chromate- or chromate-phosphate coatings. It has been shown that on a macro-scale these coatings reflect the surface topography prior to coating[61] although on a micro-scale spherical particles agglomerate to form a highly structured porous oxide which can be $>1\mu$m thick[62]. There is concern over the non-uniformity of improperly prepared and coated surfaces. In 5000 series

alloys, the first stage of development is the removal of the supposedly detrimental magnesium-rich surface oxide from the mill-finished surface[63]. The freshly-produced oxide has been reported as comprising either chromate, or mixed chromate-phosphate, depending on the treatment, with aluminium fluoride concentrated at the oxide-to-metal interface. A mechanism for the growth of such films has been proposed by Treverton et al[62] in which the fluorides remove the existing oxide while the chromates are reduced by the exposed aluminium metal. The proposed reactions are as follows:

$$2Al_2O_3 + 6H^+ + 6F^- \rightarrow 2AlF_3 + 3H_2O$$

$$2Al(metal) + 2HCrO_4^- + 8H^+ \rightarrow 2Al^{3+} + Cr_2O_32H_2O \downarrow + 3H_2O$$

In a limited number of durability trials, results indicate that these surfaces produce bonds comparable to those obtained by Boeing BAC 5555 PAA, and better than phosphoric acid or FPL etching[59]. The freshly-prepared surface is capable of retaining its bondability for at least six months; this is in marked contrast with the FPL etch. The coating time required is typically 5 to 60 seconds, in contrast with the many minutes required in conventional anodising treatments[59].

STAB 1, 2 and 3 are non-acid, non-chromate, chemical treatments. STAB 1 involves an ultra-sonic degrease (in "Gunk") followed by a rinse step and then immersion in either tap water, or, deionised water containing K_2CO_3 for 10 minutes at 80°C. STAB 2 involves a degrease followed by a room temperature soak in an ammonium hydroxide solution containing commercial cleaner (60 $g.l^{-1}$ "MICRO" in deionised water). STAB 3 comprises a dip in concentrated NaOH solution (568 $g.l^{-1}$ in deionised water) for 3 to 10 minutes followed by a hard spray rinse[102]. Little information has been given on the surface physicochemical parameters after these treatments. STAB 3 treatment gives durability results better than the FPL etch but not as good as PAA; STAB 1 and 2 give poor and highly variable results.

1.4.2.3 Electrochemical treatments

Chromic acid anodising may be carried out either with or without a subsequent phosphoric acid dip or sealing. CAA is currently the preferred treatment option of European aeroplane manufacturers. The surface oxide produced is reported to be thick, typically 1.5 to 3 μm, porous and highly structured[86], with cell walls reported to be ~30nm thick[86]. The oxide is moderately resistant to attack by moisture although hydration of the surface has been observed[107]. Prior treatment with a chromic acid etch is beneficial to long term durability, with the etch conditions being critical[126]. Bonded joints with CAA surfaces usually give much better durability results than following FPL etching. CAA treatment can be followed by a subsequent sodium dichromate[103], hot water[120] or chromic acid[67] immersion stages designed to "block" the pores in the CAA oxide, leading to a "sealed" CAA-treated adherend. Sealed CAA treated adherends produce relatively poor durability results[103], though performing well in corrosive environments[78]. CAA surfaces exposed to a subsequent phosphoric acid dip produced excellent initial bonds[110]. Poole and Watts demonstrated good durability performance with CAA plus PAD treated adherends using the wedge test configuration[109]. On balance, CAA together with PAA treated adherends produce the most consistently good, durable bonds.

Phosphoric acid anodising is currently the preferred treatment of the Boeing Aerospace Co. Boeing have reported satisfactory in-service performances over many years with bonded PAA joints[88,101]. The surface oxide has been described as being in the range 400 to 800 nm thick including ~100 nm of small protruding fibrils[86]. The oxide is highly porous, with a cell diameter of ~40 nm and with walls which are thin compared to those on the CAA oxide. The phosphate component of the oxide is thought to make it highly moisture-resistant although complete hydration of the surface has been observed after exposure to 100% RH/50°C for 72 hours[91,138]. Vermilya and Vedder[148] had previously reported that phosphate ions greatly improved the stability of anodic aluminium oxide towards water. The structure of the PAA oxide is considered to form part of an "interphase" with the subsequently applied adhesives or primers to provide good

initial and long term performance. A wide range of pretreatment options are possible since PAA is a multi-stage process. However, durability studies show the full BAC 5555 to out-perform other PAA treatments[123], although PAA is considered relatively insensitive to variations in processing parameters, certainly compared with CAE. PAA is widely considered to provide the most durable joints, though in some tests it is shown to be only comparable to[87], or less effective than[90,96,98], CAA-prepared joints.

Electron microscopy shows the PAA oxide produced after P2 etching is more dense and lacks the continuous pores which are associated with the FPL etched plus PAA surface[119]. A subsequently applied phosphoric acid dip has been shown to remove the beneficial PAA oxide.

There are limited data on the surface modification caused by *sulphuric acid anodise, sealed sulphuric acid anodise and sulphuric acid anodise plus phosphoric acid dip treatments*. Sulphuric acid anodising has been widely tested in comparative trials with PAA, CAA and FPL treated surfaces. SAA treated adherends, both un-sealed and after sealing by immersion in de-ionised water[120,136], usually demonstrate only moderate initial and long term durability results[53,66,70,78,120]. SAA treated adherends are commonly out-performed by PAA and CAA treated equivalents. In a number of studies, SAA has performed similarly to the FPL etch[78,90]. SAA followed by a phosphoric acid dip has been demonstrated to markedly improve both initial and durability results compared with the un-sealed treatment[110,115,116]. In one study, Digby and Packham[119] used SEM to demonstrate that the application of a PAD onto a previously sulphuric acid anodised surface caused the formation of "brush-like topography with features $\sim 1\mu$m in scale". The formation of such features explains the beneficial effects of the PAD when combined with this treatment.

A limited amount of information is available for *boric acid, tartaric acid, ammonium tartrate and oxalic acid anodising treatments*. From the available information it is not possible to rank these treatments in terms of durability. While some information is available regarding their surface characteristics, none of these have been fully characterised.

With *a.c. phosphoric acid and sulphuric acid anodising*, a degrease stage plus alkaline clean or FPL etch precedes anodising[48]. The structure of the oxide produced on a 5251 alloy surface by a.c. PAA is comparable to that produced by conventional PAA[48]. Durability trials show a.c. PAA treated samples have a ten-fold increase in energy absorption when tested under impact conditions, compared with degreased-only controls[50]. Varying the treatment time markedly affected the bond durability[50]. Comparative studies of a.c. PAA and SAA with conventional Boeing BAC 5555 PAA show all three treatments produce similarly good, durable bonds when impact tested[48].

1.5 DURABILITY RANKING AND JOINT FAILURE MECHANISMS

Section 1.4.2 provides an indication of the relative durability performance of the treatments identified, usually, under well-defined exposure conditions. Whilst a summary of all reported durability data is outside of the scope of this work a number of key points can be extracted from the literature :

As indicated in the references, there exists a large number of standard and "in-house" test configurations and procedures used in adhesion studies. Whilst some tests interrogate, for example, the bulk properties of the adhesive, others, are intended to provide a measure of interfacial adhesion. In addition, the range of tests has evolved to simulate conditions experienced by joints in service conditions.

Table 4 gives a summary of durability results as a function of test method and environment. In the tests highlighted in Table 4 the intention was to discriminate between different treatment-adhesive combinations in terms of their ability to sustain adhesion under known exposure conditions, to establish a "durability ranking". The selected treatments represent the three broad treatment groups: mechanical, chemical and electrochemical. The ranking is given for each individual test with a high value indicating increasing durability. To avoid the complicating effect of priming, all results presented were from joints which were either stated as being un-primed otherwise no mention of any primer was given.

A number of points emerge from this table and from the available literature:

- Untreated or degreased-only adherends consistently perform badly in a wide range of durability trials;

- Grit-blasting can produce relatively durable joints particularly when exposed relatively benign environments but, in general, grit-blasting is out-performed by both chemical and electrochemical treatments when joints are exposed to elevated temperatures and humidity;

- The chemical treatments such as CAE give, overall, intermediate results. However, there are instances where CAE out-performs either CAA or chromate-phosphate conversion coating. This highlights that CAE can give inconsistent results. This is not surprising given the range of CAE and optimised CAE treatments available;

- PAA yields either equivalent, or, as in most cases better durability results than CAA treatment in crack propagation tests. However, in lap shear tests both treatments are shown to perform similarly. Chromate-based conversion coatings, when optimised, can compare favourably with CAE and CAA.

All of the commonly-used test configurations have been demonstrated to successfully discriminate between treatments. The sensitivity of a particular test relative to another is a function of many factors, these include: the environment to which a joint is exposed; the ability of water to get to the bondline; temperature; adhesive selection, and; the stresses within the joint. Such factors combine to determine the joint failure mode.

In any durability study an understanding of the failure mechanism is important in interpreting the data.

Bonded joints are commonly aged by prolonged exposure to elevated temperatures and high humidity (or water immersion) in order to accelerate the conditions experienced in-service. In addition, stress may be applied. Under these conditions, water can reach the bondline either by diffusion through the adhesive or by migrating through cracks in the adhesive[149] or voids at the interface[21]. Given this

circumstance, moisture can influence the bonded joint in many ways, as indicated in a recent review by Bowditch[150]. Plasticisation of the adhesive can occur along with swelling or hydrolysis. Other effects include hydration or corrosion of the metal (oxide) or disruption of bonds at the interface.

The influence of water within the adhesive joint has also been studied by Brewis and co-workers[122]. It has been established that water ingress, by diffusion, can cause plasticisation of an epoxide adhesive eventually leading to a reduction in its mechanical strength. This process was shown to be reversible on drying. To complicate matters, plasticisation has also been associated with stress relief in joints leading to improved joint strengths.

One theory advanced by many workers is that the metal oxide, to which the adhesive is bonded, is mechanically weakened by hydration during exposure of joints to high relative humidities or water immersion. In this case, failure within the hydrated oxide is thought to result in poor joint durability. It has been demonstrated, by Noland[70], Davies *et al*[138] and others, that the most successful treatments, the anodic oxides, demonstrate some degree of hydration resistance whilst those which are less successful, for example the CAE, do not. With aluminium, the presence of cladding has been shown to be detrimental to durability, leading to the philosophy that "clad is bad"[88]. The poor durability is attributed to enhanced corrosion of the cladding layer. However, the occurrence of such hydration prior to joint destruction has been disputed, for example, by Bishopp *et al*[21].

Kinloch[92] has used a thermodynamic approach to explain the effect of moisture on the interface, whereby, there is a displacement of adhesive from the interface by the liquid. The work of adhesion between a material, A, and a liquid, L, is calculated from the following equation:

$$W_{AL} = \gamma_{1L} + \gamma_{2L} - \gamma_{12}$$

Where $\gamma_{1,2}$ is the interfacial energy between 1 and 2, and γ_{1L} and γ_{2L} are the surface energies of 1 and 2 in the presence of L. A positive value for W_{AL} indicates a stable interface, however, if this value is negative it is expected to be unstable.

In many durability trials, joint failure is reported to be *apparently* interfacial. However, a full understanding of the causes of joint failure requires a precise knowledge of the locus of failure; surface analytical techniques such as AES and XPS can provide the latter information. Such information has been obtained, when appropriate, in the present study.

Table 4 - A Ranking of Surface Treatments as a Function of Test Geometry and Environment.

Description of Test	Ref	Ranking Treatment						Environment / exposure time
		Untreated or degreased only	Grit blast	CAE	CAA	PAA	Cr conversion	
Tensile shear	51	-	1	2	-	-	-	Hot dry, hot humid
SLS	122	1	2	3=	3=	-	-	97 - 100% RH, 50 ± 2°C for up to 1 year
Lap shear	52	1	4	2	-	-	3	Seacoast for up to 8 years with a 1-part epoxide
Lap shear	52	1	-	2	-	-	-	RT water and also cyclic anodise wet - freeze thaw
Lap shear	52	1	-	2	-	-	3	Seacoast
SLS to ASTM 1002-72	58	1=	1=	3	-	-	4	Stressed in Alcoa ring to 3.45 MPa to failure, plus salt spray cycling. Note CAE and conversion coating rankings are reversed at 13.78 MPa.
PLS	59	-	-	-	-	1=	1=	Salt spray at 43°C for 3 weeks
PLS	60	-	-	1	-	-	2	Salt spray for up to 60 weeks
PLS	113	-	-	-	1	-	2	5% salt spray at 43°C for up to 100 days
Butt joint	134	1	-	-	-	2	-	Immersion in distilled water at 60°C
Wedge test	109	1	2=	2=	4	5	-	95% RH at 50°C for up to 14 days
Boeing Wedge	46	-	-	1	-	2	-	100% RH at 60°C
Boeing wedge	110	-	-	2	1	3	-	Immersion in distilled water at 50°C
Crack extensions to BSS 7208	111	-	-	1	2=	2=	-	95% RH at 50°C for 48 hours
DCB	123	-	-	-	1	2	-	DI water immersion at ambient
DCB	123	-	-	-	1	2	-	95 - 100% RH at 50°C for up to 400 hours
DCB	123	-	-	-	1	2	-	~ 2% salt solution for 1 year
FRP	117	-	1	2	-	3	-	85% RH at 70°C for up to 30 days

Key, 1 = worst performance, increasing numbers indicate improved durability. Note that intercomparisons can only be made between treatments for a particular set of test parameters (reading across) and not between tests (reading down).

1.6 SUMMARY

Although "satisfactory" initial bonds can be achieved when bonding to aluminium surfaces which have simply been degreased, surface modification is generally regarded as being required to optimise durability. A diverse range of mechanical, chemical and electrochemical treatments developed to achieve this have been outlined in the preceding text. The most widely used of these are the subject of standards documents[151-156].

In this review, forty one mechanical, chemical, electro-chemical or other treatments specifically designed to modify the surface of aluminium to enhance bond durability have been identified. These may be combined with a range of chemical "add-ons", such as primers, coupling agents or hydration inhibitors to stabilise the surface during storage or to further enhance bond durability.

An indication has been given, wherever possible, as to how the treatments identified modify the surface chemistry and topography, and how they perform in comparative durability trials.

In comparative trials, phosphoric acid anodising usually produces the best durability.

However, it is clear that the modified aluminium surface should not be considered in isolation. For optimum durability any treatment should be matched when appropriate, to a suitable primer and adhesive.

Because of the large number of combinations of alloys, pretreatments and adhesives, it is not possible to fully explain the relative durabilities provided by the various pretreatments. However, a number of factors have been shown to be important; all of which are possessed by the phosphoric acid anodised surface. A stable oxide is considered important as this can prevent or minimise the formation of a relatively weakly bound inorganic layer. Topography which favours mechanical keying and provides an increased area over which interfacial interactions can occur is clearly beneficial. With

phosphoric acid anodised aluminium, in particular, the adhesive is thought to form a "composite" with the oxide structure. Strong interaction between the adhesive and the substrate is necessary to prevent the displacement of the adhesive by water.

The specific advantages offered by each of the surface treatments studied in the present work are discussed in Chapter 4. It is sufficient at this point to mention that each were, in principal, likely to facilitate successful bonding and, as such, were deemed worthy of investigation.

In summary, the use of metal-to-metal bonding is now a mature subject area. A great deal of information exists on, for example, the physico-chemical effects of particular treatments on the adherends, the relative performance of different treatments in durability trials, and the possible mechanisms of joint failure. However, there still exists gaps in the current knowledge of existing bonding systems. In addition, there is currently the requirement for alternative treatments which are more environmentally-friendly to those which currently exist. A number of these conclusions are reinforced by a recent review article by Boerio et al[157].

1.7 AIMS OF THE PROJECT

- An extensive review of the literature has been conducted; the focus of this review being the influence of surface treatments used prior to the adhesive bonding of aluminium. The best-performing pretreatments identified for use in structural or other demanding applications include the well-established CAE, CAA and PAA. All of the aforementioned treatments utilise highly toxic hexavalent chromium in their processing.

  Hexavalent chromium is a Category 1 (A-1) confirmed human carcinogen and is recognised as acutely toxic with a maximum exposure limit (MEL) of $0.05mg.m^{-3}$. For reasons of personal health and environmental pressures there is currently a move away from the use of hexavalent chromium in the metal treatment industry[146]. It is, therefore, recognised that there exists a need for alternative, more benign, metal treatments to replace those currently in use. This is the main driving force behind the present study.

- The initial aim of this project was to investigate the durability performance of both established and novel metal treatments. The novel metal treatments studied in the present work were CO_2-laser ablation, and two chromate-free conversion coatings, Bonderite 777 and EP2472. The durability performance of these treatments were compared with a range of including: degrease-only; alkaline clean; grit-blast; chromate-phosphate conversion coating; CAE, and; PAA.

  Durability data have been obtained using different metal treatments and the same adherends, adhesive and exposure conditions. The established treatments were studied to provide comparative durability data and reference surfaces with which the novel treatments could be compared.

- The metal adherends used in the present study were characterised both before and after treatment. The physical changes introduced to the aluminium alloy surfaces were identified using electron microscopy (EM), whilst changes in chemistry were monitored using Auger electron spectroscopy (AES). Complementary techniques were used when appropriate. Wherever appropriate, AES and X-ray photoelectron spectroscopy (XPS or ESCA) were used to elucidate joint failure mechanisms.

- It was envisaged that the physicochemical changes introduced to the treated metal surfaces could then be related to the durability of the adhesive joints and thereby used to explain their performance. The main aim of this project being to establish scientific reasons for the durability performance of specific alloy-pretreatment-adhesive systems.

- The novel treatments under investigation have been selected with a view to establishing them as credible alternatives to the chromate-containing methods.

- In addition, a number of other related studies have been conducted; for example, the effect of surface macro-roughness on bond durability has been investigated.

- A limited number of preliminary experiments have also been conducted to establish the test procedures to be used in the subsequent durability studies. These tests investigate the effects of joint fillet geometry, adherend thickness and, the tensometer crosshead speed on single lap shear results.

CHAPTER 2 - EXPERIMENTAL

2.1 ANALYTICAL TECHNIQUES

2.1.1 AUGER ELECTRON SPECTROSCOPY

The instrument used throughout the present study was a dedicated Varian scanning Auger electron spectrometer. The base pressure prior to analysis was always less than $1x10^{-8}$ torr. In most experiments a primary electron beam of $3x10^{3}$ eV and $\sim 0.7x10^{-6}$ A was used with an analysis spot $\sim 100x10^{-6}$ m in diameter. Conditions were varied depending upon the sample requirements. For example, to analyse adhesive-coated failure surfaces a reduced beam energy of $1x10^{3}$ eV and a current of $\sim 0.2x10^{-6}$ A were used. The ion-gun used for depth profiling was the static-backfilled type operating with Ar^{+} ions of energy $3x10^{3}$ eV and a current density between 25 and $75x10^{-6}$ $A.cm^{-2}$. Quantification was achieved using experimentally derived RSFs based upon Al, Al_2O_3, MgO, ZrO_2, P_2O_5 and other appropriate reference materials. Depth scale calibration was achieved using either experimentally or theoretically derived etch rates. Further details are provided, where appropriate, in the following text.

2.1.2 X-RAY PHOTOELECTRON SPECTROSCOPY

The XPS instrument used was a VG Escalab Mark II operating with an Alkα radiation source with a photon energy of 1486.6 eV, a voltage of $15x10^{3}$ V and a current of $20x10^{-3}$ A. The instrument was operated with a base pressure in the region of $1x10^{-8}$ torr. In all cases, the surface analysed was aligned normal to the energy analyser. A pass energy of 85 eV was used for all analyses.

2.1.3 X-RAY DIFFRACTION

XRD was carried out using a Philips PW1130/00 diffractometer with Hilton Brookes automation. The copper anode was operated at $20x10^{-3}$ A and $40x10^{3}$ V emitting CuKα radiation stated as having a wavelength of 1.540562 Å. Samples were scanned from 10° to 110° at a rate of 1° per minute with a step size of 0.02°. Parameters were kept constant for each sample so that the relative peak intensities would provide some indication of the relative thicknesses of corresponding layers.

2.1.4 ELECTRON MICROSCOPY

The SEM instrument used was a Cambridge Stereoscan 360 operating with a primary electron beam energy in the range 10 to $40x10^{3}$ eV and a current in the range 50 to $\sim 200x10^{-12}$ A. All samples were sputter-coated with gold prior to examination to reduce the influence of sample charging. Magnifications were achieved up to x100000; features could be resolved as small as a few tens of nanometres. Scanning transmission electron microscopy was used in one instance, this was performed using a Joel GM 100CX instrument.

2.1.5 CONTACT ANGLES

Sessile contact angles were determined using an instrument developed in-house. In all cases triply-distilled water was used. A contact angle (θ) was determined by measuring the diameter (d) and height (h) of a drop projected onto a nearby screen using the following equation:

$$\tan (\theta / 2) = 2 h / d$$

It was demonstrated that the precision of such measurements was $\pm 2°$.

2.1.6 DIFFERENTIAL SCANNING CALORIMETRY

The instrument used incorporated a Mettler DSC 30 low temperature cell and TC 10 A processor. Scan rates were used in the range 1 to 20°C.min^{-1} with start and end temperatures of -20 and 300°C in all cases.

Preliminary investigations indicated that severe exothermic reactions resulted within the adhesive given full aluminium pans. The thickness of the adhesive layer in the pans was therefore controlled to represent the situation within the adhesive joints used in the durability studies. To facilitate this, spacers were used to provide a glueline thickness of 250μm in the pans the same as the bondline thickness in the durability studies. To confirm that the correct thickness of adhesive was used in each case, the density of the Araldite 2007 was measured to be 1.2 g.m^{-3}, from the diameter of the pans the mass of a 250μm thick layer was estimated to be approximately 8.5 μg. This compares with measured values in the range 9 to 10.5 μg; these values were acceptable.

For the T_g measurement, a fully-cured sample was scanned with at a rate of 5°C.min^{-1} within the parameters detailed above; the T_g value was taken as the mid-point between the two phase-lines.

2.2 JOINT ASSEMBLY AND TESTING

2.2.1 MATERIALS

2.2.1.1 Adherends

The aluminium alloys used were 5251, bulk composition by weight being: 0.1-0.5% Mn, 1.7-2.4% Mg, 0.15% Cu, 0.4% Si, 0.5% Fe, Al balance, and 5083, bulk composition: 0.7% Mn, 4.4% Mg, 0.15% Cr, Al balance. Except where otherwise stated, the coupons were produced on a press-tool yielding 20 x 55 mm (width x length) adherends. The aluminium adherends were either 1.6 or 2 mm thick. Mild steel adherends measuring 20 x 55 and either 1.2 or 3 mm thick were used in Section 3.1. In all cases, bonding was carried out on the burr-free surfaces of these coupons.

2.2.1.2 Adhesives

The adhesives used in the various experiments were as follows: Dunlop 525; Ciba Geigy AV/HV 100; Permabond F246; 3M's 7823 G, and; Ciba Polymers' Araldite 2001 and 2007 (AV119). A brief description of these is given in Table 5.

Table 5 - A Summary of the Adhesives used in the Present Programme.

Adhesive	Description	Recommended cure schedule
Dunlop 525	Two-part, RT cure, toughened epoxide	24h at RT plus 20 minutes at 100°C
Ciba Geigy AV/HV 100	Two-part, 60°C cure, non-toughened epoxide	3h at 60°C
Permabond F246	Two-part, RT cure, toughened acrylic	less than 10 minutes at RT
Araldite 2001	Two-part, non-toughened epoxide	24h at RT plus 90 minutes at 60°C
Araldite 2007	Single-part, toughened epoxide	2h at 120°C
3M 7823 G	Single-part, toughened epoxide	30 minutes at 180°C

2.2.2 SURFACE TREATMENTS

2.2.2.1 Degreasing

The as-received, mill-finished adherends were doubly-degreased by ultra-sonic immersion in either 1-1-1-trichloroethane or "Super Purity" acetone, both from Romil Chemicals, for periods of 10 minutes on each occasion.

2.2.2.2 Grit-blasting

The coupons were initially degreased as detailed above. Grit-blasting was carried out using a Guyson Beadblaster operating at a continuous indicated pressure of 0.6 MPa. In Section 3.1 the adherends were treated with an industrial-grade grit. For the surfaces characterised in Section 3.2.2 and subsequently used in durability trials, the following grades of alumina grit were used: 40/60; 80/120; 180/220, and; 320. The approximate mesh sizes are 425/250, 180/125, 85/65 and 45 μm respectively. In all cases, coupons were held approximately 4 cm from the nozzle and treated by passing the bonding area under the nozzle a number of times until the area appeared uniformly treated. After grit-blasting, the coupons were again doubly-degreased to remove surface detritus.

2.2.2.3 CO_2-laser treatment

During laser treatment the bonding area on the coupons was irradiated using a Laserbrand L450 pulsed transversely excited atmospheric (TEA) CO_2-laser, emitting at 10.6 μm. The TEA CO_2-laser emits a broad beam of $\sim$10 cm^2 which is then focused to irradiate an area of $\sim$10 mm^2 to provide an energy density of 20 J.cm^{-2}. This relatively high energy density is required to create a plasma above the surface of the metal which facilitates the cleaning process. The small area of the focused beam made it necessary to raster the sample to treat the entire bonded area. Various treatment conditions were used; these are detailed in Section 3.2.3.

2.2.2.4 Bonderite 705, Chromate-Phosphate Conversion Coating

In Section 3.3.3 the coupons were either degreased plus alkaline cleaned, or, degreased then alkaline cleaned and then Bonderite 705 conversion coated. The alkaline clean was carried out by immersion in 5% Oakite NST for 10 minutes at 50°C.

In Section 3.3.4 a "standard" treatment was used, as follows: degrease as before followed by cleaning with Pyroclean 71 (20g.l^{-1} @ 65°C for 5 minutes) + Aluma Etch 700 (4% w/v NaOH, 75 ml.l^{-1} AE700 @ 50°C for 5 minutes) + rinse + HNO_3 desmut (10% v/v @ 20°C for 30 seconds) + rinse. Following this, the coupons were immersed in Bonderite 705 proprietary solution for 5 minutes at 20°C.

The coupons were then rinsed in deionised water and dried in an air oven at 120°C for 10 minutes.

2.2.2.5 Bonderite 777, Chromate-Free Conversion Coating

The first six steps were as detailed in Section 2.2.2.4. Following these, the coupons were immersed in Bonderite 777 proprietary solution for 5 minutes at 20°C and dried as detailed above.

2.2.2.6 EP2472, Chromate-Free Conversion Coating

The first six steps were as detailed in Section 2.2.2.4. Following these, the coupons were immersed in EP2472 proprietary solution for 5 minutes at 20°C and dried as detailed above.

2.2.2.7 Chromic acid etching

An "optimised" CAE treatment was used; the optimised FPL etch. Coupons were first degreased in "Super Purity" acetone in an ultra-sonic bath as previously detailed, these were then immersed in a 10% aqueous solution of Pyroclean 71, Brent Europe Ltd, for 15 minutes at 55±2°C. After thorough washing in warm tap water, a water break test was carried out; the result was invariably positive. The coupons were then treated in a seeded chromic acid solution for 30 minutes at 62±2°C. One litre of solution contained

9.9g $Na_2Cr_2O_7.2H_2O$ and 304g concentrated sulphuric acid. Seeding was carried out by the addition of 3.4g $CuSO_4.5H_2O$ and 9.3g $(Al_2(SO_4)_3.16H_2O$ per litre of solution. After immersion, the coupons were washed in cold running tap water for 20 minutes then dried in an air oven at 40°C for 30 minutes.

2.2.2.8 Phosphoric acid anodising

PAA treatment was carried out to the full Boeing BAC 5555 process specification[158].

2.2.3 JOINT ASSEMBLY

Single lap shear (SLS) joints were used in all tests. Joints were assembled with 10 mm overlaps on a custom-built jig. Except when otherwise stated, adhesive spew fillets were removed prior to curing by double-wiping with a clean spatula; see Section 3.1.1. Prior to bonding, ~1% by weight of 250μm "Ballotini" glass spheres were mixed into the adhesive to control bondline thickness. Joints were clipped together using small bull-dog clips during the cure stage. The adhesives were cured according to the manufacturers instructions, see Table 5.

2.2.4 TESTING PROCEDURES AND EXPOSURE CONDITIONS

Initial joint strengths were determined using a Lloyd 2000R tensometer. An initial jaw separation of 70 mm was chosen. Except during the work detailed in Section 3.1.2, a cross-head speed of 6 mm.minute^{-1} was used throughout the present study. Two load cells were used, these were rated at either 5 kN or 10 kN. To be consistent, the same load cell was used throughout each individual experiment. Both load cells were NAMAS calibrated at the time of use.

In the unstressed trials, joints were fully immersed in deionised water at 60±2°C.

In the stressed durability studies, joints were assembled into chains of six joints and inserted into Maddison-type tubes, see Figure 3. Stress was applied by compression of both the vernier and main pre-calibrated springs. Stress levels were chosen in the range 0.2 to 1.5 kN. The tubes were immersed in deionised water at 60±0.5°C. In these

tests, times-to-failure were measured for up to six replicate joints.

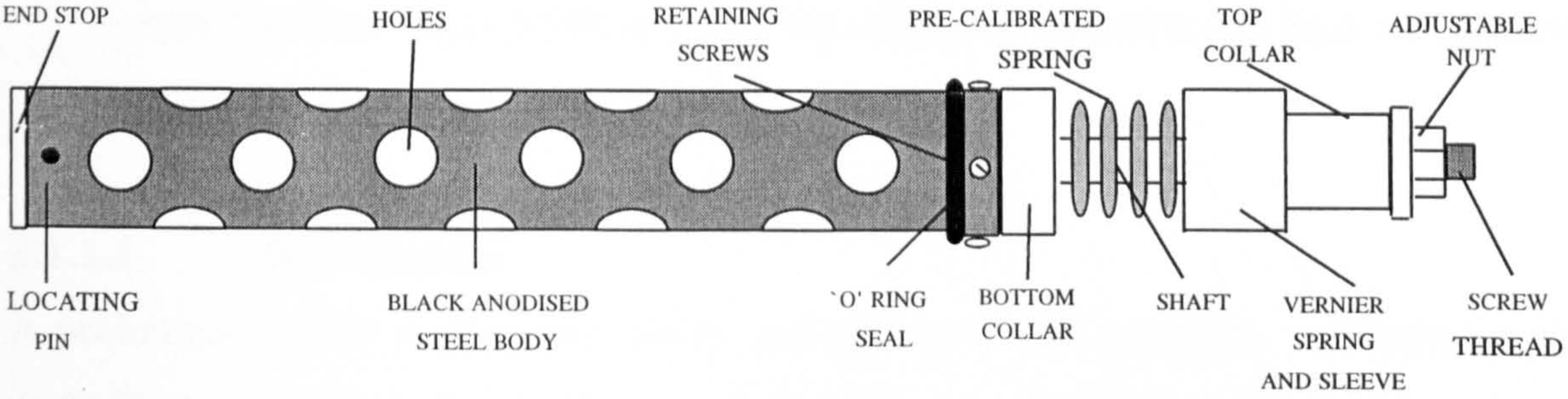

Figure 3 - To Show the Main Features of the Maddison-type Stress Tube.

DSC showed the glass transition temperature, T_g, of the AV119 adhesive used in the durability trials to be approximately 117°C; this compares well with the a value of 110 to 120°C, depending upon the cure schedule used, quoted by Ciba Polymers. Whilst it is recognised that exposure to water will reduce the T_g of the adhesive, the value of 117°C is significantly higher than the maximum temperature of 60±2°C to which the joints were exposed.

CHAPTER 3 - RESULTS

3.1 PRELIMINARY TESTS

3.1.1 THE INFLUENCE OF JOINT SPEW FILLET GEOMETRY AND ADHEREND THICKNESS ON THE PERFORMANCE OF SLS ADHESIVE JOINTS

3.1.1.1 Introduction

A preliminary study was carried out to identify the extent to which variations in joint spew fillets affect both the absolute strengths and reproducibility of SLS joints. One of the objectives of this study being to establish the protocol for joint preparation to be used in the subsequent durability studies. Tests were carried out by varying the fillet geometry and measuring initial SLS joint strengths with grit-blasted mild steel adherends. Three different geometries were used: no fillet; half-fillet and full-fillet. Two different adherend thicknesses were used: 1.2, and; 3 mm. Results were obtained with both toughened and non-toughened epoxide adhesives.

The mild steel adherends were grit-blasted using the procedure outlined in Section 2.2.2.2. SLS joints were assembled as detailed in Section 2.2.3 with 10 mm overlaps. The adhesives used were Dunlop 525 and Ciba Geigy AV/HV 100; these adhesives are toughened and non-toughened epoxides respectively.

In the joints requiring the full-fillet geometry, no attempt was made to remove any excess adhesive exuding from the joints prior to curing. In contrast, with the joints requiring either half- or no-fillets the excess adhesive was removed prior to curing by double-wiping with a spatula. In the joints requiring no-fillets, any adhesive which exuded from the joints during the cure stage was removed by careful filing, being careful not to undercut the joint. Five replicates of each joint were prepared. Initial joint strengths were determined using the procedure outlined in Section 2.2.4.

3.1.1.2 Test Results

A compilation of joint strength data are given in Tables 6 and 7 which give the average, of five, initial joint strengths with their standard deviations and percentage variations (standard deviation / mean) as a function of adhesive type and fillet geometry.

Table 6 - A Summary of Initial Joint Strengths with Grit-blasted 1.2 Mild Steel Adherends as a Function of Fillet Geometry.

Adhesive	Fillet geometry	Joint strength (N)	Percentage variation
Toughened epoxide (Dunlop 525)	Full	3491±253	7.2
	Half	3311±59	1.8
	None	3229±64	2.0
Non-toughened epoxide (Ciba Geigy AV/HV 100)	Full	2705±121	4.5
	Half	2425±132	5.4
	None	2157±57	2.6

Table 7 - A Summary of Initial Joint Strengths with Grit-blasted 3 mm Mild Steel Adherends as a Function of Fillet Geometry.

Adhesive	Fillet geometry	Joint strength (N)	Percentage variation
Toughened epoxide (Dunlop 525)	Full	3970±233	5.9
	None	3895±215	5.5
Non-toughened epoxide (Ciba Geigy AV/HV 100)	Full	4970±145	2.9
	None	5080±159	3.1

3.1.2 THE INFLUENCE OF STRAIN RATE BEHAVIOUR ON THE PERFORMANCE OF SLS ADHESIVE JOINTS

3.1.2.1 Introduction

The second stage in establishing the importance of a strictly-defined testing procedure was to investigate the effect of variations in strain rate behaviour with SLS bonded joints. In this study, the strain rate applied to the joint was adjusted by varying the cross-head speed of the tensometer. The adherends used were, again, grit-blasted mild steel measuring 20 x 55 x 3 mm. The adherends were treated and bonded using the procedures detailed in Sections 2.2.2.2 and 2.2.3. The adhesives used were Ciba Geigy AV/HV 100, a non-toughened epoxide and Permabond F246, a two-part toughened acrylic.

Bond testing was carried out using the Lloyd 2000R tensometer and a 10 kN load cell; the crosshead speed was varied from 1 to 50 mm.minute^{-1}. The adherends were held in position by pins rather than the usual grips to avoid the possibility of slippage in the jaws.

3.1.2.2 Test Results

The results, presented in Table 8 and in Figure 4, give the mean, of five, initial joint strengths and their accompanying standard deviations as a function of crosshead speed.

Table 8 - A Summary of Initial Joint Strengths as a Function of Strain Rate with Two Different Adhesives.

Adhesive	Crosshead speed (mm per minute)	Average joint strength (N)	Standard deviation (N)
Non-toughened epoxide (Ciba Geigy AV/HV 100)	1	3812	410
	10	4278	760
	50	3844	756
Two-part acrylic (Permabond F246)	1	4336	736
	10	4837	644
	50	6013	514

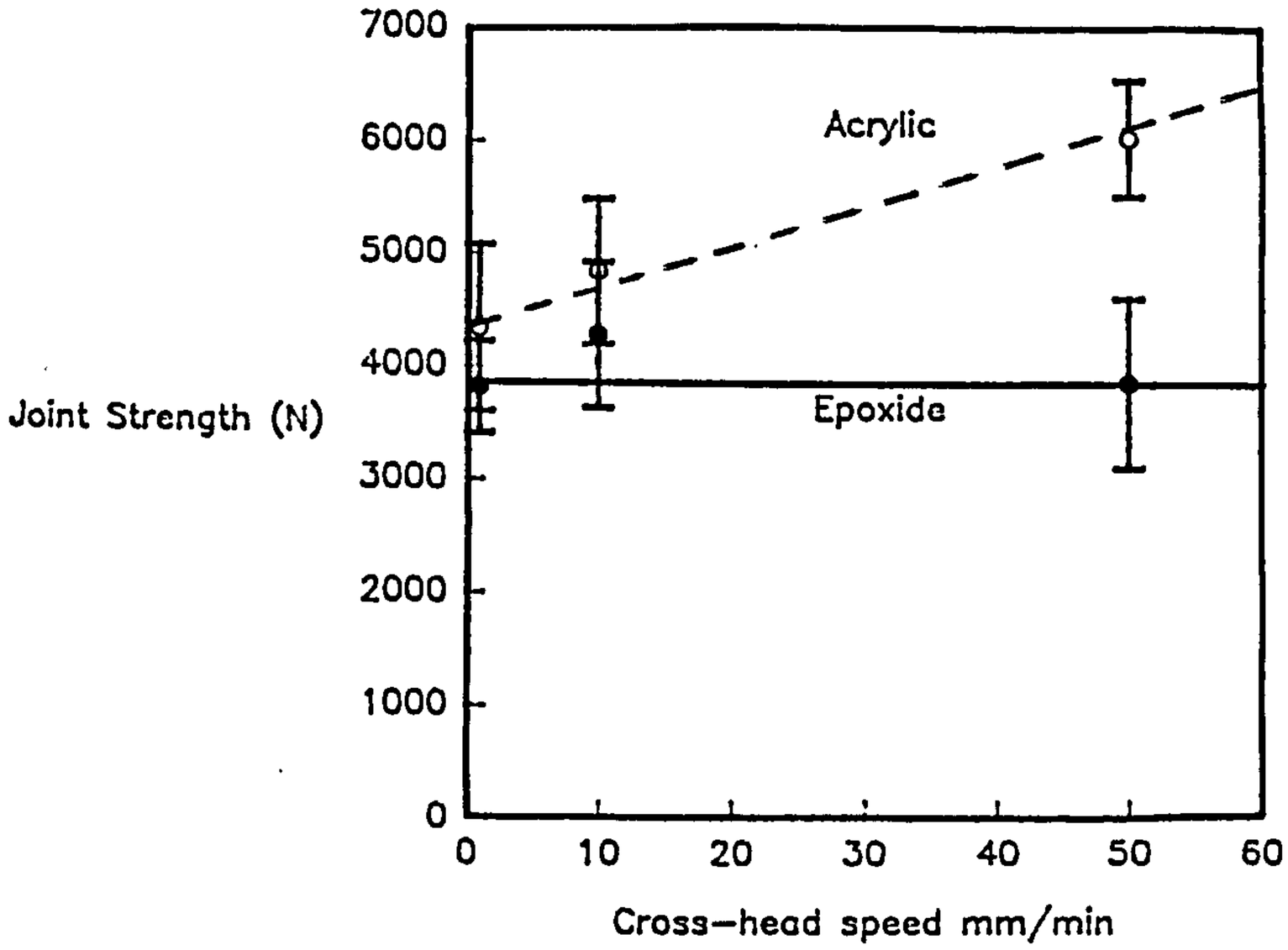

Figure 4 - To Show the Initial Strength of SLS Joints Produced with Acrylic and Epoxide Adhesives as a Function of Testing Speed.

3.2 SURFACE CHARACTERISATION OF TREATED ADHERENDS

The following section provides details of the physicochemical changes introduced to the surface of the adherend materials by the different treatments used in the present study.

AES depth profiles were obtained to provide surface and sub-surface chemical compositions. The surface topography was studied using electron microscopy. SEM was carried out in all cases, whilst STEM was used in one instance when the resolution of the SEM was not sufficient to provide the required information. In addition, profilometry was used to provide a quantitative assessment of the roughness parameters on the degreased-only and grit-blasted surfaces in Sections 3.2.1 and 3.2.2. Profilometry was not applied to the study of the micro-rough surfaces produced by most of the other treatments. The finite probe size used by this technique, being 2μm in diameter, prevents meaningful data from being obtained in these instances. Water contact angles were used, as appropriate, to provide complementary data on surface cleanliness and wettability.

Surface characterisation was carried out to establish base-line data underpinning the subsequent durability trials and hydration studies. This information fulfils two requirements: with the established treatments, it was necessary to ensure that the treatments carried out produced surfaces comparable to those reported in the literature thereby providing a check that the treatments were performed satisfactorily, and; for the novel treatments, the degree of surface physicochemical modification to the aluminium surface has been established, these data can then be intercompared with those from the established treatments and furthermore correlated with the durability results.

3.2.1 DEGREASED

The sheet material supplied was visibly contaminated with press lubricant. The material in this condition was unsuitable for bonding and no characterisation was carried out on the as-supplied aluminium alloy.

The minimum adherend surface preparation which was carried out was a double-degrease, as detailed in Section 2.2.2.1. Due to the ongoing nature of research it was necessary to obtain more than one batch of aluminium 5251 alloy. For comparison, surface characterisation was carried out on degreased-only material from two separate batches, labelled 1 and 2, from the same supplier.

AES depth profiles from degreased-only samples cut from two separate batches of aluminium 5251 alloy are presented in Figures 5a and 5b. The surface compositions are given in Table 9.

Table 9 - Surface Compositions (atom%), as Determined by AES, from Degreased-only Aluminium 5251 Alloy Samples from Two Different Batches of Material.

Batch Number	O	Al	Cl	C	Mg	Ca	S
1	51.7	14.6	0.0	24.6	7.4	0.6	1.1
2	48.7	8.5	0.9	29.6	12.5	0.0	0.0

The level of carbon contamination present on the two degreased-only surfaces was in the range ~25 to 30%. Such high levels were despite a two-stage treatment being used. It is significant that the carbon levels rapidly decrease with depth in the profiles, thereby, indicating that this material is surface specific. This level represents complete monolayer coverage of the substrate by organic contamination. It is likely that this contamination is strongly adsorbed or chemisorbed since it was not removed by the double-degrease treatment.

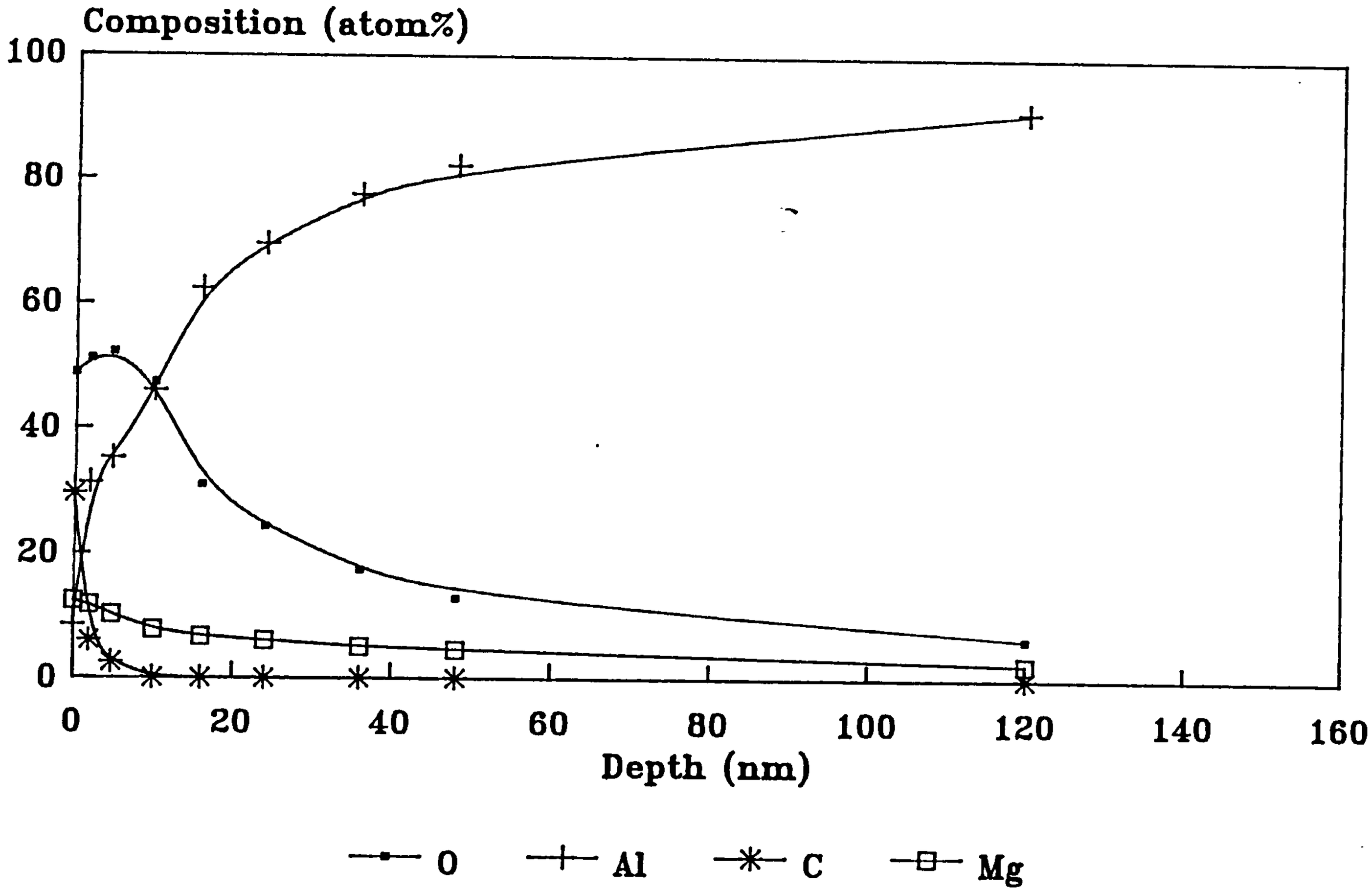

Figure 5a - AES Depth Profile from a Sample of Degreased-only Aluminium 5251 Alloy, Batch 1.

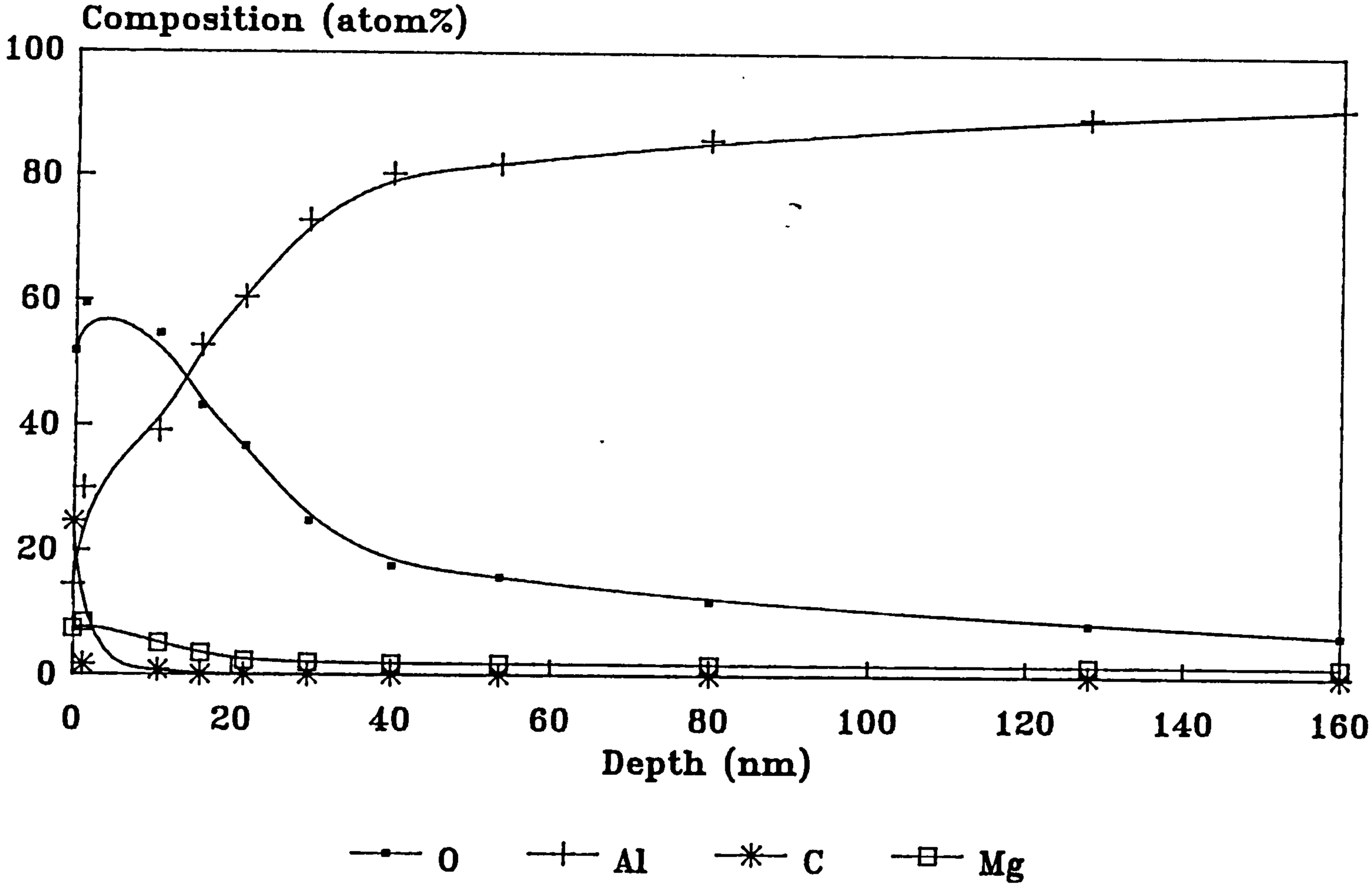

Figure 5b - AES Depth Profile from a Sample of Degreased-only Aluminium 5251 Alloy, Batch 2.

Water contact angles were obtained in three separate areas on a single degreased-only substrate, the mean value was ~50°. Such a high water contact angle is further indication of surface contamination. The contact angles were obtained within a few seconds of degreasing to reduce the possibility of post-treatment contamination affecting the results.

The ratio of the metallic species-to-oxygen indicates that, on the surface, in both instances there is more oxygen present than might be expected from Al_2O_3 and MgO. It is possible that the excess oxygen present is associated with the carbon otherwise the metals might have hydrated or there might be adsorbed water from the ambient.

An important feature of the surface oxide is the high Mg/Al levels observed throughout. The bulk alloy contains ~2% Mg and, as such, has a Mg/Al value of ~0.02. Mg/Al values were observed as high as 1.5 in the outermost layers of the oxide. The importance of the surface enrichment of Mg will be discussed later in the text.

To be consistent, throughout the present study, the thickness of the surface oxide has been defined as the depth at which the oxygen level decreases to half of its maximum value. Using this criteria, it can be estimated from Figures 5a and 5b that the oxide layer is 22 and 25 nm thick on samples from batches 1 and 2 respectively. The oxide layers are therefore similar in thickness in both batches.

SEM micrographs, at up to x5000 magnification, showed that the surface texture was similar on degreased-only samples in both batches of material. From Figure 5c and 5d, it can be seen that the degreased-only surface appears largely planar with embedded particles, rolling lines and areas of loosely-bound oxide present. The lack of surface macro-roughness was confirmed by the profilometry data presented in Table 10.

Figure 5 - SEM Micrographs of Degreased-only Aluminium 5261 Alloy at c. x410 and, d. x5000 Magnification.

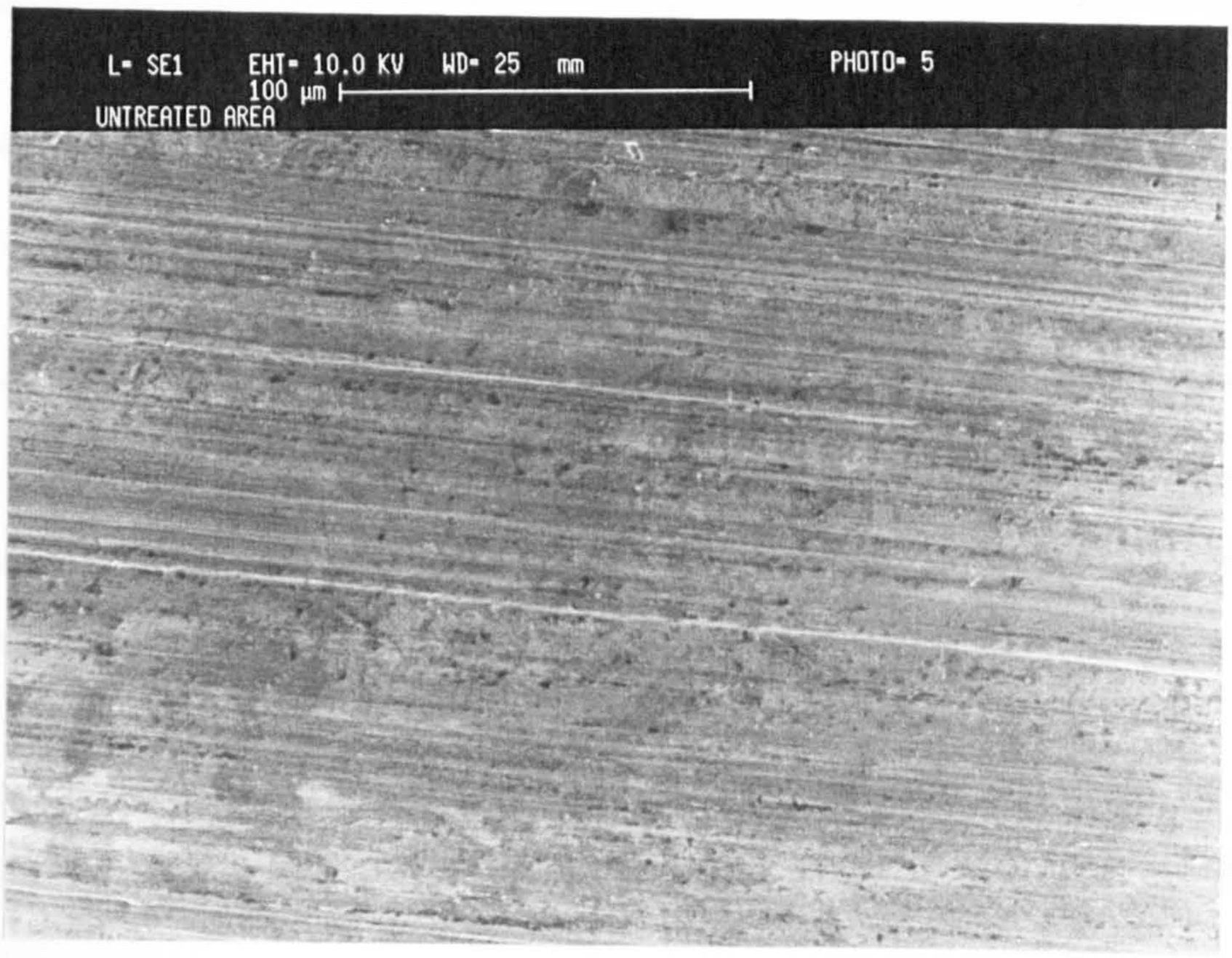

Table 10 - Profilometry Data from a Degreased-only Aluminium 5251 Alloy Surface.

Roughness parameter	Along rolling lines	Perpendicular to rolling lines
R_a (μm)	0.1	0.4
R_q (μm)	0.2	0.4
R_t (μm)	3.5	2.3

Where: the R_a value is the arithmetic mean deviation of the profile from the mean line; the R_q value is the root-mean-square equivalent of R_a, and; R_t is the peak-to-valley parameter.

As indicated in the above table, and as expected, the data from the degreased-only coupons were different when scanned either across or along the rolling lines.

3.2.2 GRIT-BLASTED

Grit-blasting was carried out using the procedure detailed in Section 2.2.2.2, using four different sizes of alumina grit.

AES depth profiling was carried out through the oxide on an 80/120 grade grit-blasted surface; this grade of grit was the most widely used in the durability studies. The resultant AES depth profile is presented in Figure 6a. The profile indicates that, as with the degreased-only treatment, the surface is contaminated with a thin layer of organic contamination. The oxide contains higher levels of Mg than the bulk material, but not such high levels as the degreased-only material. The thickness of the passivating oxide layer is approximately 11 nm. This value is much less than that previously measured on the degreased-only samples.

Surface compositions were determined, by AES, after treatment with all four sizes of grit; a compilation of these is given in Table 11. A compilation of surface Mg/Al

values is given in Table 12.

Table 11 - Surface Compositions (atom%), as Determined by AES, from Grit-blasted Aluminium 5251 Alloy Surfaces

Grade of grit	S	Cl	C	Ca	O	Al	Mg
320	0.0	0.0	3.5	1.2	67.7	27.6	0.0
180/220	0.6	0.0	7.2	1.9	63.3	23.0	4.0
80/120	0.8	0.0	8.7	1.3	63.6	20.5	5.1
40/60	0.7	0.0	3.5	2.4	67.5	21.8	4.1

Table 12 - A Compilation of Surface Mg/Al Values, as Determined by AES, along with Water Contact Angles as a Function of Grit-size.

Grade of grit	Mg/Al value	Mean water contact angle (°)
320	<< 0.1	83
180/220	0.17	64
80/120	0.25	69
40/60	0.19	89

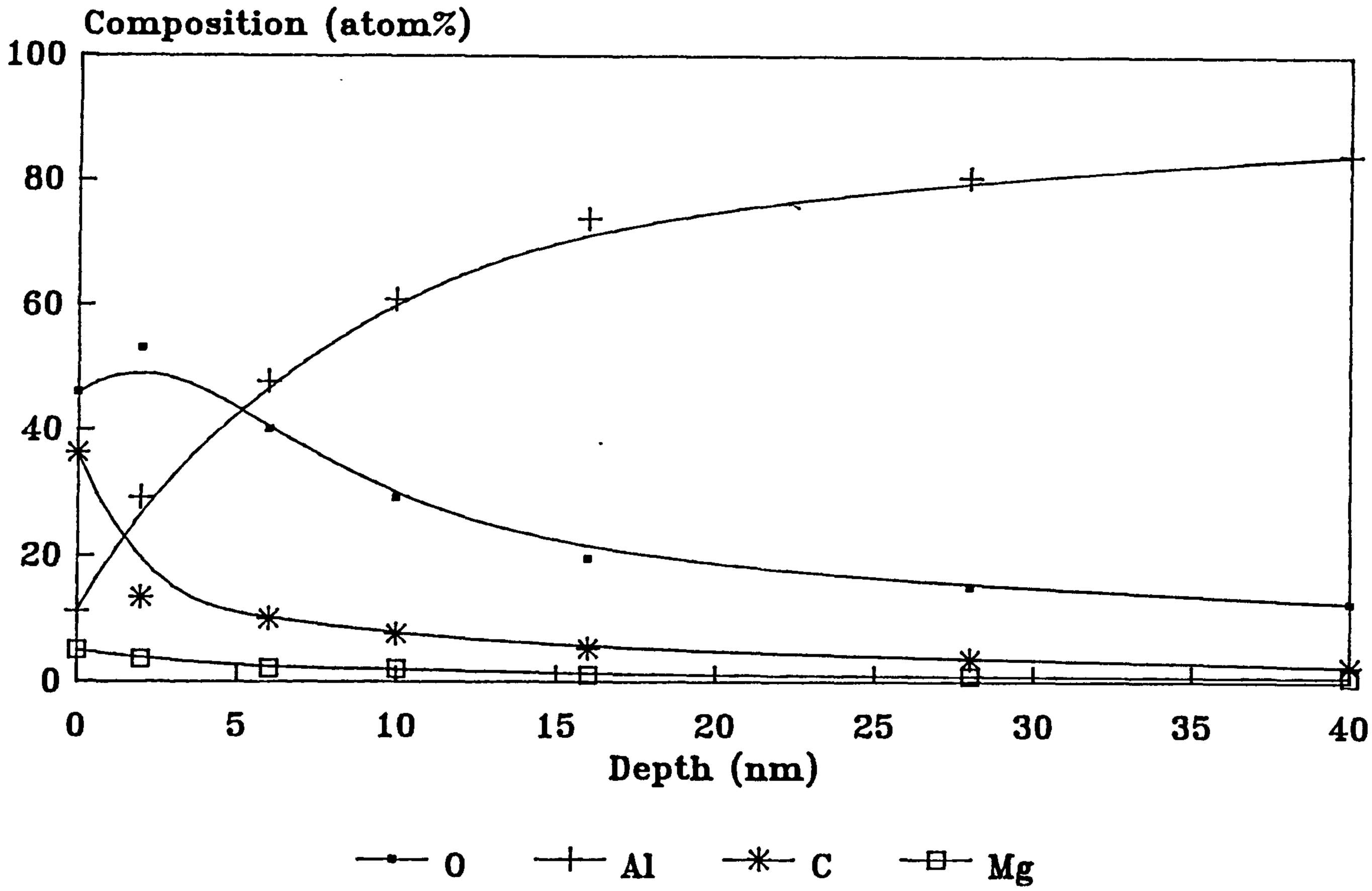

Figure 6a - AES Depth Profile from a Sample of 80/120 grade Grit-blasted Aluminium 5251 Alloy.

The carbon levels on these surfaces were much reduced from the degreased-only surfaces. It should be noted that there is an apparent inconsistency between the low levels of organic contamination and the high contact angles measured; see Table 12.

Water contact angles were determined in three separate areas on grit-blasted and subsequently degreased surfaces, as previously described, these were determined within 20 seconds of degreasing to reduce the effect of post-treatment contamination. The high contact angles observed, in the range 64 to 89°, indicate a high degree of surface organic contamination. Such contamination was not observed in the AES results. It is possible that loosely-bound organic material might be desorbed by the vacuum or under the influence of the electron beam.

Significantly, no Mg could be detected on the 320-grade grit-blasted surface; a Mg/Al value of $<<0.1$ is quoted in Table 12 since magnesium might be present below the detection limits of AES. The other three grades gave consistent results, with Mg/Al values of ~ 0.2.

Electron micrographs from 320, 80/120 and 40/60 grade grit-blasted surfaces at x1300 magnification are given in Figures 6b to 6d. The grit-blasted samples exhibit a uniform degree of treatment across their surfaces with all of the features of the degreased-only surface removed. All of the grit-blasted surfaces have more angular features than that which was degreased-only. The surface features were smaller and less deep when using the 320 grade grit compared with the broader but deeper features produced using the 40/60 grit. The 80/120 grade grit produced a similar surface texture to the 40/60.

A quantitative view of these surfaces is given in the profilometry data presented in Table 13. The values given are representative of a number of areas scanned on each coupon.

Table 13 - A Summary of Profilometry Data as a Function of Alumina Grit-size.

Roughness parameter	Grade of grit			
	320	180/220	80/120	40/60
R_a (μm)	0.9	1.2	2.7	2.9
R_q (μm)	1.3	1.6	3.5	3.6
R_t (μm)	13.4	12.8	23.6	20.2

The R_a values from the grit-blasted surfaces show variations ranging from 0.9 to 2.9μm for the 320 and 40/60 grade grit-blasted surfaces respectively. A similar, factor of x3, variation is also observed in the R_q values. These data, when combined with the peak-to-valley parameter values, R_t, indicate a general increase in surface roughness with increasing grit size. However, it is apparent that the two finer grades of grit produce similar surface profiles as do the two coarser grades.

Figure 6 - SEM Micrographs of b. 40/60, c. 80/120 and, d. 320 Grade Grit-blasted Aluminium 5251 Alloy at Approximately x1300 magnification.

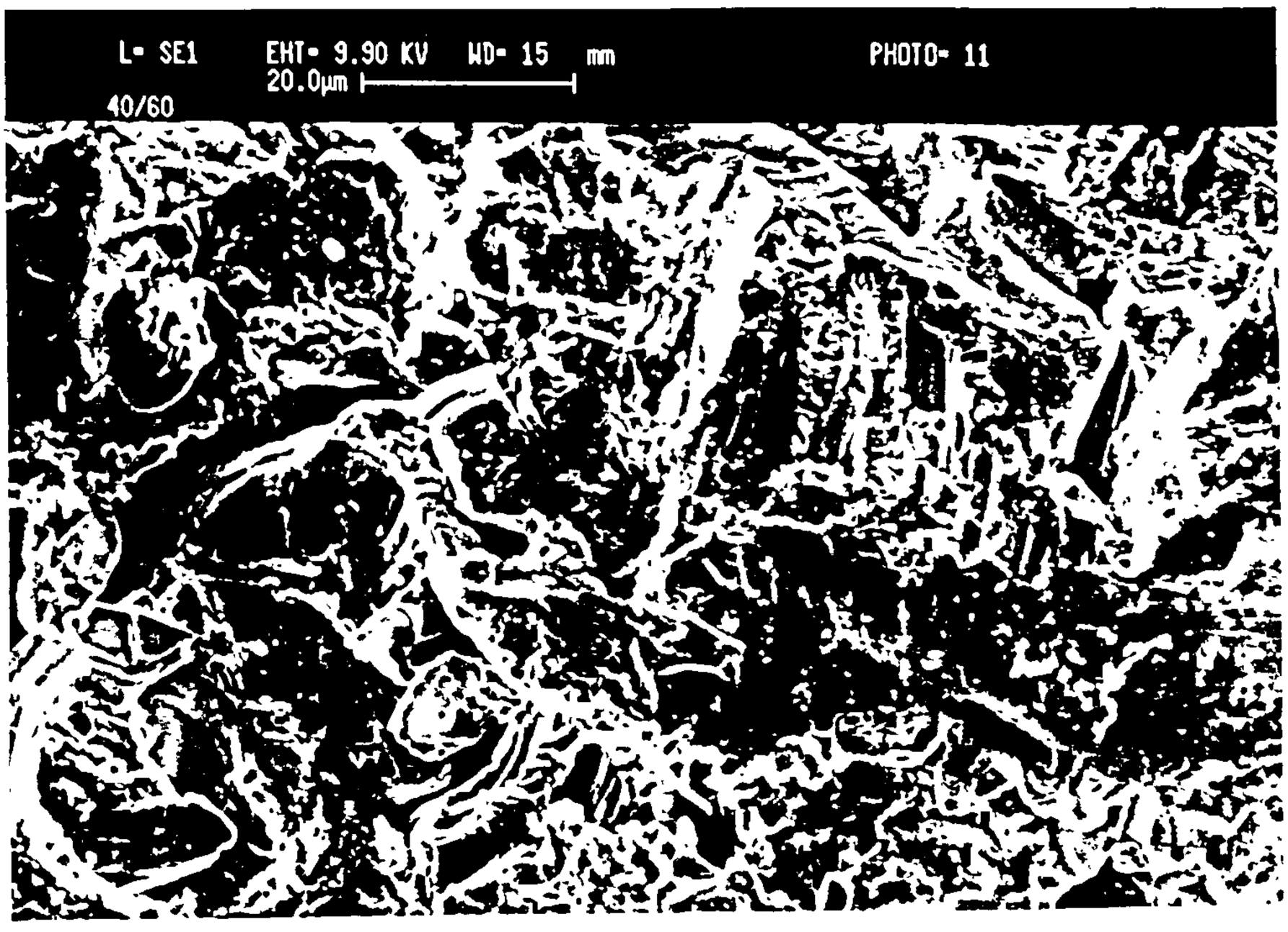

Table 13 - A Summary of Profilometry Data as a Function of Alumina Grit-size.

Roughness parameter	Grade of grit			
	320	180/220	80/120	40/60
R_a (μm)	0.9	1.2	2.7	2.9
R_q (μm)	1.3	1.6	3.5	3.6
R_t (μm)	13.4	12.8	23.6	20.2

The R_a values from the grit-blasted surfaces show variations ranging from 0.9 to 2.9μm for the 320 and 40/60 grade grit-blasted surfaces respectively. A similar, factor of x3, variation is also observed in the R_q values. These data, when combined with the peak-to-valley parameter values, R_t, indicate a general increase in surface roughness with increasing grit size. However, it is apparent that the two finer grades of grit produce similar surface profiles as do the two coarser grades.

Figure 6 - SEM Micrographs of b. 40/60, c. 80/120 and, d. 320 Grade Grit-blasted Aluminium 5251 Alloy at Approximately x1300 magnification.

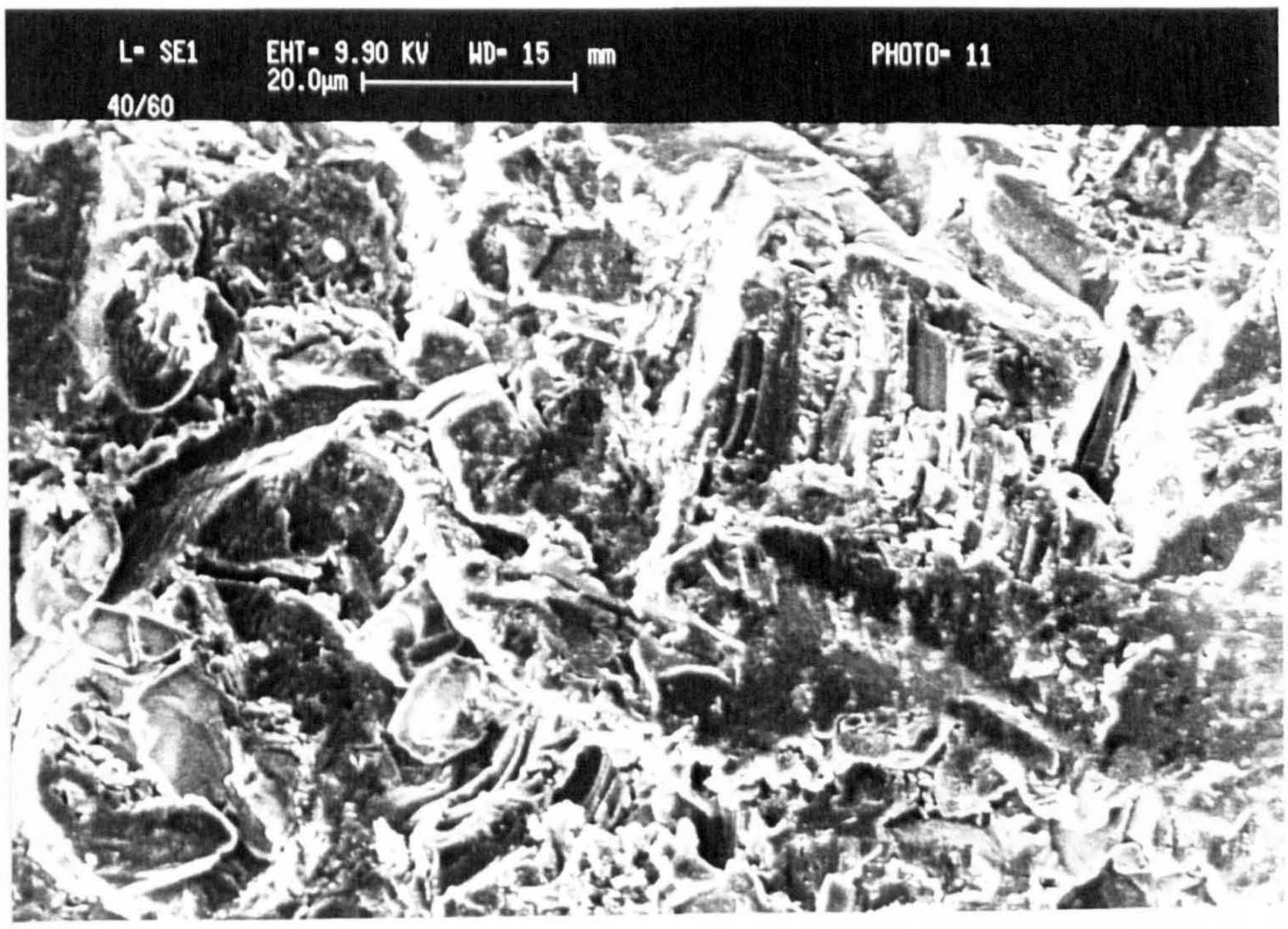

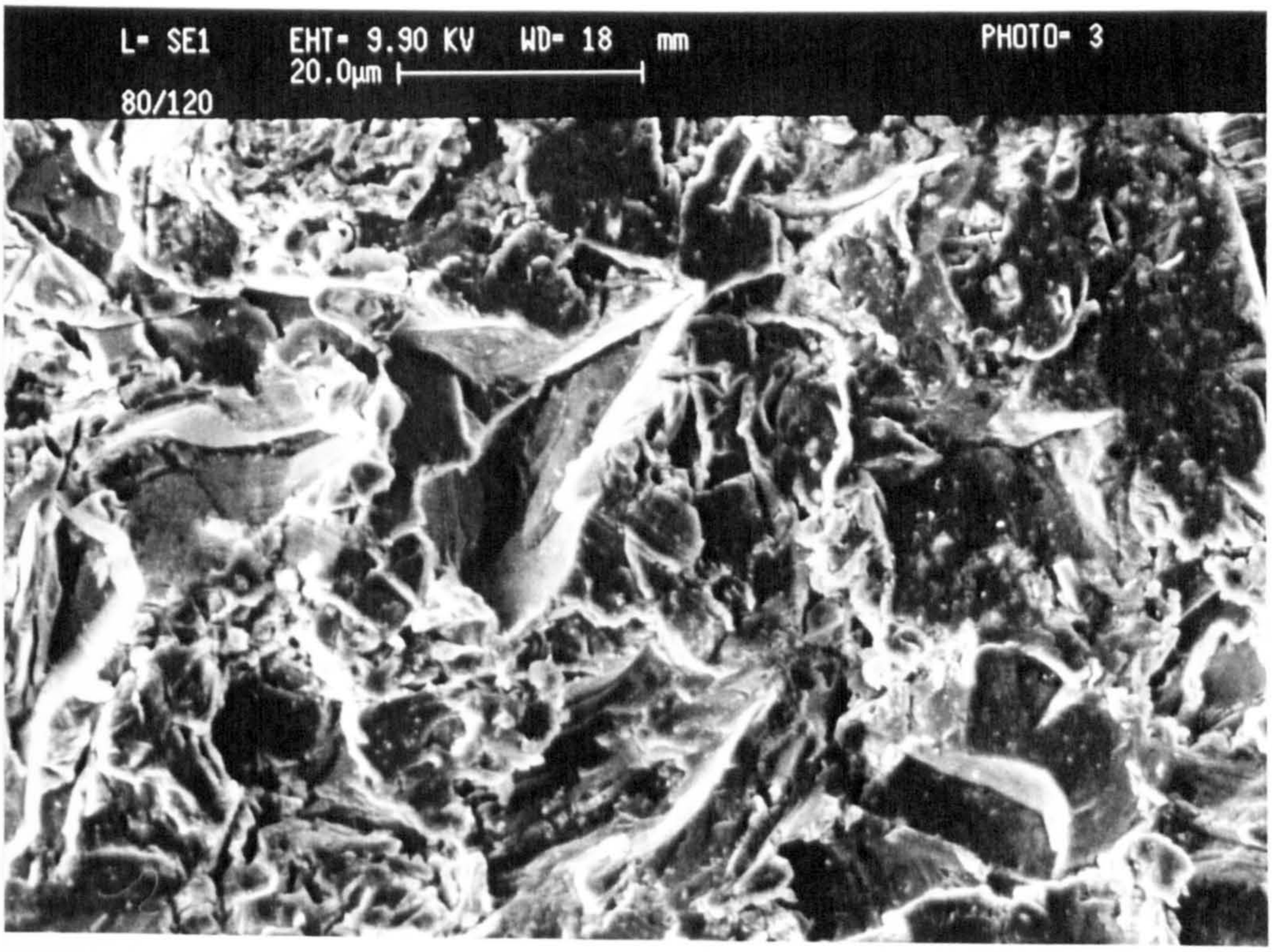
L= SE1
EHT= 9.90 KV
WD= 18 mm
PHOTO= 3
20.0µm
80/120

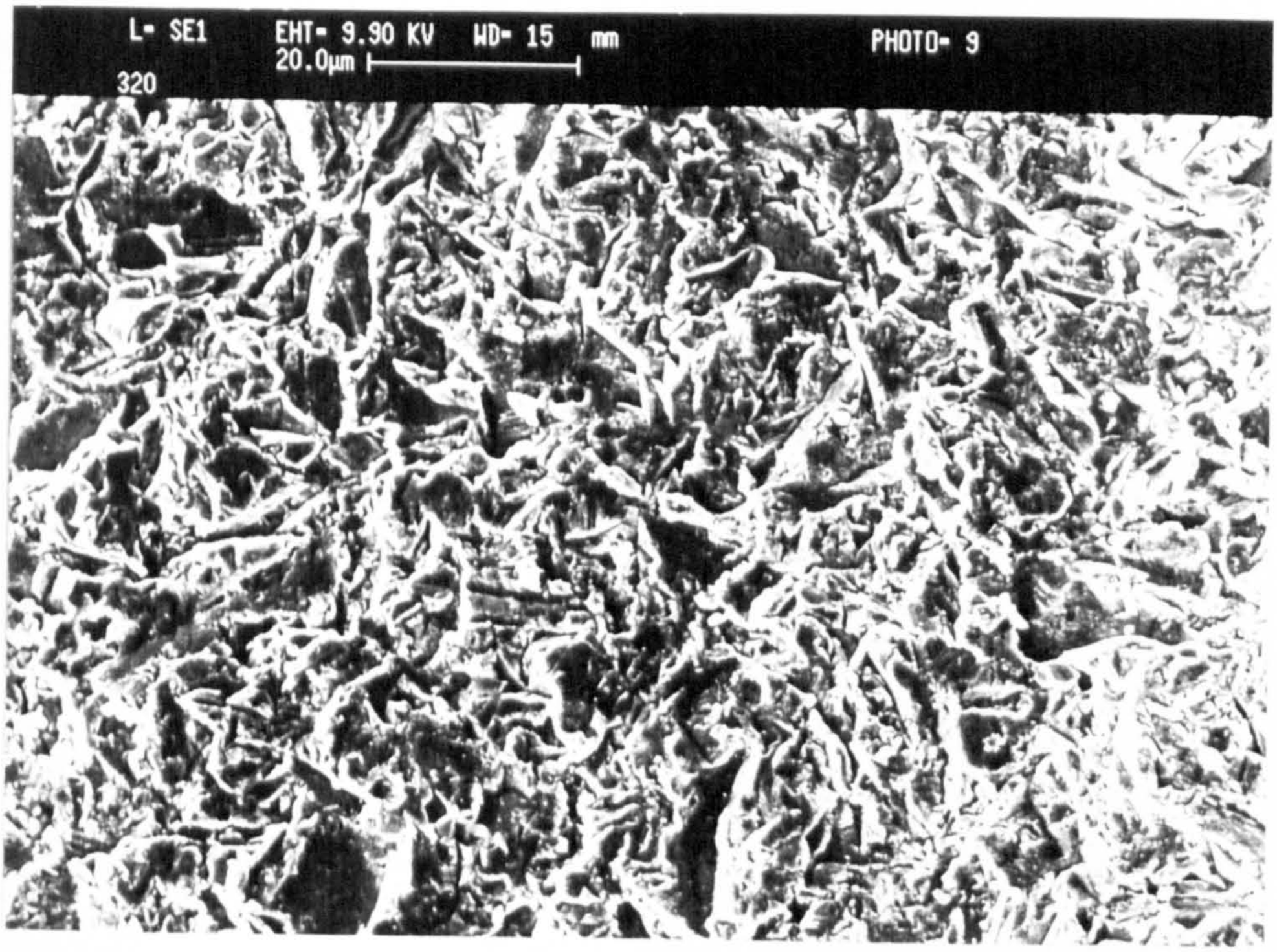
L= SE1
EHT= 9.90 KV
WD= 15 mm
PHOTO= 9
20.0µm
320

3.2.3 CO_2-LASER ABLATED

3.2.3.1 Aluminium 5251 alloy

Aluminium 5251 alloy coupons were first degreased, the coupons were then CO_2-laser ablated with each point on the surface receiving 30 pulses with a half-second duration inbetween. The results of AES analysis on the laser-treated aluminium alloy are given in Table 14 and in Figure 7a. Table 14 gives the results from surface survey scans in both laser-treated and degreased-only regions of the same sample. These results are representative of those obtained from a number of areas from within each region.

The data presented in Table 14 indicate that there is a reduction in the levels of surface carbon from ~30% on the double-degreased surface to 0% with the laser-treated. This result indicates that the CO_2-laser treatment effectively removes organic material which is residual following the degrease process. It should be noted that the detection limits of AES for carbon in the Al_2O_3 matrix is less than 1%.

Also, as indicated in the previously-mentioned table, there is an accompanying decrease in the Mg/Al value in the outermost part of the oxide layer as a consequence of the laser treatment.

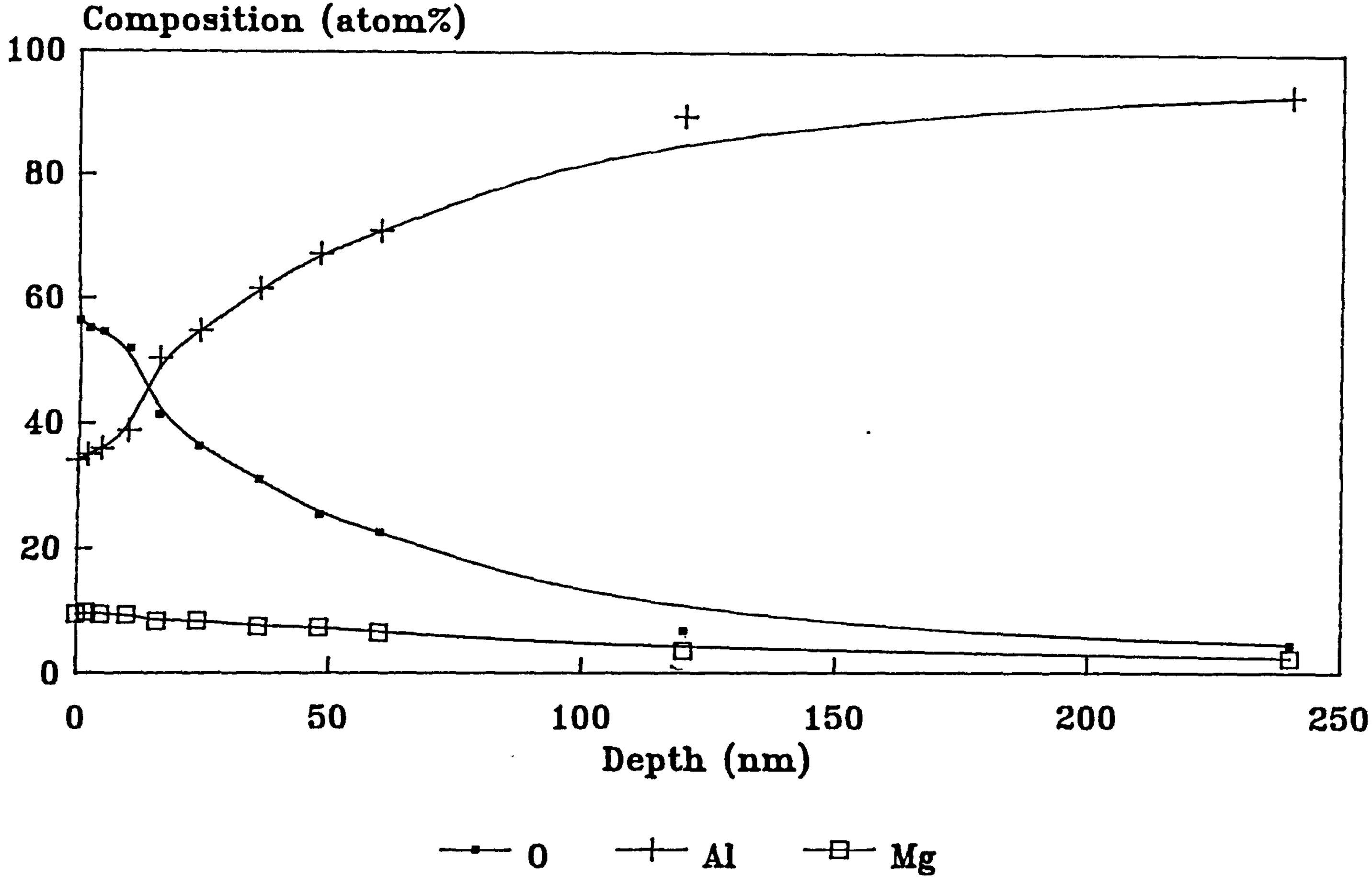

Figure 7a - AES Depth Profile from a Sample of CO_2-laser Treated Aluminium 5251 Alloy.

Table 14 - AES data (atom%) from Survey Scans in Degreased-only and CO_2-laser Treated areas of the Same Coupon.

	Element				
Analysis area	O	Cl	C	Al	Mg
Degreased-only	48.7	0.9	29.6	8.5	12.4
Laser-treated	56.4	0.0	0.0	34.1	9.6

The depth profile, given in Figure 7a, illustrates the variations in oxide composition with depth in the laser-treated area. This profile should be compared with Figure 5a which was a degreased-only coupon from the same batch of alloy. Comparing results, it can be seen that the laser-treatment causes a slight thickening of the surface oxide from ~21 nm to ~42 nm.

The surface topography was studied by SEM at magnifications up to x20000. Micrographs with magnification of x400 and x5000 from representative laser-treated areas are given in Figures 7b and 7c. The surface features are broadly similar in both degreased-only and laser-treated areas, with rolling lines, apparently loosely bound oxide and embedded particulates visible in both cases. No differences could be observed at the higher magnification levels, the only differentiating feature between these surfaces being that, at low resolution, the rolling lines do not appear as prominent on the laser-treated compared degreased-only surface; thereby indicating that some degree of surface melting had occurred.

Figure 7 - SEM Micrograph of CO_2-laser Treated Aluminium Alloy at b. x400 and c. x5000 Magnification.

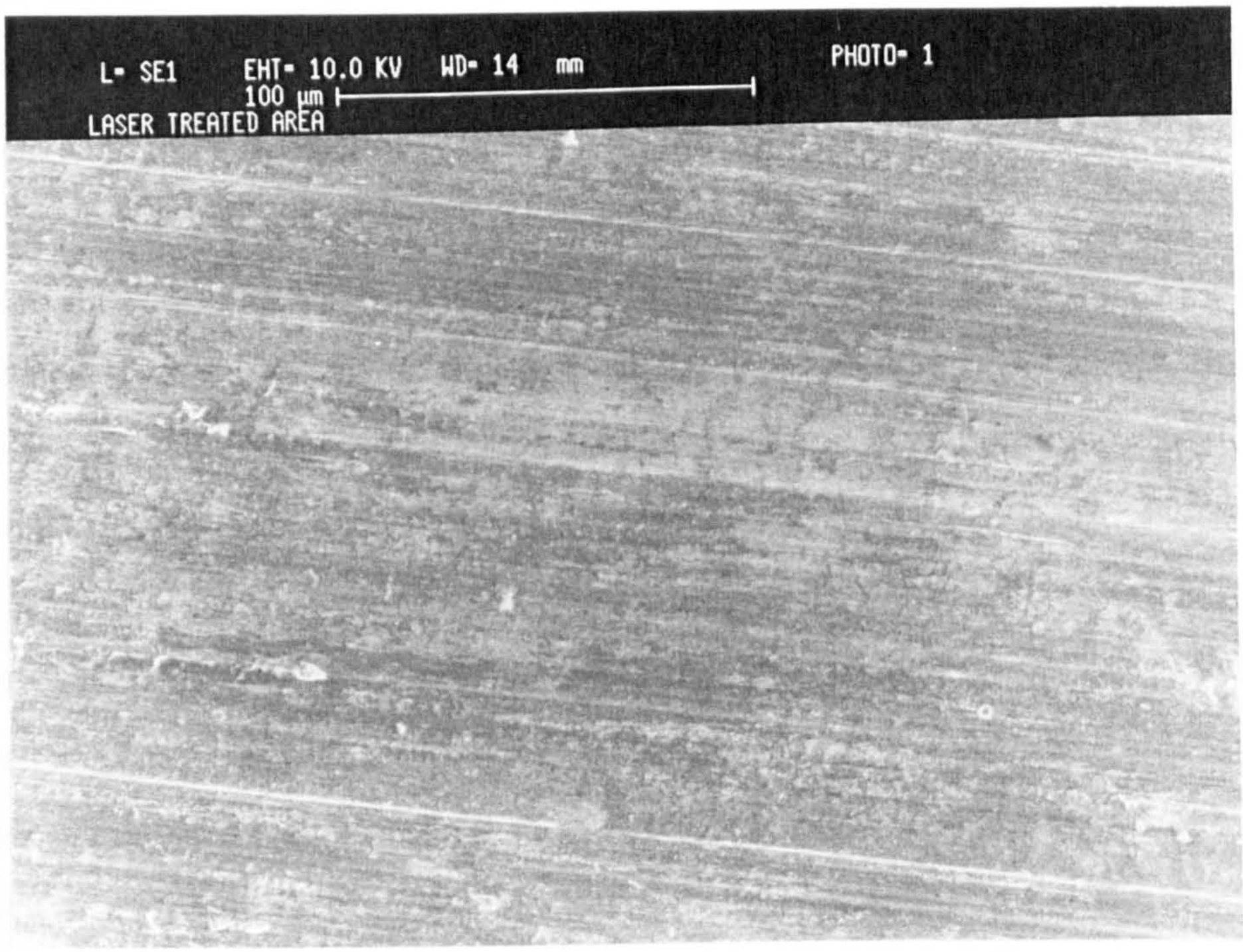

3.2.3.2 Mild steel

The as-received CR1 mild steel had a characteristic matt grey colour with a visible oily deposit on the surface. As might be expected the oily deposit appeared to be removed when the coupons were degreased. The CO_2-laser treated surfaces were not, however, degreased but received 40 pulses at each point on the raster within the bonded area.

The bonded area in all samples contained areas of different colouration. Both AES analysis and SEM were carried out in three characteristic areas on separate coupons, these being: degreased-only; laser-treated and shiny grey in appearance, and; laser-treated and dark blue.

The results of AES analyses are presented in Table 15 and in Figures 8a to 8c. The table gives surface compositions in terms of atom percent whilst the figures present the depth profiles through the oxide layer in all three of the aforementioned areas. For clarity, only the elements O, C, Fe and Ca have been included in the figures. Note that the carbon levels in Figures 8b and 8c were so low that they did not show above the base line and so were not included in these plots.

Table 15 - Surface Compositions (AES data) from Degreased-only and CO_2-laser Treated Areas on CR1 Mild Steel.

Surface treatment	O	P	S	Cl	C	Ca	Fe
Degreased-only	28.4	1.2	1.3	3.5	45.1	7.0	13.5
Laser treated	61.6	0.0	0.8	1.1	1.2	8.7	26.6

A compilation of oxide thicknesses, estimated from Figures 8a to 8c, is given in Table 16.

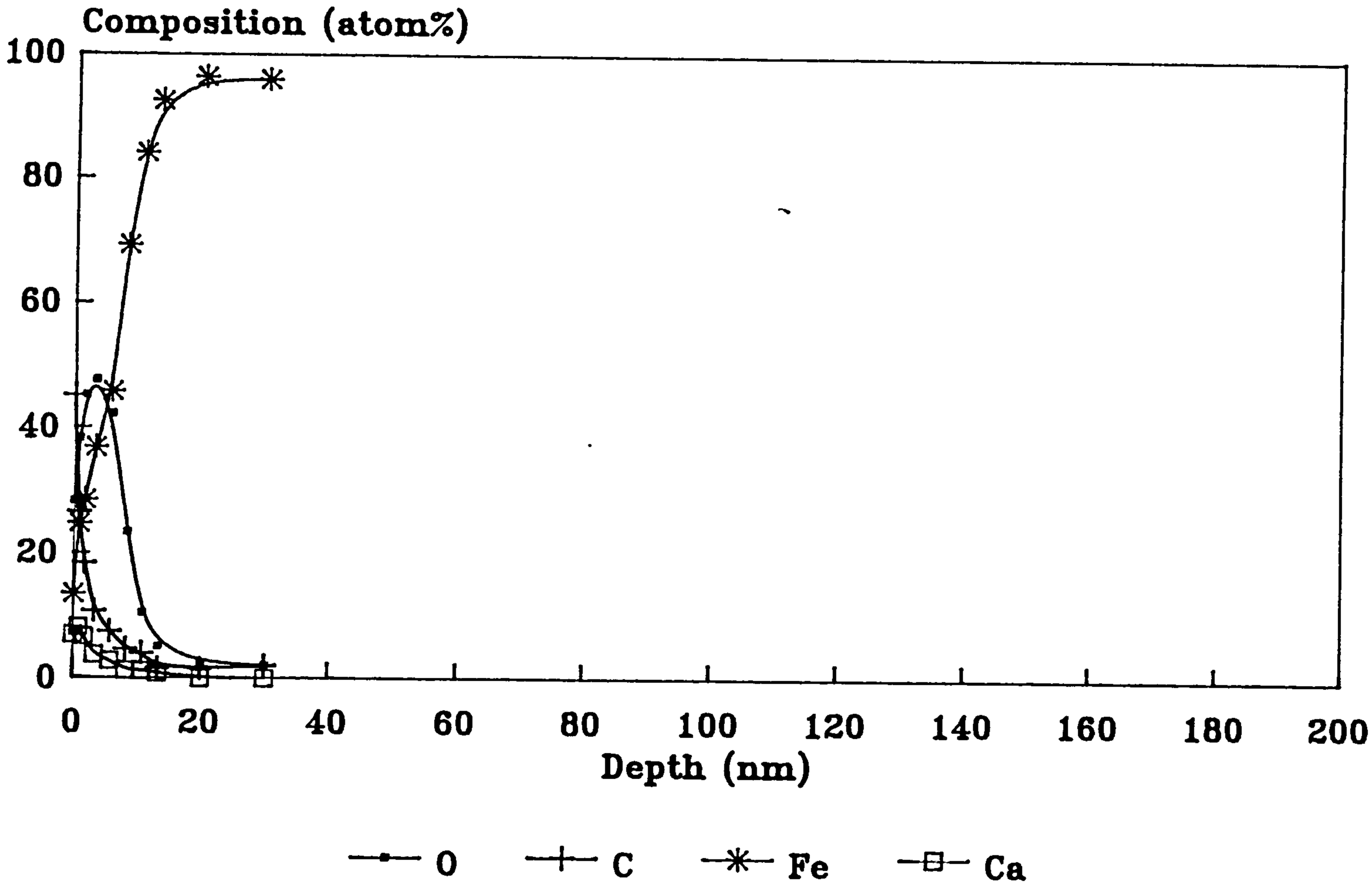

Figure 8a - AES Depth Profile from a Degreased-only CR1 Mild Steel Sample.

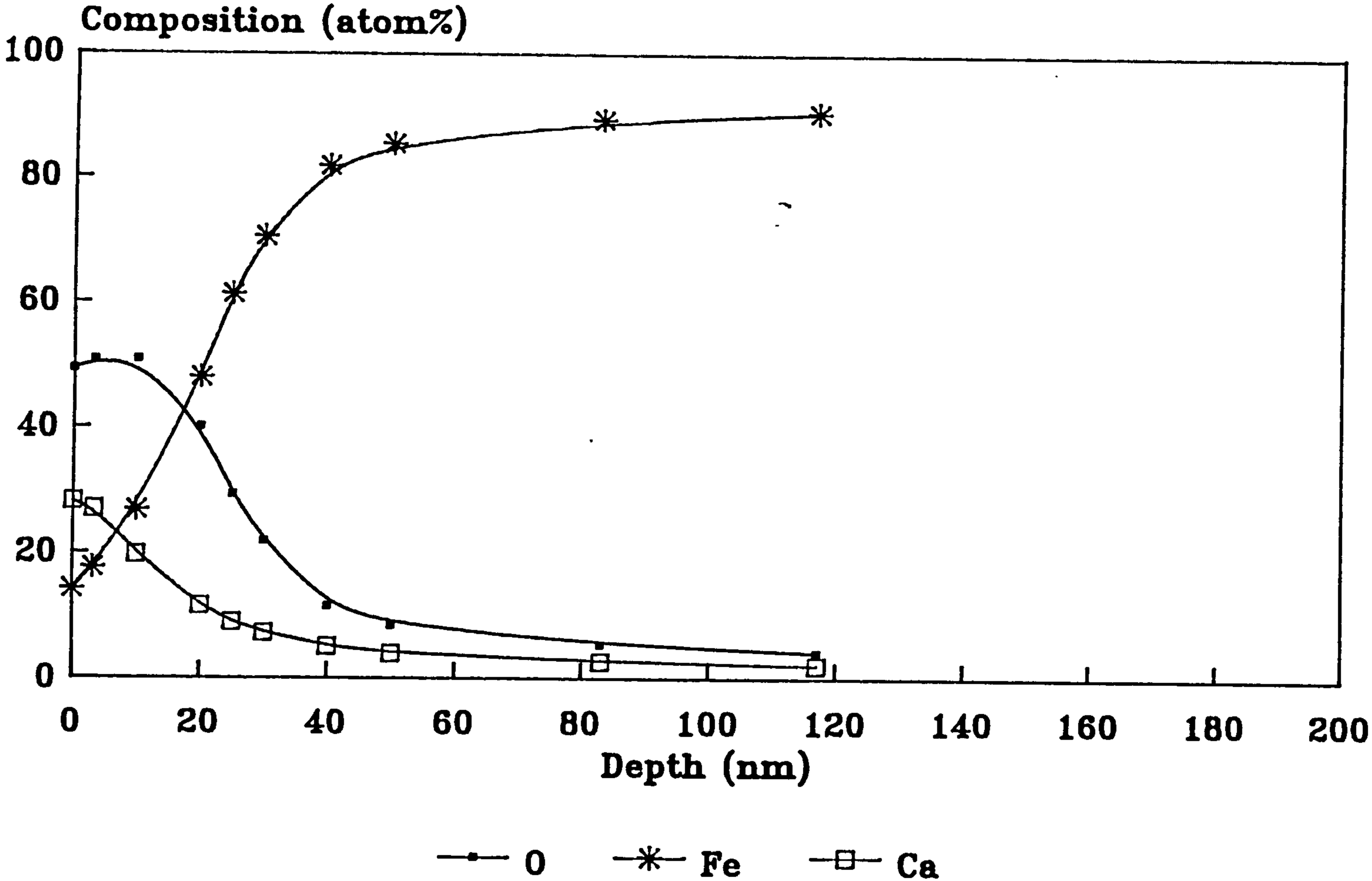

Figure 8b - AES Depth Profile from a CO_2-laser Treated CR1 Mild Steel Sample - Shiny Grey Area.

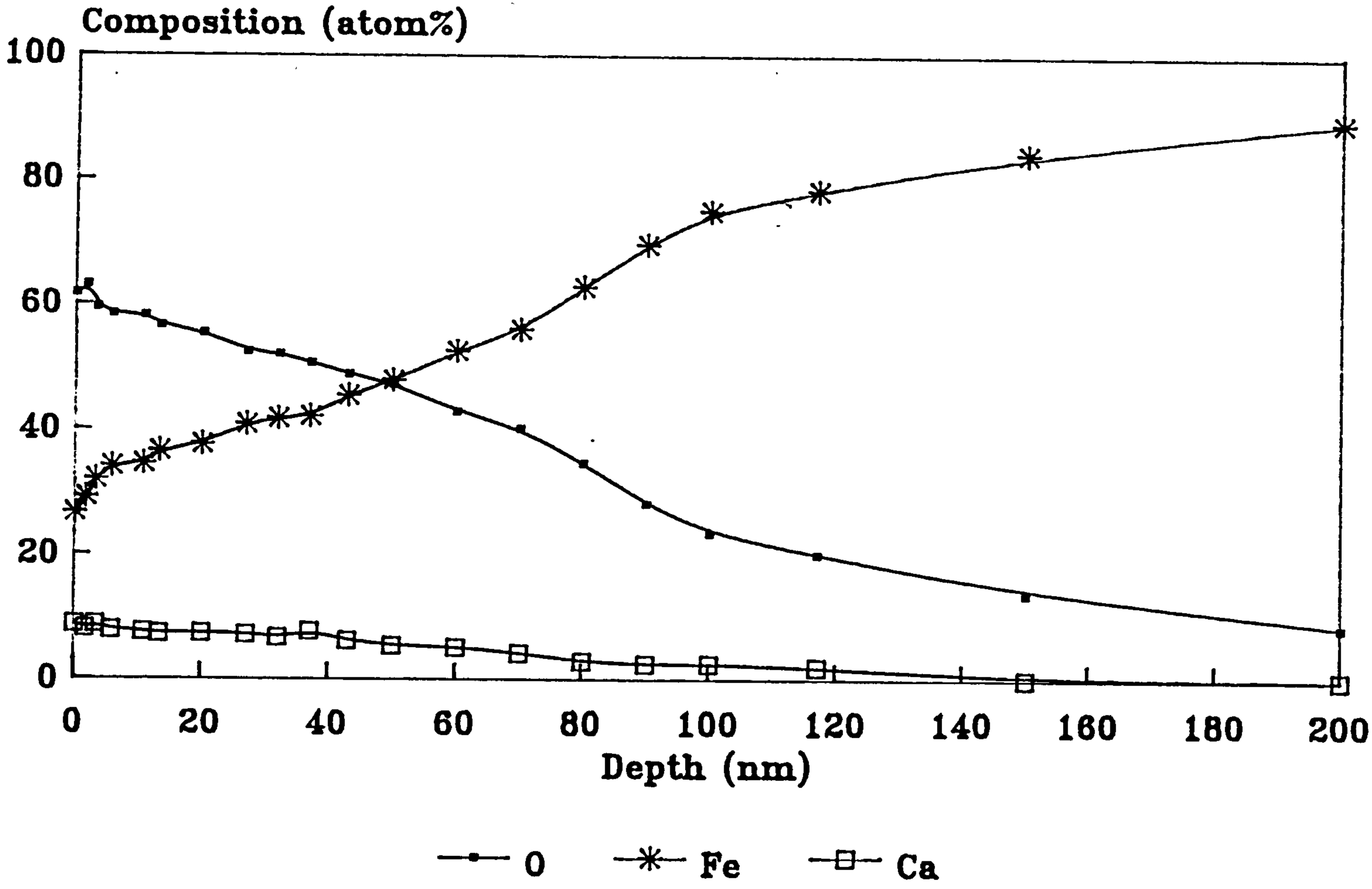

Figure 8c - AES Depth Profile from a CO_2-laser Treated CR1 Mild Steel Sample - Dark Blue Area.

Table 16 - A Compilation of Oxide Thicknesses for Treated CR1 Mild Steel.

Surface treatment	Oxide thickness (nm)
Degreased-only	8
Laser treated - shiny grey	28
Laser treated - dark blue	85

Note that there has been considerable thickening, compared with the pre-existing surface oxide, as a result of the CO_2-laser treatment.

The significant changes in surface chemistry, as a function of treatment, were also reflected in the topographical information in the SEM images. These are given in Figures 9 to 11. The SEM images are from the three areas of interest at high magnification, x13000.

Figure 9 - SEM Micrograph from a Degreased-only CR1 Mild Steel Sample at x13000 Magnification.

Figure 10 - SEM Micrograph from a CO_2-laser Treated CR1 Mild Steel Sample, Shiny Grey in Colour, at x13000 Magnification.

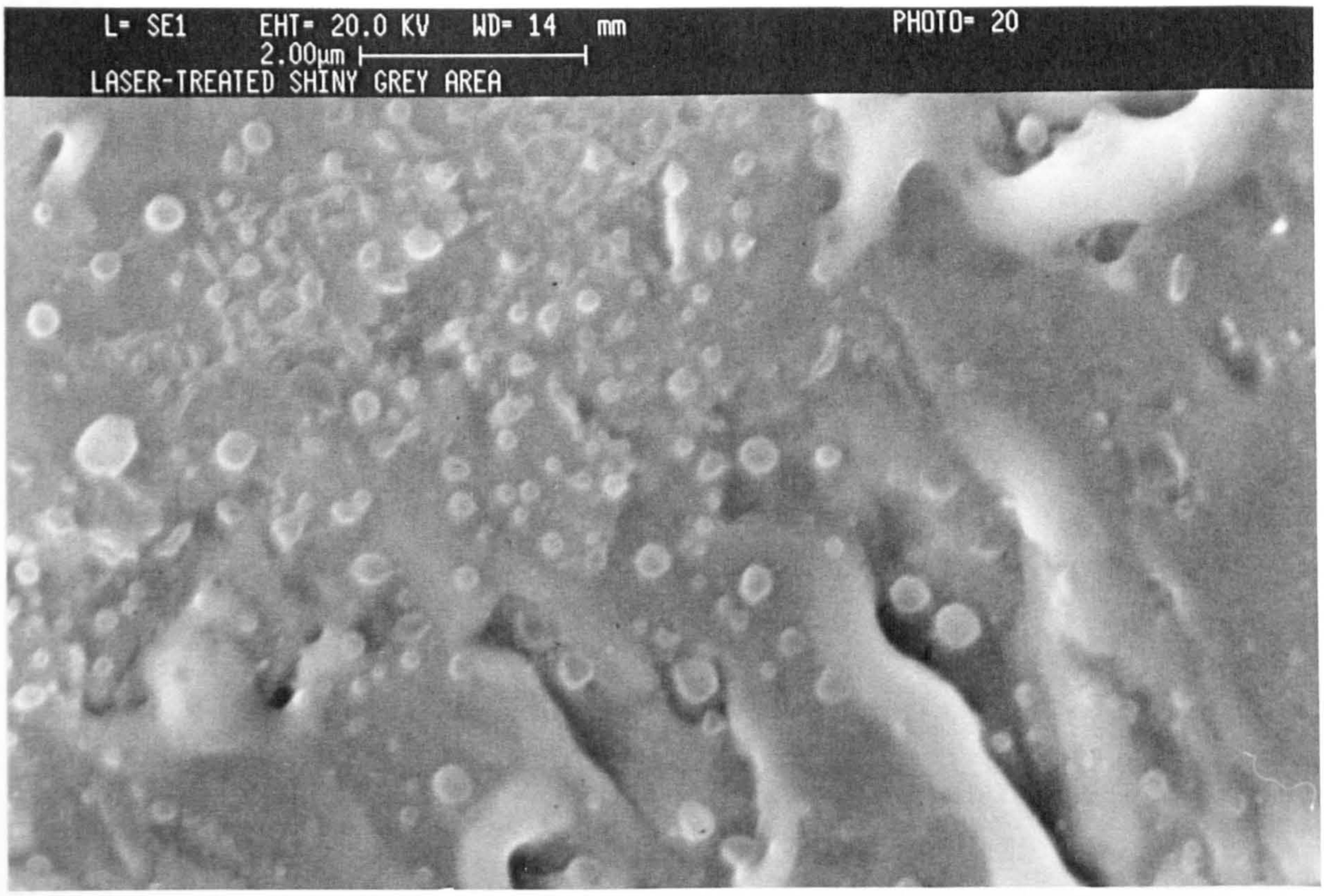

Figure 11 - SEM Micrograph from a CO_2-laser Treated CR1 Mild Steel Sample, Dark Blue in Colour, at 13000 Magnification.

3.2.4 BONDERITE 705 CONVERSION COATED

3.2.4.1 Aluminium 5251 Alloy

AES was used to determine the composition of the film produced by chromate-phosphate conversion coating for treatment times of 5, 15, 30 and 60 seconds; see Figures 12a to 12d. Figure 12e provides comparative data for the alkaline cleaned only surface.

These figures illustrate the compositional variations as a function of depth through the oxide and provide a more detailed analysis of such films than has so far been presented in the literature. For clarity and ease of comparison, carbon has not been included in these figures; similarly, magnesium has been omitted when present at bulk alloy levels, less than ~2%.

Compositions were based on Al_2O_3, P_2O_5 and Cr_2O_3 reference materials. Depth scale calibration was achieved using an etch rate determined by measuring the time taken to etch through a 1000 second Bonderite 705 conversion coating, the thickness of which was estimated from both SEM and ball cratering[159] to be in the range 0.95 to 1 μm. This depth scale calibration procedure was undertaken to minimise the errors previously associated with the characterisation of porous coatings on aluminium[94]. The etch rate calculated was subsequently applied to all of the aluminium depth profiles in the present study.

From these figures an estimated thickness for the coating present after each pretreatment can be estimated, a compilation of these is given in Table 17.

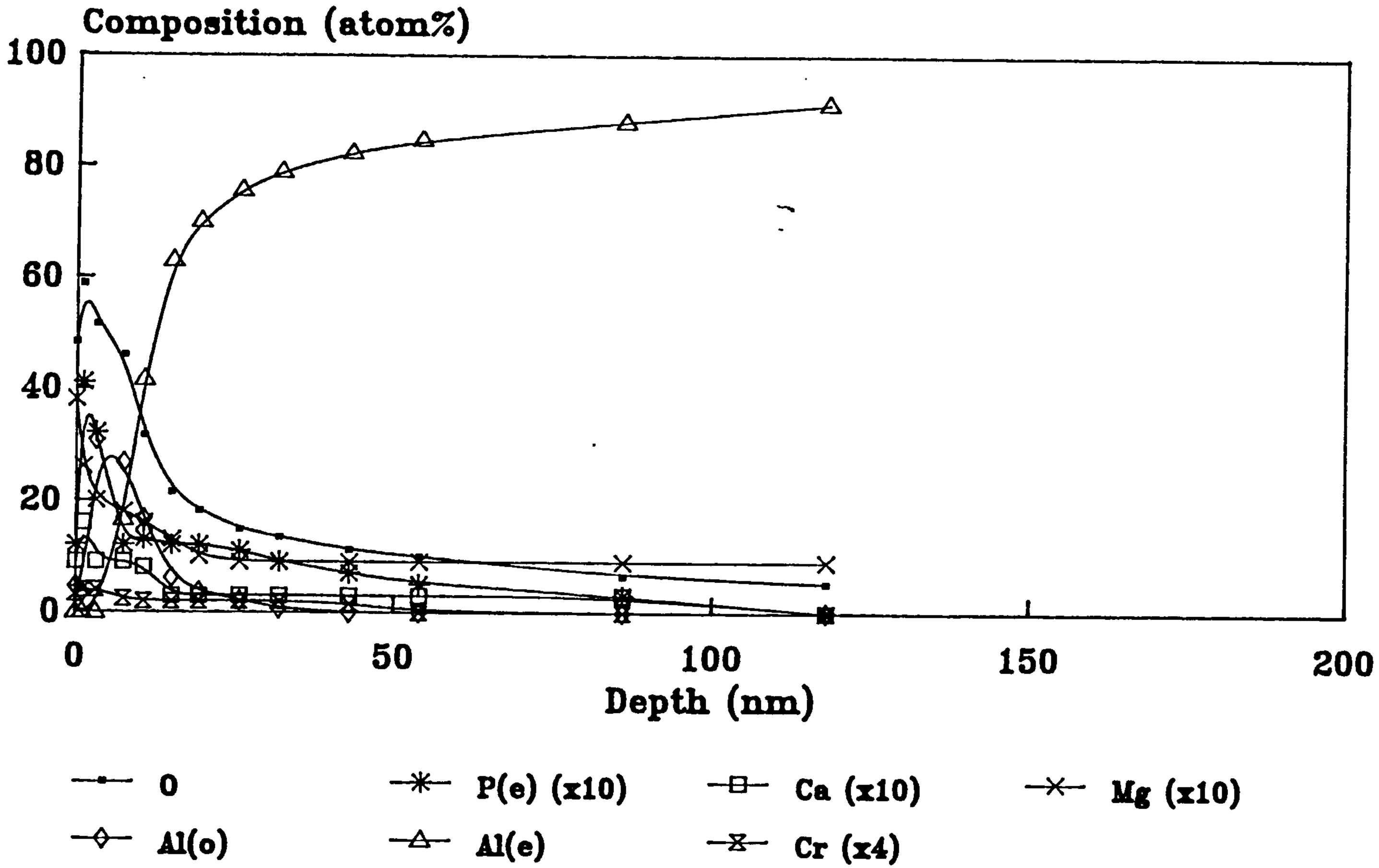

Figure 12a - AES Depth Profile Through the Film Produced Following Bonderite 705 Treatment for 5 Seconds on an Aluminium 5251 Alloy Sample.

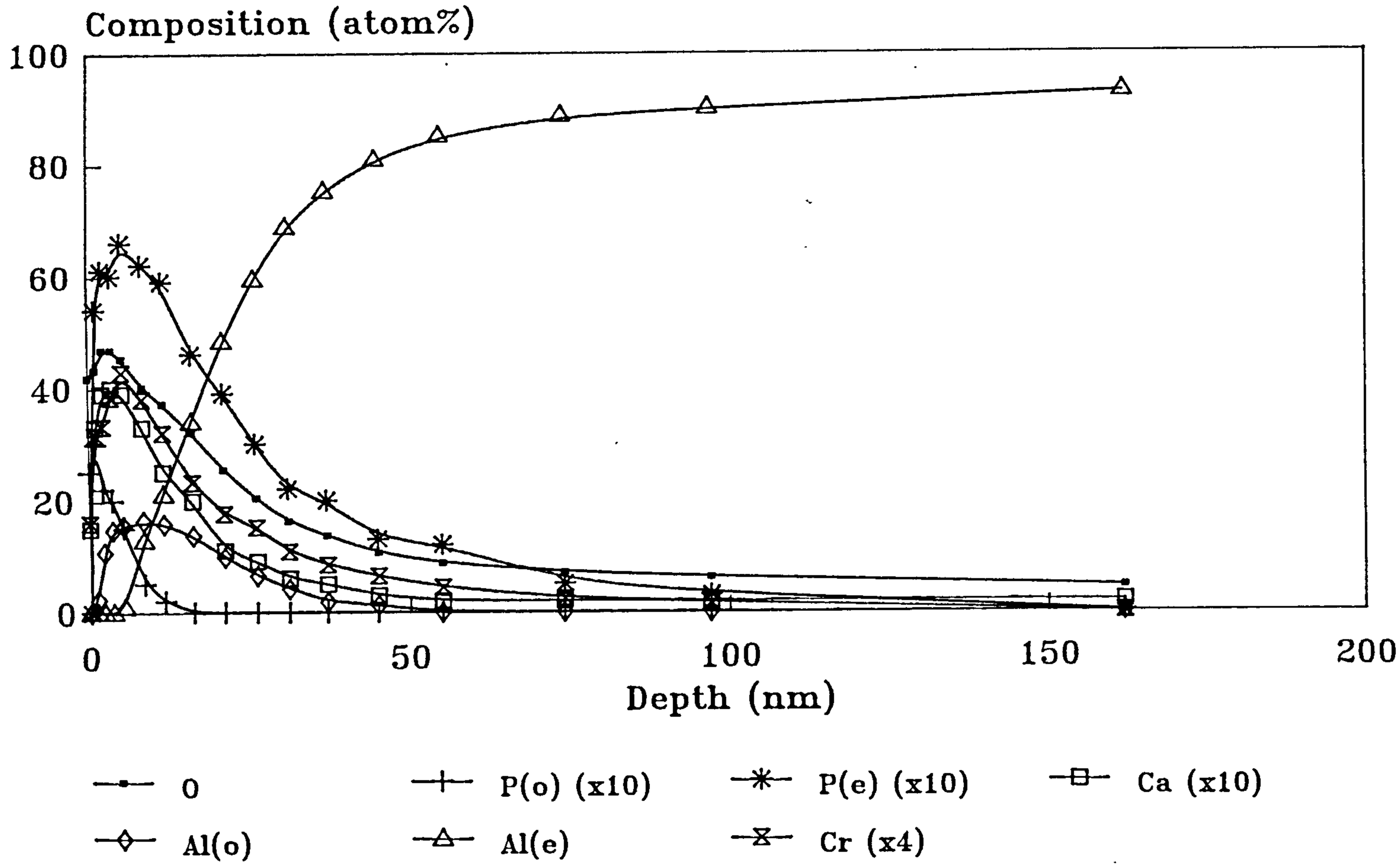

Figure 12b - AES Depth Profile Through the Film Produced Following Bonderite 705 Treatment for 15 Seconds on an Aluminium 5251 Alloy Sample.

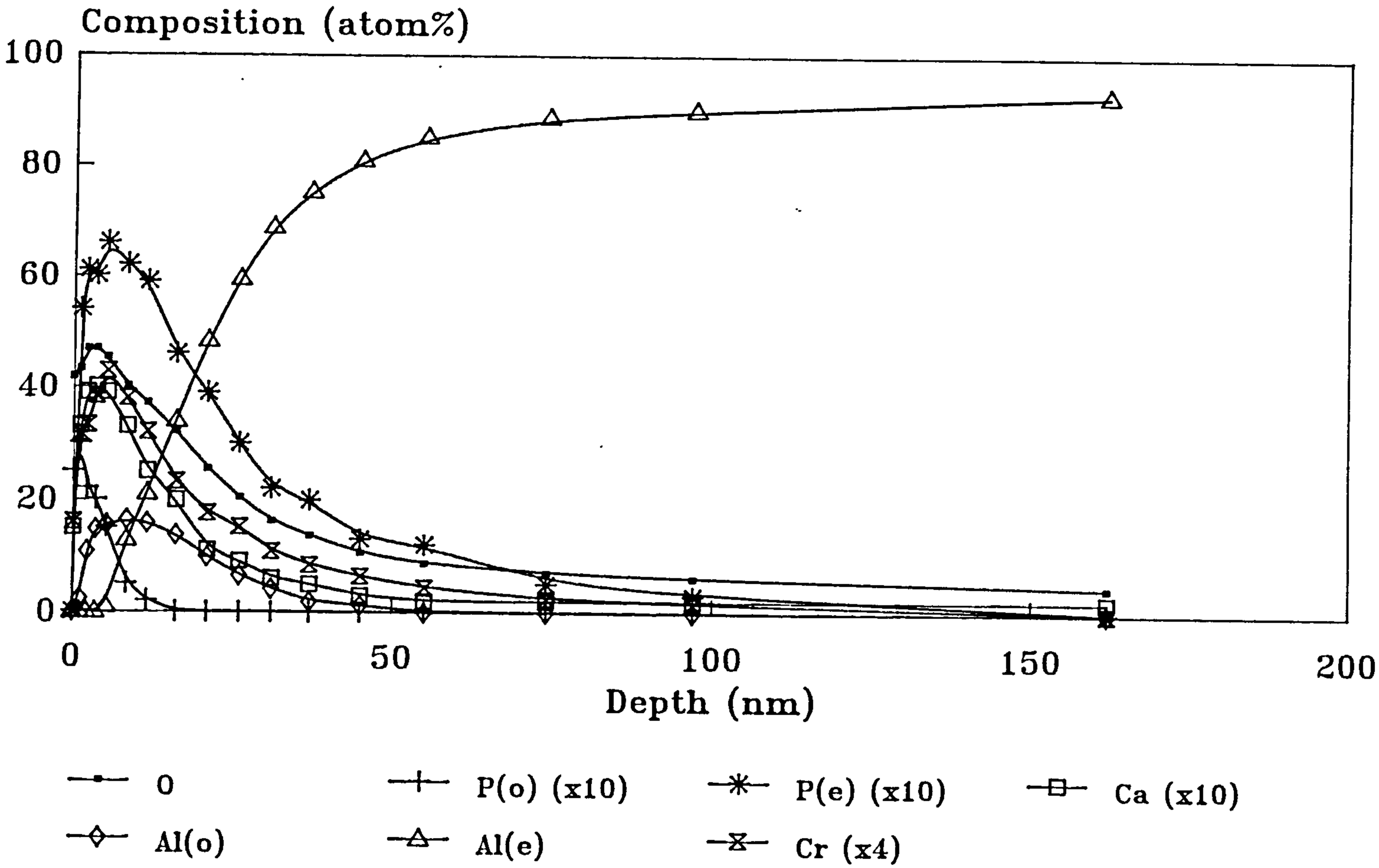

Figure 12b - AES Depth Profile Through the Film Produced Following Bonderite 705 Treatment for 15 Seconds on an Aluminium 5251 Alloy Sample.

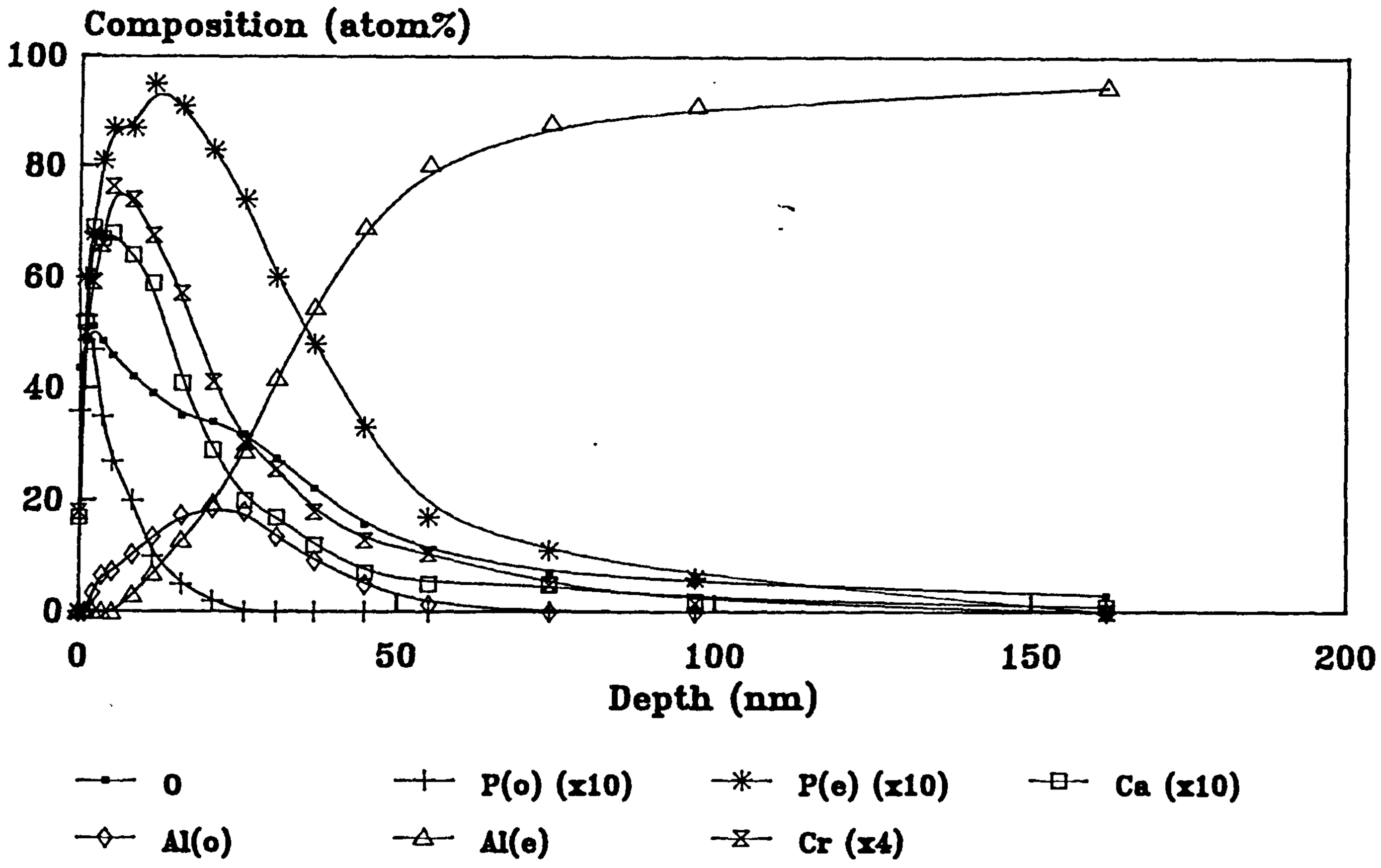

Figure 12c - AES Depth Profile Through the Film Produced Following Bonderite 705 Treatment for 30 Seconds on an Aluminium 5251 Alloy Sample.

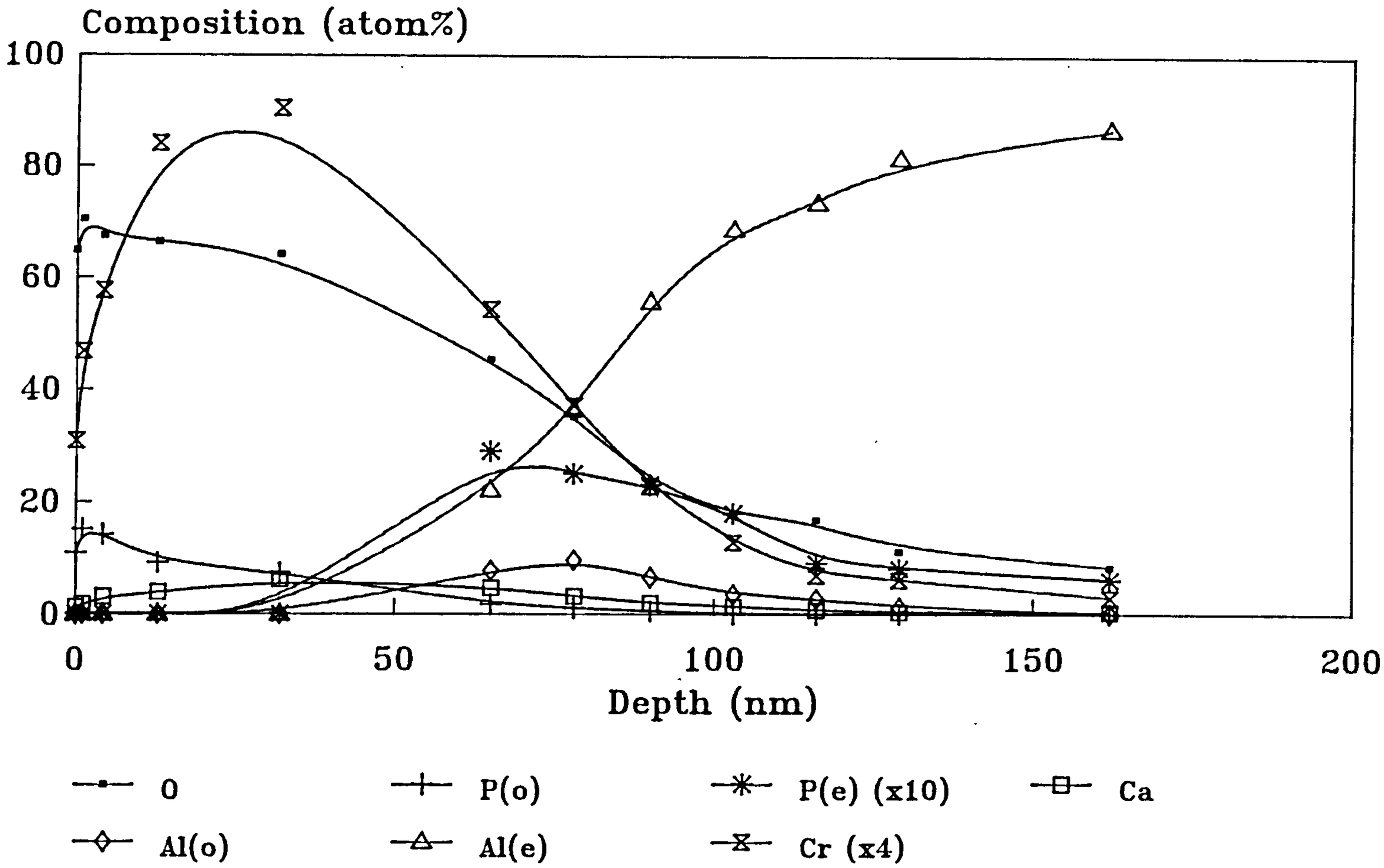

Figure 12d - AES Depth Profile Through the Film Produced Following Bonderite 705 Treatment for 60 Seconds on an Aluminium 5251 Alloy Sample.

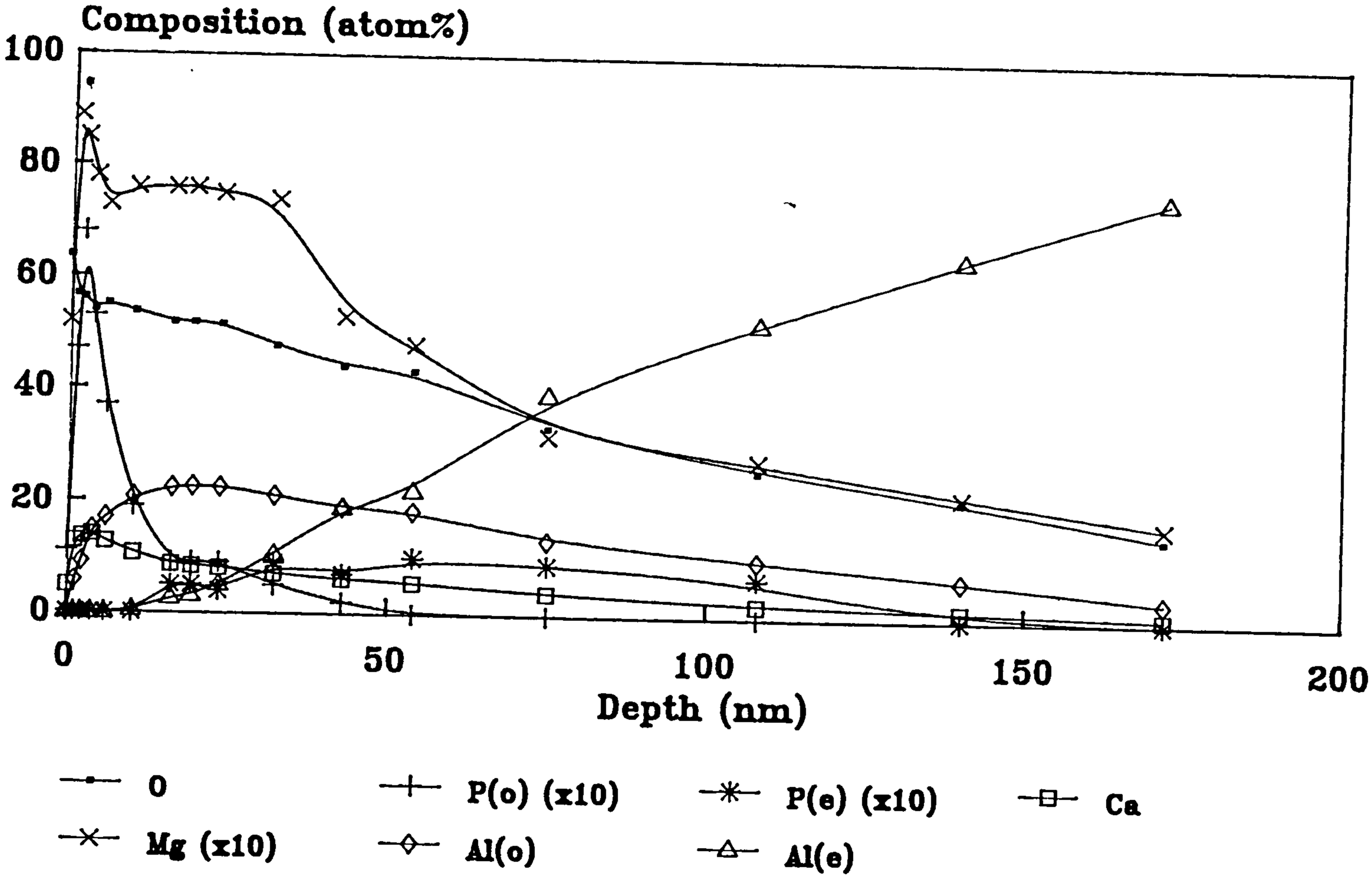

Figure 12e - AES Depth Profile Through the Oxide Layer on an Alkaline-cleaned Aluminium 5251 Alloy Sample.

Table 17 - The Thickness of a Bonderite 705 Conversion Coating Film as a Function of Treatment Time (seconds) at 22°C.

Treatment time (s)	Oxide thickness (nm)
5	12
15	22
30	34
60	86

Comparing the data presented in Figures 12a to 12e with those in Table 17 it can be concluded that in the initial stages of film formation the pre-existing oxide is rapidly removed, within a few seconds. The conversion coated film then develops, with its desirable chemistry, at a constant rate of 86 $nm.min^{-1}$ for the treatment times studied. This growth rate is comparable to that measured by DeLaet *et al* for a similar conversion coating process, albeit, at a higher growth temperature[160].

Significantly, the AES results indicate that the conversion coated layer contains phosphorous in the pentavalent oxidation state with the phosphorous L_3VV peaks at 95 and 110 eV[94]. The high oxidation state (most likely to be as a phosphate) component would be expected to inhibit hydration of the oxide during exposure to water[138,148]. There was, however, no evidence of the fluorine-rich layer at the film-substrate interface which has previously been reported[62,160]; levels of the order of a few percent were observed throughout the coatings. This layer is supposed to form by reaction with the HF in solution; clearly, the highly-soluble AlF_3 has been removed in this instance prior to film formation.

For the main durability trials a standard 5 minute Bonderite 705 treatment was carried out as recommended by Brent; further details are given in Section 2.2.2.4. The

composition of the chromate-phosphate conversion coating was consistent with that reported above. A mixed chromium and phosphorous containing oxide was again shown to be present, see Figure 13a.

The 5 minute Bonderite 705 film was shown by SEM to be ~230 nm thick and to be highly cracked; see Figures 13b to 13d. The SEM images indicate that large areas of the coating have become detached to reveal the rippled appearance of the underlying etched metal. In addition, these images reveal that there is a significant amount of surface detritus which has not been removed in the final rinse stage. Within the limited resolution of the SEM, the surface texture on the Bonderite 705 treated adherends in this study appeared to be wavy or undulating rather than porous. It is possible that, as a consequence of the extended treatment time, the expected filaments of oxide have agglomerated to form a close-packed, continuous film.

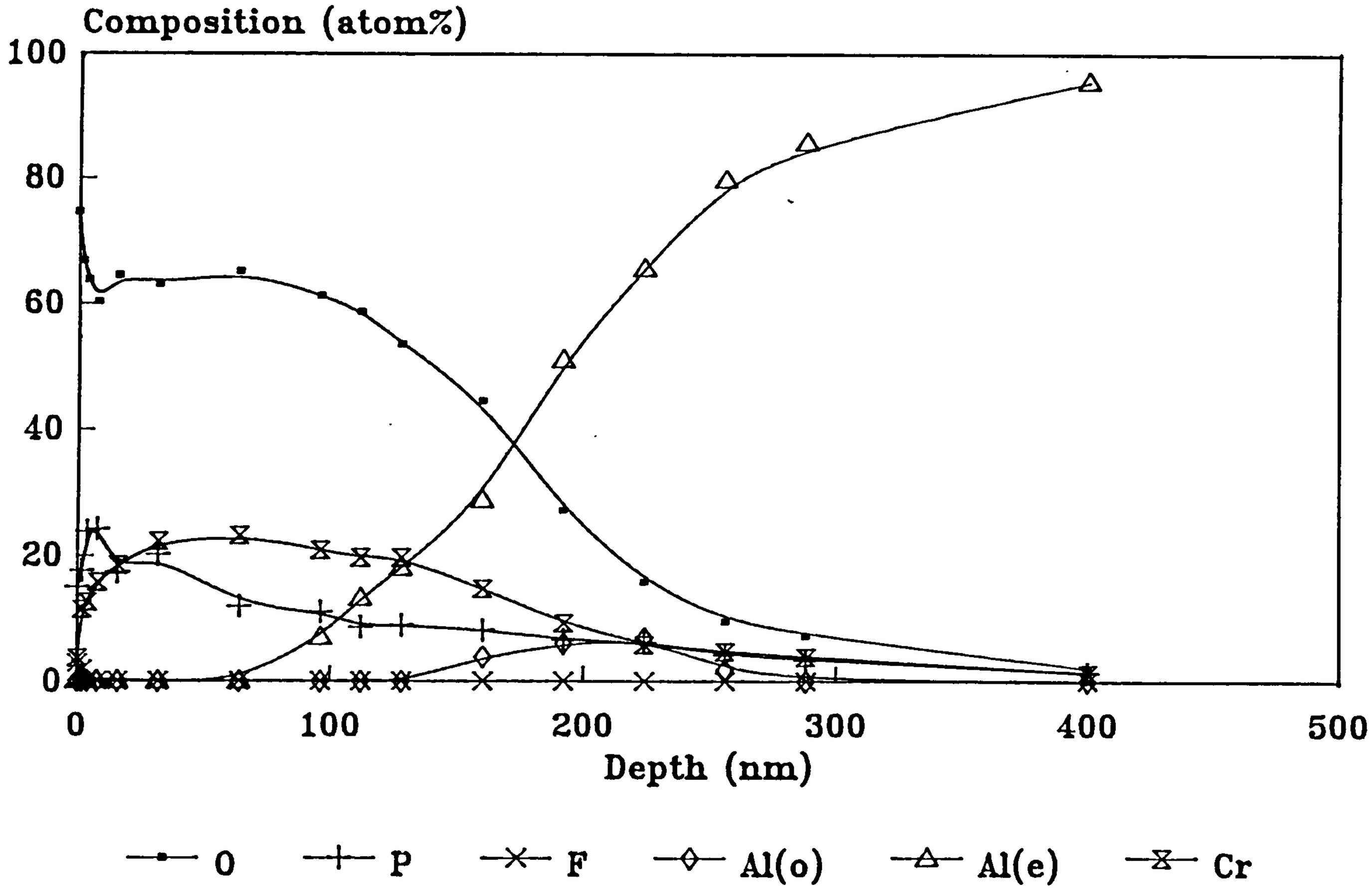

Figure 13a - AES Depth Profile Through the Film Produced Following Bonderite 705 Treatment for 5 Minutes on an Aluminium 5251 Alloy Sample.

Figure 13 - SEM Micrographs of the Aluminium 5251 Alloy Surface Following Bonderite 705 Treatment for a Period of 5 Minutes at b. x2400, c. x19000, and d. x32000 Magnification.

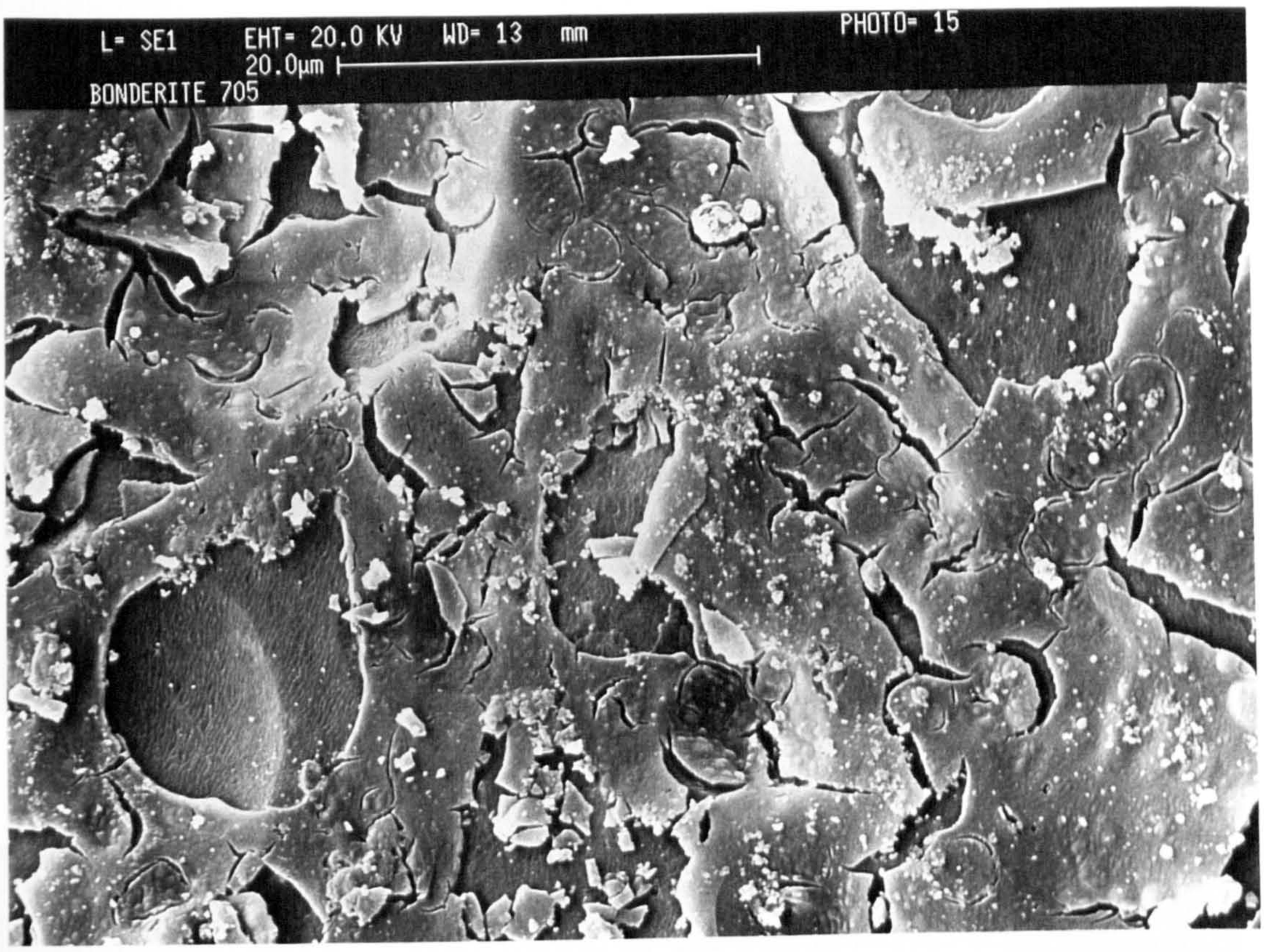

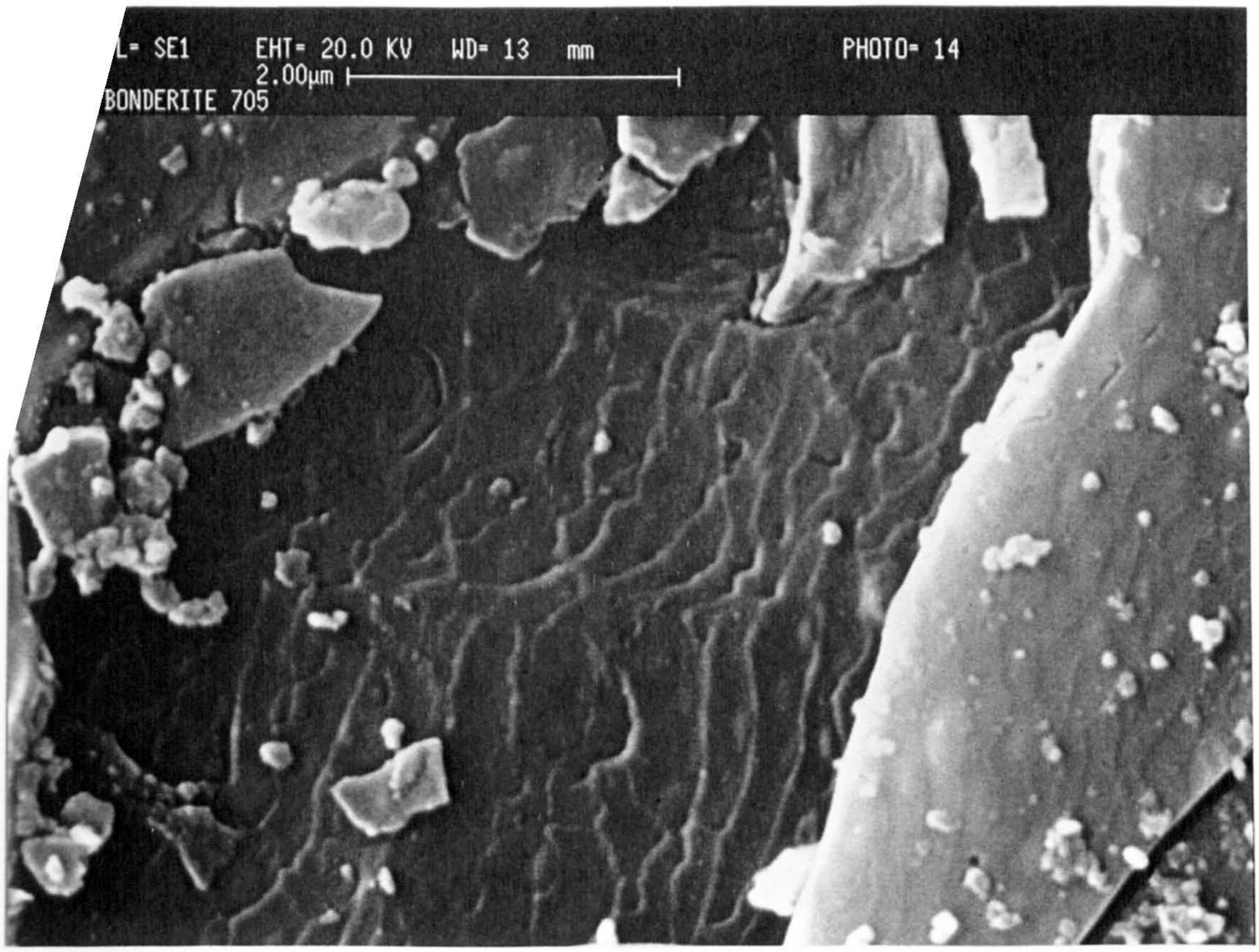
L= SE1 EHT= 20.0 KV WD= 13 mm PHOTO= 14
2.00µm
BONDERITE 705

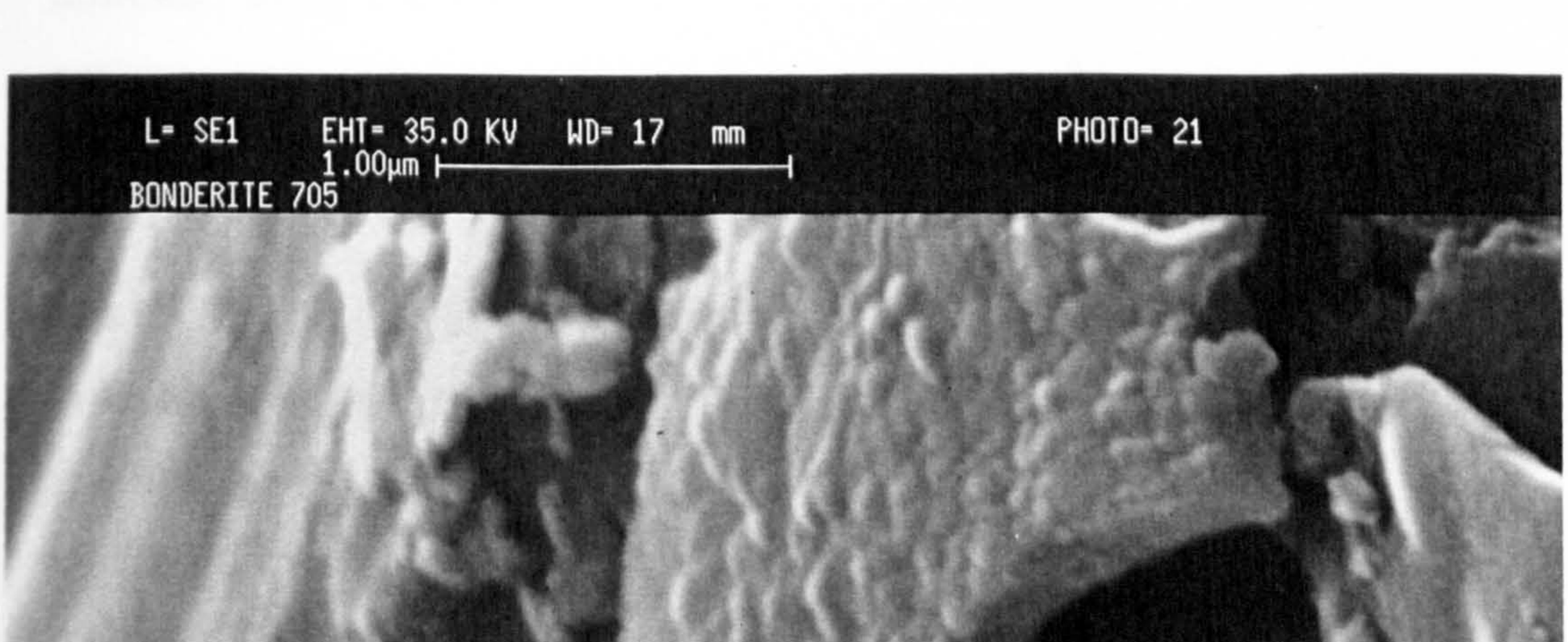
L= SE1 EHT= 35.0 KV WD= 17 mm PHOTO= 21
1.00µm
BONDERITE 705
Distance = 243 nm

3.2.4.2 Aluminium 5083 Alloy

As with the 5251 alloy, depth profiling was carried out using AES on alkaline cleaned-only and 1000 second conversion coated surfaces. The results show a thick magnesium-rich oxide on the alkaline cleaned 5083 surface similar to that seen on the 5251 alloy. Also, as with the 5251, SEM examination of a 1000 second film on 5083 alloy confirmed its thickness to be approximately 1 μm with a highly fissured coating structure similar to that illustrated in Figure 13b.

3.2.5 BONDERITE 777 CONVERSION COATED

The results of AES analysis on the Bonderite 777 treated material are given in Figure 14a. The AES results show that the Bonderite 777 conversion coating produces a much thinner film than that produced by the Bonderite 705 process, being approximately 15-20 nm thick (compared with ~230 nm). These results also indicate that there are two distinct phases within the layer, the inner 7-8 nm comprises mainly Al_2O_3 whilst the outer 7-8 nm is mainly ZrO_2. Phosphorous, calcium and fluorine are present throughout the film. The calcium could possibly derive from the rinsing stage, however, since it was not observed in either of the other conversion coatings this is, perhaps, unlikely. As with the Bonderite 705, the phosphorous present in the Bonderite 777 film was in the high oxidation state.

The SEM images, in Figures 14b and 14c, indicate that the Bonderite 777 process produces a scalloped surface texture with sharp ridges present. The size of these features is in the range 0.5 to less than 0.1μm across. The surface appears to be uniformly treated with none of the patchiness observable after the Bonderite 705 treatment. Small particles of debris were also present on this surface.

It is interesting to note that the surface texture produced by the Bonderite 777 process is comparable to that following the optimised CAE.

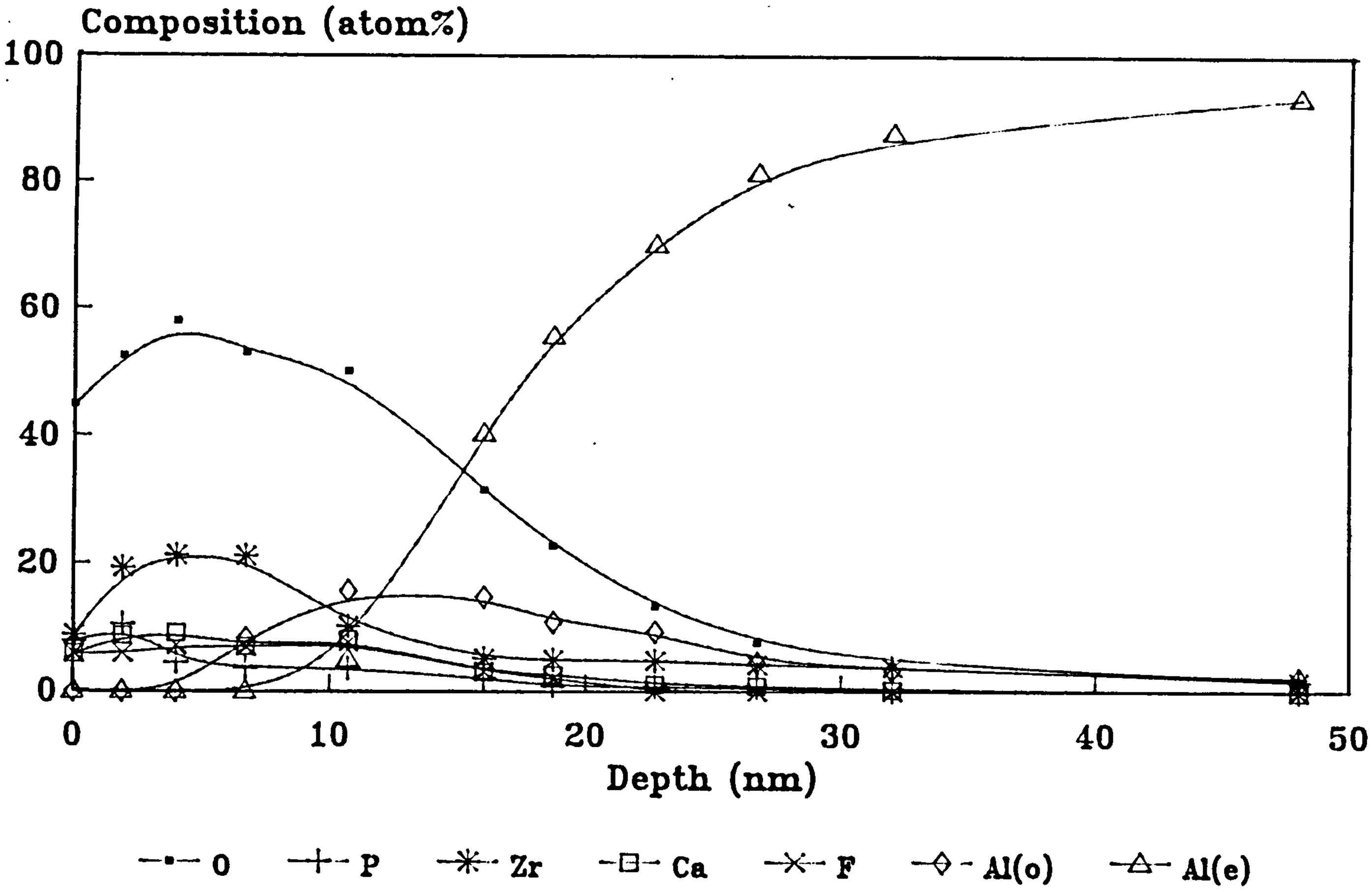

Figure 14a - AES Depth Profile Through the Film Produced Following Bonderite 777 Treatment for 5 Minutes on an Aluminium 5251 Alloy Sample.

Figure 14 - SEM Micrographs of the Aluminium 5251 Alloy Surface Following Bonderite 777 Treatment for a Period of 5 Minutes at b. x2300 and c. x19000 Magnification.

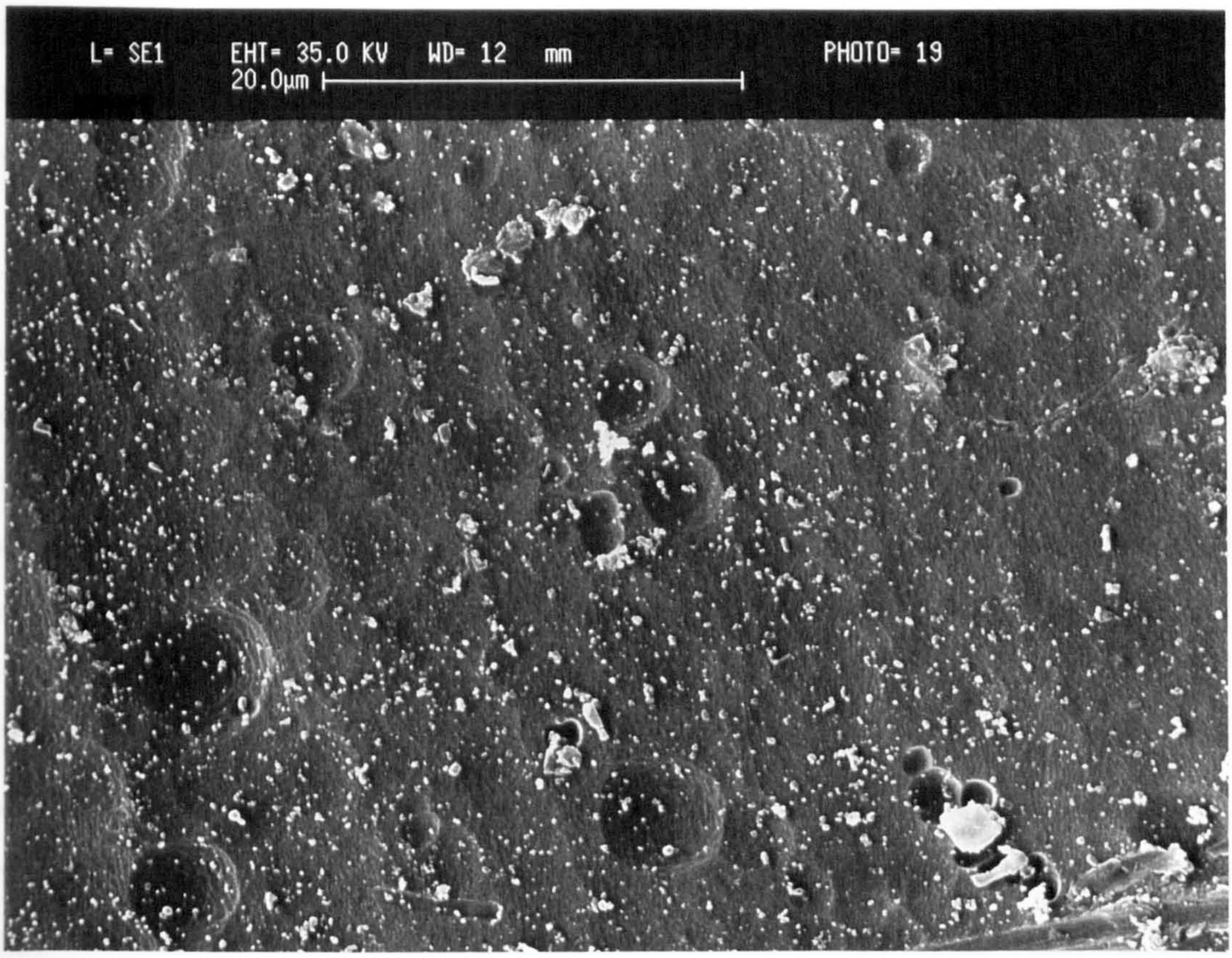

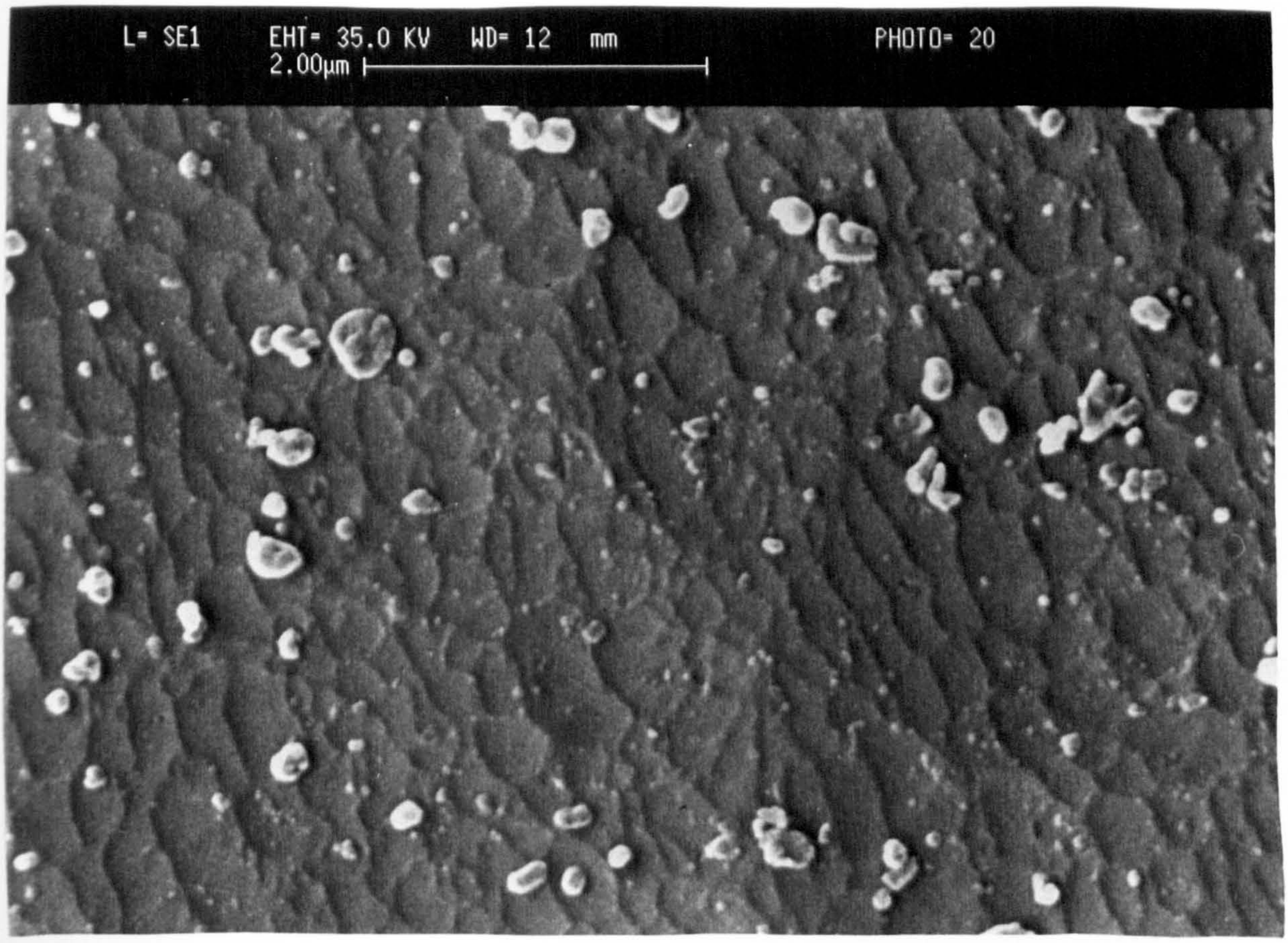

3.2.6 EP2472 CONVERSION COATED

AES results, presented in Figure 15a, indicate that the EP2472 process produces a film containing both organic and inorganic components. The inorganic phase contains phosphorous and zirconium oxides, however, no direct information is available regarding the organic component. AES analysis indicates that the EP2472 film is ~50 nm thick.

The SEM images, in Figures 15b and 15c indicate that the there is uniform coverage of the substrate by the EP2472 film. On a macro-scale the surface texture appears to contain a series of large scallops up to ~20μm in diameter. On a micro-scale the surface appears highly nodular. The nodules are approximately 0.1 μm in diameter or less. STEM cross sections, with x100000 magnification, confirm that the thickness of the film is ~50 nm, and that it is filament-like in structure; see Figure 15d.

It is not, at present, possible to determine the precise chemical and structural nature of the EP2472 film. It is possible that the film comprises either filaments of oxide with an organic coating, or, small particles of oxide each individually coated and agglomerated to form filaments or there is a complex metal-organic complex formed by the process.

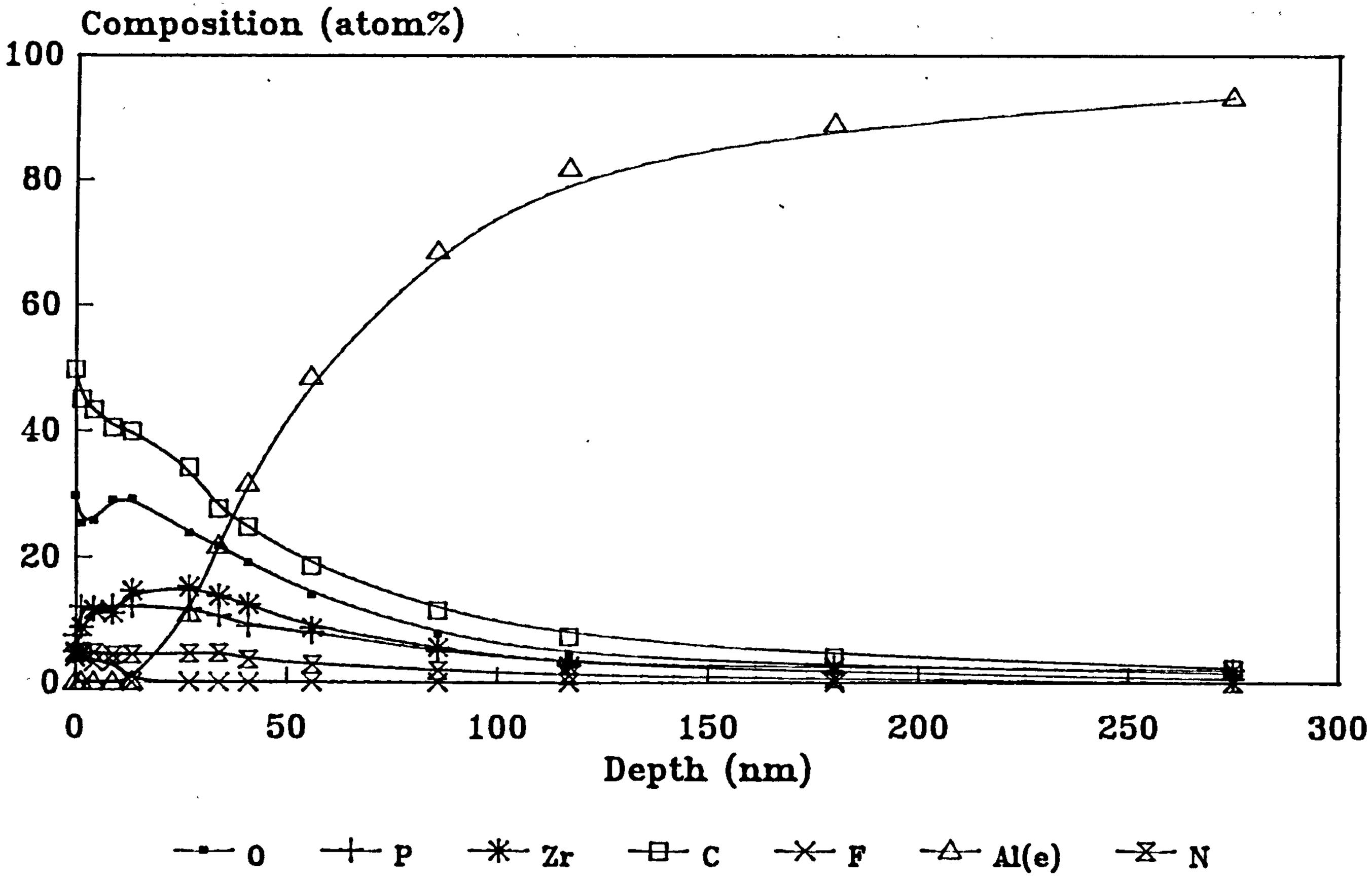

Figure 15a - AES Depth Profile Through the Film Produced Following EP2472 Treatment for 5 Minutes on an Aluminium 5251 Alloy Sample.

Figure 15 - SEM Micrographs of the Aluminium 5251 Alloy Surface Following EP2472 Treatment for a Period of 5 Minutes at b. x2400, c. x19000, and an STEM Micrograph at x100000 Magnification.

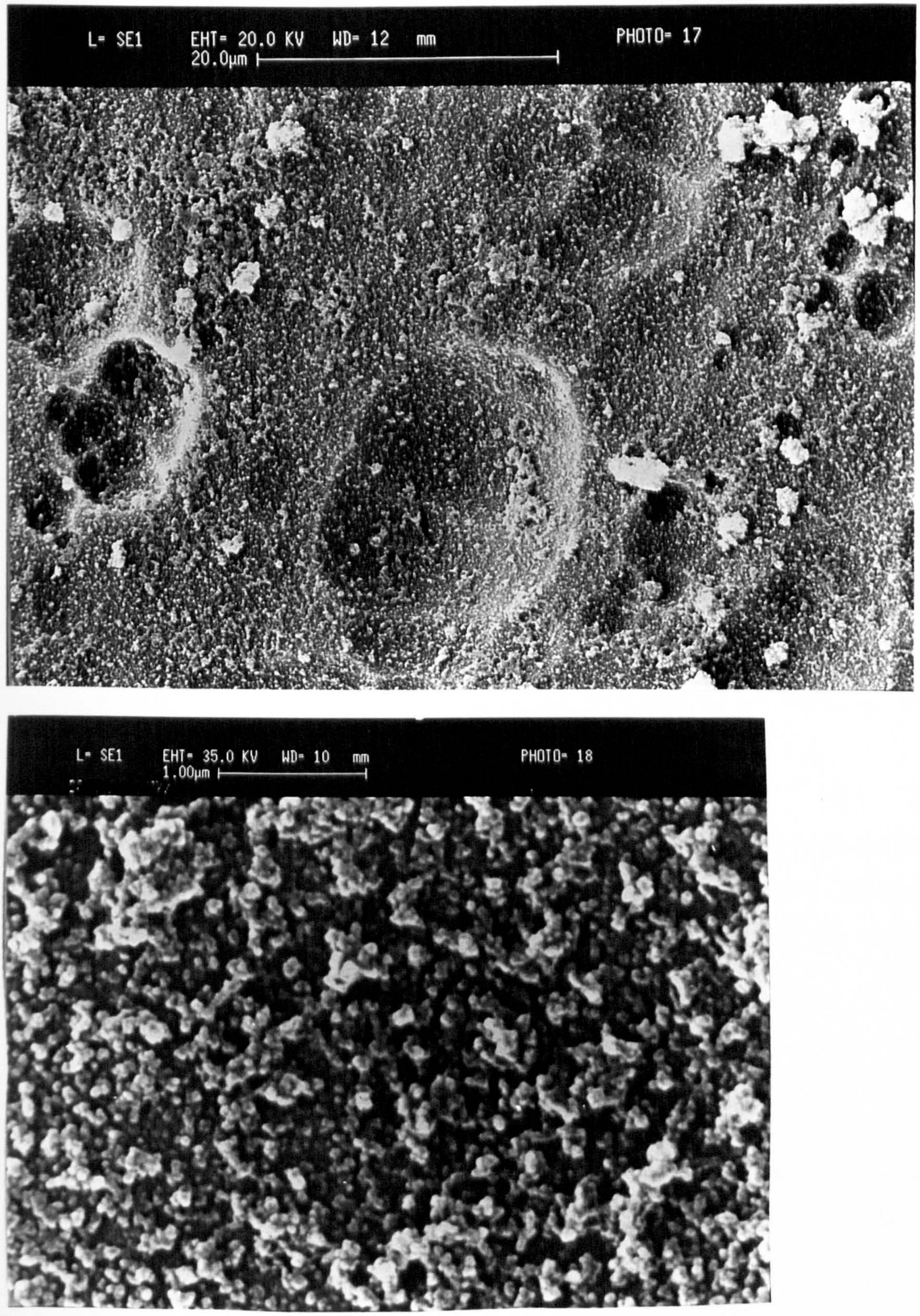

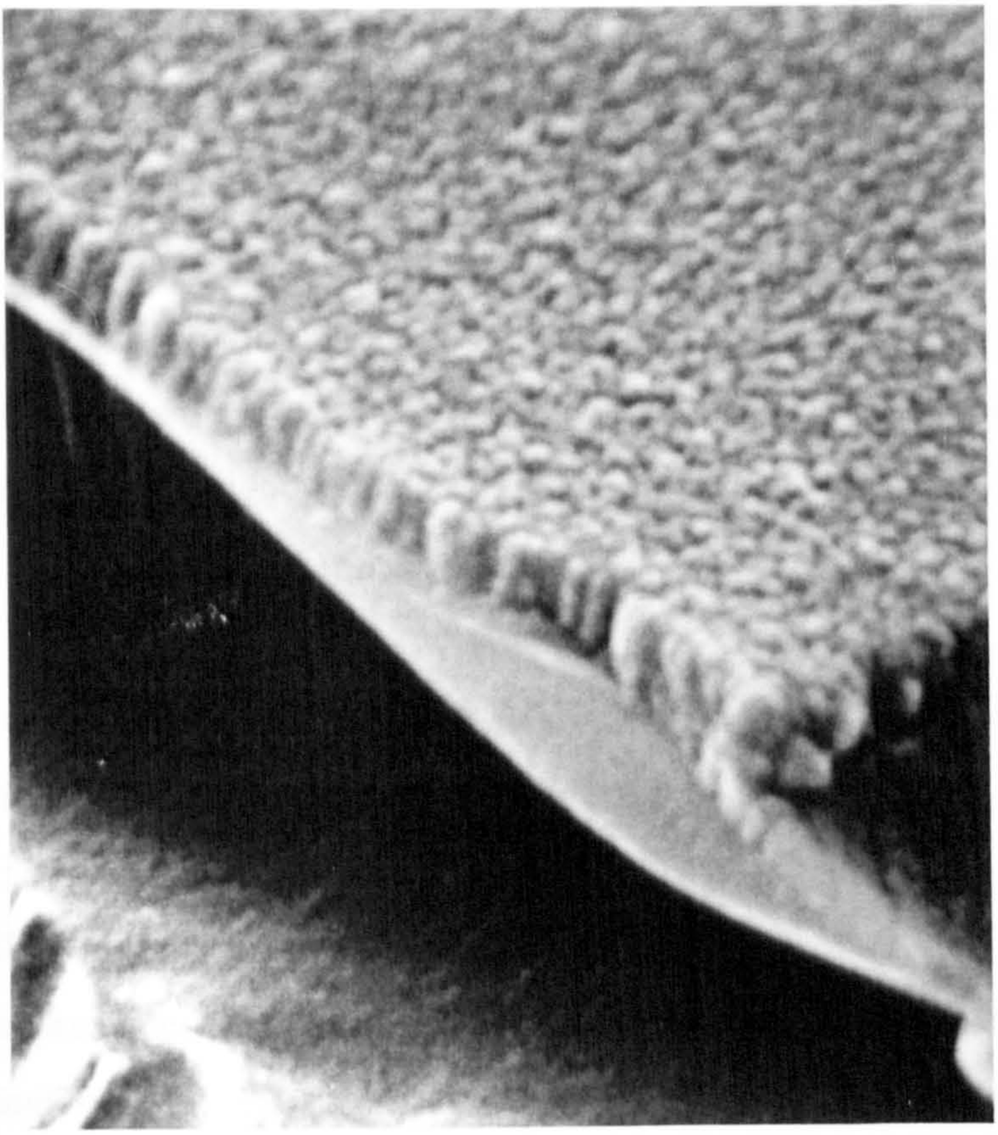

3.2.7 CHROMIC ACID ETCHED

An AES depth profile from the optimised CAE surface is presented in Figure 16a; from this, the oxide thickness can be seen to be approximately 18 nm thick. From the Al:O ratios the oxide appears to comprise mainly Al_2O_3.

Significantly, there is no magnesium enrichment in the CAE oxide layer thereby indicating that the pre-existing oxide has been removed by the etch process. There is, however, some surface organic contamination, most likely to be adsorbed adventitious material from the ambient. This is not entirely unexpected given the high surface energy of the freshly-prepared metal oxide.

The SEM images in Figures 16b and 16c illustrate the scalloped surface texture reported previously by many workers; see Section 1.4.2.2.

3.2.8 PHOSPHORIC ACID ANODISED

The AES data presented in Figure 17a are entirely consistent with those reported by Sun *et al*[94] and others. The outer few nanometres of the oxide structure being phosphate-based whilst within the bulk of the film the Al:O ratio remains constant and consistent with the presence of Al_2O_3. The oxide thickness can be estimated, from Figure 17a, to be ~ 660 nm thick.

The SEM micrographs in Figures 17b and 17c indicate that, on a macro-scale the PAA surface appears very similar to that following optimised CAE treatment. However, when viewed in cross-section, and, at a high magnification of x76000, the expected porous, columnar structure is revealed.

The thickness of the oxide layer produced in the present study can be more directly measured by SEM and estimated to be approximately 600-630 nm. This value is within the range reported by other workers and is in good agreement with the AES data reported above where the depth scale calibration was achieved using an empirically-derived etch rate as described in Section 3.2.4.1.

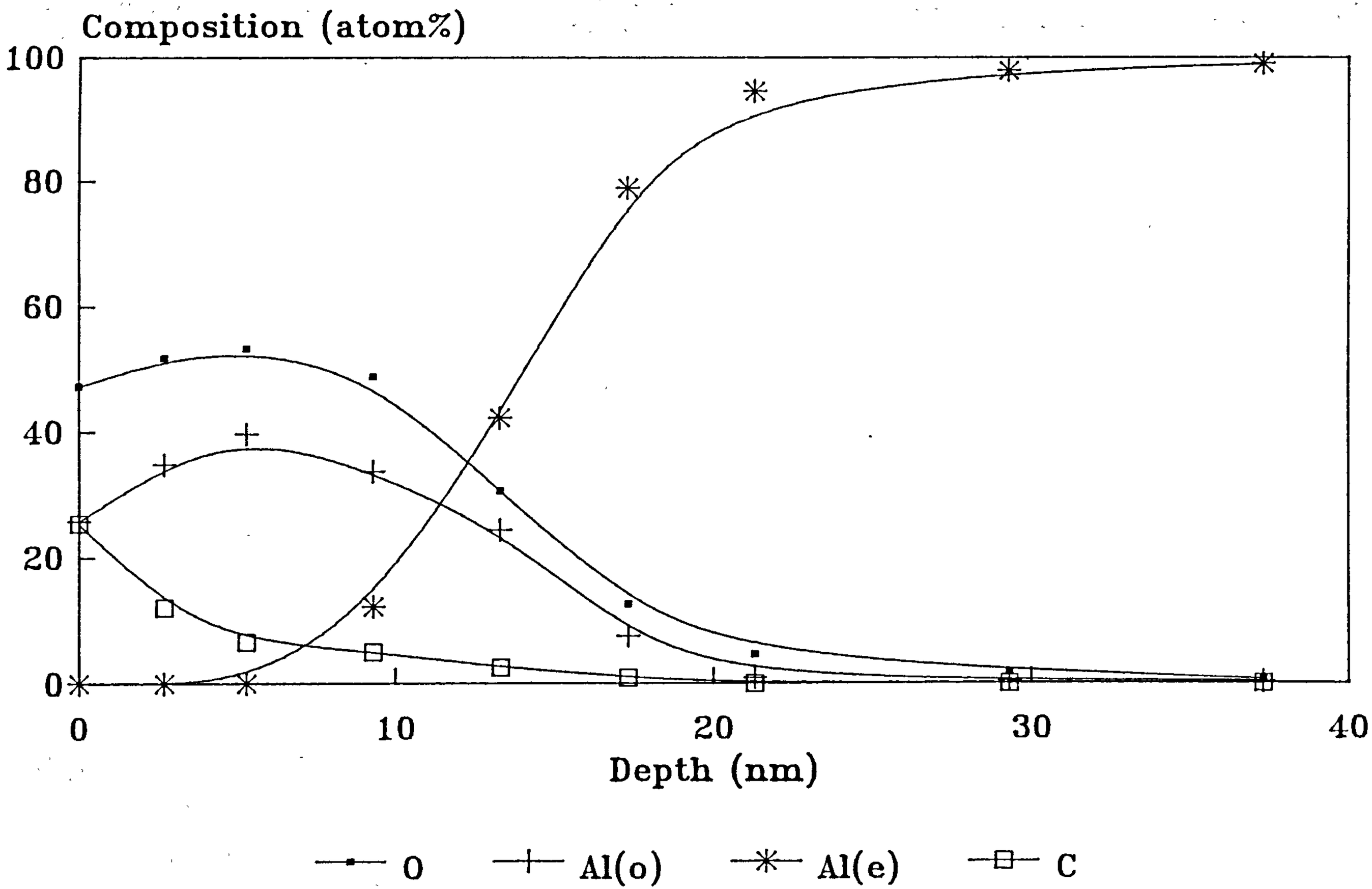

Figure 16a - AES Depth Profile Through the Oxide Layer Produced Following an Optimised CAE Treatment on an Aluminium 5251 Alloy Sample.

Figure 16 - SEM Micrographs of the Aluminium 5251 Alloy Surface Following an Optimised CAE Treatment at Magnifications of b. x2700 and c. x13000.

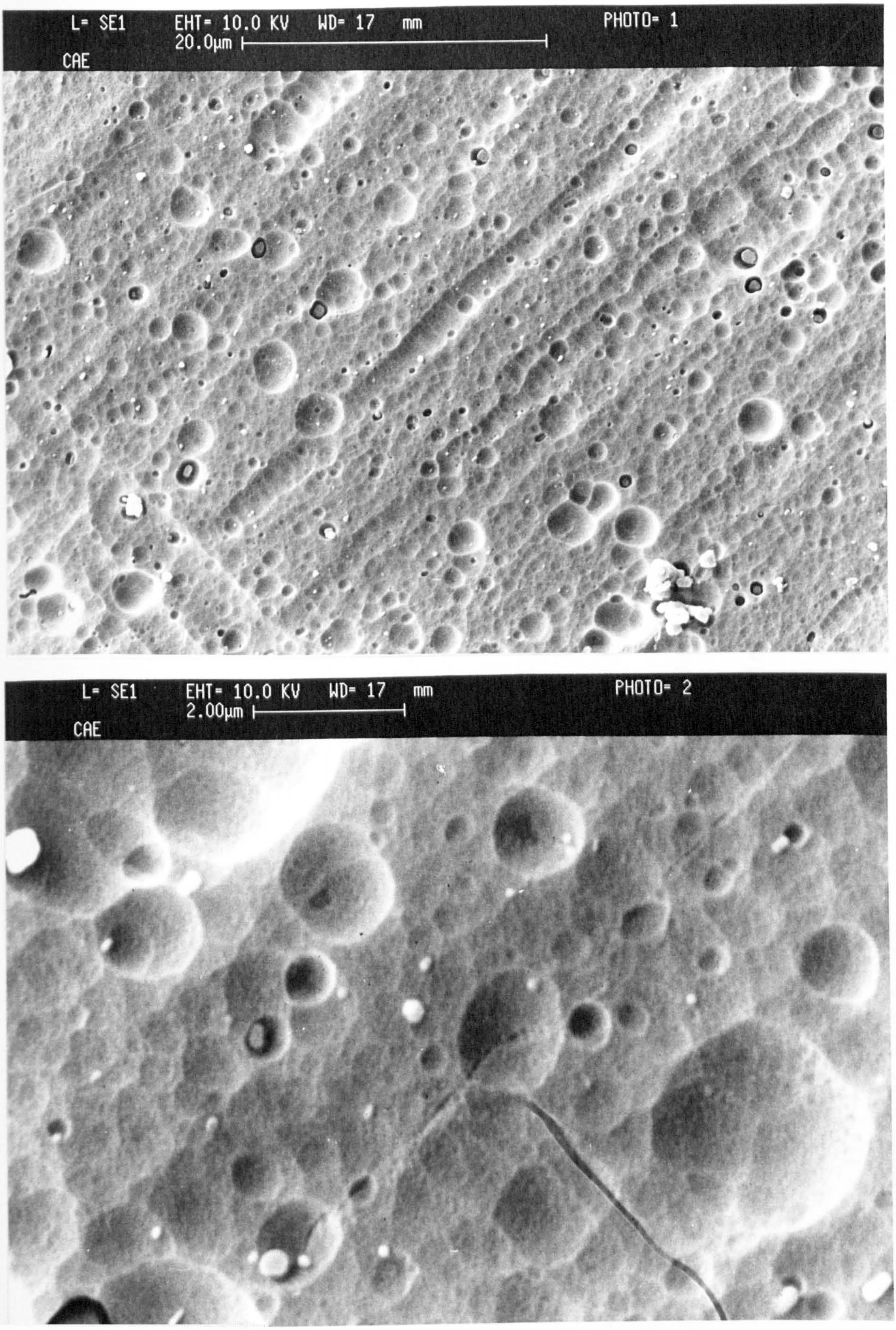

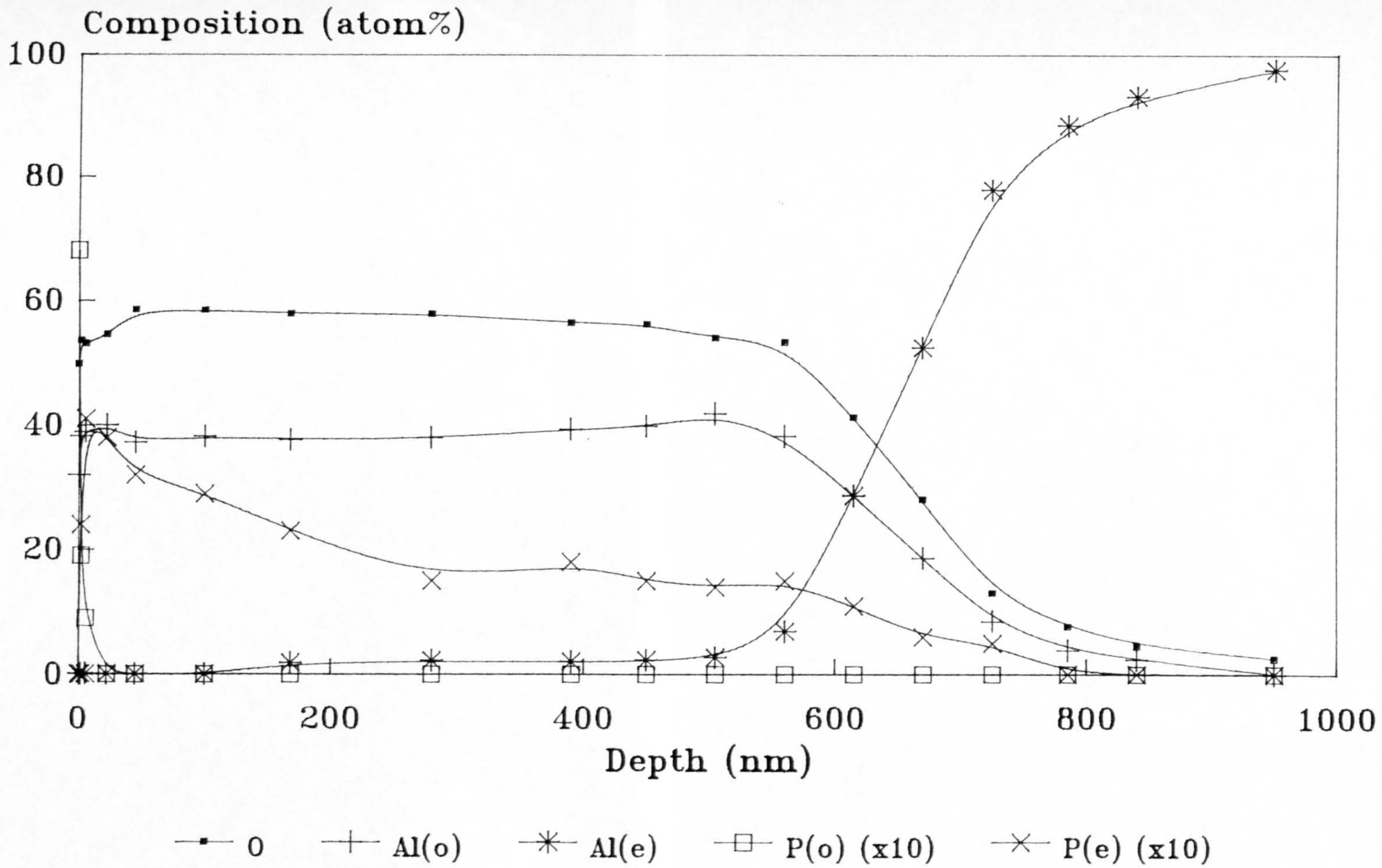

Figure 17a - AES Depth Profile Through the Oxide Layer Produced Following the Boeing BAC 5555 PAA Treatment on an Aluminium 5251 Alloy Sample.

Figure 17 - SEM Micrographs of the Aluminium 5251 Alloy Surface Following the Boeing BAC 55555 PAA Treatment at Magnifications of b. x13000 and c. x76000.

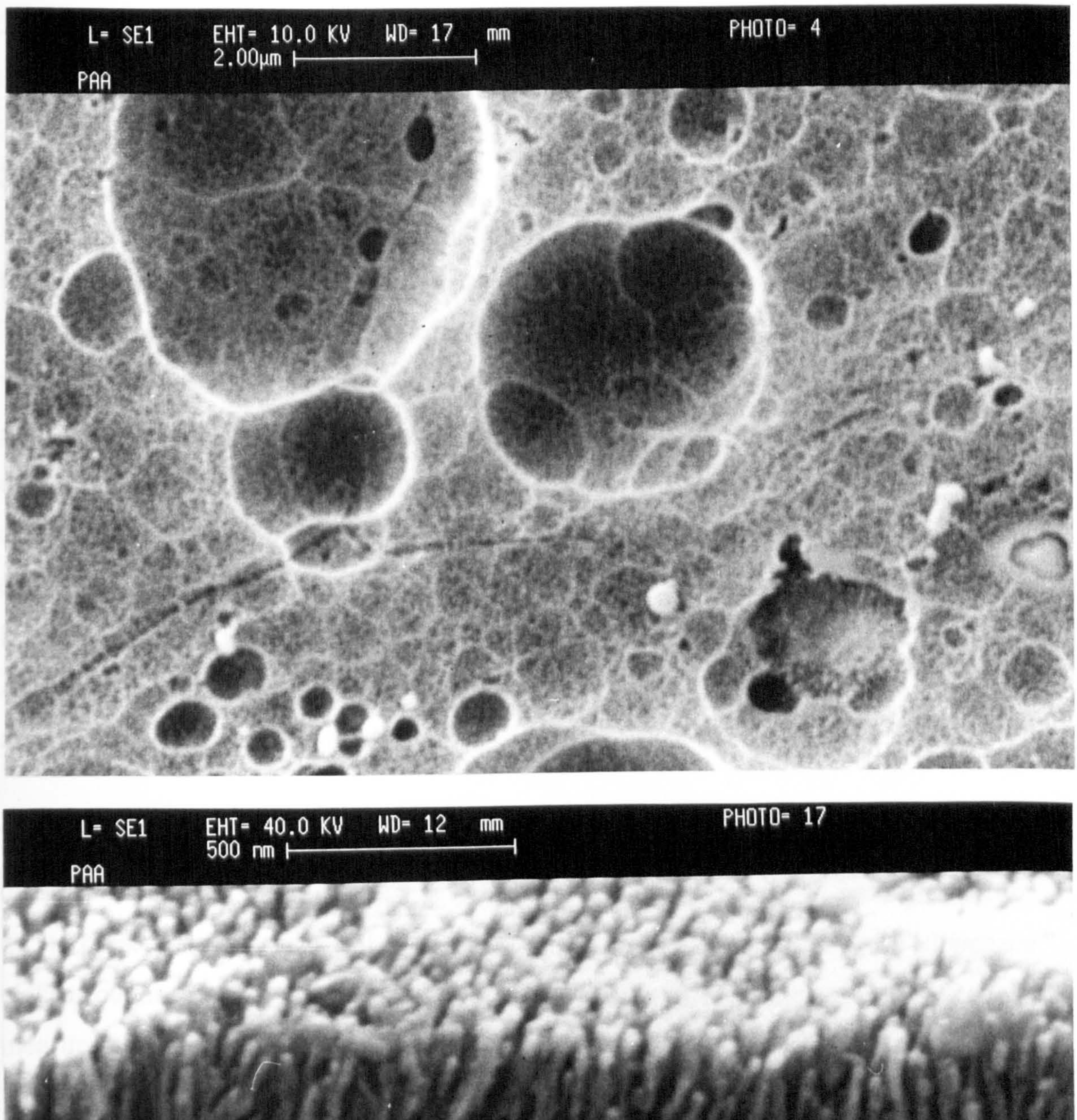

3.3 DURABILITY TRIALS

3.3.1 THE INFLUENCE OF SURFACE MACRO-ROUGHNESS ON THE DURABILITY OF ALUMINIUM ALLOY-EPOXIDE JOINTS

3.3.1.1 Introduction

As previously reported, the most effective chemical and electrochemical treatments for the adhesive bonding of aluminium impart a high degree of surface micro-roughness. The most generally accepted definition of micro-roughness is that given by Venables where he defines micro-rough surfaces as having fine structures with dimensions of 0.1 μm or less[46]. It is proposed that treatments such as chromic acid etching and chromic or phosphoric acid anodising produce small features which, when fully wetted by the applied adhesive, produce a "micro-composite interphase". This facilitates a high degree of micro-mechanical interlocking, a much increased surface area over which interactions can occur and the possibility of stress relief at the tips of the structure. As previously discussed, STEM has been used to observe features on these surfaces as small as a few nanometres.

It is not so clear what effect surface macro-roughness, where surface features have dimensions in the region of 1μm or greater, has on metal-to-metal bond durability. In the present study, surfaces have been engineered with different degrees of surface macro-roughness and the resultant effect on unstressed lap shear joints has been measured.

To produce varying degrees of macro-roughness, aluminium alloy coupons have been grit-blasted with four sizes of alumina grit. The resultant changes in surface topography have been characterised using SEM and profilometry whilst surface chemistry has been studied using AES. These data are reported in Section 3.2.2.

By correlating the data from the aforementioned surface analytical techniques with both initial joint strengths and durability results we can isolate the influence of macro-

roughness from that of surface chemistry.

The adhesive chosen was Araldite 2007 (AV119). Single lap shear joints were assembled with 20 x 10mm overlaps. Bond testing was carried out using the procedure previously described. Initial joint strengths were determined within 24 hours of assembly followed by testing of joints after exposure to DI water at 60±2°C, for time periods of 24, 85 and 211 days. The joints were exposed in the unstressed condition. Four replicate joints were tested at each stage. Failed joints were assessed by optical inspection, and, in some instances by XPS.

3.3.1.2 Bond testing

The results of bond testing are given Table 18 and Figure 18. These give initial joint strengths and residual values after various exposure times as a function of surface treatment.

Table 18 - Joint Strength Data from Initial Controls and Unstressed Exposed Joints.

Treatment	Initial joint strength (N)	Joint strengths after exposure for 24 days (N)	Joint strengths after exposure for 85 days (N)	Joint strengths after exposure for 211 days (N)
Degreased-only	3938±178	3964±434	4392±146	4365±277
320	5803±91	5556±307	4768±125	4127±330
180/220	5940±107	5545±230	4591±161	4506±103
80/120	5693±452	4979±343	4315±164	3854±194
40/60	5975±117	5368±353	3931±174	3498±200

Joint strengths are given with their standard deviations. The results presented in the above table indicate that all four sets of grit-blasted adherends provide similar initial joint strengths of ~6000 N whilst with the degreased-only adherends this value was close to 4000N.

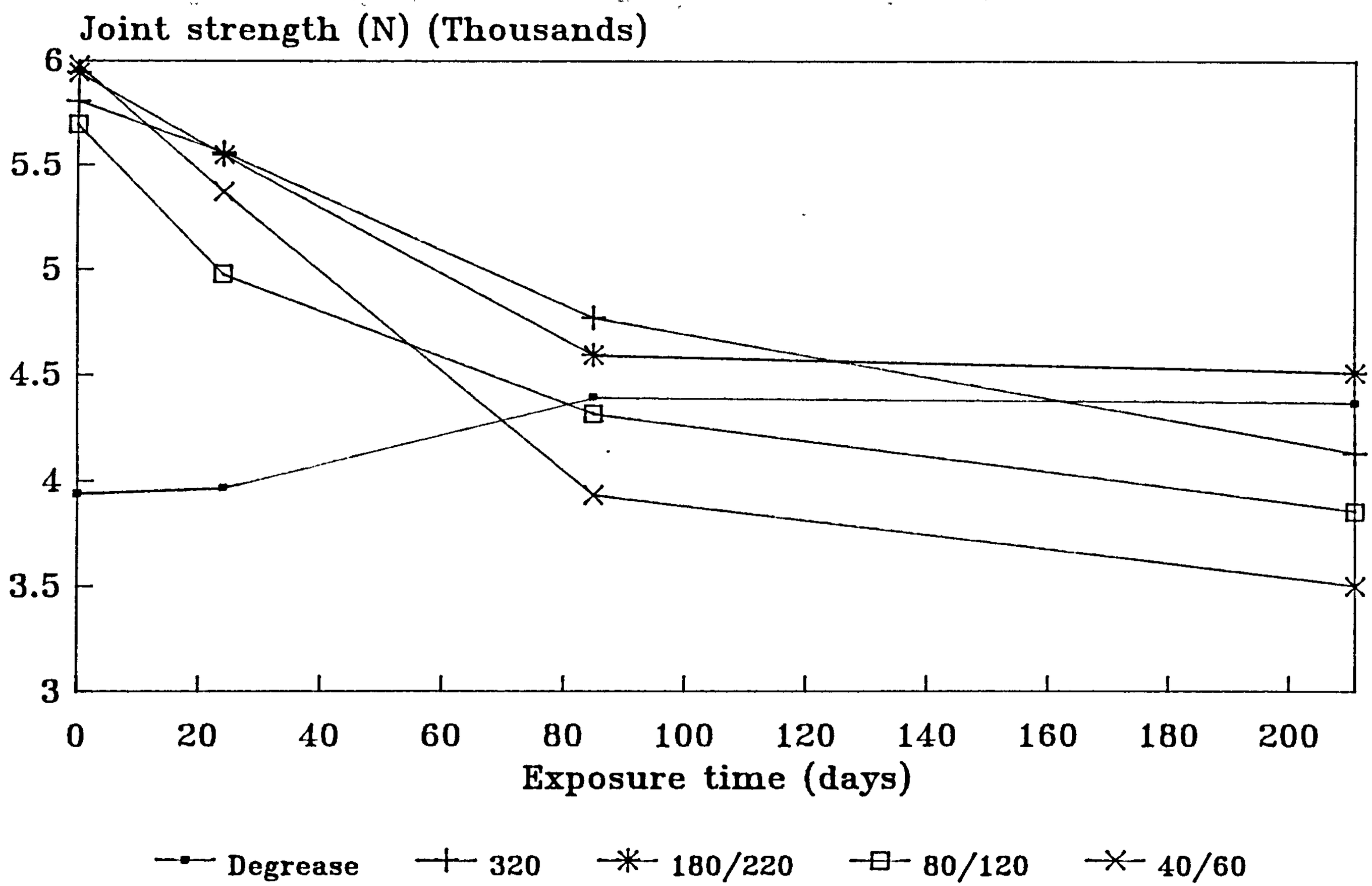

Figure 18 - To Show the Strength of Unstressed SLS Joints Exposed by Immersion in DI Water at 60°C for up to 211 Days with Four Grit-sizes.

The durability results indicate that with the degreased-only adherends there is no loss in joint strength with exposure times up to 211 days. Indeed, there is evidence of a slight increase in joint strengths with this system with exposure.

In contrast, with the grit-blasted adherends there is a gradual decrease in joint strengths after 24, 85 and 211 days exposure in all cases. Significantly, there is no major difference in either the absolute joint strengths or the percentage strength retention of joints produced with 320-grade compared with 180/220 grade grit-blasting. The percentage loss in joint strength after treatment with the coarser (40/60) grade grit is, however, significantly greater than with the finer grades.

3.3.1.3 Failure analysis

All failed joints were inspected optically using a microscope with up to x45 magnification. In addition, the degreased-only and other selected joints were investigated using XPS to accurately determine their failure modes.

Optical inspection of both initial controls and exposed degreased-only joints indicated a mixed failure mode in all cases; the majority of the joint exhibiting apparent interfacial failure but with some cohesive failure of the adhesive, and, transfer of metal onto the adhesive side of the failed joints indicating some failure within the oxide.

XPS results from degreased-only joints also indicate the same, mixed failure mode in all cases; see Table 19. Considering the ratio of the peaks from the metallic species to the carbon the amount of metal indicated on the adhesive side of the joint tested after 85 days exposure is reduced indicating that the failure mode is, if anything, becoming more cohesive within the adhesive or interfacial with time. This result is consistent with the observed slight increase in mean failure loads with exposure time.

Table 19 - XPS Data from Fracture Surfaces with Degreased-only Aluminium 5251 Alloy Joints Exposed by Immersion in DI water at 60°C.

Exposure time (days)	Fracture surface	Elements observed
0	metal side	Al, Si, C, Mg, N, O
0	adhesive side	Al, Si, C, Mg, N, O
24	metal side	Al, C, Mg, N, O, Na
24	adhesive side	Al, C, Mg, N, O, Na
85	metal side	Al, C, Mg, N, O, Na
85	adhesive side	Al, Si, C, Mg, O

Visual inspection of initial joints produced using grit-blasted adherends indicated a mixed failure mode, again, with apparent interfacial failure and cohesive failure both within the adhesive and the adherends. Significantly, little or no metal could be observed on the adhesive side of failed, exposed joints. This indicates that disruption of interfacial bonds had occurred, with the grit-blasted adherends, as a result of exposure to the DI water.

3.3.2 THE EFFECTIVENESS OF CO_2-LASER ABLATION AS A PRETREATMENT FOR BONDING ALUMINIUM AND MILD STEEL

3.3.2.1 Introduction

Laser treatment of metals offers a number of important advantages over other pretreatment methods for bonding. A number of which are detailed below:

Environmental compatibility: laser cleaning requires no solvents or chemical processing of any kind. It is a simple, single-stage process which eliminates the requirement for degreasing;

Economic cost: CO_2-lasers are amongst the cheapest and most efficient of all industrial lasers. Running costs are very low;

Versatility: although only aluminium and mild steel adherends have been used in the present work, the optical properties of most metals are similar and it is likely that most metals will respond to laser treatment. For example, TEA CO_2-laser treatment of titanium has been studied for use in dental applications[161]. In this case an improvement in shear strengths of a factor of 40 was observed with laser treated Ti-PMMA joints compared with untreated controls;

Treatment rate: the maximum cleaning rate established in the present study is approximately 0.5 $cm^{-2}.second^{-1}$ and as such is not, at present, suitable for large-scale treatment. However, this rate could be much increased by process optimisation;

Precision: the ability to focus the laser into a fine spot enables localised areas to be treated. This might be important in critical applications;

Safety: 10.6 μm radiation is absorbed by standard plastic sheet or safety glasses, it is therefore easy to protect against. If a powerful lens is used for focusing then the flux density of the beam rapidly decreases from the point of cleaning until it becomes quite

harmless.

Many of the advantages of laser treatment have previously been mentioned by Buchman *et al* in their consideration of excimer laser treatment as a surface treatment[162].

In this study, AES and SEM were used to identify physicochemical changes introduced to the degreased-only aluminium surface by CO_2-laser treatment. These results were correlated with initial joint strength data obtained using both Araldite 2001 and 2007 adhesives. Stressed durability data were obtained using the Araldite 2007.

In addition, limited studies have been carried out to investigate the effects of CO_2-laser treatment on CR1 mild steel adherends.

3.3.2.2 Aluminium 5251 alloy

Degreased then laser-treated coupons were assembled into single lap shear joints, with 10 mm overlaps, within a few seconds of treatment. Other such joints were prepared using the same adherend material and the following surface treatments: degrease-only; grit-blast with 80/120 grade grit and grit-blast plus silane (Union Carbide A187, applied from a 1% aqueous solution). To be consistent with previous studies, tensile testing was carried out using a 10 kN load cell, a crosshead speed of 2 $mm.min^{-1}$ and with an initial jaw separation of 40 mm.

A compilation of joint strength data for the various surface treatments and using the Araldite 2001 is given in Table 20.

Table 20 - Initial Strengths of Treated Aluminium 5251 Alloy Joints with Araldite 2001, a Two-part Epoxide Adhesive.

Surface treatment	Initial joint strength (N)	Percentage strength increase
Degrease-only	2910±250	-
CO_2-laser treatment	3550±117	22
Grit-blast	4270±240	47
Grit-blast plus silane	4490±410	54

The joint strength values given in Table 20 are averages of at least 4 measurements, with their accompanying standard deviations. The percentage strength increases are with respect to the degrease-only treatment. As indicated, the laser treatment provided a 22% increase in initial joint strengths over the degreased-only controls. However, the CO_2-laser did not perform as well as the grit-blast or grit-blast plus silane.

Given this result, the laser treatment was deemed worthy of further investigation. A different adhesive, Araldite 2007, was used on the same aluminium alloy. These further studies were aimed at assessing the impact of CO_2-laser treatment on stressed bond durability to more fully evaluate its usefulness for more demanding applications.

The following treatments were used in the further study: degrease-only; degrease plus laser-treatment; degrease plus grit-blast, and; Bonderite 705 conversion coating. In this experiment, the laser-treated adherends were again assembled into joints within 30 seconds of treatment.

Initial joint strengths were determined for all adherend-treatment systems with three replicate joints in all cases. Stressed durability results were obtained using the Maddison-type tubes, as previously detailed, with applied loads of 1 and 1.5 kN. The time-to-failure of three replicate joints was measured; see Section 2.2.4.

Initial SLS joint strengths from degreased-only, laser-treated, grit-blasted and conversion coated aluminium joints are presented in Table 21.

Table 21 - Initial Strengths of Treated Aluminium 5251 Alloy Joints with Araldite 2007, a Single-part Epoxide Adhesive.

Surface treatment	Initial joint strength (N) ±1 standard deviation
Degrease-only	1895±184
CO_2-laser treatment	4876±843
Grit-blast	4687±160
Conversion coating	4057±313

Table 22 presents data from stressed durability tests.

Table 22 - Mean Time-to-failure (Hours) of Stressed SLS Aluminium 5251 Alloy Joints as a Function of Surface Treatment.

Treatment	Applied load (N)	
	1000	1500
Degrease-only	19	<1
CO_2-laser treatment	532	158
Grit-blast	465	223
Conversion coating	547	367

3.3.2.3 Mild steel

Process optimisation

Having demonstrated the ability of the CO_2-laser treatment to remove organic material from the aluminium alloy surface it was decided that the degrease stage was unnecessary with the mild steel adherends.

To optimise the treatment process, in order to identify when the surfaces were fully cleaned, contact angles were determined on coupons after treatment by either 0, 1, 3, 5 , 15 or 20 laser pulses in each area. The results of this experiment are presented in Figure 19.

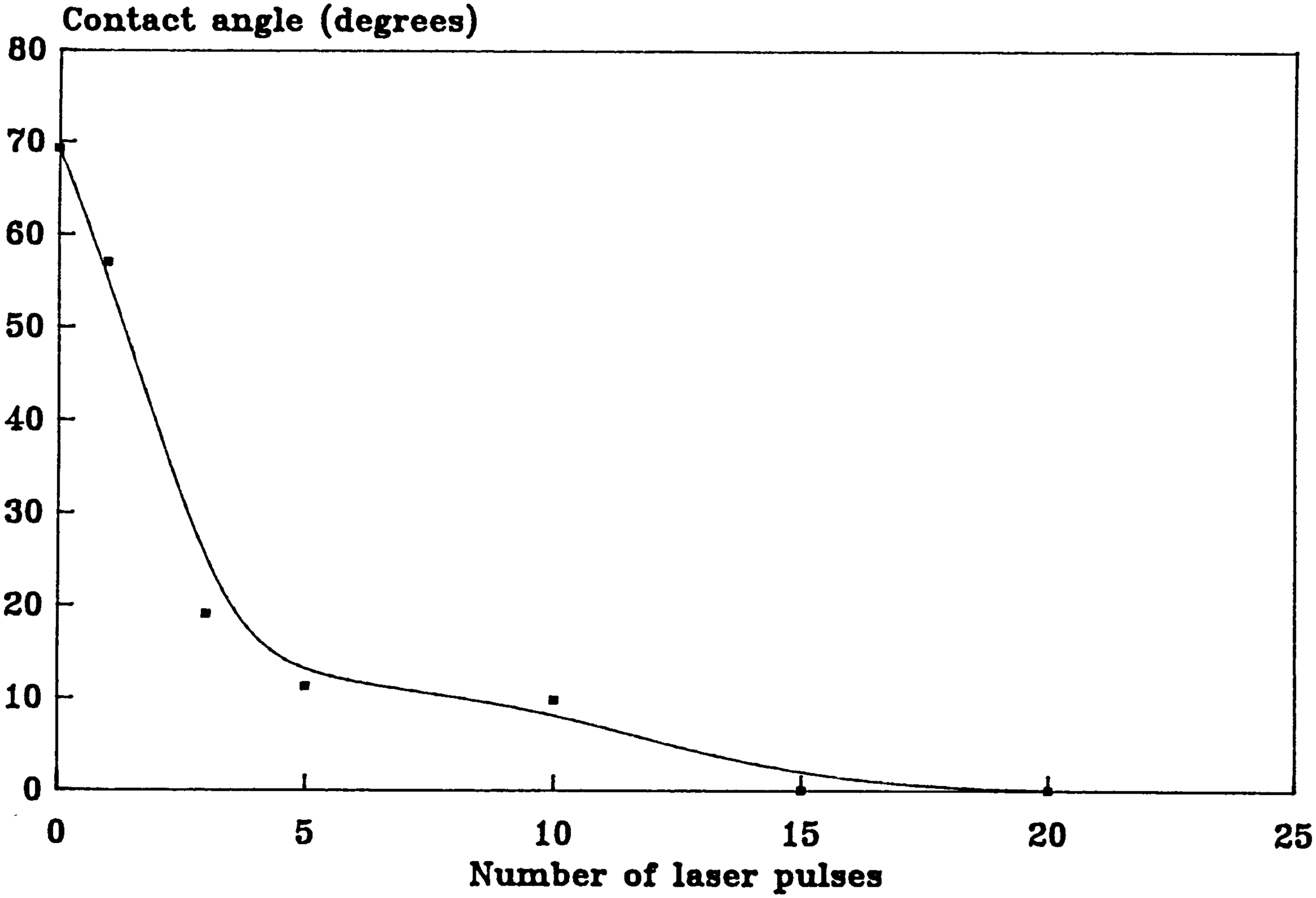

Figure 19 - To Show the Variations in Contact Angle Measurements, Using Triply-distilled Water, with the Number of CO_2-laser Pulses Incident in a Single Area; with As-received CR1 Mild Steel.

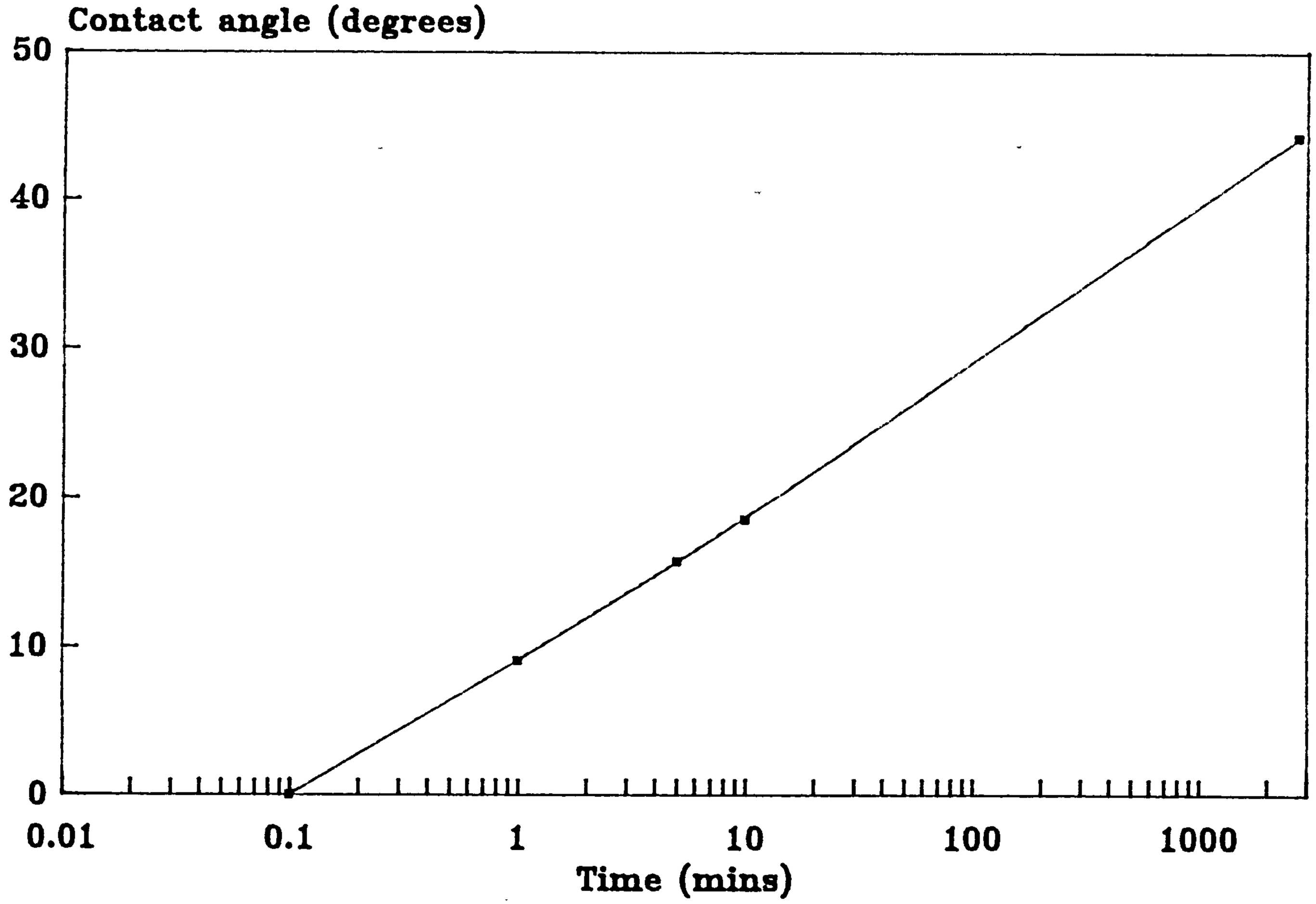

Figure 20 - To Show the Variations in Contact Angle Measurements, Using Triply-distilled Water, with the Surface Exposure Time (SET) for a Clean CR1 Mild Steel Surface.

Figure 19 illustrates that the initial contact angle on the degreased-only surface was approximately 70° with a zero degree contact angle obtained after more than 15 pulses in each area of the raster. To be certain of complete removal of any organic material it was decided to use 40 laser pulses per area as a standard treatment for mild steel throughout the subsequent work.

It was observed that, after this number of pulses, different areas within the treated region appeared to have different colouration, ranging from shiny grey to pale yellow to dark blue.

In addition, it was decided to investigate the influence of surface exposure time (SET); the delay time between treatment and bonding, on both initial joint strengths and bond durability. Contact angles were again used, in this instance, to monitor the rate of surface contamination as a function of exposure time in a laboratory environment. Contact angles were determined for surface exposure times up to 2760 minutes, as presented in Figure 20.

The results in Figure 20 indicate that, to optimise wettability, it would be beneficial to bond as soon as possible after treatment. A contact angle of approximately 10° resulted after a SET of only one minute indicating a degree of organic contamination after this limited time.

In order to determine the effect of SET upon joint strengths surfaces were bonded either immediately after treatment (SET estimated to be approximately 30 seconds) or after a SET of 2760 minutes. Initial joint strengths and unstressed durability results were determined from joints utilising these two SET values.

Bond testing

Unstressed durability results were obtained with the steel adherends and the following treatments: degrease-only; laser-treatment; degrease plus grit-blast; and degrease plus grit-blast plus silane application. Three replicates were used in all cases. For the

durability trials, the joints were immersed in DI water at 60±2°C for a period of 12 weeks.

Initial SLS joint strengths and durability results determined using a number of surface treatments are given in Table 23.

Table 23 - Initial Strengths and Unstressed Durability Data from Treated CR1 Mild Steel Joints with Araldite 2007, a Single-part Epoxide

Treatment	Initial joint strength (N) ±1 standard deviation	Joint strength (N) after exposure for 12 weeks ±1 standard deviation
Degrease-only	3552±700	3073±732
CO_2-laser treatment, SET 30s	5203±138	3920±309
CO_2-laser treatment, SET 2760m	4939±307	3979±622
Grit-blast	5240±350	5410±120
Grit-blast plus silane	5160±260	5610±270

With mild steel, the laser treatment increases initial SLS joint strengths from approximately 3500 N to approximately 5000 N; this is comparable to those produced with grit-blasted and silane treated adherends. However, the unstressed durability performance of the laser-treatment does not compare favourably with either the grit-blast or grit-blast plus silane.

3.3.3 THE INFLUENCE OF CHROMATE-PHOSPHATE CONVERSION COATING OF ALUMINUM ON THE IMPACT BEHAVIOUR OF ADHESIVE JOINTS

3.3.3.1 Introduction

In certain applications the dynamic behaviour of bonded structures may be of critical importance. For example, the collapse of vehicle bodyshells in collision must be controlled in order to minimise deceleration forces on passengers. It follows that, under impact conditions, adhesive bondlines must remain intact to facilitate energy absorption by the deformation of component panels

For this reason, the impact test method was considered appropriate to be used in the present study. This method provides a measure of the energy absorbed by an adhesive joint whether it be by the bond or in deformation of the adherends.

The impact test geometries specified in BS and ASTM methods use thick adherends and are often unrepresentative of real engineering structures. Alternative configurations, based on T-peel joints and box-sections, have sometimes been utilised[163,164]. Short diffusion path (perforated) lap joints have been used in the current work to study the effects of surface treatment conditions on impact behaviour.

The pretreatment method studied was Bonderite 705, a chromate-phosphate conversion process which was developed for high volume automotive applications.

Aluminium alloys 5251 and 5083 were chosen as adherends since these are of industrial interest; the adherends were 1.6mm thick. The selected adhesive was 3M's 7823 G, a single component, toughened epoxide, cured for 30 minutes at 180°C.

The surface treatments used are detailed in Section 2.2.2.4. On the 5251 alloy coupons, Bonderite 705 treatment times of 5, 15, 30 and 60 seconds were chosen. With the 5083 alloy, treatments were carried out for 1, 10, 100 and 1000 seconds.

Perforated lap shear coupons, measuring 35 x 20mm, were treated and bonded in the single lap shear configuration with 10 mm overlaps. The initial energy absorbtion was measured using three replicates with unexposed joints. The remaining joints were immersed in DI water at 75°C, for 7 days. Impact testing was performed on a variable mass pendulum instrument adjusted to provide an initial impact velocity of 3.5 $m.s^{-1}$.

3.3.3.2 Surface analysis

In the present work, with the 5251 alloy, the average rate of film growth for coating times up to 60 seconds was 86 $nm.min^{-1}$, as determined by AES. This value compares with 96 $nm.min^{-1}$ reported for a similar chromate-phosphate treatment[165], but which was carried out at 60°C.

SEM was used to highlight differences in surface topography prior to bonding; the oxide present after alkaline cleaning was shown to be patchy in nature ie. highly variable in thickness across the surface. Comparing surfaces after treatment times of 15 and 60 seconds; after a 60 second treatment a more complete film with fewer cracks is present when compared with the 15 second treatment. Neither of these coatings exhibit the same patchiness in the surface topography that was evident prior to conversion coating.

Examination by STEM of the oxide present after the alkaline cleaning stage and after the 60 second coating revealed comparable surface micro-roughness.

3.3.3.3 Bond testing and failure analysis

In bonding trials, using 5251 alloy adherends which had been either alkaline cleaned only or alkaline cleaned plus conversion coated (treatment times of up to 60 seconds at room temperature), cohesive failures within the adhesive were observed in all cases when inspected using optical microscopy. However, after 7 days exposure to water significant losses in energy absorption occurred. XPS was used to determine the locus of failure for both initial and exposed joints. Qualitative results from XPS analysis of

fracture surfaces are presented in Table 24.

Table 24 - XPS Results from Fracture Surfaces Exposed by Impact Testing.

Fracture surface	Treatment time (seconds)	Exposure	Elements observed
A	60	No	Si, C, N, O
B	60	No	Si, C, N, O
C	0	Yes	Si, C, P, O, Al, P, Mg
D	0	Yes	Si, C, N, O
E	60	Yes	Si, C, N, O, Al
F	60	Yes	Si, C, N, O, Al

In Table 24, A,B and C,D and E,F are the opposing fracture faces revealed after impact testing. Results from surfaces A and B confirm cohesive failure within the adhesive when impact testing unexposed joints with Si and O attributable to the Ballotini and with C and N associated with the epoxide. In contrast, analysis of fracture surfaces E and F indicate that after exposure to water some cohesive failure is observed within the coating since Al is observed on both surfaces. Analysis of surfaces C and D indicates a degree of interfacial failure in joints incorporating alkaline cleaned only surfaces, with both Al and Mg observed only on the 'metal' side of the failed joint.

Table 25 presents joint strength data obtained over the range of coating thicknesses produced on the 5083 aluminium alloy both before and after environmental exposure.

Table 25 - Effects of Bonderite 705 Conversion Coating Treatment Time on the Energy Absorption of both Initial and Exposed Joints.

Surface treatment	Energy absorption (J) Initial	Exposed
Alkaline clean only	5.0	0.3
Chromate-phosphate - 1 second	6.2	1.7
Chromate-phosphate - 10 seconds	5.6	1.6
Chromate-phosphate - 100 seconds	4.6	1.6
Chromate-phosphate - 1000 seconds	1.2	0.5

After 7 days in water at 75°C, energy absorption retention levels of approximately 30% were achieved on conversion coated surfaces, compared to the 6% value found with alkaline cleaning only. Severe bond-line porosity was observed in specimens with the thickest coating which is associated with the markedly reduced initial performance.

Of particular interest is the cohesive failure observed within the 1000 second film after exposure. SEM revealed areas where detachment of the coating had occurred. In addition, AES analysis carried out in such a region showed the film to be much thinner than that present on the unbonded sample. This is confirmation of failure within the coating after what might be regarded as an excessively long treatment time.

3.3.4 A COMPARISON OF CHROMATE-PHOSPHATE AND CHROMATE-FREE CONVERSION COATINGS FOR THE ADHESIVE BONDING OF ALUMINIUM

3.3.4.1 Introduction

Conversion coatings offer a number of advantages over other surface treatments being, simple, rapid processes which are routinely used for coil-to-coil treatment lines. Conversion coatings produce a surface film by interaction with the underlying base material[166]. The passivation and adhesion promoting properties of such films makes them suitable for a wide range of applications[167-169]. Conversion coatings are used, for example, in the automotive, aerospace and domestic appliance industries; their main application is as a prepaint treatment for metals[167-173]. In addition, their usefulness has been demonstrated for metal treatment prior to adhesive bonding; see Sections 1.4.2.2 and 3.3.3.

The most commonly-used conversion coatings are based on chromate or chromate-phosphate chemistry, for example the Bonderite 705 process previously discussed and the commonly-used Alodine 1200. However, alternative chromate-free processes are becoming more widely used because of the toxicity of the hexavalent chromium used in the conventional process. In the present study, the Bonderite 705, an established chromate-containing treatment has been compared to Bonderite 777 and EP2472, both of which are chromate-free conversion coatings. The optimised CAE and PAA have been studied for comparative purposes.

Aluminium 5251 alloy coupons were used throughout this work. After surface treatment the coupons were assembled into SLS joints with 10 mm overlaps. The adhesive used was Araldite 2007. Three replicates of all joints were prepared, with the exception of the degreased-only joints in which case up to six replicates were used.

Initial joint strengths and stressed durability data were obtained using the procedures previously described. Stressed joints were exposed by immersion in deionised water

at 60±2°C. Times-to-failure of the replicate joints were measured at applied loads in the range 0.2 to 1.5 kN. The results of the surface analytical studies on treated adherends are presented in Section 3.2.

3.3.4.2 Bond Testing

Initial joint strengths for the seven treatments under investigation are given in Table 26.

Table 26 - Initial SLS Joint Strengths as a Function of Surface Treatment

Surface treatment	Joint strength (N) (±1 std.dev.)
Degrease-only	1895±184
Grit-blast	4687±160
Bonderite 705	4057±313
Bonderite 777	5677±194
EP2472	5444±379
CAE	6485±180
PAA	6810±56

The degreased-only adherends produced, by far, the worst initial joint strengths. Of the others, the chromate-phosphate treatment, Bonderite 705, was out-performed by grit-blasting whilst the chromate-free treatments, Bonderite 777 and EP2472 out-performed all of these treatments. The optimised CAE and PAA performed best of all.

The results of stressed durability trials are given in Appendix 3 and illustrated in Figures 21a and 21b, which present the mean times-to-failure, T_f, of SLS joints as a function of applied load. In addition, Figures 21c and 21d illustrate these data in terms of LnT_f versus mean stress (MPa).

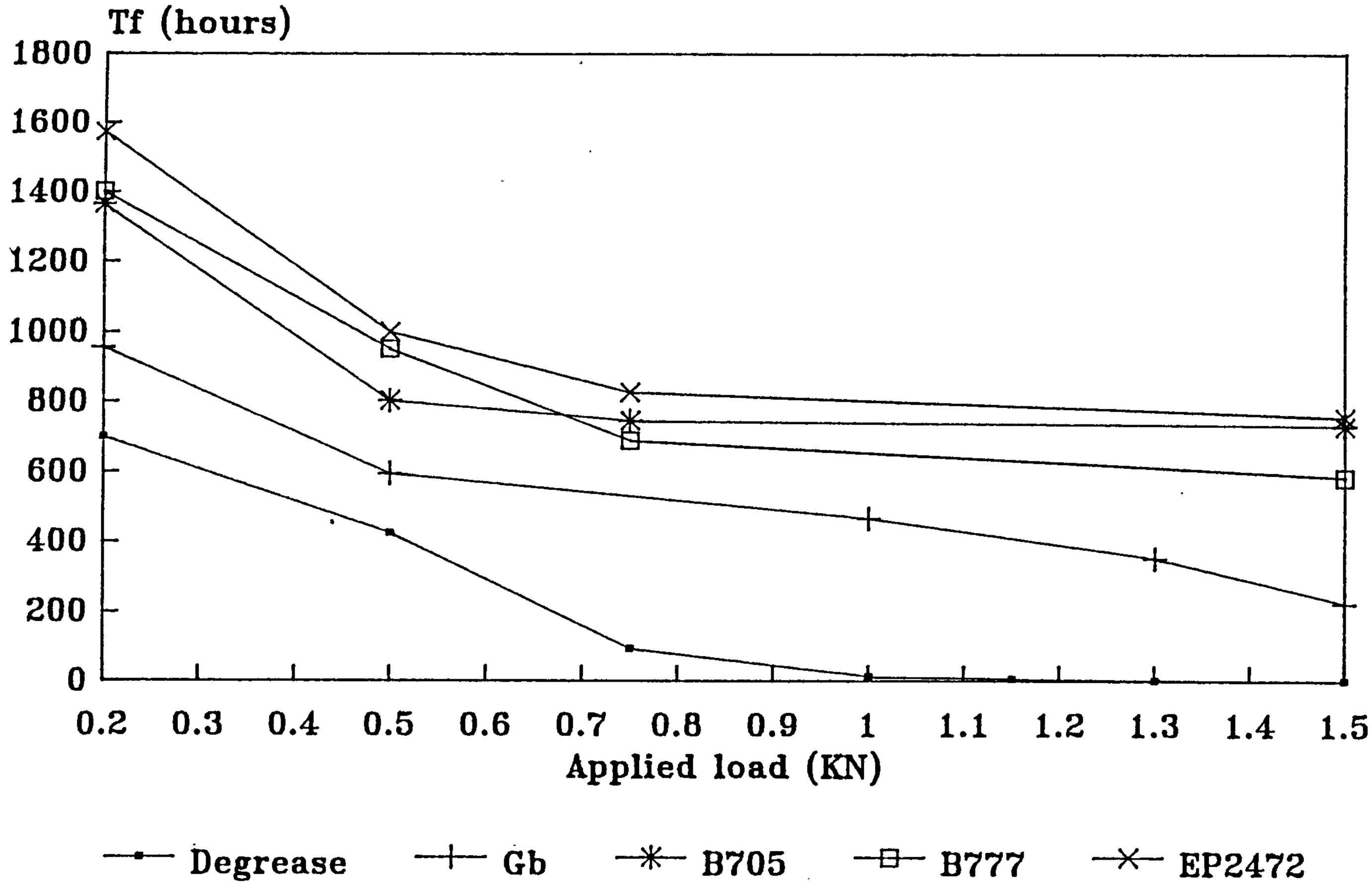

Figure 21a - To Show the Mean Times-to-failure, T_f, of SLS Joints as a Function of Applied Load with Simultaneous Immersion in DI water with the Following Treatments: Degrease-only; Grit-blast; B705; B777, and; EP2472.

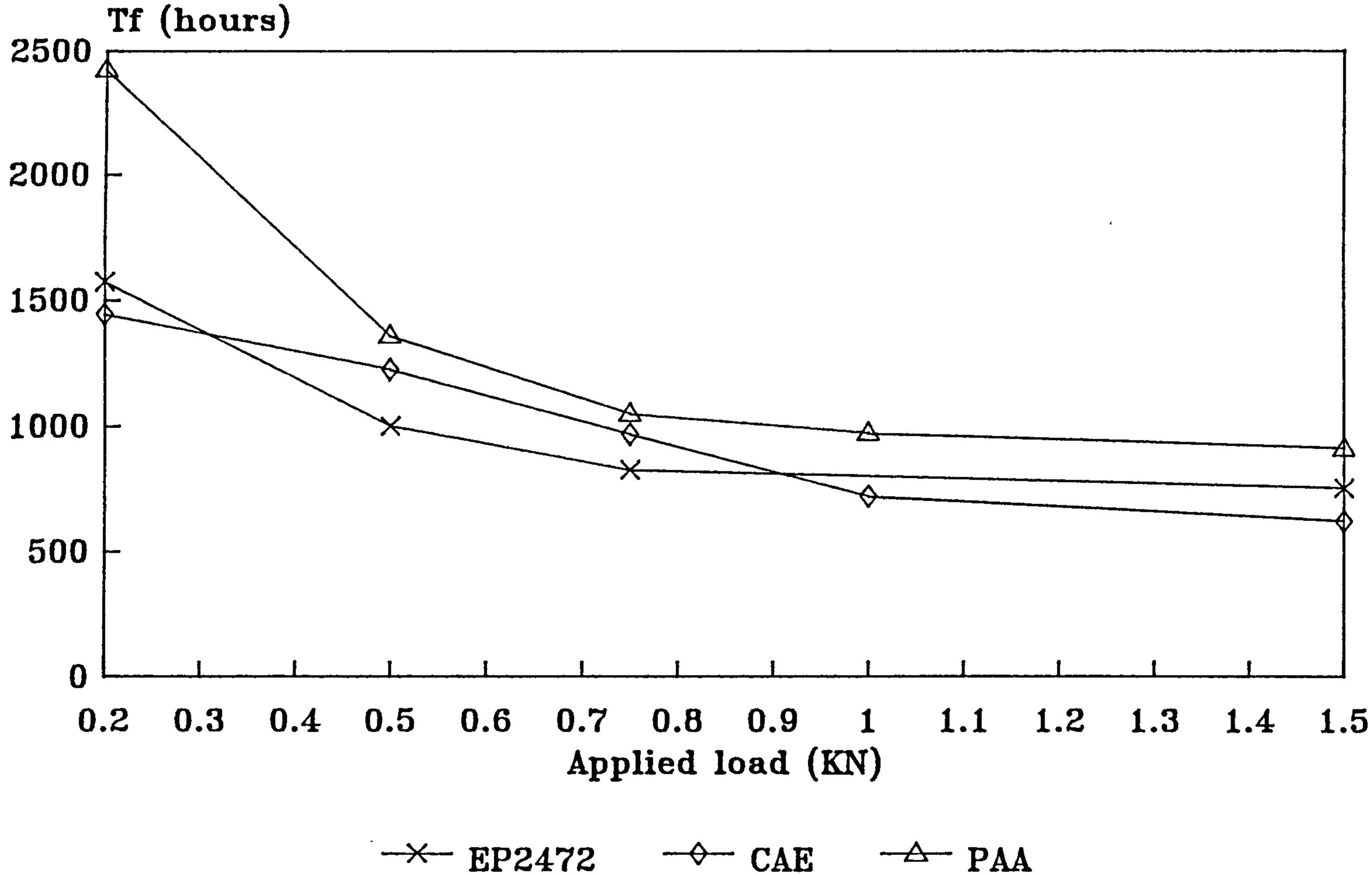

Figure 21b - To Show the Mean Times-to-failure, T_f, of SLS Joints as a Function of Applied Load with Simultaneous Immersion in DI water with the Following Treatments: EP2472; optimised CAE and PAA.

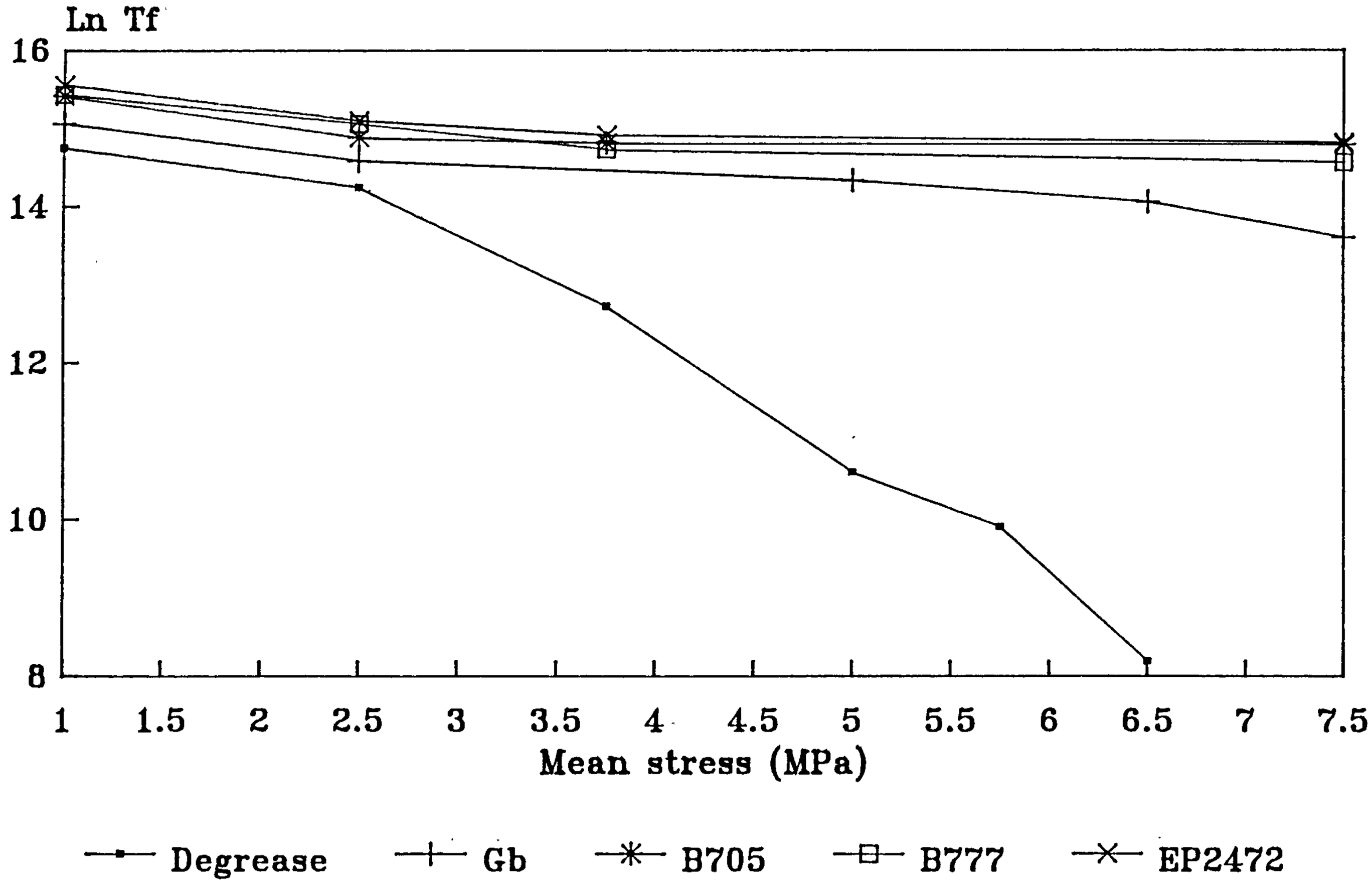

Figure 21c - To Show the Natural Logarithm of the Mean Times-to failure, Ln T_f, of SLS Joints as a Function of Mean Applied Stress with Simultaneous Immersion in DI water with the Following Treatments: Degrease-only; Grit-blast; B705; B777, and; EP2472.

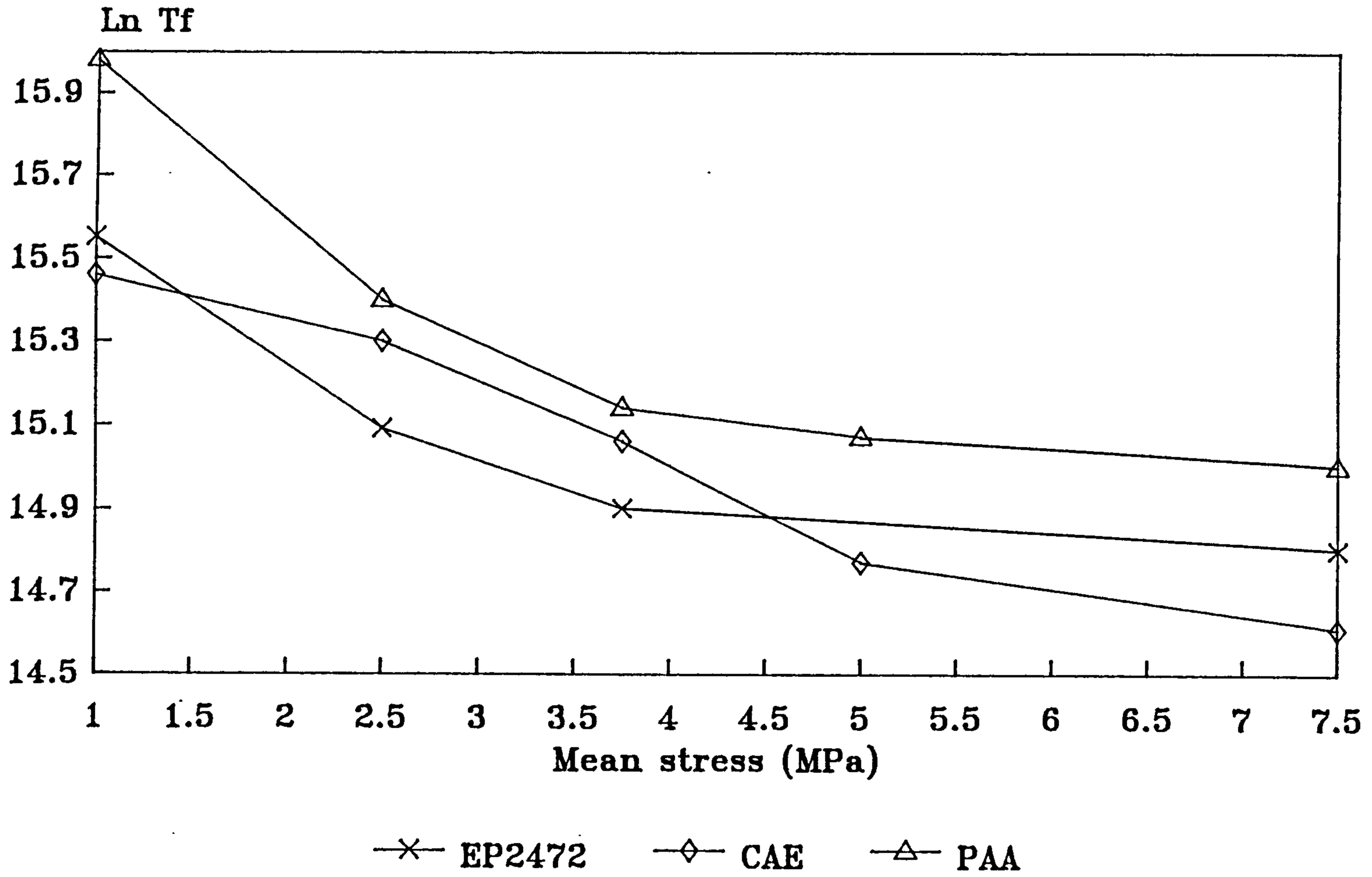

Figure 21d - To Show the Natural Logarithm of the Mean Times-to-failure, Ln T_f, of SLS Joints as a Function of Mean Applied Stress with Simultaneous Immersion in DI water with the Following Treatments: EP2472; optimised CAE and PAA.

3.3.4.3 Failure Analysis

A combination of optical inspection, AES, XPS and SEM were used to evince the failure modes from these joints. The results of these analyses are incorporated in the discussion in Section 4.2.4.

3.4 HYDRATION STUDIES OF TREATED ALUMINIUM

Studies were undertaken to establish the resistance of selected metal treatments to hydration, and, to determine the changes in surface topography caused by this effect. The topographical information being of importance in the locus of failure studies discussed in Section 4.2.4.

In all cases, bare, treated aluminium 5251 alloy coupons were immersed in DI water at 60±2°C for various periods of time to replicate the exposure conditions used in many of the durability studies in the present programme. The degreased-only, grit-blasted, conversion coated, CAE and PAA material was studied after exposure for periods of 20 and 120 hours. In addition, the EP2472 treated material was studied after similar exposure for up to 550 hours. SEM was used to study the changes in morphology as a result of surface hydration as a function of exposure time whilst XRD was used to provide hydration state information.

3.4.1 DEGREASED

Figures 22a to 22c indicate that extensive modification of the degreased-only surface results as a consequence of DI water exposure at 60°C after as little as 20 hours exposure. The "cornflake-like" structure reported by Venables *et al*[1] could be clearly observed, see Figure 22c. These smaller structures completely cover the surface. Larger needle-like structures were also present, these extend to ~5-10 μm from the surface and cover approximately 10-20% of the surface area. After 120 hours exposure the underlying, smaller features were still visible, whilst the needle-like structures increased in size; after this time, there is almost complete coverage of the surface by the larger features.

XRD data indicate that the surface altered layer produced after 120 hours exposure comprises mainly bayerite but with evidence of some gibbsite present; both are forms of aluminium hydroxide $Al(OH)_3$.

Figure 22 - SEM Micrographs to Show the Hydration Products on the Degreased-only Aluminium 5251 Alloy Surface Following Exposure to DI Water at 60°C for a. and b 20 Hours, and c.120 Hours.

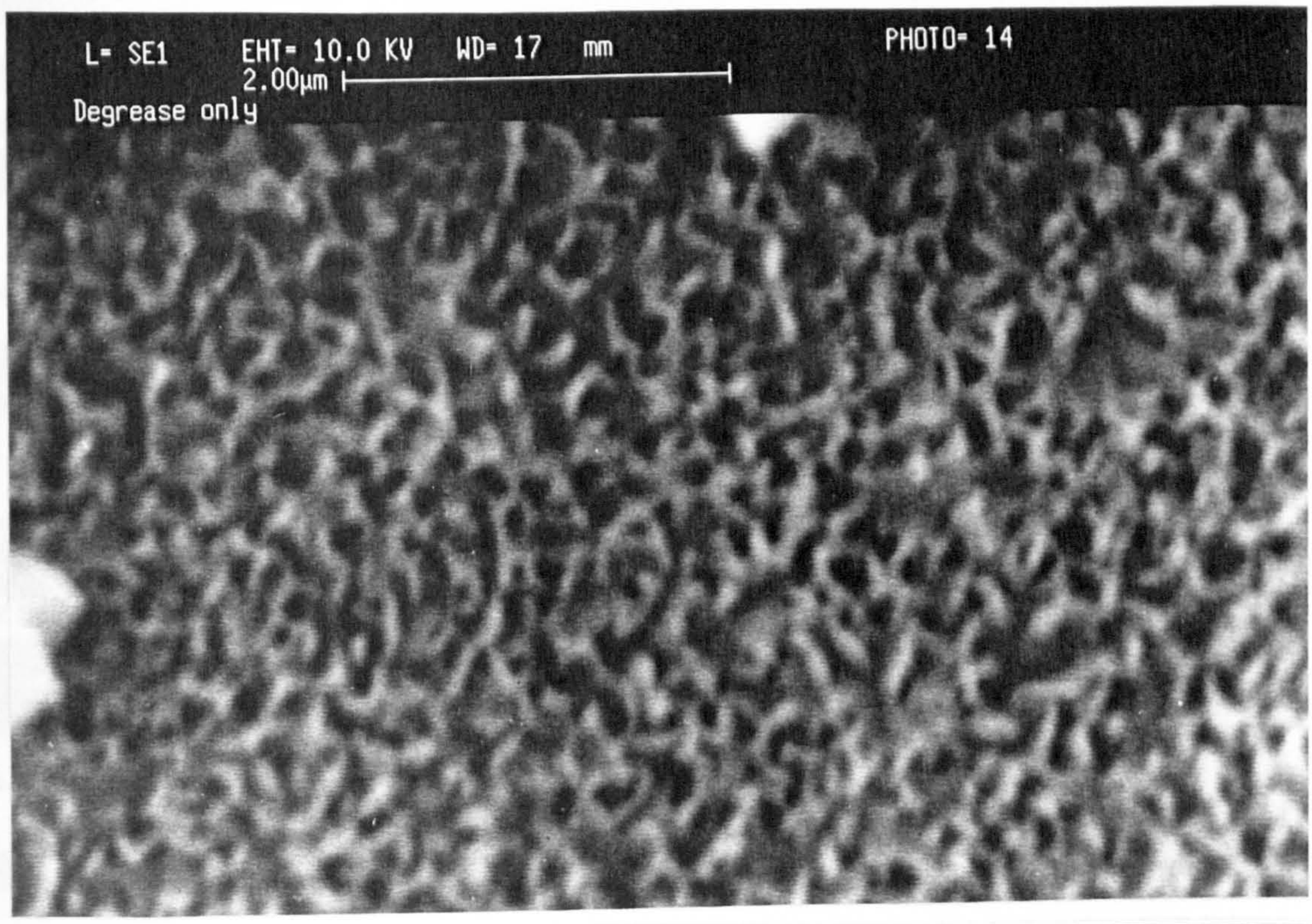

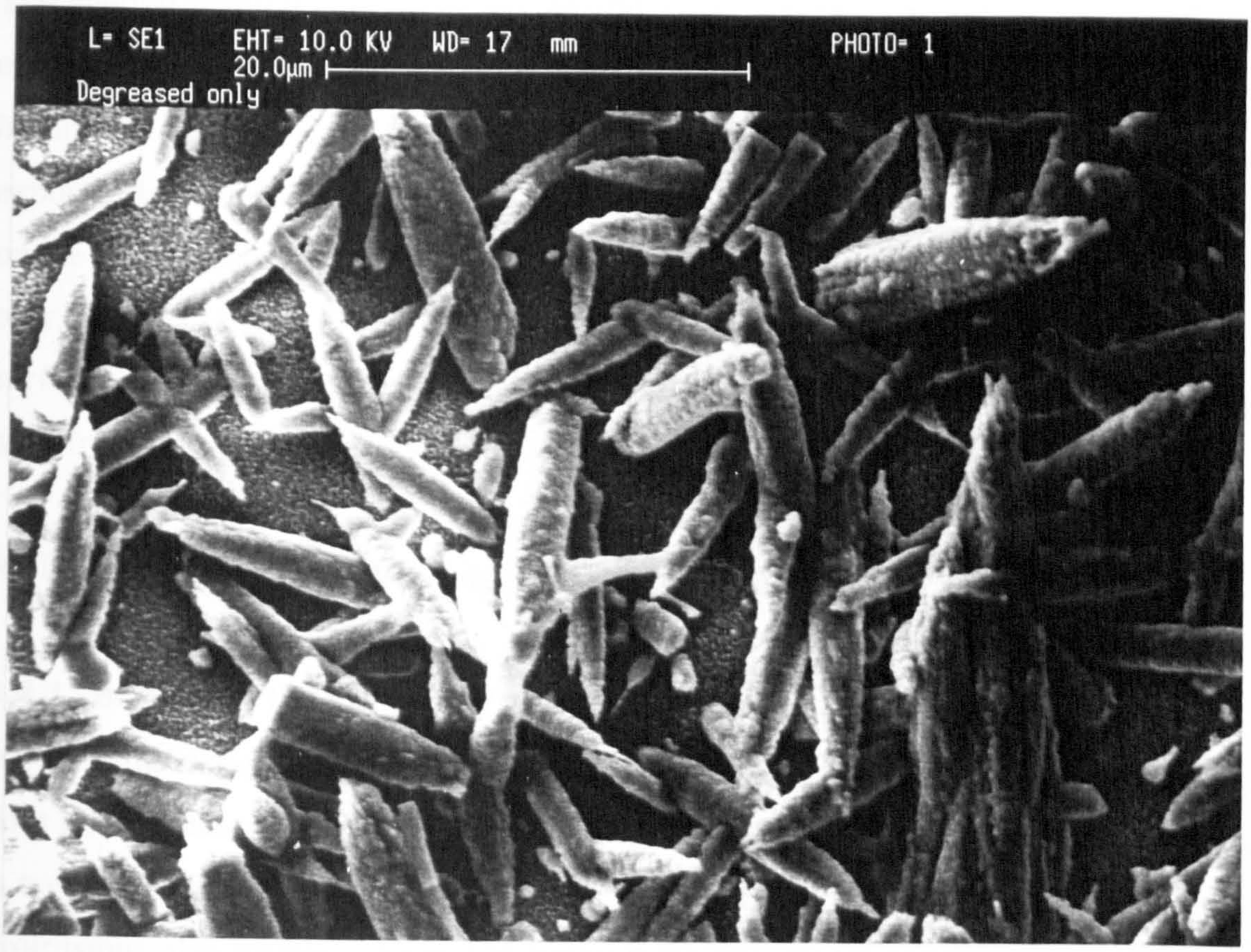
L= SE1
EHT= 10.0 KV
WD= 17 mm
PHOTO= 1
20.0µm
Degreased only

3.4.2 GRIT-BLASTED

The angular features present on the 80/120 grade grit-blasted surface were no longer evident after 20 hours exposure; see Figures 23a and 23b. Complete coverage could be observed by the same "cornflake-like" structures as were present on the similarly exposed degreased-only surfaces. Such coverage creates a smoother surface texture on the macro-scale compared with the freshly-treated material. As with the degreased-only material, large, cylindrical features could also be observed protruding from the surface. The size and packing density of these larger features increased with exposure time from 20 to 120 hours.

XRD again indicated bayerite and, probably, gibbsite present.

3.4.3 BONDERITE 705 CONVERSION COATED

At the same exposure times, the Bonderite 705 surface exhibited similar features to both the degreased-only and grit-blasted surfaces. After exposure for 20 hours there is complete coverage by the smaller-scale hydration products with larger "flake-like" protrusions also visible. After 120 hours there is complete surface coverage by the larger 10-20 μm sized features; see Figures 24a and 24b.

XRD shows the larger-sized features to be of bayerite.

3.4.4 BONDERITE 777 CONVERSION COATED

The Bonderite 777 surface was modified by exposure to DI water at 60°C in the same manner and at approximately same rate as the Bonderite 705 treatment; see Figures 25a and 25b.

3.4.5 EP2472 CONVERSION COATED

The scallops and nodular features on the EP2472 surface were largely unaltered after exposure for up to 120 hours, see Figure 26a. Only after exposure for an extended period of 550 hours could evidence of hydration be observed in the SEM images; see Figure 26b.

Figure 23 - SEM Micrographs to Show the Hydration Products on the Grit-blasted Aluminium 5251 Alloy Surface Following Exposure to DI Water at 60°C for a. 20 Hours, and b. 120 Hours.

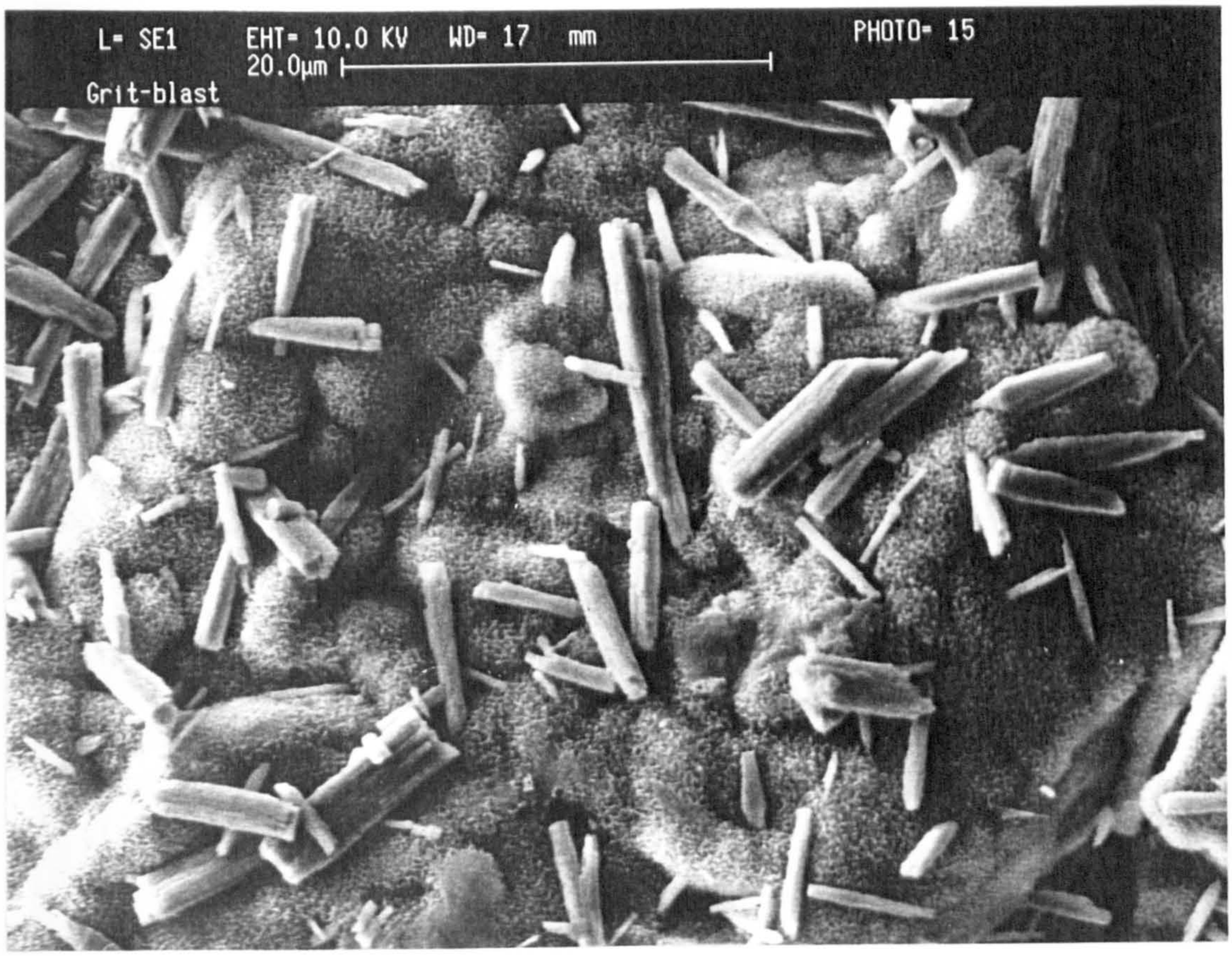

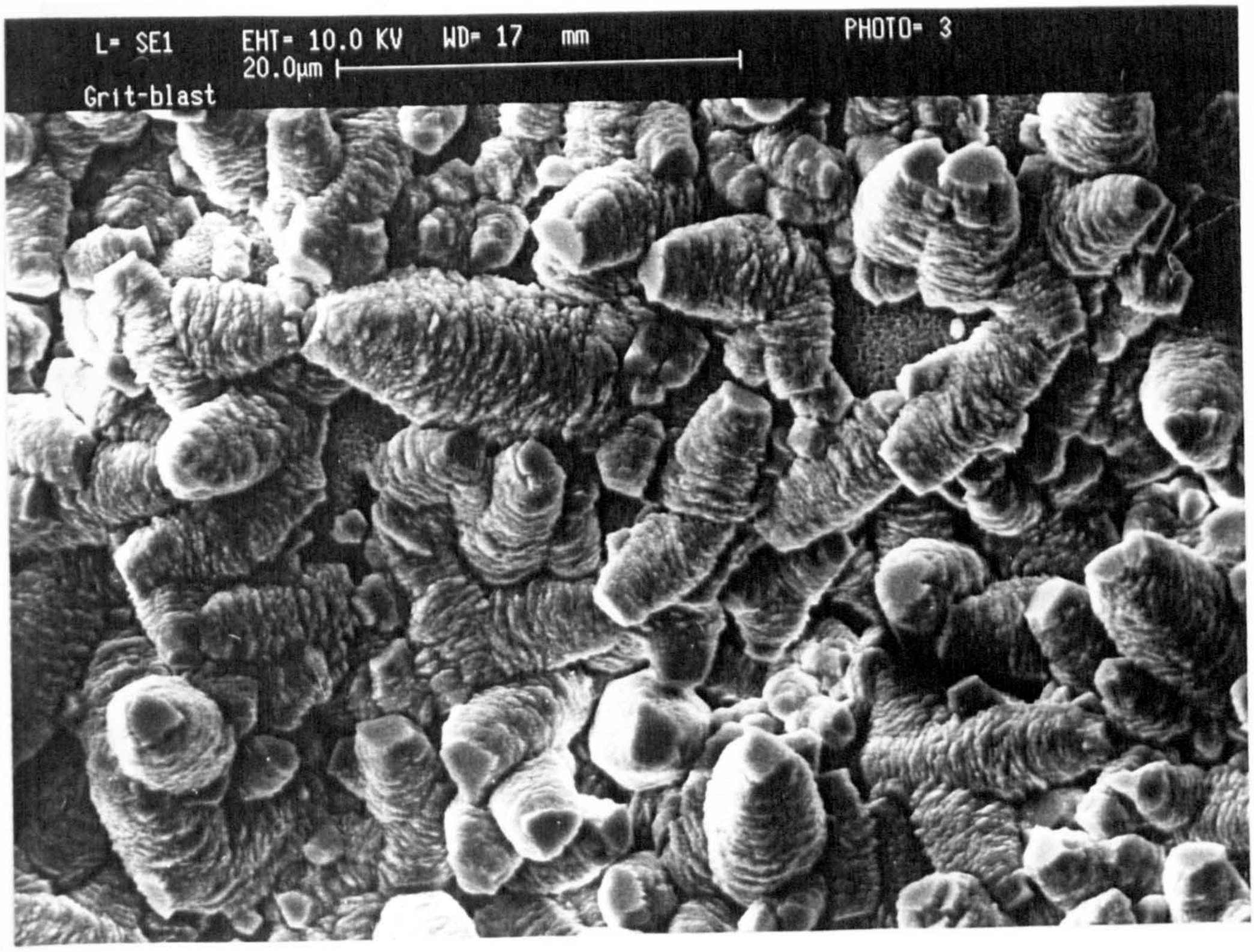

Figure 24 - SEM Micrographs to Show the Hydration Products on the Bonderite 705 Treated Aluminium 5251 Alloy Surface Following Exposure to DI Water at 60°C for a. 20 Hours, and b. 120 Hours.

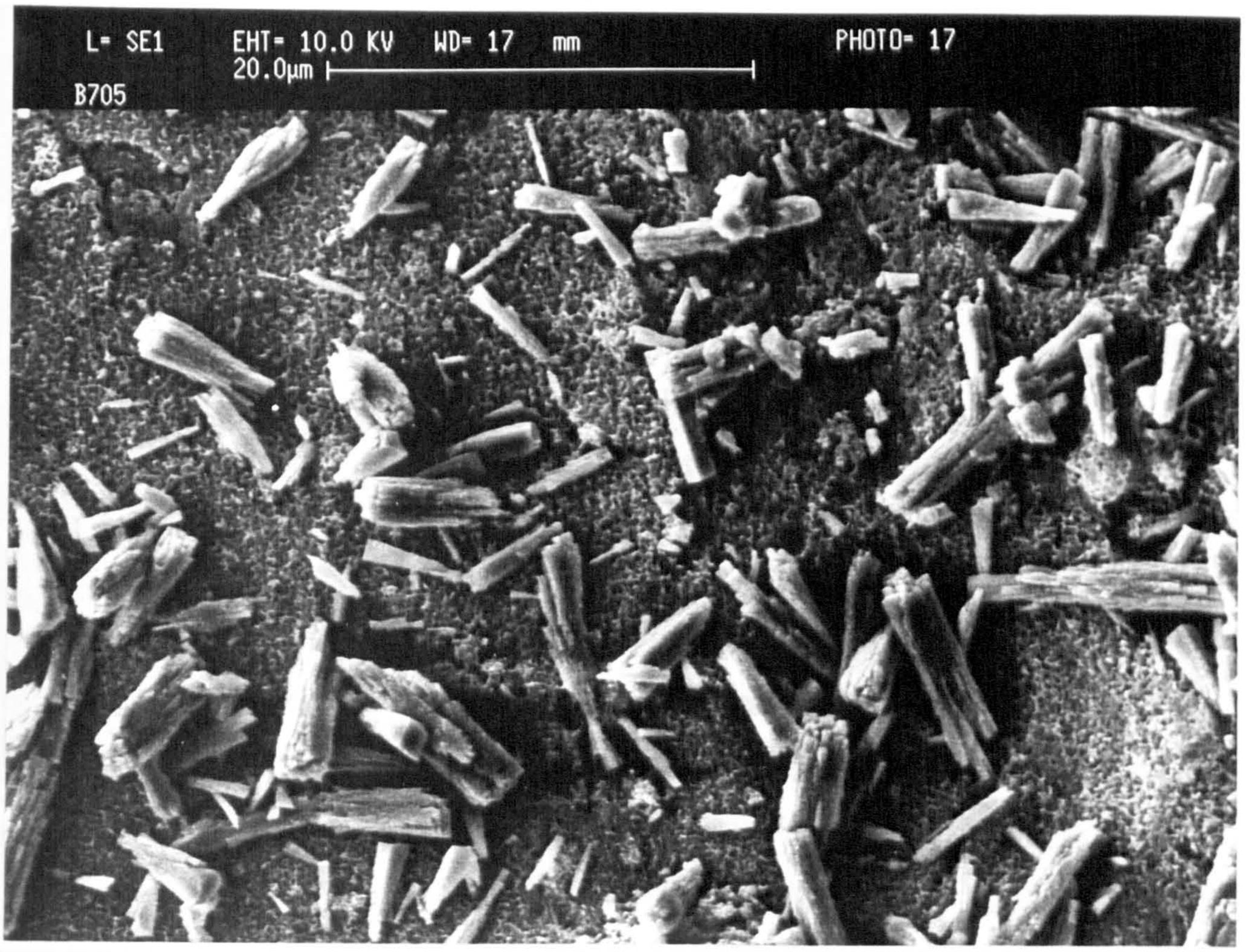

Figure 25 - SEM Micrographs to Show the Hydration Products on the Bonderite 777 Treated Aluminium 5251 Alloy Surface Following Exposure to DI Water at 60°C for a. 20 Hours, and b. 120 Hours.

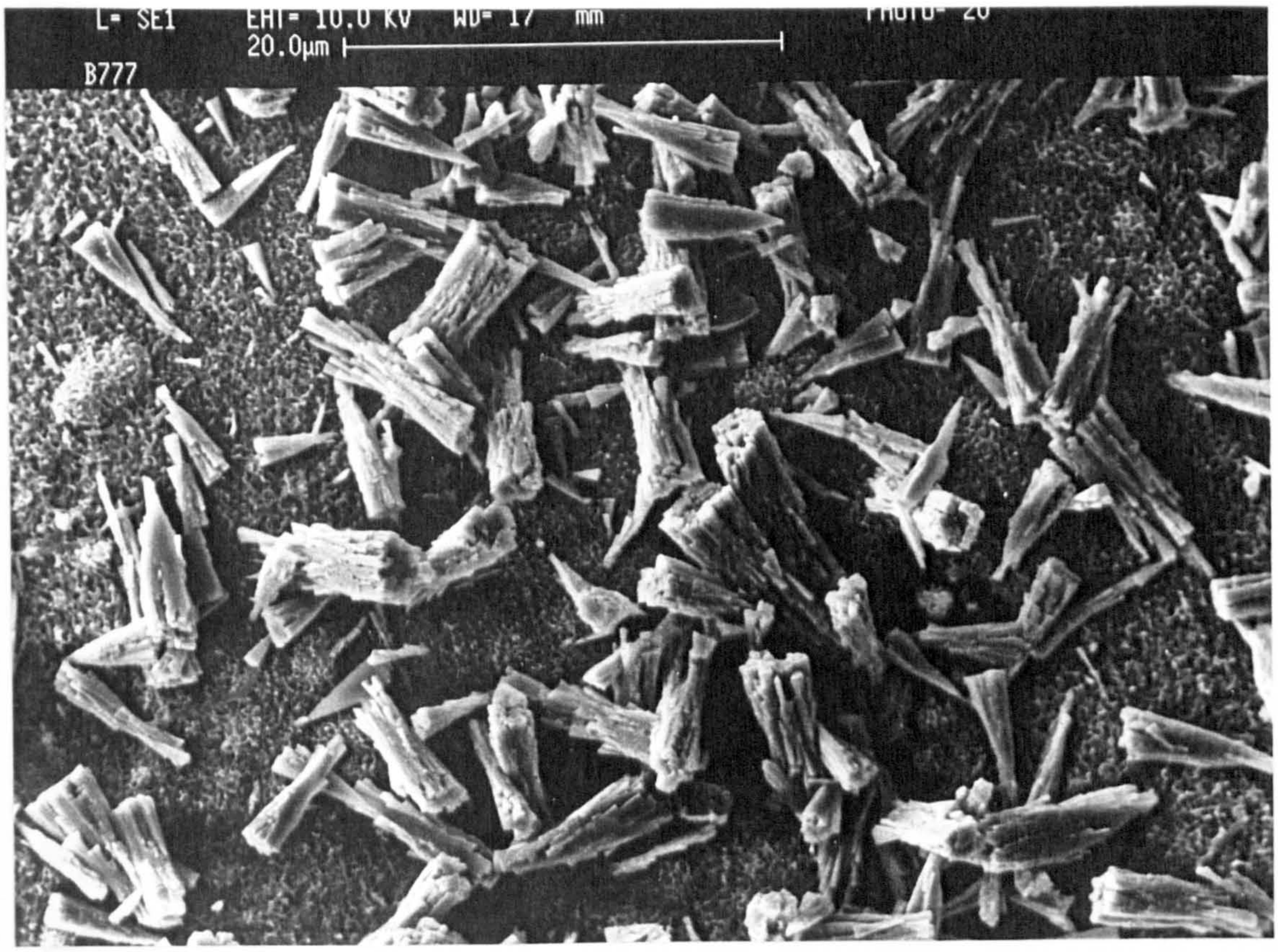

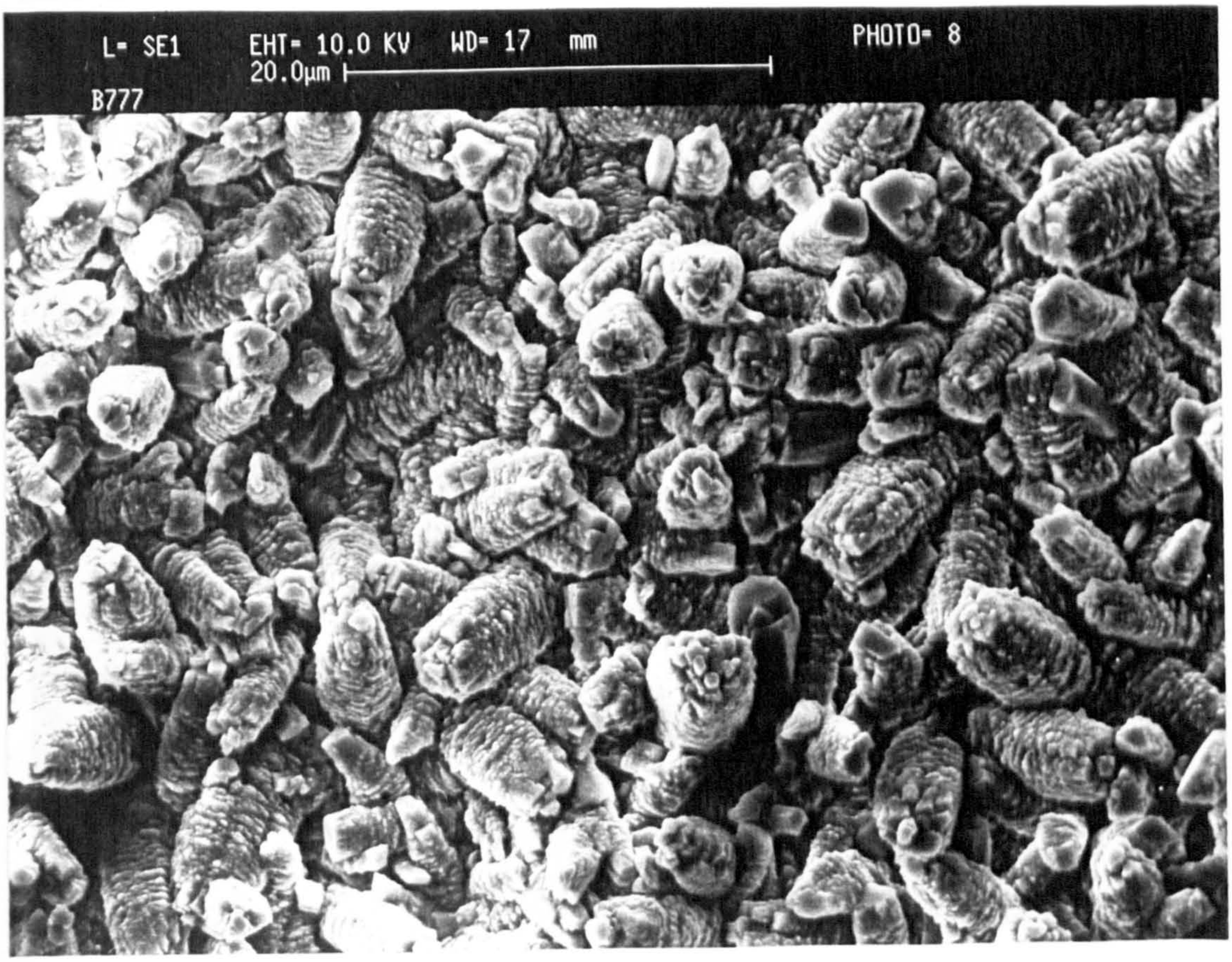

Figure 26 - SEM Micrographs to Show the Hydration Products on the EP2472 Treated Aluminium 5251 Alloy Surface Following Exposure to DI Water at 60°C for a. 120 Hours, and b. 550 Hours.

3.4.6 CHROMIC ACID ETCHED

After 20 hours exposure, the CAE treated material had undergone severe hydration. The underlying "corn-flake" like material was present, however, larger features up to 10μm in size were shown by SEM to cover 50 to 60% of the surface; see Figure 27.

XRD indicates the presence of bayerite only.

3.4.7 PHOSPHORIC ACID ANODISED

The PAA surface appears to hydrate at approximately the same rate as all of the other metal treatments apart from the EP2472. Large hydration products were again formed after 20 hours at 60°C which cover 70-80% of the surface. In this instance the hydration products have a distinctive "sea-anemone"-like appearance; see Figure 28.

XRD again indicates the products to comprise mainly bayerite.

Figure 27 - SEM Micrograph to Show the Hydration Products on the Optimised CAE Treated Aluminium 5251 Alloy Surface Following Exposure to DI Water at 60°C for 20 Hours.

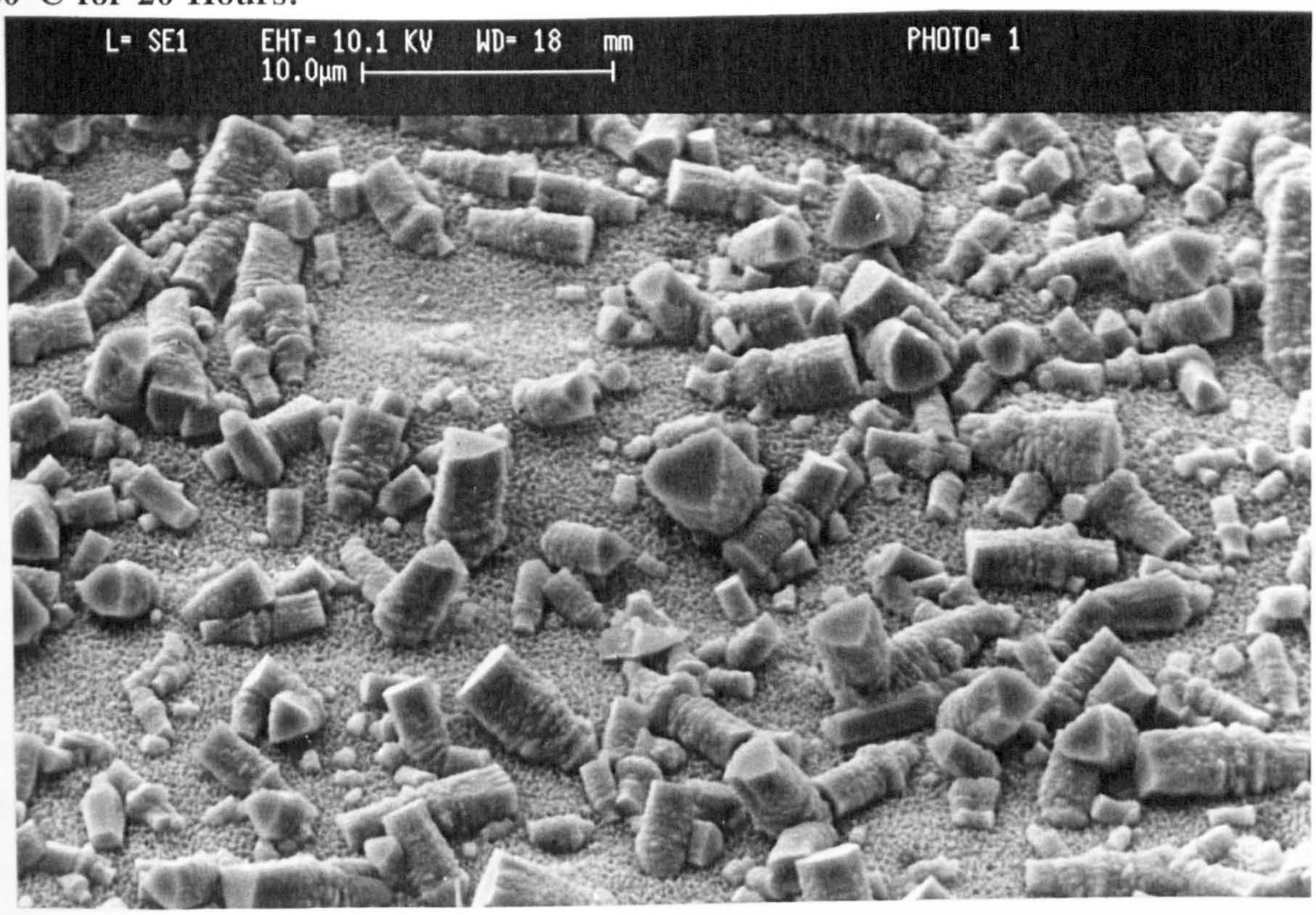

Figure 28 - SEM Micrograph to Show the Hydration Products on the Boeing BAC 5555 PAA Treated Aluminium 5251 Alloy Surface Following Exposure to DI Water at 60°C for 20 Hours.

CHAPTER 4 - DISCUSSION

4.1 TEST PARAMETERS

4.1.1 THE INFLUENCE OF JOINT SPEW FILLET GEOMETRY AND ADHEREND THICKNESS ON THE PERFORMANCE OF SLS ADHESIVE JOINTS

Comparing results, in Table 6, from joints with no-fillets and those with full-fillets and using 1.2 mm adherends and the toughened epoxide, it can be seen that there is a slight increase in both absolute joint strengths and in the percentage variations (standard deviation divided by the mean) with increasing fillet size. Qualitatively, this result is in agreement with that predicted. Adams and co-workers and others[174-176]. have demonstrated using the finite-element method (FEM) and Moiré interferometry that the peel, shear and principal stresses in this type of joint are at a maximum at the leading edges of a joint and within the adhesive. The presence of a fillet on this edge facilitates a reduction in peak stresses for a given load. Therefore, a fillet permits a greater load to be applied before joint failure.

The lack of control over the size of the full-fillet configuration means that there is little control over the degree of stress reduction and, thereby, leading to increased variability in joint strength results. The greater degree of control over the fillet size when using either the half- or no-fillet configurations leads to a reduction in the variability in test results; this effect was observed.

The data from joints using the high modulus, non-toughened epoxide show a smaller peak change in percentage variations when compared with the low modulus toughened epoxide but greater differences in absolute values. The much increased load capacity of the joints containing the non-toughened epoxide and the full-fillet can be attributed to the difference in modulus of these adhesives. Crocombe and Adams[174] used FEM

analysis to demonstrate that peel, shear and the principal stresses within a SLS joint all decrease with increasing adhesive modulus. It is suggested that this is possible because a higher modulus adhesive is more capable of transferring the load to the adhesive and hence the fillet, thereby, reducing the average stress in the overlap region.

With the thicker (3mm) adherends only the two extremes ie. the full- and no-fillet geometries were considered. The data in Table 7 show that there is little or no relationship between fillet geometry and subsequent joint strengths or percentage variations. These data are also in agreement with those predicted by Crocombe and Adams[174] who concluded that the influence of the spew fillet has a reduced effect with increasing adherend thickness.

Considering the data from the no-fillet joints in Tables 6 and 7, it can also be seen that, with both adhesives, there is a large increase in the absolute joint strengths with increasing adherend thickness. This indicates that there is a reduction in the stresses within the joint with increasing adherend thickness.

Kinloch[12] has summarised work combining Volkerson's analysis, assuming that the adhesive is a linear elastic solid which deforms only in shear, and that by Hart-Smith, again, assuming elastic behaviour of the adhesive. It is argued that increasing the thickness of the adherend leads to a reduction in the maximum stress concentrations and thereby an increase in joint strengths. However, reducing the adherend thickness increases the transverse tensile stresses. The consequence of this is that increasing the adherend thickness facilitates an increase in joint strengths but only up to a certain level[12]. The reduction in stress within the adhesive can be attributed to an increase in the load bearing capacity of the thicker, stiffer adherend, thereby reducing the load on the adhesive. The reduction of the load on the adhesive lessens the influence of the fillet. This is not the case with thinner adherends than those used in the present work where the increased flexibility of the adherend is considered to permit better stress transfer to the fillet than with the thicker adherends.

Increasing the adherend thickness has a much larger influence with the high modulus compared with the low modulus adhesive. With the high modulus material there are high levels of stress within the adhesive, most of which are transferred to the adherends with increasing adherend thickness. In contrast, with the low modulus adhesive much of the stress is already accommodated by the adherend.

With the thinner adherends, the percentage variation of joints using the toughened epoxide and half-fillets are of the order of $\sim 2\%$. This demonstrates that there is no measurable benefit in using the no-fillet geometry.

It is recognised that a full quantitative evaluation of the data presented in this section is not possible without recourse to mathematical modelling techniques such as FEM. However, by considering the stresses acting in these systems there is good qualitative agreement between the experimental data presented and that predicted by such techniques.

In summary:

- Toughened epoxides have been chosen as the preferred adhesive-type for the durability studies in this research programme.

- To produce the desired reproducibility in data using toughened epoxide adhesives, the half-fillet geometry is to be used in all subsequent work.

4.1.2 THE INFLUENCE OF STRAIN RATE ON THE PERFORMANCE OF SLS ADHESIVE JOINTS

The results presented in Figure 4 indicate that, within the range used, the non-toughened epoxide shows no sensitivity to strain rate, whilst the two-part acrylic shows joint strengths increasing linearly.

The relative performance of both adhesives can be explained in terms of their varying degrees of cross-linking[177]. The two-part acrylic is only slightly cross-linked and so the polymer chains are able to move relative to each other at low strain rates. Under this condition the adhesive has only a low modulus. At the higher strain rate such movement of the polymer molecules cannot so easily occur and so the adhesive becomes stiffer giving it a higher modulus. The increased modulus enables the acrylic adhesive to accommodate higher loads at the increased strain rate[177].

In contrast, the non-toughened epoxide has a high degree of cross-linking and so the polymer chains cannot deform in the same way as the acrylic. The epoxide maintains its modulus at the different strain rates and consequently shows no variation in joint strength with changes in this parameter.

In summary:

- With some adhesives, for example, the two-part acrylic used in this test, variations in strain rate can have a profound effect on the measured strength of an SLS joint. However, this was not the case with the non-toughened epoxide.

- Since an epoxide adhesive was selected for use in further studies, it was clear that the SLS joint strength results would not be critically dependent upon the strain rate conditions used.

- A constant value for the cross-head speed of 6 mm per minute was chosen for use throughout the present programme.

4.2 DURABILITY TRIALS

4.2.1 THE INFLUENCE OF SURFACE MACRO-ROUGHNESS ON THE DURABILITY OF ALUMINIUM-EPOXIDE JOINTS

Correlating data from Tables 13 and 18 it can be concluded that the degree of macro-roughness as measured by profilometry and observed directly by SEM has been demonstrated to have no measurable effect on the initial strength of SLS joints. There is, however, a small but significant influence on the durability of epoxide-aluminium joints.

The data presented in Table 13 indicate that the coarser grades of grit, 40/60 and 80/120, produce much larger surface features with R_t values in the range 20 to ~23 microns compared with 12 to 14 microns for the finer grades, 320 and 180/220. Table 18 shows that the smoother surfaces with the lowest roughness (R_a, R_q and R_t) values performed better in unstressed durability trials than those with much higher figures.

Interestingly, initial joint strengths with degreased-only adherends are ~30% lower than the comparable values obtained with treated adherends. This result indicates that the increased roughness and modified oxide introduced to the aluminium surface by the grit-blast is beneficial at least in terms of initial joint strengths.

XPS data, in Table 19 indicate a high degree of failure within the surface oxide with the degreased-only samples. This result is consistent with the presence of a cohesively-weak surface oxide, however, the lack of surface roughness might contribute to the observed poor initial joint strengths.

Optical inspection, using up to x45 magnification, indicates a mixed failure mode with the unexposed grit-blasted adherends. In all cases, a combination of apparent interfacial and cohesive failure within both the adherend and adhesive was observed.

Similar failure modes were observed with exposed grit-blasted joints, however, in these cases there did appear to be some disruption of interfacial bonds as a consequence of exposure to DI water at 60°C. This effect would account for the reduction in joint strengths as a function of exposure time.

The following explanation is offered to account for the fact that the smoother surfaces performed better in durability than the rougher: It is postulated that there is incomplete wetting of the metal surfaces by the adhesive after grit-blasting. Such incomplete wetting might then result in voids at the metal-adhesive interface which could facilitate the transport of water. The presence of water at the interface is then thought to have caused the weakening of bonds in this region. The rate of ingress of water and consequently its damaging effects are thought to be more pronounced given the larger asperities and troughs on the rougher surfaces.

Poor wettability of the grit-blasted surfaces has been directly observed by measurement of contact angles, see Table 12. Contact angles in the range 64 to 89° indicate some contamination of the grit-blasted surfaces prior to bonding, this is despite the double-degrease stage used after this treatment and prior to bonding. It would be expected that, irrespective of surface roughness, an uncontaminated aluminium-magnesium oxide produce a zero degree contact angle with water.

This latter point was demonstrated experimentally by laser ablation of the 80/120 grade grit-blasted surface. In this experiment, an initial contact angle of 69° was measured on a degreased-only surface this was reduced to 0° after laser-cleaning. No change in surface texture would be expected as a result of the relatively mild laser treatment which might account for this change in contact angle results.

Additional evidence of contamination on the grit-blasted and degreased surfaces is given by the presence of carbon in the AES data presented in Table 11.

4.2.2 THE EFFECTIVENESS OF CO_2-LASER ABLATION AS A PRETREATMENT FOR BONDING ALUMINIUM AND MILD STEEL

Whilst laser treatment has been used to modify the surface of polymers, for example, PMMA[178], PVC[179] , PEI[179] and polycarbonate[179], and ceramics such as alumina and silicon nitride[179]. There has, however, been little work carried out on laser treatment to enhance adhesion to previously untreated aluminium.

Much of the work carried out to date has utilised excimer rather than CO_2-lasers. In one study[180], excimer laser treatment was shown to improve joint strengths to sealed anodised 2024-T3 aluminium alloy by up to 150%. This improvement was attributed to the removal of material from the previously sealed pores. The resultant increase in surface roughness and porosity was deemed to have enabled a higher degree of mechanical interlocking and hence adhesion.

However, as detailed in Section 3.3.2, other laser-types are potentially useful, in particular, CO_2-lasers were deemed worthy of study offering the major advantages of being relatively cheap to purchase and operate, whilst providing the possibility of large area coverage. For example, CO_2-lasers are used for ornamental and structural restoration where these previously mentioned features are a tangible benefit[181]. For these, and other reasons as detailed in Section 3.3.2, CO_2-laser ablation has been considered of interest to the present study.

4.2.2.1 Aluminium

The effectiveness of the CO_2-laser treatment on aluminium 5251 alloy was originally demonstrated using Araldite 2001. The results given in Table 20 indicate that this adhesive-treatment-alloy system is sensitive to changes in the surface condition. The CO_2-laser treatment can be seen to provide a 22% increase in initial joint strengths; this level is, however, less than that provided by the other mechanical treatments tested.

In the above mentioned study, Araldite 2001, a two-part epoxide, was used. The cure schedule for Araldite 2001 was 24 hours at room temperature plus a 60°C post-cure for 1 hour. In the second part of this work, Araldite 2007, a single-part 120°C cure was used for comparison. The resultant initial joint strengths are given in Table 21. It is interesting to note that, when compared with degreased-only controls, only a modest increase in initial joint strength was provided with the lower temperature curing adhesive whilst there was $>100\%$ increase with the higher temperature curing material. In the latter case, the initial joint strengths with the CO_2-laser treatment were similar to, or greater than, those obtained with either the mechanical (grit-blast) or chemical (conversion coating) treatments.

The results of stressed durability trials with the single-part epoxide are presented in Table 22. These data indicate that, at the lower applied load (1 kN), the degreased-only joints performed significantly worse than the other treatments. However, the CO_2-laser treatment had similar mean times-to-failure to the grit-blast and Bonderite 705 conversion coating.

With the higher applied load (1.5 kN), the stressed durability performance of the CO_2-laser treatment was significantly worse than the chemical treatment but only marginally inferior to the mechanical treatment. There was, however, a significant increase in the mean time-to-failure of laser treated joints compared with the degreased-only material. The much improved joint performance resulting after CO_2-laser treatment of the adherends compared with degreasing combined with the fact that there was little change in surface texture after laser treatment implies that the improvement was a consequence of there being more interaction between the adhesive and the laser-treated surface than in the degreased-only case.

Comparing AES data in Table 14, it is apparent that following a two-stage ultra-sonic degrease treatment there is a relatively high degree of contamination residual on the aluminium surface. It is likely that this contamination is strongly adsorbed or bonded to the surface. In contrast, the laser-treated area shows no evidence for the presence

of organics. The detection limit for carbon in this matrix is ~1 atom%. This result indicates that CO_2-laser treatment can effectively remove contamination from the aluminium surface which might otherwise obscure surface features, provide a weak boundary layer, reduce surface wettability by the adhesive or act as a barrier to the formation of interfacial bonds.

Contact angle measurements confirm that superior wettability is provided by the laser-treatment. The water contact angle with the CO_2-laser treated aluminium was zero compared with ~50° with the solvent degreased material.

AES depth profiling indicates that CO_2-laser ablation treatment modifies the degreased-only aluminium surface not only by the removal of residual organic contamination but also by modification of the oxide layer. The oxide layer increases in thickness following laser-treatment and there is an accompanying decrease in the Mg:Al ratio in the near surface. Although there is evidence of a change in the macro-roughness, with a reduction in the prominence of the rolling lines, there is no evidence, within the resolution of SEM, of a change in the surface micro-roughness following CO_2-laser treatment.

The difference in Mg:Al ratios in the surface region may be significant; this aspect will be discussed in Section 4.4.5.

4.2.2.2 Mild steel

As indicated in Table 23, all three surface treatments provide a significant increase in initial joint strengths compared with the degreased-only controls. The CO_2-laser treatment gives comparable initial results to the commercially-used grit-blast plus silane treatment. However, whilst the grit-blasted and grit-blasted plus silane treated adherends showed no loss in joint strengths after exposure the degreased-only and laser treated surfaces did. In absolute terms, the CO_2-laser treated surfaces performed better than the degreased-only surfaces in the durability test; this situation is reversed in terms of the percentage strength retention.

With mild steel, a surface exposure time (SET) of up to approximately 2 days has no detrimental effect on either initial joint strengths or the durability performance of subsequently produced joints. However, surface contamination is evident from contact angle measurements after as little as one minute after treatment.

With the mild steel adherends, the results from the surface scans, see Table 15, indicate that, as with aluminium, a significant level of organic contamination remains on the surface after the degrease stage. The AES data confirm that the organic material was almost completely removed after CO_2-laser treatment. This result was verified by contact angle measurements in which values of 0°, 70° and 70° were recorded for the laser treated, degreased-only and as-received (oily) material respectively.

The AES depth profiles indicate that, unlike the aluminium, there was a large increase in surface oxide thickness over the degreased-only control as a consequence of CO_2-laser treatment; see Figures 8a to 8c and Table 16. The AES data further indicate that there was some variability in the thickness of the surface oxide across the bonded area despite each area having received the same degree of laser treatment. The presence of calcium in the depth profiles could not be accounted for. Care was taken to avoid contamination as a result of handling the surfaces post-treatment. The calcium is more likely to be attributable to some processing aid which has been incorporated within the surface oxide.

SEM micrographs also reflect the fact that there is a large interaction between the CO_2-laser and the mild steel; see Figures 9 to 11. The degreased-only surface appeared patchy with prominent cracks in the surface. In the shiny grey laser treated area there was evidence of some surface melting with what appear to be small droplets of metal or metal oxide over the surface. In addition, the previously observed cracks appeared to be closing-up, being more rounded at the edges. Figures 11a and 11b show that the dark blue laser treated area appeared noticeably different in surface texture to the other areas whether viewed at either high or low magnification. At low

magnification the dark blue CO_2-laser treated area appeared much smoother than either the shiny grey laser treated area or the degreased region. This was confirmed when viewed at a greater magnification when no discrete cracks could be observed and the surface had a glassy appearance.

The results indicate that there was severe surface melting with the steel adherend; this effect was not so apparent with the aluminium. In order to explain this result it was decided to calculate the expected surface temperature for both aluminium and mild steel as a consequence of CO_2-laser treatment.

Initial predictions of surface temperature were made from the equation given below:[182]

$$T = (2 \times F / K) (\kappa \times t / \pi)^{0.5}$$

$$\text{where } F = (1 - R) \times I$$

where I is the flux density of the laser ($J.cm^{-2}$), R is the reflectivity of the metal at 10.6μm, κ is the thermal diffusivity of the metal, K is the thermal conductivity of the metal, t is the pulse duration and T is the increase in temperature at the surface of the metal after a single pulse. This equation is a simplification of that given in reference 182.

The high reflectivity of metals to 10.6 μm radiation, together with their high thermal conductivities give a calculated increase in surface temperature of just a few hundred degrees, insufficient to induce surface melting. Reflectivity values of 0.975 and 0.967 were used in this calculation for aluminium and steel respectively[183]. From this, it was concluded that the oxide was formed by the impact of high energy ions produced in the resultant plasma.

The mechanism of laser-surface interaction which facilitates these changes is not given in the literature. From the surface analysis information acquired in this study and other observations, the following mechanism is proposed: the high reflectivity of the aluminium, and to a lesser extent the mild steel surface, means that the laser interaction is dominated by the plasma formed immediately above the surface and which is probably initiated by loosely bound material on the surface. This plasma is visibly blue-purple in colour. This hot plasma then radiates to the surface resulting in some further heating and subsequent oxidation.

Noticeable heating of the metal adherends was a result of absorption of the ultra-violet light produced by the plasma as opposed to the far infra-red radiation directly from the laser. There was insufficient energy in the laser to produce X-rays in the plasma. A simple substantiation was accomplished by exposing a metal coupon to excessive plasma and non-plasma radiation with a similar fluence in both instances (being slightly above and below plasma threshold). The plasma radiation induced considerable heating of the bulk material, whilst non-plasma radiation produced no noticeable effect.

The mechanism detailed above is proposed to explain the observed laser-metal interactions which produce the resultant benefits in terms of bond performance.

4.2.3 THE INFLUENCE OF CHROMATE-PHOSPHATE CONVERSION COATING OF ALUMINIUM ON THE IMPACT BEHAVIOUR OF JOINTS

It has been demonstrated that the Bonderite 705 chromate-phosphate conversion coating introduces many desirable features to the aluminium surface, being: potentially micro-rough; wettable, and; potentially hydration resistant.

Figure 12e shows that a thick magnesium-rich oxide is still present after alkaline cleaning in Oakite. Comparison with Figures 12a to 12d it can be seen that this oxide is removed in the initial stages of conversion coating. The developing chromate-phosphate film can be seen to have a constant growth rate for the treatment times used.

Fluorine could be observed, both at the surface and within all of the conversion coated films, at levels up to a few atom percent. The importance of fluorine is stressed in the film formation mechanisms proposed by both Treverton *et al*[63] and Brown *et al*[61]. There is a disparity between the AES depth profiles in the present work and XPS depth profiles given by Treverton *et al*[63]. In the aforementioned work by Treverton *et al* phosphorus levels decrease rapidly with depth leading to the conclusion that the phosphorus is situated on the surface of the oxide particles which form the conversion coating film. In contrast, in the present work phosphorus is observed throughout the film irrespective of film thickness.

The surface film comprises a highly-complex oxide structure which is relatively uniform in its coverage, highly micro-rough and thick, up to $\sim 1\ \mu m$. These conclusions are in good agreement with those obtained by other workers investigating the effects of chromate-phosphate treatment on commercially pure (99.5%) aluminium.[61,63]

These benefits have been demonstrated to significantly improve both the initial energy absorption and durability performance. It has, however, been demonstrated that over-treatment leads to a thick, mechanically weak oxide layer which is associated with poor bond performance.

It has been established that, as with crack propagation, peel and static shear tests, the impact behaviour of bonded aluminium is significantly influenced by surface treatment and environmental exposure.

4.2.4 A COMPARISON OF CHROMATE-PHOSPHATE AND CHROMATE-FREE CONVERSION COATINGS FOR THE ADHESIVE BONDING OF ALUMINIUM

As indicated in the Section 1.4.2, characterisation of chromate, chromate-phosphate and other conversion coated surfaces has been carried out by a number of workers. These studies utilise analytical techniques such as: SEM, SIMS, AES and XPS to elucidate the film formation mechanisms and to study the physico-chemical characteristics of the resultant films. Such techniques have also been used in the present study.

Static stress and simultaneous exposure by water immersion have been used as a measure of joint durability, as these conditions might be experienced by structural joints in service conditions.

The adverse effect of applied stress has been demonstrated in work by Minford[3]. In one trial, he reported that after exposure to 52°C and 100% RH for 700 days, unstressed vinyl phenolic and two-part RT epoxide joints retained over 88% of their initial strengths. However, under the same conditions of temperature and humidity, the joints failed in less than 100 minutes when a stress of 2MPa was applied.

Minford also compared the effect of various pretreatments of both clad and bare aluminium on the time-to-failure of joints exposed to sodium chloride solution[58]. In both cases, acid etching, anodising in sulphuric acid and a conversion coating treatment were superior to degreasing and grit-blasting. In another study[53], he compared the effect of various treatments on the time-to-fail of joints bonded with a one-part nitrile modified epoxide and exposed to 52°C and 100% RH. The durability increased in the order:

$$\text{degreased} < \text{sulphuric acid anodised (sealed)} < \text{sulphuric acid anodised (unsealed)} < \text{CAE} \approx \text{CAA} < \text{PAA}$$

The various parameters that affect durability have been examined using stress tests. Bethune[72] demonstrated the beneficial effect of a primer containing a corrosion inhibitor. Russel and Garnis[95] showed that an etchant consisting of sodium sulphate, ferric sulphate, sulphuric acid and nitric acid gave a similar performance to a standard FPL etch in time-to-failure tests.

Applied stress may or may not affect the residual strength of joints. Parker[118] reported that with CAE treated aluminium bonded with a 120°C curing epoxide, applied stress under various environments did not affect residual strengths. In contrast, Cotter and Kohler[96] reported that stress has a large detrimental effect on residual strengths for CAE and PAA treated aluminium bonded with either a "modified epoxide" or a nitrile-epoxide.

Interesting work has been carried out by Schwartz[80] in which single lap shear joints were stressed to 50% and 60% of their ultimate failure loads (ufl) in 95% RH at a temperature of 60°C. In this work, the adherends were treated by either by chromic acid etching (FPL etch) or PAA; the adhesives used were either FM123-2 or EA9628. The failure times at an applied load of 50% ufl with FM123-2 were 27h and 13h for the CAE and PAA respectively. These values increased to 63.5h and 55.5h with the EA9628 adhesive. From the relatively poor performance of the PAA treatment it was concluded by Schwartz that the mechanical behaviour of the adhesive was a dominant factor in joints exposed to high stress levels. A similar conclusion has been drawn by Hennemann and Brockmann[98] who have stated that "ageing under load is only a suitable method to evaluate the load capability of the adhesive itself and not for the adhesion".

In summary, the effect of exposing a joint to elevated temperatures and water under stress is particularly severe. It might be argued that such severe conditions might change the joint failure mechanism from that seen in service and, as such, the results presented are of limited value. However, provided the mechanism of failure is not changed, it is clearly very useful to accelerate the normal failure by increased

temperature, stress and water concentration

The effects of water on a joint are detailed in the literature[96,150], it is worth noting that, according to Kinloch[184], "stress probably increases the rate of diffusion of the ingressing medium", in this case water. The effect of stress on both the adhesive and the interface is to reduce their activation energies to bond breaking[185,186] that is to say make it more likely that polymer-polymer or polymer-substrate interactions will be destroyed.

A consideration of the work by Zhurkov and Kurskov[186] indicates that a plot of LnT_f versus stress should be linear assuming the same failure mechanism at all stresses. The activation energy for the formation of polymer-polymer bonds, E_a, can be calculated from DSC analysis invoking the theory proposed by Zukas *et al*[44]. In the present study, a value of 64.9 kJ.mole^{-1} was calculated using this procedure for the AV119 adhesive, this compares with a value of approximately 65 kJ.mole^{-1} reported for DGEBA. This value of E_a can be used, in the derivation of the Arhenius equation proposed by Zhurkov and Kurskov[186], to lead to a model for prediction of joint lifetimes. The presence of water in the present test environment does, clearly, provide a complicating factor.

The possibility of predicting lifetimes for joints experiencing relatively benign service conditions from short-term stressed durability tests where joints are exposed to more extreme ambient conditions has been addressed by Levi[83]. Levi has proposed a model for the estimation of joint lifetimes based upon a comparison of stressed and unstressed durability data with joints exposed to hot water ageing. His model was described as "promising".

Clearly, it is essential to establish the joint failure mechanism in order to fully understand what parameter is being measured, whether it is the cohesive properties of the adhesive or whether it is a measure of the interaction of the adhesive with the surface.

AES, XPS, SEM and visual inspection using optical microscopy were carried out in the present study to determine joint failure mechanisms. These results were then correlated with the surface analysis data presented in Section 3.2 to explain the joint strength data presented in Section 3.3.4.

As expected, with all treatments, the mean times-to-failure decrease with increasing applied load. The degreased-only joints had the lowest times-to-failure at every applied load. This effect is particularly evident at the higher loads. For example, a mean time-to-failure times of approximately 20 hours was recorded with the degreased-only adherends at an applied load of 1 kN; this compares with more than 450 hours with the other treatments. At all applied loads the mechanical treatment (grit-blasting) was out-performed by the conversion coating treatments. Considering the conversion coatings, at loads of 0.2 and 0.5 kN the EP2472 treated joints had the longest time-to-failure with the B705 and B777 performing similarly. At loads of 1 kN or greater, all three conversion coatings perform similarly.

The optimised CAE performed similarly to the EP2472, however, at all applied loads the PAA treated adherends had the longest times-to-failure.

A measure of the variability of the SSLS data can be evinced from Table A3.1 in Appendix 3. The greatest variability in times-to-failure was observed with the degreased-only treatment. These data reflect the non-uniform nature of the mill-finished surface oxide and the limitation of the degrease process producing a degree of variability in the surface condition prior to bonding. In all other cases there is a much tighter population of times-to-failure reflecting a degree of uniformity in the surface treatments carried out. These data will be considered in more detail below:

4.2.4.1 Degreased-only

As reported in Section 3.3.1.3 initial joints with degreased-only adherends failed with a mixed mode with apparent interfacial failure and cohesive failure within both the adhesive and metal oxide. A similar failure mechanism was indicated by AES on joints with an applied load of 0.2 kN and by SEM when 1.5 kN was applied; see Figures 29a and 29b. It is apparent that the largely planar, friable surface oxide on the degreased-only adherends is not capable of sustaining an applied load for prolonged periods of time.

4.2.4.2 Grit-blasted

Surface treatment by grit-blasting provides an intermediate level of performance, below that observed using the conversion coatings but better than with degreased-only adherends. Visual inspection indicated the same failure mechanism with both initial and stressed joints; a combination of apparent interfacial failure and cohesive failure within the adhesive. In one instance, with an exposed joint stressed to 1.5 kN, SEM indicated the presence of hydration products on the metal surface post-failure. Significantly, none were observed on the adhesive side of the failed joint. It is therefore most likely that hydration of the exposed adherend occurred after failure and prior to removal of the fractured joints from the test environment; see Figures 30a and 30b.

Figure 29 - SEM Micrographs to Show a. the Metal, and b. the Adhesive Sides of a Joint Prepared with Degreased-only Adherends Following SSLS Testing at a Load of 1.5 kN and Simultaneous Immersion in DI Water at 60°C.

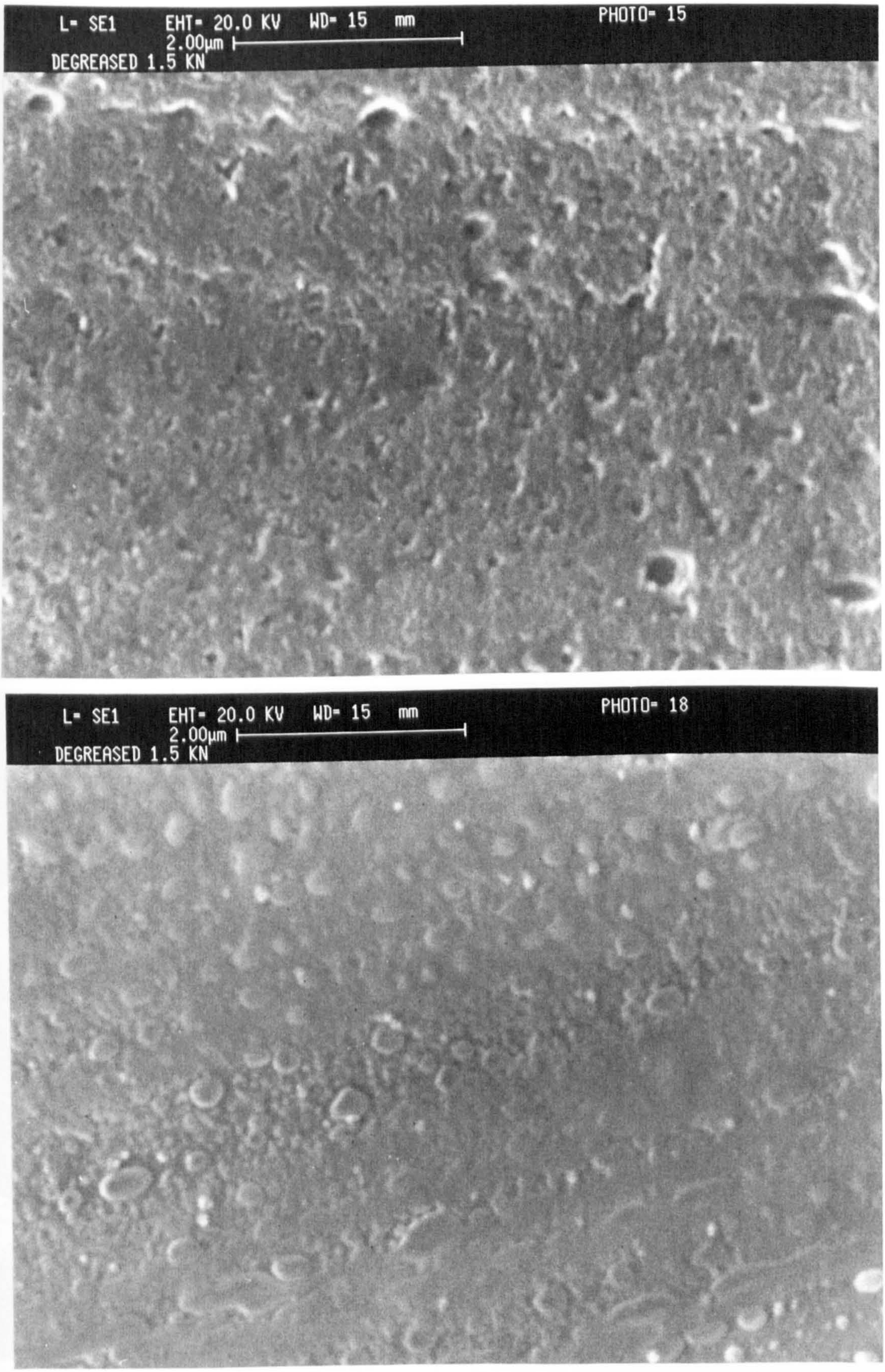

Figure 30 - SEM Micrographs to Show a. the Metal, and b. the Adhesive Sides of a Joint Prepared with Grit-blasted Adherends Following SSLS Testing at a Load of 1.5 kN and Simultaneous Immersion in DI Water at 60°C.

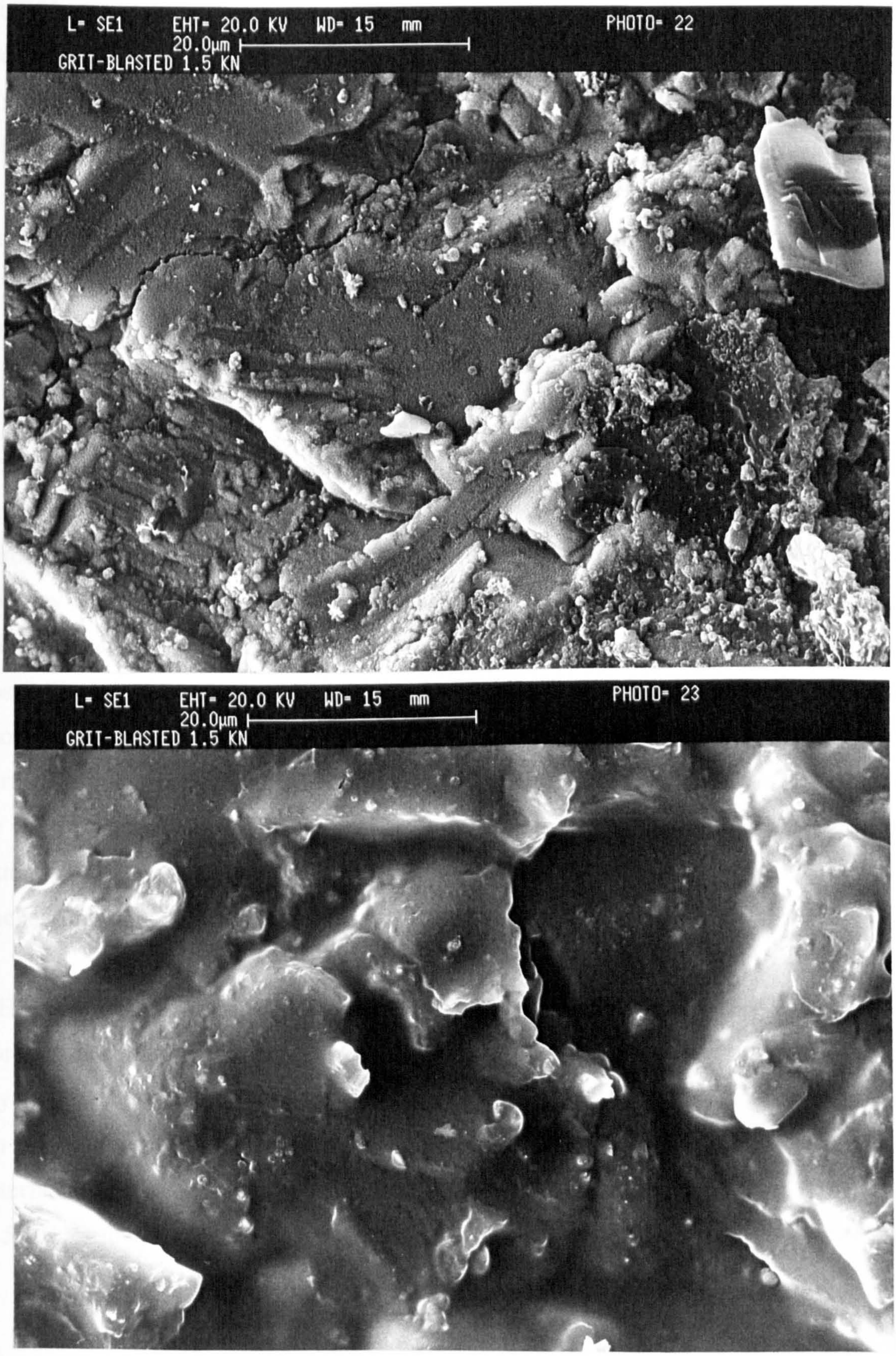

4.2.4.3 Bonderite 705 Conversion Coated

The composition of the chromate-phosphate conversion coating is reported in Section 3.2.4; a mixed chromium and phosphorous containing oxide is present. As previously detailed, the high oxidation state phosphate component would be expected to inhibit hydration of the oxide during exposure to water. In the present work, a "standard" 5 minute Bonderite 705 coating was used and there was no attempt at process optimisation. The Bonderite 705 film was shown by SEM to be ~230 nm thick and to be highly cracked. Treverton *et al*[63] observed cracks in the surface oxide with the same type of conversion coating. The "mud crack" type morphology was attributed to shrinkage of the coating as water evaporated from between the particles in the gel formed on the metal surface. The SEM images indicate that large areas of the coating have subsequently become detached.

According to the mechanism of film formation proposed by Treverton *et al*[63] the chromate-phosphate conversion coating comprises small, spherical particles of chromium (III) oxide which join together to form a filament-like structure. The film porosity introduced by such features would be desirable for improved bond durability, providing both an extended interface across which interactions can occur and also the possibility of micro-mechanical interlocking. Such features were observed with the shorter treatment times. However, within the limited resolution of the SEM, the surface texture on the Bonderite 705 treated adherends in the present study appears to be wavy or undulating rather than porous. It is possible that, as a consequence of the extended treatment time, the filaments of oxide have agglomerated to form a close-packed, continuous film.

AES indicated that initial joints failed partly within both the adhesive and the conversion coating. This is evidence of over-treatment providing a mechanically-weak layer. There was no evidence for the presence of aluminium, phosphorus or chromium on the adhesive side of joints which failed with an applied load of 1 kN indicating interfacial failure or failure within the boundary polymer. SEM of joints stressed to 1.5 kN further indicate a near-interfacial failure mechanism, perhaps with a limited

amount of detachment of the weakly-bound oxide from the metal surface; see Figures 31a and 31b.

Figure 31 - SEM Micrographs to Show a. the Metal, and b. the Adhesive Sides of a Joint Prepared with Bonderite 705 Treated Adherends Following SSLS Testing at a Load of 1.5 kN and Simultaneous Immersion in DI Water at 60°C.

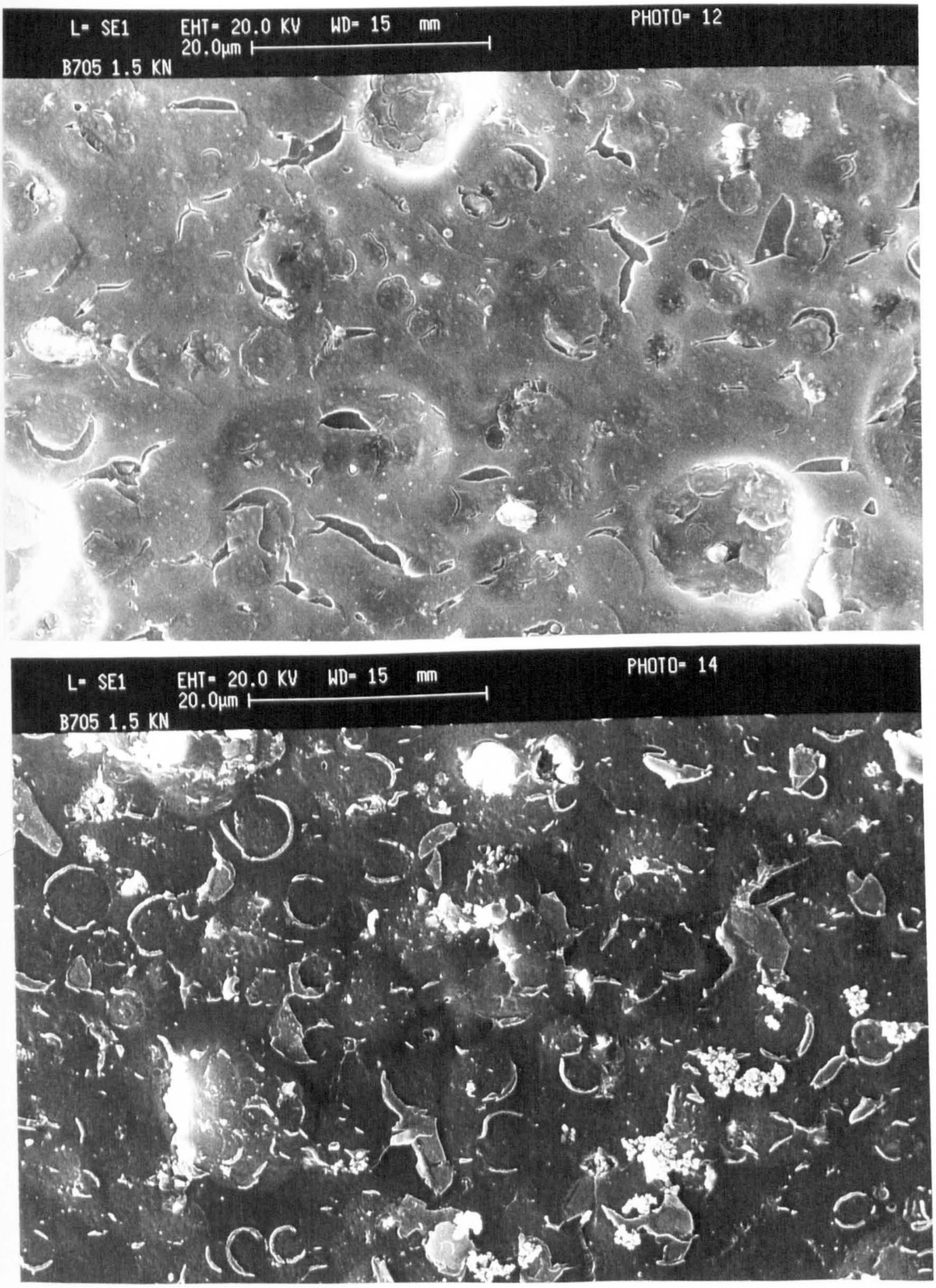

4.2.4.4 Bonderite 777 Conversion Coated

AES analysis on the Bonderite 777 treated surfaces indicate that this process produces a much thinner film than that produced by the Bonderite 705, being approximately 15 to 20 nm thick; there are two distinct phases within the layer, the inner 7-8 nm comprises mainly Al_2O_3 whilst the outer 7-8 nm is mainly ZrO_2 with phosphorous, calcium and fluorine present throughout. As with the Bonderite 705, the phosphorous present in the Bonderite 777 film was in the high oxidation state. The SEM images indicate that the Bonderite 777 process produces a scalloped surface texture comparable to that on the optimised CAE sample. This conclusion was confirmed by atomic force microscopy.

Visually, all Bonderite 777 joints appeared to fail interfacially. On joints stressed to 1 kN, no metal was observed by AES on the adhesive side of the failure whereas a thin layer of organic material was present on the metal side. Joints under an applied load of 1.5 kN failed in a similar manner. SEM indicated that the rippled surface texture of the treated metal was reflected in the detached adhesive; see Figures 32a and 32b.

Figure 32 - SEM Micrographs to Show a. the Metal, and b. the Adhesive Sides of a Joint Prepared with Bonderite 777 Treated Adherends Following SSLS Testing at a Load of 1.5 kN and Simultaneous Immersion in DI Water at 60°C.

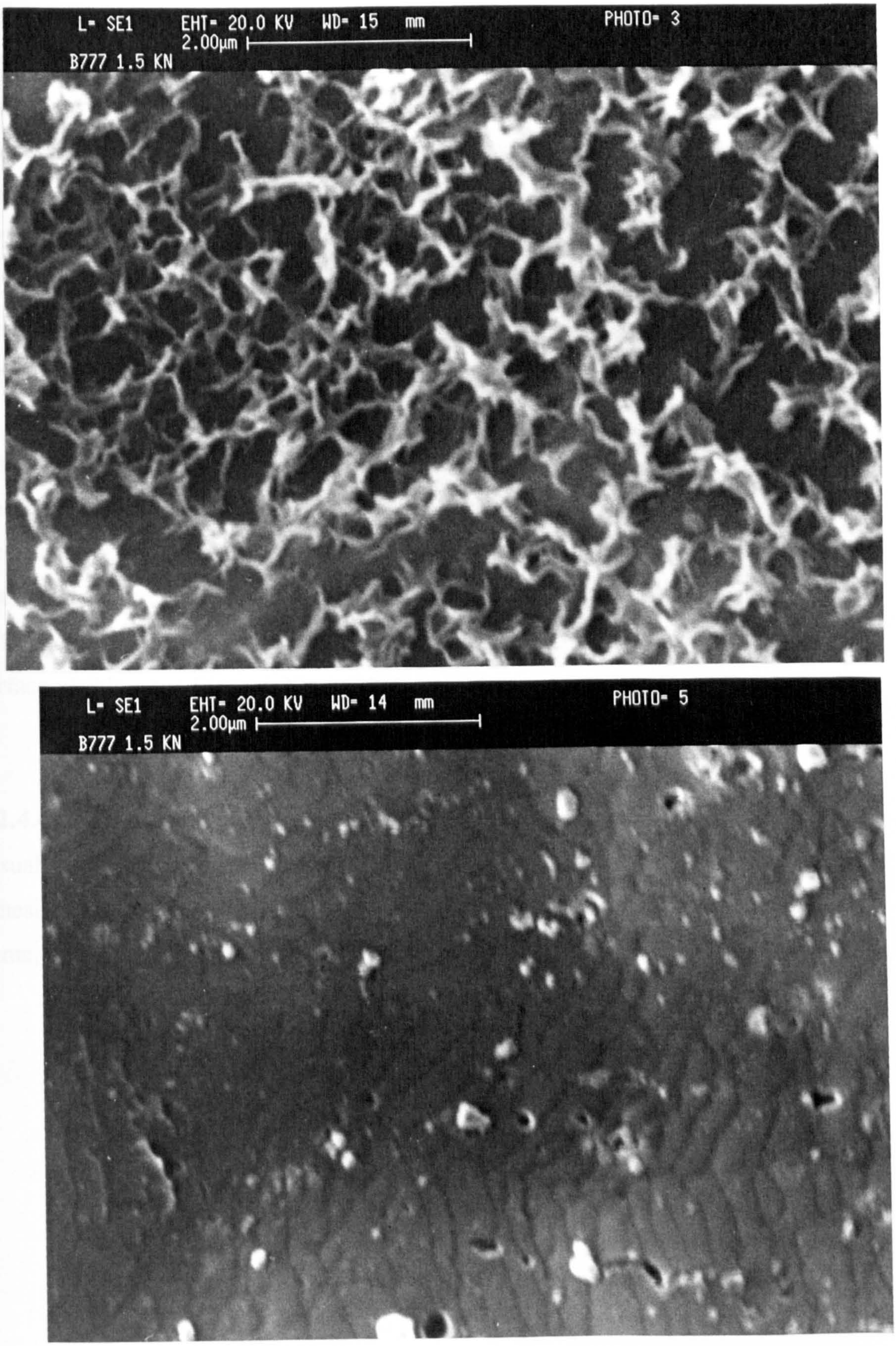

4.2.4.5 EP2472 Conversion Coated

AES results indicate that the EP2472 process produces a film containing both organic and inorganic components. This type of structure, a combination of zirconium-based chemistry with a polymer, has been reported by Schram *et al*[187]. There are, however, a number of differences between the films produced by the EP2472 conversion coating, used in the present work, and the Alodine 4830/4831 process studied by the aforementioned workers. Firstly, the EP2472 film contains phosphorous which is absent in the Alodine 4830/4831 film. Also, there is much more zirconium in the EP2472 conversion coating compared with the Alodine 4830/4831. In addition, the EP2472 film is much thicker (~50 nm) than the Alodine 4830/4831 film (<10nm) previously reported[187]. The SEM images indicate that on a micro-scale the surface appears highly nodular; the nodules are approximately 0.1 μm in diameter or less.

Visually, initial joints appeared to fail interfacially. Joints which failed with an applied load of 0.2 kN showed no evidence for the presence of metal on the adhesive side of the failure with carbon, nitrogen, and zirconium on the metal surface indicating interfacial or near interfacial failure. Joints loaded to 1.5 kN appeared, using SEM, to fail cohesively through the adhesive with none of the nodular features on the treated surface visible.; see Figures 33a and 33b.

4.2.4.6 Chromic Acid Etched

Visual inspection indicated that initial joints failed mainly interfacially but with some cohesive failure of the adhesive. A similar mechanism was observed with stressed joints, as evinced by SEM; see Figures 34a and 34b.

Figure 33 - SEM Micrographs to Show a. the Metal, and b. the Adhesive Sides of a Joint Prepared with EP2472 Treated Adherends Following SSLS Testing at a Load of 1.5 kN and Simultaneous Immersion in DI Water at 60°C.

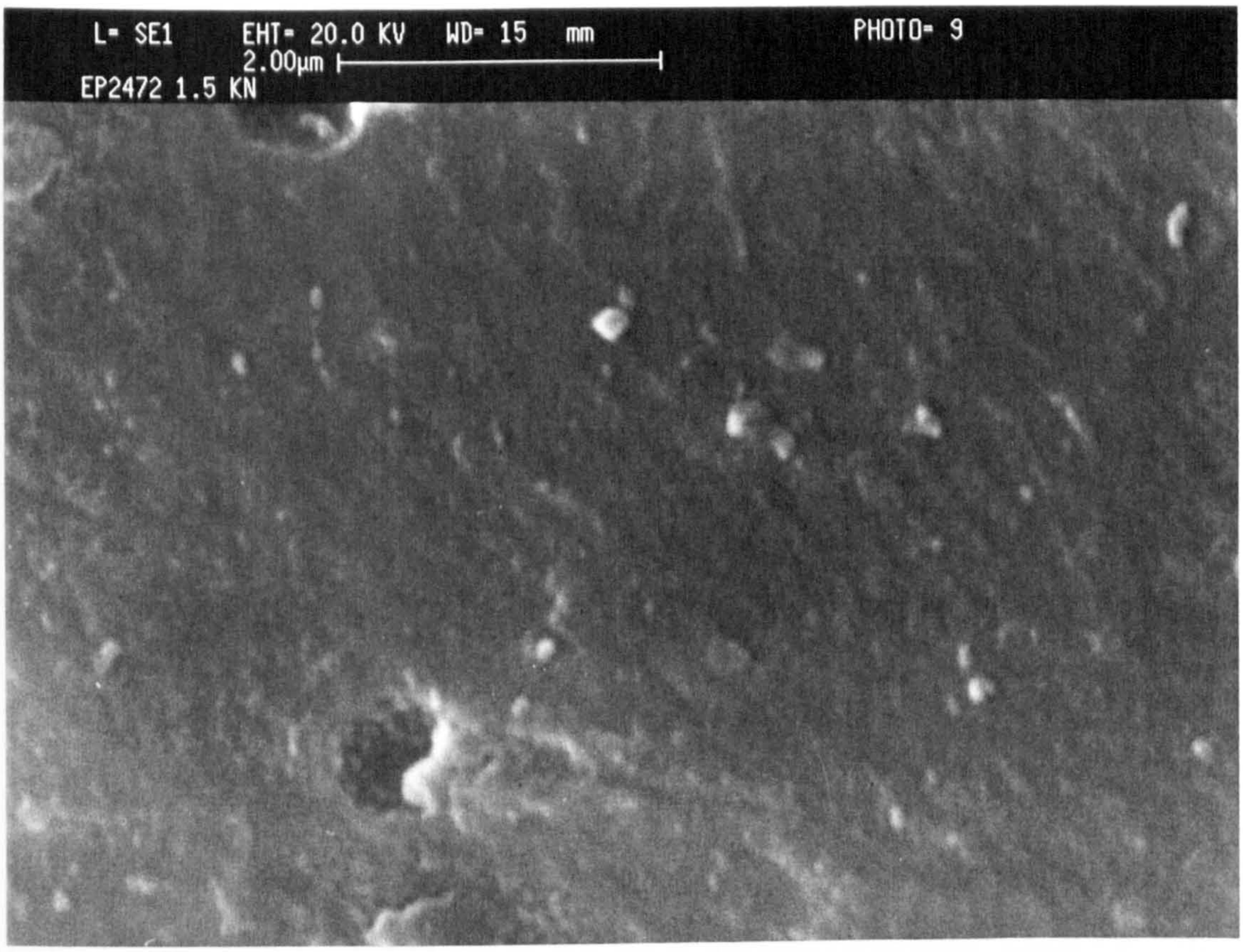

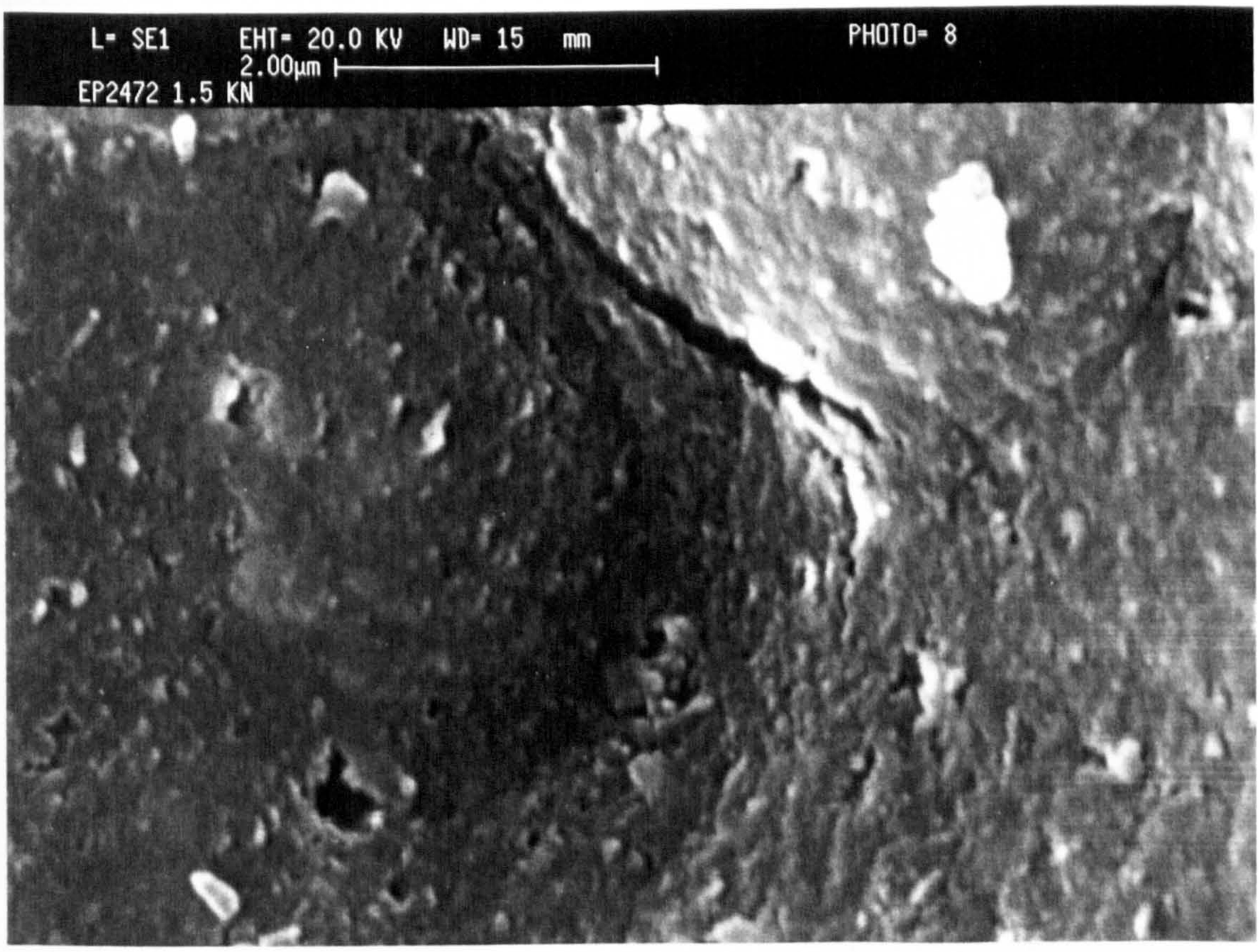

Figure 34 - SEM Micrographs to Show a. the Metal, and b. the Adhesive Sides of a Joint Prepared with Optimised CAE Treated Adherends Following SSLS Testing at a Load of 1.5 kN and Simultaneous Immersion in DI Water at 60°C.

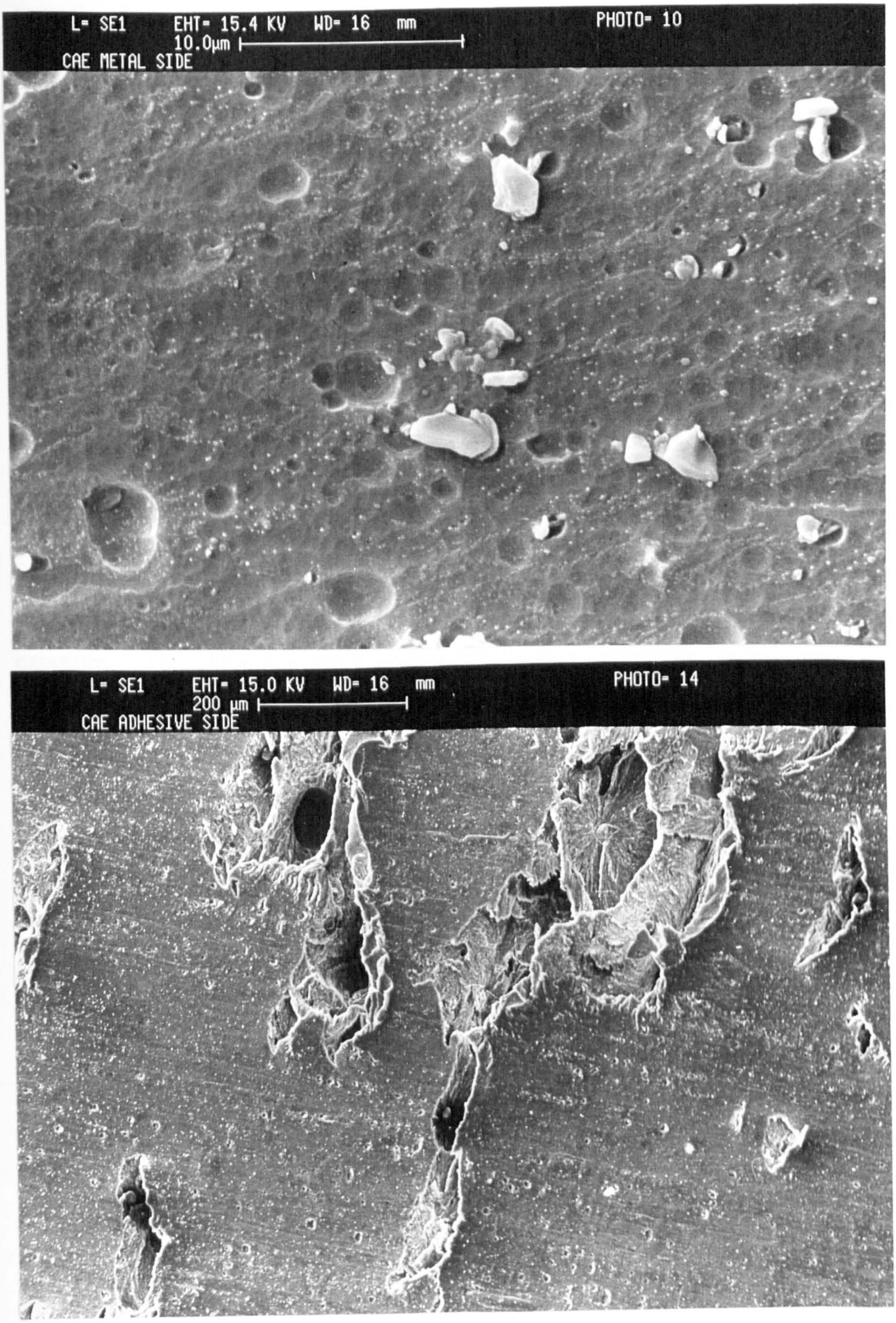

4.2.4.7 Phosphoric Acid Anodised

Visual inspection indicated that both initial and stressed joints failed cohesively within the adhesive. Typical SEM images are presented in Figures 35a and 35b from initial controls. Significantly, with the PAA joints the LnT_f versus stress plots deviate from the predicted straight line at low applied loads. This could be evidence of plasticisation of the adhesive after extended exposure times resulting in stress relief within the joints.

Surface characterisation and bond durability results have been presented for the three different conversion coating treatments and four controls. The chromate-phosphate process has been shown by Sheasby *et al*[59,60,188] to be an effective surface treatment for aluminium. In their work, conversion coatings were incorporated into an integrated design and manufacturing process for adhesively-bonded car bodies from aluminium sheet. As a part of the evaluation process, zirconium- and chromium-based conversion coatings were considered alongside chromic acid etching (CAE) for the treatment of aluminium prior to bonding. In unstressed durability tests SLS joints were exposed to salt-spray for up to 60 weeks. Overall, the zirconium-based conversion coating performed comparably to the CAE with residual strengths of ~6 MPa after 60 weeks exposure. The chromium-based conversion coating performed much better with residual strengths of ~16 MPa after the same exposure. The superior performance of the chromium-based conversion coating was confirmed by stressed humidity tests, whereby, SLS joints were exposed to temperature cycling between 43-48°C and 5 MPa stress. In these tests, using the same (unnamed) adhesive zirconium-based conversion coated joints lasted ~15 days whilst with the chromium-based treatment joints lasted >320 days. In the UK patent GB 2 139 540 A, chromate-phosphate conversion coated joints are compared with those prepared with the Boeing BAC 5555 phosphoric acid anodise (PAA) process. With aluminium 2117 and 5251 alloys the conversion coating produces comparable initial joint strengths to the PAA with values in the range ~15-16 MPa. Furthermore, with unstressed joints exposed to salt-spray exposure for 8 weeks the surface treatments performed similarly with strength retention levels in the range ~60-70%.

Figure 35 - SEM Micrographs to Show a. the Metal, and b. the Adhesive Sides of a Joint Prepared with BAC 5555 PAA Treated Adherends Following SSLS Testing at a Load of 1.5 kN and Simultaneous Immersion in DI Water at 60°C.

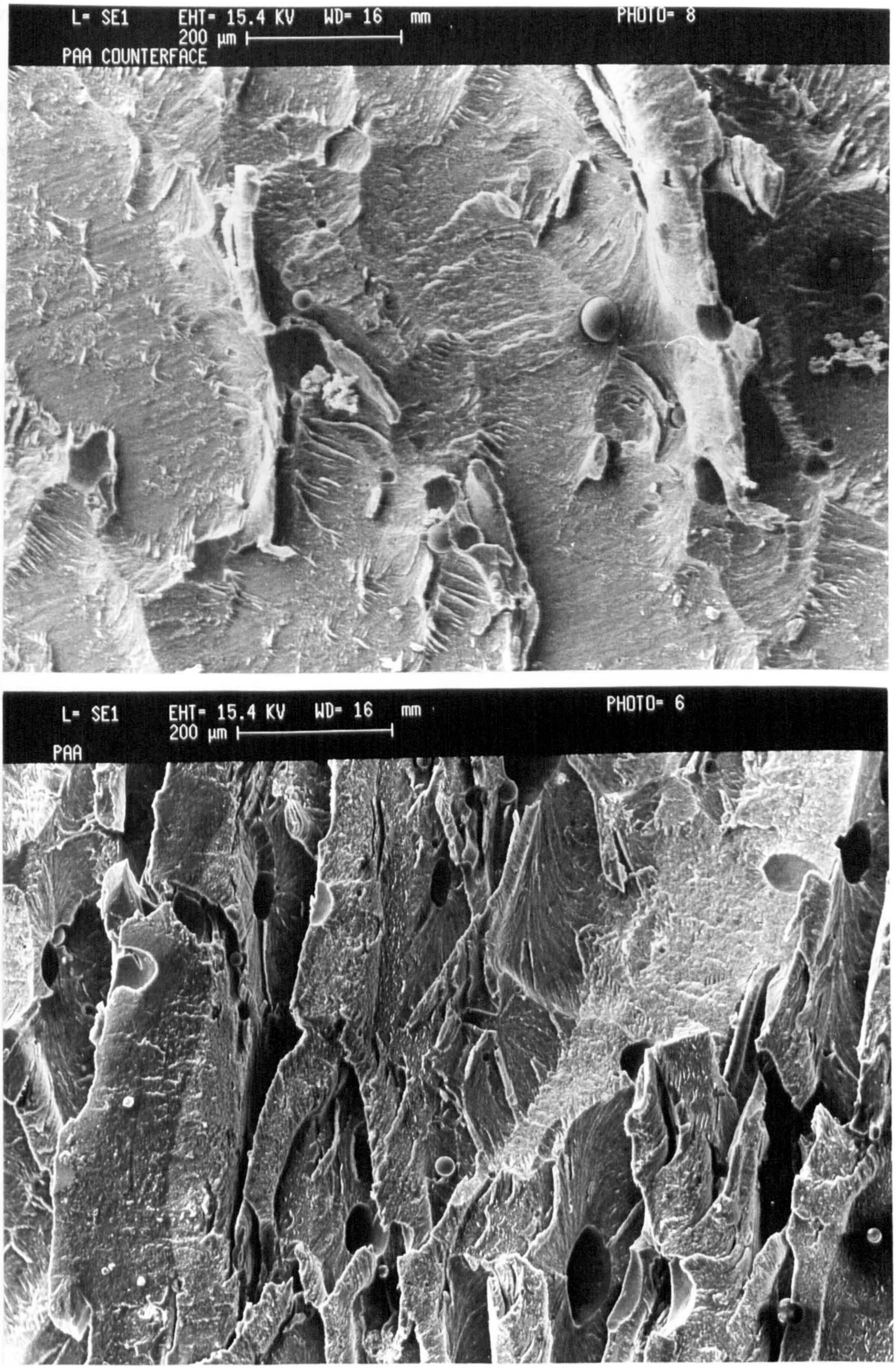

Work by Minford also highlights the beneficial effects of conversion coatings[3,52]. In one study[52], Minford compared the performance of Alodine 1200, a chromate conversion coating, with degreasing, grit-blasting and a number of acid etches. With a two-part epoxide the conversion coating gave poor initial control strengths (8.7MPa) but demonstrated excellent durability with 90% strength retention after 8 years exposure in an industrial atmosphere. However, after 2 years exposure to a seacoast atmosphere the conversion coated joints retained ~34% of their initial joint strengths. Acid etched joints used in the same trials had 0% strength retention after this time. The poor initial joint strengths and relatively good durability was also reflected in tests with a single-part epoxide. Initial joint strengths were 18.4 and 36.8MPa for conversion coated and acid etched joints respectively. However, after 4 years exposure to the seacoast environment the conversion coating showed 97% strength retention, whilst the acid etched joints retained no joint strength. In the present work, the chromate-phosphate conversion coating out-performed both the degrease-only and grit-blasting treatments, in line with Minford's results.

In the present work, no process optimisation was carried out as "standard" treatment times were used. The SEM images from the Bonderite 705 treated surface indicate that over-treatment might have occurred with a cracked, non-continuous and non-porous oxide layer produced. There are a number of possible explanations for the improved durability results produced by the Bonderite 705 treated, as compared with the grit-blasted adherends; there is some micro-mechanical interlocking with surface features unresolved by SEM; there is increased chemical interaction between the epoxide and the chromate-phosphate conversion coated compared with the grit-blasted surface, or; the Bonderite 705 conversion coating produces a more hydration resistant surface.

The possibility of micro-mechanical interlocking and the increased area over which interactions can occur have been proposed as being responsible for the generally good durability performance of the FPL etch[18,90]. These benefits could also be responsible for the good durability performance of the Bonderite 777 treated joints. The FPL etch

is not recommended for bonding of primary structures because of doubts over the uniformity of treatment[88] and the inability of the oxide layer to resist attack by moisture[70,88]. The potential for increased hydration resistance and the apparently uniform coverage provided by the Bonderite 777 process means that this treatment could possibly provide additional benefits to those offered by the FPL etch.

The EP2472 conversion coating contains both inorganic and organic components. The inorganic component is based upon zirconium and phosphorus chemistry; whilst the nature of the organic part is unknown. It is likely that when the EP2472 treated adherend is bonded, a region of graded composition is formed between the metal adherend and the polymeric adhesive, ie. an interphase, rather than there being a discreet interface between the adhesive and the adherend. Irrespective of any surface interaction with the adhesive, the highly micro-rough, nodular surface created by the EP2472 process would, if fully wetted by the adhesive, provide an ideal surface topography for bonding.

The extended "interphase" formed by the PAA provides the best bonding surface of those used in the present study.

In summary:

- Surface analysis by AES and SEM highlight differences in topography and chemistry between the three "standard" conversion coatings with 5 minute treatment times at 20°C.

- Initial joint strength results indicate that both the mechanical and chemical treatments provide significant improvements compared with the degreased-only control.

- All three conversion coatings out-performed both the degrease-only and the grit-blast treatments in the stressed durability trials.

- In the stressed durability trials, the chromate-free treatments out-performed the established chromate-phosphate conversion coating at low applied loads (0.2 and 0.5 kN). All conversion coatings performed similarly at loads $\geq$1 kN.

- The chromate-containing optimised CAE performed similarly to the EP2472 process. However, as in many other studies, the PAA provided the best initial joint strengths and durability as measured by static stress in a hot-wet environment.

- The effects of applied stress in combination with elevated temperatures and water immersion on adhesive joints has yet to be fully investigated. These three factors are experienced by many joints in service and, therefore, it is appropriate that they should be studied in combination if durability results are to reflect service conditions. It is likely that at low applied loads the increased exposure times to water and elevated temperatures prior to failure enables water ingress to be a contributory factor in joint failure. However, at high applied loads creep of the adhesive might be the dominant failure mechanism.

4.3 HYDRATION STUDIES OF TREATED ALUMINIUM

Modification of the degreased-only, grit-blasted, Bonderite 705, Bonderite 777, optimised CAE and PAA treated surfaces was evident after immersion in DI water at 60°C for as little as 5 hours. Complete coating by "cornflake-like" structures resulted in as little as 20 hours with all of the aforementioned treatments; these structures have previously been reported to comprise boehmite or pseudo-boehmite. In addition, larger crystalline features were present after an extended exposure time up to 120 hours. The features, observed by SEM, were consistent with the presence of larger hydration products on these surfaces. XRD was used to confirm that the larger features were hydration products, $Al(OH)_3$, with the bayerite form present in all cases and gibbsite occasionally observed.

Significantly, none of the aforementioned treatments afforded any measurable hydration resistance to the aluminium 5251 alloy compared with simply degreasing under the exposure conditions used. It is important to note that the same exposure conditions, namely, full immersion in DI water at 60°C were used in many durability trials in the present programme.

The patchiness of the Bonderite 705 treatment could account for its poor performance in this experiment with hydration possibly being initiated in the bare areas.

The Bonderite 777 process produces a relatively thin passivating or barrier layer originally devised as a prepaint or prelacquer process and not as a stand-alone process for surface passivation[189]. This relatively thin film, extending to only ~15 nm, contrasts with the many tens of microns of anodic oxide used for passivation of architectural aluminium.

The hydration of CAE and PAA treated aluminium has been widely discussed in the literature. For example Venables[46] reports that, as a result of immersion in DI water at 80°C, the incubation time for the CAE surface before the onset of corrosion was

approximately 2 minutes whilst for PAA values were recorded as high as 15 to 16 hours.

In addition, Davis *et al*[138] used a combination of X-ray photoelectron spectroscopy (XPS), scanning transmission electron microscopy (STEM) and electron diffraction (ED) to determine the decomposition mechanism of the BAC 5555 PAA oxide as a consequence of immersion in 100% RH at 50°C. It was established that an overlayer of decomposition product was produced after 72 hours exposure. ED showed this to be boehmite. Crystallites of a further product were observed after 192 hours. ED identified that these crystallites were of bayerite. It was concluded that the freshly-prepared PAA surface comprised a combination of $AlPO_4$, Al_2O_3 and H_2O. The phosphate component of this layer was proposed to decompose by the following mechanism:

$$AlPO_4 \rightarrow Al_2O_3 \rightarrow AlOOH \rightarrow Al(OH)_3$$

It is suggested that it is the time taken for the initial reaction to occur which rate limits the decomposition mechanism, thereby, providing the PAA surface with a degree of hydration resistance. It should be noted, however, that the exposure time of joints in the present durability trials is large compared with these incubation times.

The EP2472 treatment provides the best resistance to hydration of those studied in the present work. No surface modification was evident after 120 hours and only limited changes were introduced to the surface after 550 hours exposure. The complex nature of the EP2472 film chemistry prevents a full understanding of the reasons for this performance at the present time.

It should be noted that AES was not used to study the hydration performance of these treatments due to the possible influence of the vacuum on the hydrated oxide by the vacuum. The possibility of a reversible reaction occurring has been identified by Nylund and Olefjord[190].

4.4 SURFACE PARAMETERS

It was reported in Section 1.1, that the following adherend surface parameters might be modified by a particular treatment in order to optimise bond durability: roughness, hydration resistance, contamination-level, wettability and chemistry.

The present research programme provides information on each of these topics and how they inter-relate, as discussed below:

4.4.1 ROUGHNESS

Chemical and electrochemical treatments have been demonstrated to form micro-rough surfaces which, if fully wetted, form a "micro-composite interphase". For example, the Bonderite 705 process, if optimised, provides a columnar porous structure which provide good initial bonds and durability. However, it has also been demonstrated that over-treatment forms poor initial joint strengths and reduced durability whilst retaining the same surface chemistry. The production of a planar rather than a porous surface, at least partly, accounts for this effect.

A complicating factor is evinced by the formation of the characteristic "mud crack" type morphology, with the thicker Bonderite 705 conversion coatings, caused by the loss of water from the film. This effect influences the subsequently-produced joint in two ways: the loss of water leads to a mechanical weakening of the film so that joint failure can become cohesive within this layer, and; if a high temperature curing adhesive is used, further water loss occurs from the conversion coating during the cure stage leading to the displacement of adhesive from the surface and the formation of voids within the adhesive. This results in poor initial joint strengths due to the lack of adhesive-adherend interaction and a reduction in durability since water is able to rapidly penetrate the joint through the voids.

A similar effect has been observed, by the present author, on hot dipped galvanised zinc (HDG) surfaces treated by commercially-used chromate- and phosphate-based conversion coatings. In both instances, the treatments produced the required micro-rough surfaces by the formation of the hydrated metal oxides on the HDG surface; however, water loss from the conversion coatings during the cure of a subsequently applied 190°C curing epoxide adhesive resulted in large voids in the adhesive and little contact between the adhesive and the substrate[191].

As discussed in Section 4.2.1, the degree of surface macro-roughness can have an influence on both initial joint strengths and durability. Initial joint strengths are much improved by providing macro-rough, as opposed to a planar, surfaces possibly due to increased areas over which interactions can occur or, as previously mentioned, by the reduction of stresses within the joint due to the formation of an "interphase". However, it is significant that a reduction in durability has been demonstrated with macro-rough surfaces which might be incompletely wetted by the adhesive. Such a situation could also result in voids at the adhesive-adherend interface which might facilitate rapid transport of water to the bondline with the resultant disruption of interfacial bonds.

In summary, surface micro-and macro-roughness are required to optimise initial joint strengths and durability. The manner in which such roughness is produced can profoundly influence the joint performance. Surface roughness is only beneficial if the features are properly wetted by the subsequently applied adhesive. If not, the resultant voids can have an adverse effect on durability by providing pathways for the rapid ingress of water to the joint.

4.4.2 HYDRATION RESISTANCE

Many durability studies relate the performance of aluminium joints with different surface treatments exposed to elevated temperatures usually combined with a high relative humidity (RH) or full immersion in water. A number of approaches have been taken to explain the performance of different alloy / adhesive / treatment systems in

such studies.

There are two methods by which water can enter the metal-to-metal joint. Firstly, transported by capillary action along the interface as discussed above. Secondly, and the most commonly considered effect is diffusion through the permeable adhesive. The rate at which water ingresses into the SLS joint has been modelled assuming Fickian diffusion[122,192]. In the work by Brewis *et al*[122], using the Fickian Diffusion model, it was found that there was good agreement between the loss of SLS joint strength with chromic acid etched (CAE) adherends and the total water absorbed. This correlation led to the conclusion that "the loss of strength is primarily dependent upon the water uptake within the adhesive".

The aforementioned work, along with that of other workers, has been concerned with the effects of water within the joint. For example, in a recent paper by Bowditch[150], three main explanations were proposed to account for the damaging effects of water on joints: Firstly, water is absorbed by the adhesive; initially, this might lead to plasticisation and to improved joint performance by the relief of shrinkage stresses within the adhesive which were created during the cure stage. However, it is recognised that prolonged exposure to water or its vapour might cause a mechanical weakening of the adhesive or boundary polymer which would have a detrimental effect upon the joint; Secondly, water might displace adhesive at the interface thereby destroying the inter-atomic bonds between the metal and the polymer, again leading to a reduction in joint strength; Thirdly, and most significantly in the context of this section, by hydration of the omnipresent aluminium oxide is thought to occur, thereby, leading to a cohesively weak zone within which joint failure occurs.

Joint failure by this third mechanism has been reported by many workers. For example, in 1975, Bethune[72] outlined studies conducted using CAE treated adherends in SLS joints which were simultaneously exposed to 100% RH at 60°C and stress, in the range 2.1 to 8.3 MPa. The joints stressed to 8.3 MPa had a maximum survival times of approximately 20 days whilst those exposed to 4.2 MPa survived for 80 days.

In all cases failure was attributed to hydration and weakening of the CAE oxide. Supporting evidence was provided by SEM which observed hydration products on both metal and adhesive sides of the failed joints. Bethune concluded from this work, that, in order to provide durable joints with aluminium, the treated surface should be "highly resistant if not inert".

The aforementioned review article by Venables[46], published in 1984, details a number of projects carried out by representatives of Boeing into joint failure analysis and the related topics of hydration formation and the use of inhibitors. In wedge tests conducted at 65°C, 100%RH ,again with CAE adherends, it was reported that 60 nm of hydrated metal oxide was attached to the adhesive side of the failed joint. This compares with a previously determined CAE oxide thickness of 20 nm. It was again concluded that the metal oxide had hydrated and become detached from the adherend. The factor of three increase was attributed to swelling as a result of hydration. AES was used to indicate that the hydration product was boehmite ($Al_2O_3.H_2O$) and pseudo-boehmite ($Al_2O_3.2H_2O$). This result was confirmed by ED.

Venables concluded that: "the long-term durability of metal-polymer bonds is determined to a great extent by the environmental stability (or lack of it) of the oxide that is responsible for promoting good bond strengths".

As a consequence of such work, it is widely thought that the metal treatment used prior to bonding of aluminium should provide a degree of hydration resistance. This aspect has been studied to a limited extent by Noland[70] and, in more detail, by Davis *et al*[138].

The purpose of the work detailed in Section 4.3 was to identify the rate at which hydration occurred on aluminium alloy surfaces which had undergone one of a range of different treatments. It should be noted that bare adherends were used in the present work. The complicating factors introduced by hydration inhibitors, which might be incorporated into an adhesive, is outside of the scope of the present study.

From the aforementioned work it could be concluded that both untreated and treated adherends would all undergo hydration within the timescales of the many durability trials; this includes both the commonly-used CAE and PAA and the novel conversion coatings used in this programme. The time taken for water to get into the joint is a limiting factor.

This was measured experimentally using anhydrous copper sulphate-loaded Araldite AV119 where exposure times of approximately 8 to 10 weeks were required in the unstressed condition for complete saturation of 20 x 10 mm overlap joints in DI water at 60°C.

It is therefore concluded that the hydration resistance of treated aluminium surfaces cannot fully explain their performance in accelerated durability trials with SLS joints. It is possible that, in some of the reported cases indicating failure within a hydrated oxide, post-failure exposure has occurred with subsequent hydration of the bare adherend. This effect has been observed in the present study.

Perhaps of more significance in determining the rate of metal hydration is the choice of adhesive used; some adhesives contain hydration inhibitors whilst others do not. In a recent paper by Brewis and Critchlow[193], aluminium 5251 adherends were treated using CAE, assembled into T-peel joints and then immersed in DI water at 60°C for a period of 19 days. The adhesives used were 3M's 3532, a two-part polyurethane, and Araldite 2007, a single-part epoxide. The joints utilising the polyurethane demonstrated poor durability and failed within a weakly-cohesive hydrated layer. In contrast, the Araldite 2007 exhibited much better durability and a mixed failure mode, being mainly interfacial with some cohesive failure within the adhesive. It is not known whether either of the adhesives used contain hydration inhibitors, as such information is not readily available. However, it is significant that the choice of adhesive is the only variable in these two instances where one adherend underwent hydration and the other did not. Differences in diffusion coefficients may also contribute to this effect.

Recent work by Bremont and Brockmann[194] indicates that the alloy type has a significant effect upon the hydration resistance. In particular, the magnesium content of the surface is considered to be important in this aspect. This will be discussed in Section 4.4.5.

4.4.3 WETTABILITY

All clean metal oxides have high energy surfaces which should give zero-degree contact angles when wetted with water or organic compounds with reasonably low viscocity. Typically, surface energies should be of the order of 1 $J.m^{-2}$ compared with approximately 73 $mJ.m^{-2}$ required for water to spread[39].

Many studies have used contact angles to determine surface energies; however, as the data presented in Figure 20 indicate, under normal laboratory conditions atomically-clean metal surfaces readily adsorb organic contamination in a matter of seconds. This is indicated by the general increase in θ_c with surface exposure time (SET). The resultant effect is that the contact angle measured after only a limited SET does not reflect the surface energy of the freshly-treated material. This problem is exacerbated if a degree of drying is required, for example with a wet chemical process. This was studied by cleaning a flat piece of aluminium metallised silicon wafer with the CO_2-laser to produce a zero degree contact angle with water; after 30 minutes in an air oven at 120°C the surface gave a contact angle of 70 to 80°. The adsorption of organic material could lead to erroneous measurement of surface energies and the work of adhesion.

Furthermore, double-degreased surfaces have been demonstrated to provide a contact angle of approximately 50° indicating some possibly chemisorbed material. This might be different given a vapour degrease rather than an ultra-sonic immersion treatment. AES results from double-degreased surfaces confirm the presence of organic contamination.

As discussed in the previous section, an incompletely wetted surface can lead to voids in the interfacial region with the resultant loss in joint performance.

The beneficial effect of increasing the surface wettability was observed with the CO_2-laser cleaned aluminium alloy. The laser-cleaned 5251 aluminium alloy surface produces only limited changes in surface chemistry and topography; there is, however, a measurable increase in initial joint strength and durability. Different effects were observed with different adhesives.

A complicating factor is if the organic present is absorbed by the adhesive then there may be no loss in joint performance. For example, in some industrial situations the Bonderite 705 surface is primed with a controlled "contaminant" which reduces the surface energy and enables the surface to be stored for many months prior to bonding with no loss in performance. This effect was observed in our study where the mild steel surfaces were either bonded immediately after laser treatment or left unbonded for approximately two days. After the extended SET the contact angle was approximately 45°. The joints performed similarly in terms of both initial joint strengths and durability to those bonded after only 30 seconds.

4.4.4 CONTAMINATION-LEVEL

Surface contamination by rolling oils and lubricants occurs on all mill-finished metals. Such material would be expected to reduce the wettability as discussed above, provide a barrier to the formation of interfacial bonds and mask desirable surface topography.

In all of the studies presented herein the miniumum surface treatment involved a solvent degrease thereby removing the majority of the contaminants.

The main source of surface contamination occurring post-treatment and prior to bonding is adventitious organics as indicated by the contact angle versus SET plot; see Figure 20. As discussed in Section 4.4.3 this may or may not have an impact upon joint performance depending upon whether or not this is absorbed by the adhesive.

4.4.5 CHEMISTRY

Of particular concern in the present section is the role of magnesium, an alloying element in aluminium 5251, on bond performance. The influence of high levels of magnesium at the aluminium alloy surface has been shown by Kinloch *et al*[97] to be associated with poor bond durability, although it was pointed out that other factors may be operating. In other studies, for example that by Poole and Watts[109], this correlation was not observed. It is appropriate to compare the results obtained in the present study with those of other workers. AES was used in Sections 3.2.1 and 3.2.2 of the present study to determine variations in surface magnesium content; these data can be combined with the SEM data in Section 3.2.2 to isolate the influence of surface chemistry on the joint strength data from that of the topography.

Surface Mg:Al ratios for the grit-blasted samples are given in Table 12. Comparing the surface texture parameters for the 320 and 180/220 grit-blasted surfaces in Table 13, it can be seen that these treatments produce similar surface profiles. There is, however, a difference in surface magnesium composition in these two instances. The 180/220 grade grit produces a surface which is relatively rich in magnesium compared with the 320 grade. This difference is not reflected in either the initial joint strength data or those obtained after exposure; see Table 18.

The presence of surface magnesium therefore seems to have no detrimental effects on initial SLS joint strengths or their unstressed durability performance. Further evidence was provided by the unstressed durability performance of degreased-only SLS joints. The data presented in Table 18 indicate that there is no significant change in the joint strengths with the degreased-only adherends after exposure for up to 211 days. It is clear from the data in Table 19 that the failure modes are similar for both initial and exposed joints with degreased-only adherends. It is therefore concluded that there has been no reduction in interfacial adhesion between the adhesive and the magnesium-rich oxide on the degreased-only surface after exposure to DI water at 60°C for up to 211 days. In addition, the often suggested failure mechanism by which the magnesium-rich oxide is hydrated to form a cohesively-weak layer has not been observed. In

summary, the magnesium-rich oxide on this alloy appears to provide relatively hydrolytically stable bonds and does not appear to readily hydrate.

The poor initial joint strengths produced by this surface suggests two possibilities: the magnesium-rich oxide itself is cohesively weak, or; that its planar rather than textured nature has a significantly detrimental effect on subsequent joint strengths.

This result is in contrast with the aforementioned work by Kinloch *et al*[134]. They found that for degreased-only joints, adherends formed from high magnesium containing aluminium alloys performed less well in durability trials than those containing little or no magnesium. In that study, degreased-only NE4 adherends (a similar alloy to 5251) retained only ~20% of their initial joint strengths after immersion in deionised water for 62 days at 60°C. However, they used a different adhesive in a butt joint configuration. The adhesive used in the present study i.e. Araldite 2007 is known to impart excellent durability and, furthermore, it is known that the butt joint configuration can be more sensitive to environmental exposure than the single lap shear configuration. It was proposed by Kinloch *et al*[134] that the high magnesium content within the oxide would be expected to affect the rate of oxide hydration and that such hydration would lead to a cohesively weak oxide. In that study, degreased-only adherends had surface Mg:Al ratios up to 0.3. In the present study, the presence of magnesium, even at the relatively high levels observed after grit-blasting, seems to have little influence on either initial joint strength or durability. This conclusion is in line with that of Poole and Watts[109], who, using a 120°C-curing modified epoxy supported film adhesive, assessed durability by the Boeing wedge test. The present work shows that magnesium at a higher level (Mg:Al ratios >0.5), on the degreased-only surface, facilitates a change in the failure mechanism i.e. there is cohesive failure within the magnesium-rich oxide. Whilst this mechanism has a detrimental effect on initial joint strengths, excellent durability, in terms of percentage strength retention with exposure time, was observed with the degreased-only adherends.

In contrast, it was noted that the adhesive used in the present study provided excellent durability with degreased-only aluminium alloy despite the high magnesium content in the surface region. This effect was observed in recently reported work by Brémont and Brockmann[194]. In their study, the surface compositions of degreased-only AlMg3 and clad AlCuMg2 alloys were correlated with bond durability results. The exposure conditions for aluminium alloy-epoxide SLS joints were either full immersion in water at 70°C for up to 12 weeks, or, exposure to 5% salt-spray at 35°C for up to 6 weeks. The Mg/Al values for the AlMg3 and clad AlCuMg2 alloys were approximately 1.2 and 0.4 respectively; the former result indicating a similarly high degree of surface magnesium enrichment in the degreased-only aluminium-magnesium alloy as in the present study. The clad alloy would be expected to have little or no magnesium in the outer layers since a relatively pure aluminium layer, approximately 50 μm thick, would be present as the cladding. Following 8 weeks exposure to water at 70°C the AlMg3 alloy joints retained approximately 100% of their initial strengths whilst the clad AlCuMg2 adherends retained only 52%. Interestingly, with grit-blasted AlMg3 adherends the surface Mg/Al values reduced to approximately 0.1 and the joints retained only 85% of their initial values after 8 weeks in this test. It was concluded that, "the morphology of the metal substrate seems to play a less important role than the surface composition and, in particular, the Al/Mg ratio on the hydrolytic stability". To verify this statement, XPS was used in joint failure studies. With the clad AlCuMg2, XPS demonstrated full hydration of the oxide layer with resultant joint failure whilst the degree of corrosion of the AlMg3 joints was described as "limited". A similar improvement in durability performance was observed with joints prepared with degreased-only AlMg3 compared with clad AlCuMg2 alloy adherends and exposed to the corrosive salt-spray environment. One firm conclusion drawn from this work by Brémont and Brockmann is that "a high magnesium content in the oxide layer leads to a better hydrolytic stability of the bonded joint"; attributable to the "high stability of magnesium oxides". This conclusion is in good agreement with the statements made above from the present study, and is apparently opposed to that by Kinloch and co-workers[97,134].

CHAPTER 5 - CONCLUSIONS

A number of novel or developmental treatments have been considered in terms of both how these treatments modify the aluminium 5251 alloy surface and how the changes introduced influence the durability of subsequently-produced joints.

The following surface treatments were studied: grit-blasting; Bonderite 705, a chromate-phosphate conversion coating; Bonderite 777, a zirconia-based conversion coating; EP2472, a mixed phase conversion coating, and; CO_2-laser ablation. These treatments were compared to degreased-only, chromic acid etched and phosphoric acid anodised controls.

Grit-blasting was demonstrated to remove the pre-existing, planar, friable, magnesium-rich oxide on the mill-finished and degreased-only surface. This is followed by the formation of a macro-rough surface with roughness parameters and precise surface chemistry dependent upon the grade of alumina grit used. These changes facilitate an increase in initial joint strengths over degreased-only controls. However, in terms of the percentage strength retention, and in some cases absolute values in unstressed durability trials, grit-blasted adherends performed worse than those which had been simply degreased. The unfavourable unstressed durability performance was attributed to poor wettability of the grit-blasted surfaces enabling rapid transport of water to the adhesive-adherend interface resulting in the destruction of interfacial bonds. The stressed durability performance of the grit-blasted joints was far superior at all loads to the degreased. The exceptionally poor performance of the degreased-only adherends was attributed largely to failure within the oxide.

Optimisation of the Bonderite 705 treatment enabled the production of a micro-rough, highly complex, mixed oxide structure. In impact tests this treatment was shown to be effective in terms of initial energy absorption and in durability compared to alkaline cleaning. Extended treatment times were shown to provide a planar surface with

reduced joint test performance. A "standard", rather than optimised, Bonderite 705 film was shown to provide stressed durability performance better than the grit-blast but slightly worse than the optimised chromic acid etch.

The Bonderite 777 process has been shown to produce a similar surface texture to the optimised chromic acid etch and to perform similarly in stressed durability. There are, however, differences in the surface chemistry in these two cases; the Bonderite 777 process provides a zirconium-based oxide with a phosphate component whilst the optimised chromic acid etch produces an aluminium oxide surface.

The most promising of the conversion coatings studied is the EP2472 treatment. This process produces a highly nodular, mixed organic-inorganic phase deposit. Such a surface provides good initial SLS joint strengths and durability comparable to or better than the optimised chromic acid etch. It does not, however, provide such good durability as the phosphoric acid anodise.

With aluminium, the CO_2-laser ablation process provides little or no change in surface texture but does modify the surface and sub-surface chemistry. The most noticeable effect is the complete removal of surface organic contamination which, at least in part, provides a significant increase in initial joint strengths and stressed durability. A larger effect was observed when the CO_2-laser interacted with mild steel adherends. The formation of an atomically-clean, glassy surface was shown to provide an increase in initial joint strengths to that produced by grit-blasting plus silane application. However, the unstressed durability performance was not so convincing. A mechanism has been proposed to explain the laser-surface interaction.

It was mentioned, in the *Introduction*, that a number of key physico-chemical parameters were widely recognised as necessary to provide enhanced durability of the untreated material. A consideration of these parameters has been given. Also, of significance, is the role of surface hydration in the joint failure mechanisms. It is concluded that at the test temperatures used there is no direct correlation between the

rate of hydration and the type of surface treatment, and, that hydration of the metal oxide did not appear to be a significant factor in the failure of any of the joints in the main durability trials.

In addition, other factors are considered which are considered to be relevant in preparing aluminium surfaces for bonding such as the role of surface magnesium and surface exposure times. Such information advances the current understanding on the role of surface parameters on adhesive bonding and is vital in understanding the effectiveness of surface treatments for this application.

CHAPTER 6 - FUTURE STUDIES

Further studies are required if the chromate-free conversion coatings and CO_2-laser ablation treatments are to be validated for use as commercially-viable treatments prior to structural adhesive bonding. The use of double cantilever beam specimens and a consideration of the fracture mechanics is essential to quantitatively asses the performance of these treatments.

A greater understanding is required of the mechanism of adhesion between the epoxide adhesive and treated aluminium surfaces. SSIMS, XPS and infra-red (IR) analyses have been used with model systems by Boerio, Ishida, Koenig and others to provide such information. A research programme is planned to combine these techniques in a study using monolayer-thin adhesive films deposited onto model substrates to, hopefully, provide evidence for the formation of covalent bonds between the adhesive and the adherend. The experimental protocol established is expected to be adopted for similar studies on technologically-important surfaces. If evidence for covalent bonding can be established, the next stage would be to determine the influence of stress and water thereon.

Information on the reaction kinetics could be obtained by determination of activation energies for polymer-metal bond formation, E_a, from differently-treated metal powders. The treatments providing a large value of E_a should, theoretically, provide good stressed durability. It would be interesting to obtain this relationship experimentally.

Electrochemical studies are in progress to more fully quantify the hydration rates of the different surface treatments. These data would provide a better indication of the correlation between surface hydration and bond durability. In combination, conductive adhesives could be used in exposed joints to directly measure the degree of surface hydration beneath the adhesive layer. Similarly, for aluminium alloys, the influence

of high versus low levels of surface magnesium could be studied in terms of their hydration rates. Although it is known that magnesium oxides are the more stable in alkaline media, the mixed oxides or hydrated oxides found on pretreated surfaces provide some complicating factors.

The majority of studies within this programme have utilised a single-part structural epoxide. Other adhesives could be considered. Similarly, only a limited range of tests have been used in the present programme. It is envisaged that a range of test configurations, for example SLS, SSLS, wedge, TDCB, blister, napkin ring and peel will be used with a single adherend and a range of treatments to establish the parameters evaluated by each method. Surface analysis could be used to precisely identify the failure modes.

The EP2472 process is particularly promising, optimisation experiments are in progress to get the T_f versus applied load line closer to that of the PAA. To date, treatment times have been varied; other parameters such as pH and temperature are to be optimised.

Preliminary neutron scattering experiments have already been conducted at the Institut Laue-Langevin (ILL), Grenoble to study the influence of in-situ stresses within unaged and aged joints under static loading. Initial results from this study indicate extremely high residual stresses in freshly-prepared epoxide-mild steel joints with much reduced levels in specimens aged for approximately 10 days in DI water at 60°C. Further investigations into the measurement and causes of such stresses are the subject of current collaborative work between ILL and Loughborough University.

REFERENCES

1. "Adhesives in engineering", A.J.Kinloch, *I.Mech.E. 1996 Preprint No.8.*
2. "Primary bonded aircraft wing construction", P.K.Nelson and W.D.Sanders, *Proc.27th Nat.SAMPE Symposium*, May 4-6, 1982, 967-977.
3. *Handbook of Aluminum Bonding Technology and Data*, J.D.Minford, Marcel Dekker, New York, 1993.
4. *Adhesive Bonding of Aluminum Alloys*, Eds.E.W.Thrall and R.W.Shannon, Marcel Dekker, New York, 1985.
5. "Adhesive bonding of aircraft primary structures", L.J.Hart-Smith, *S.A.E.*, 1980, 99-113.
6. "Bonding methods, the Airbus A300 as an example", *Aircraft Engineering*, May 1979, 28.
7. "Chapter 5: Aluminium adherends", D.M.Brewis in *Durability of Structural Adhesives*, Ed.A.J.Kinloch, Applied Science Publishers, 1983, 215-254.
8. "Review of surface pretreatments for aluminium", G.W.Critchlow and D.M.Brewis, *Int.J.Adhesion & Adhesives*, 1996, **16**, 255-275.
9. "Adhesion and surface analysis", D.M.Brewis and G.W.Critchlow, *J.Adhesion*, 1995, **54**, 175-199.
10. "Predicting the fatigue life of adhesively-bonded joints", A.J.Kinloch and S.O.Osiyemi, *J.Adhesion*, 1993, **43**, 79-90.
11. "Durability of adhesive bonds to aluminium", D.W.Levi, *J.Appl.Polym.Sci:Appl.Polym.Symp.32*, 1977, 189-199.
12. "Chapter 6: Mechanical behaviour of adhesive joints" in *Adhesion and Adhesives, Science and Technology*, A.J.Kinloch, Chapman and Hall, London, 1987, 188-263.
13. "Chapter 3: Standard mechanical test procedures" in *Structural Adhesive Joints in Engineering*, R.D.Adams and W.C.Wake, Elsevier Applied Science Publishers, London, 1984, 115-142.
14. "Theories of adhesion", K.W.Allen in *Handbook of Adhesion*, Ed.D.E.Packham, Longman Scientific & Technical, 1992, 473-475.

15. "Chapter 1: Introduction", D.M.Brewis in *Surface Analysis and Pretreatment of Plastics and Metals*, Ed.D.M.Brewis, Applied Science Publishers, 1982, 1-10.
16. "Chapter 3: Mechanisms of adhesion" in *Adhesion and Adhesives, Science and Technology*, A.J.Kinloch, Chapman and Hall, London, 1987, 56-100.
17. *Fundamentals of adhesion*, Ed.L.-H.Lee, Plenum Press, New York, 1991.
18. "Oxide morphologies on aluminum prepared for adhesive bonding" J.D.Venables, D.K.McNamara, J.M.Chen, T.S.Sun and R.L.Hopping, *Appl.Surf.Sci.*, 1979, **3**, 88-98.
19. "The effects of fluorine contamination on the microstructure and bondability of aluminum surfaces" J.M.Chen, T.S.Sun and J.D.Venables, *SAMPE J.*, July-August 1978, 22-27.
20. "Prebond handling of aluminum surfaces for adhesive bonding", D.K.McNamara, J.D.Venables, T.S.Sun, J.M.Chen and R.L.Hopping, *Proc.11th Nat.SAMPE Tech.Conf.*, November 13-15 1979, 740-751.
21. "Effects of the environment on bonded aluminium joints: an examination by electron microscopy", J.A.Bishopp, E.K.Sim, G.E.Thompson and G.C.Wood in *Adhesion 13*, Ed.K.W.Allen, Elsevier Applied Science, 1989, 201-219.
22. "Instrumental techniques for the surface analysis of materials", G.W.Critchlow, *Trans.IMF.*, 1996, **74**(3), 108-114.
23. *Practical Surface Analysis, Second Edition, Volume 1 - Auger and X-ray Photoelectron Spectroscopy*, Eds.D.Briggs and M.P.Seah, John Wiley and Sons, Chichester, 1990.
24. *Modern Techniques of Surface Science*, D.P.Woodruff and T.A.Delchar, Cambridge University Press, Cambridge, 1986.
25. *Practical Surface Analysis by Secondary Ion and Neutral Mass Spectrometry*, Eds. D.Briggs and M.P.Seah, John Wiley and Sons, Chichester, 1992.
26. *Methods of Surface Analysis*, Ed. J.M.Walls, Cambridge University Press, Cambridge, 1989.
27. *An Introduction to Surface Analysis by Electron Spectroscopy*, J.F.Watts, Oxford University Press, Oxford, 1990.

28. *Quantitative Surface Analysis for Materials Science*, G.C.Smith, The Institute of Metals, London, 1991.

29. *Handbook of Auger Electron Spectroscopy*, Physical Electronics Industries Inc., Minnesota, USA, 1976.

30. "Chapter 4 - Depth profiling in AES and XPS", S.Hofmann in *Practical Surface Analysis, Second Edition, Volume 1 - Auger and X-ray Photoelectron Spectroscopy*, Eds.D.Briggs and M.P.Seah, John Wiley and Sons, Chichester, 1990, 149.

31. "Pure element sputter yields using 500-1000 eV argon ions", M.P.Seah, *Thin Solid Films*, (1981), **81**, 279-287.

32. "Instrumentation", J.C.Rivière in *Practical Surface Analysis, Second Edition, Volume 1 - Auger and X-ray Photoelectron Spectroscopy*, Eds.D.Briggs and M.P.Seah, John Wiley and Sons, Chichester, UK, 1990, 51-60.

33. "Recent developments in spatially resolved ESCA", R.L.Chaney, *Surf.Interface Anal.*, 1987, **10**, 36-47.

34. *Handbook of X-ray Photoelectron Spectroscopy*, Physical Electronics Industries Inc., Minnesota, USA, 1979.

35. "Spectral interpretation", D.Briggs and J.C.Rivière in *Practical Surface Analysis, Second Edition, Volume 1 - Auger and X-ray Photoelectron Spectroscopy*, Eds.D.Briggs and M.P.Seah, John Wiley and Sons, Chichester, UK, 1990, 85-141.

36. *Fundamentals of Surface and Thin Film Analysis*, L.C.Feldman and J.W.Mayer, Elsevier Science Publishing, New York, 1986, 167-173.

37. *Powder Diffraction File: Alphabetical Index - Inorganic Phases*, Chief Ed. W.F.McClune, J.C.P.D.S., Int.Centre for Diffraction Data, Swathmore, USA, 1987, and; *X-ray Powder Diffraction Files*, A.S.T.M, Philidelphia, 1960.

38. *Electron Microscopy and Analysis*, P.J.Goodhew, Wykham Publications, London, 1975.

39. "Chapter 6 - Thermodynamics of wetting: from its molecular basis to technological application", D.G.Rance in *Surface Analysis and Pretreatment of Plastics and Metals*, Ed.D.M.Brewis, Applied Science Publishers, London, 1982, 121-152.

40. "Contact angles, wetting, and adhesion: a critical review", R.J.Good, J.Adhesion.Sci.Technol., 1992, 6(12), 1269-1302.

41. *Introduction to Thermal Analysis: Techniques and Applications*, M.E.Brown, Chapman and Hall, London, 1988.

42. "Adhesion of aluminum for application in the automotive industry: cross-linking at interfaces", L.Martin and W.Brockmann, *Proc.Euradh '96*, 3-6 September 1996, Cambridge, U.K., 595-600.

43. "Kinetic analysis of derivative curves in thermal analysis", T.Ozawa, *J.Thermal Analysis*, 1970, **2**, 301-324.

44. "Kinetics of epoxy-amine cure reactions at alumina surfaces", W.X.Zukas, S.E.Wentworth and M.S.Sennett, *Proc.16th Annual Meeting of the Adhesion Soc.*, 21-26 February 1993, Williamsburg, Virginia, USA, 187-190.

45. "Adhesion in bonded aluminium joints for aircraft construction", W.Brockmann, O.-D.Hennemann, H.Kollek and C.Matz, *Int.J.Adhes.Adhes.*, 1986, **6**(3), 115-143.

46. "Review: adhesion and durability of metal - polymer bonds", J.D.Venables, *J.Mat.Sci.*, 1984, **19**, 2431-2453.

47. "Adhesive bonding of aluminum alloys", Eds.E.W.Thrall and R.W.Shannon, (1985), Marcel Dekker, New York.

48. "UK patent No.2 167 443A", A.Maddison, P.G.Sheasby and N.C.Davies, Published 29th May 1986.

49. "A.C. anodizing of aluminium in phosphoric acid", D.J.Arrowsmith, D.A.Moth and A.Maddison, *Trans.IMF*, 1987, **65**, 38-44.

50. "Durability of adhesive joints under impact conditions", G.W.Critchlow and A.Maddison, *Surf.Interf.Anal.*, 1991, **17**(7), 539-541.

51. "How weathering and aging affect bonded aluminum", R.F.Wegman, W.M.Bodnar, E.S.Duda and M.J.Bodnar, *Adhesives Age*, (1967), **10**, 22-26.

52. "Durability of structural adhesive bonded aluminum", J.D.Minford, *Adhesives Age*, March 1978, **21**(3), 17-23.

53. "Comparison of aluminum adhesive joint durability as influenced by etching and anodizing pretreatments of bonded surfaces", J.D.Minford, *J.Appl.Polym.Sci.*, 1977, **32**, 91-103.

54. "The morphology and mechanism of formation of porous anodic films on aluminium", J.P.O'Sullivan and G.C.Wood, *Proc.Royal Soc.Lond.*, 1970, **A**(317), 511-543.

55. "Joint durability studies with abraded, etched, coated and anodized adherends", J.D.Minford, *Proc.Org.Coat.Appl.Polym.Sci.*, 1982, **47**, 189-193.

56. "Adhesive bonding of aerospace materials - surface characterisation of metallic adherends", M.Charbonnier, M.Romand, A.Roche and F.Gaillard, *Int.J.Adhes.Adhes.*, 1986, **6**(4), 199-206.

57. "An XPS study of chromate pretreatment of aluminum", J.A.Treverton and N.C.Davies, *Metals Technology*, 1977, **4**(10), 480-489.

58. "Effect of surface preparation on stressed aluminum joints in corrosive saltwater exposure", J.D.Minford, *Adhesives Age*, 1980, **23**(10), 36-41.

59. "UK Patent No.GB 2 139 540 A", P.G.Selwood, A.Maddison and P.G.Sheasby, Published 14th Nov. 1984.

60. "Evaluation of adhesives for aluminium structured vehicles", W.F.Marwick and P.G.Sheasby, *S.A.E.Tech.Paper*, 870151, 1987.

61. "The morphology, structure and mechanism of growth of chemical conversion coatings on aluminium", G.M.Brown, K.Shimizu, G.E.Thompson and G.C.Wood, *Corrosion Sci.*, 1992, **33**(9), 1371-1385.

62. "Topographical and surface chemical studies of chromate-phosphate pretreatment films on aluminium surfaces", J.A.Treverton, M.P.Armor and A.Bosland, *Corrosion Sci.*, 1992, **33**(9), 1411-1426.

63. "The effect of pretreatment on the high strain rate behaviour of adhesively bonded aluminium", A.Maddison and G.W.Critchlow, *Proc.16th Annual Meet.Adhes.Soc.*, Feb. 1993, 73-76.

64. "Effect of certain hostile environments on adhesive joints", C.Kerr, N.C.MacDonald and S.J.Orman, *J.Appl.Chem.*, 1967, **17**, 62-65.

65. "Outdoor durability of adhesive joints under stress", G.F.Carter, *Adhesives Age*, 1967, **10**, 32-37.

66. "Surface preparation for adhesive bonding", C.W.Jennings, *Appl.Polym.Symp.19*, 1972, 49-61.

67. "A comparative test for bondline corrosion: Clad versus bare aluminum", N.L.Rogers, *Proc.5th Nat.SAMPE.Tech.Conf.*, 1973, 160-183.

68. "Surface oxide on etched aluminium", A.W.Smith, *J.Electrochem.Soc.*, 1973, **120**(11), 1551-1557.

69. "The relation of surface condition after pretreatment to bondability of aluminum alloys", P.F.A.Bijlmer and R.J.Schliekelemann, *SAMPE Quarterly*, 1973, **5**(1), 13-27.

70. "Some factors for achieving environmental resistance in 120°C structural adhesives", J.S.Noland, *Adhes.Sci.and Technol.*, 1975, **9**(A), 413-428.

71. "Kinetics of surface energy degradation of metals, 1. Humidity effects on Al 2044-T3 at 23°C", D.H.Kaelble and P.J.Dynes, *J.Coll.Int.Sci.*, 1975, **52**(3), 562-571.

72. "Durability of bonded aluminum structure", A.W.Bethune, *SAMPE.J.*, Aug.-Sept. 1975, 4-10.

73. "Effect of surface exposure time on bonds to aluminium", D.W.Levi, W.C.Tanner, M.C.Ross, R.F.Wegman and M.J.Bodnar, *J.Appl.Polym.Sci.*, 1976, **20**, 1475-1482.

74. "A study of FPL etching process used for preparing aluminum surfaces for adhesive bonding", W.J.Russell and E.A.Garnis, *SAMPE Quarterly*, 1976, **7**(5), 5-12.

75. "Surface analysis of 2024 aluminum after treatment with sulphuric - chromic acid solutions", N.T.McDevitt and W.L.Baun, *J.Electrochem.Soc.*, 1976, **123**, 1058-1061.

76. "Interface reactions and their influence on the long-term properties of metal bonds", W.Brockmann, *Adhesives Age*, 1977, **20**(6), 30-34.

77. "Mechanisms of surface degradation of aluminum after the standard FPL etch for adhesive bonding", T.Smith, *J.Appl.Polym.Sci.*, 1977, **32**, 11-36.

78. "Bonding to sealed chromic acid anodize", N.L.Rogers, *J.Appl.Polym.Sci.*, 1977, **32**, 37-50.

79. "Comparative stressed durability of adhesive bonded aluminum alloy joints", W.M.Scardino and J.A.Marceau, *J.Appl.Polym.Sci.*, 1977, **32**, 51-63.

80. "Effects of adherend surface treatment on stressed durability of adhesively bonded aluminum alloy", H.S.Schwartz, *J.Appl.Polym.Sci.*, 1977, **32**, 65-90.

81. "Chromate - free process for preparing aluminum for adhesive bonding", W.J.Russell, *J.Appl.Polym.Sci.*, 1977, **32**, 105-117.

82. "PABST Environmental testing of adhesive bonded joints", R.W.Shannon and E.W.Thrall, *J.Appl.Polym.Sci.*, 1977, **32**, 131-144.

83. "Durability of adhesive bonds to aluminum", D.W.Levi, *J.Appl.Polym.Sci.*, 1977, **32**, 189-199.

84. "Effects of chemical and thermal treatments on the composition of 2024 aluminum adherend surfaces", T.S.Sun, J.M.Chen and J.D.Venables, *Appl.of Surf.Science*, 1978, **1**, 202-214.

85. "The effects of fluorine contamination on the microstructure and bondability of aluminum surfaces", J.M.Chen, T.S.Sun and J.D.Venables, *SAMPE J.*, July-Aug. 1978, 22-27.

86. "Oxide morphologies on aluminum prepared for adhesive bonded aircraft structures", J.D.Venables, D.K.McNamara, J.M.Chen, T.S.Sun and R.Hopping, *Nat.SAMPE Tech.Conf.10*, 1978, 362-376.

87. "Etching and anodizing pretreatments and aluminum joint durability", J.D.Minford, *SAMPE Quarterly*, 1978, **9**(4), 18-27.

88. "Surface preparation - the key to bondment durability", J.C.McMillan, *NATO AGARD Lecture Series 102*, Lecture 7, March 1979.

89. "Prebond handling of aluminium surfaces for adhesive bonding", D.K.McNamara, J.D.Venables, T.S.Sun, J.M.Chen and R.L.Hopping, *11th Nat.SAMPE Tech.Conf.*, Nov. 13-15 1979, 740-751.

90. "Comparison of surface treatments of aluminium and their influence on long term strength of metal bonds", W.Brockmann and O.-D.Hennemann, *11th Nat.SAMPE Conf.*, Nov. 13-15 1979, 804-816.

91. "Characterisation of aluminum surfaces prepared for adhesive bonding", J.D.Venables, D.K.McNamara, T.S.Sun, B.Ditchek, J.M.Chen and R.L.Hopping, *Proc.Struct.Adhes.Bonding Conf.Technol.Conference*, Nov. 13-15 1979, 12-23.

92. "Interfacial fracture mechanical aspects of adhesive bonded joints - A review", A.J.Kinloch, *J.Adhesion*, 1979, **10**(3), 193-219.

93. "Oxide morphologies on aluminum prepared for adhesive bonding", J.D.Venables, D.K.McNamara, J.M.Chen, T.S.Sun and R.L.Hopping, *Appl.Surf.Sci.*, 1979, **3**, 88-98.

94. "Interpretation of AES depth profiles of porous Al anodic oxides", T.S.Sun, D.K.McNamara, J.S.Ahearn, J.M.Chen, B.Ditchek and J.D.Venables, *Appl.Surf.Sci.*, 1980, **5**, 406-425.

95. "Process and composition of low toxicity for preparing aluminum surfaces for adhesive bonding", W.J.Russel and E.A.Garnis, US Patent No. 4,212,701, Published July 15th, 1980.

96. "The influence of surface pretreatment on the durability of adhesively-bonded aluminium alloys in humid and corrosive environments", J.L.Cotter and R.Kohler, *Int.J.Adhesion & Adhesives*, 1980, **1**(1), 23-28.

97. "Bonding and failure mechanisms in aluminium alloy adhesive joints", A.J.Kinloch and N.R.Smart, *J.Adhesion*, 1981, **12**(1), 23-35.

98. "Surface morphology and its influence on adhesion", O.-D.Hennemann and W.Brockmann, *J.Adhesion*, 1981, **12**(4), 297-315.

99. "Techniques of measuring the interfacial aging mechanisms in metal bonds", H.Kollek and W.Brockmann, *26th Nat.SAMPE Symp.*, April 28-30 1981, 770-780.

100. "Seeding of FPL solution", L.F.Cottrell, D.L.Trawinski, S.P.Kodali, R.C.Curley, D.K.McNamara and J.D.Venables, *27th Nat.SAMPE Conf.*, May 4-6 1982, 44-52.

101. "Service history of phosphoric acid anodized aluminum structure", D.B.Arnold and C.S.Carter, *27th Nat.SAMPE Symp.*, May 4-6 1982, 769-776.

102. "Mechanism of bond endurance after surface treatment of aluminum for bonding (STAB) in nonchromate alkaline solution", T.Smith, *J.Adhesion*, 1982, **14**, 145-174.

103. "Evaluation of a primary anticorrosion surface treatment for adhesively bonded aluminum structure", R.V.Wolff, *28th Nat.SAMPE Symp.*, April 12-14 1983, 1155-1161.

104. "Effects of cure temperature and pressure on adhesive bond properties of P_2 etched aluminum", S.Quick, *28th Nat.SAMPE Symp.*, April 12-14 1983, 1116-1122.

105. "The effect of rinse water pH on the bondability of FPL-pretreated aluminum surfaces", D.K.McNamara, L.J.Matenzo, J.D.Venables, J.Hallayer and S.P.Kodali, *28th Nat.SAMPE Symp.*, April 12-14 1983, 1142-1154.

106. "Some effects of alloying elements on the performance of bonded aluminium alloy joints", R.J.Moulds, *Int.J.Adhesion & Adhesives*, 1984, **4**(1), 23-25.

107. "Oxide films on aluminium alloys: characterization and adhesion to epoxy resins", R.J.Young, M.Assefpour-Dezfuly, E.H.Andrews and A.J.Kinloch, *Conf.Ser.Inst.Phys.Anal.1983*, 1984, **68**, 347-350.

108. "Use of hydration inhibitors to improve bond durability of aluminum joints", G.D.Davis, J.Ahearn, L.J.Matienzo and J.D.Venables, *J.Mat.Sci.*, 1985, **20**, 975-988.

109. "Effect of alloy composition and surface pretreatment on the durability of adhesive-bonded aluminium alloy", P.Poole and J.F.Watts, *Int.J.Adhesion & Adhesives*, 1985, **5**(1), 33-39.

110. "A new pretreatment for the adhesive bonding of aluminium", D.J.Arrowsmith and A.W.Clifford, *Int.J.Adhesion & Adhesives*, 1985, **5**(1), 40-42.

111. "Influence of pretreatment rinse waters on the durability of adhesive-bonded aluminium alloys", W.McGarel, H.A.Farnham and R.McGuckin, *Int.J.Adhesion & Adhesives*, 1986, **6**(2), 89-92.

112. "Physico-chemical characterisation of aluminium alloy surfaces after sulphochromic pickling prior to bonding", J.Cuntz and M.Villatte, *Int.J.Adhesion & Adhesives*, 1986, **6**(4), 221-224.

113. "The use of perforated lap shear specimens to test the durability of adhesive-bonded aluminium", D.J.Arrowsmith and A.Maddison, *Int.J.Adhesion & Adhesives*, 1987, 7(17), 15-24.

114. "Bonding of aluminium alloy with some phenolic adhesives and a modified epoxy adhesive, and strength changes on exposure to moist air at 50°C", J.Comyn, D.M.Brewis and T.Tredwell, *J.Adhesion*, 1987, **21**(1), 59-78.

115. "Etching aluminium for adhesive bonding", D.J.Arrowsmith, C.A.Moth and C.M.Vickery, *Trans.IMF*, 1988, **66**(4), 112-115.

116. "The surface characterisation and adhesive bonding of aluminium", R.J.Davies and A.J.Kinloch in *Adhesion 13*, Ed.K.W.Allen, Elsevier Applied Science, 1989, 19-22.

117. "Effects of the environment on bonded aluminium joints: an examination by electron microscopy", J.A.Bishopp, E.K.Sim, G.E.Thompson and G.C.Wood in *Adhesion 13*, Ed.K.W.Allen, Elsevier Applied Science, 1989, 201-219.

118. "Environmental durability of aluminium joints with different pretreatments", B.M.Parker, *Int.J.Adhesion & Adhesives*, 1993, **13**(1), 47-51.

119. "Pretreatment of aluminium: topography, surface chemistry and adhesive bond durability", R.P.Digby and D.E.Packham, *Int.J.Adhesion & Adhesives*, 1995, **15**(2), 61-73.

120. "Adhesive bonding on anodized aluminum", P.F.A.Bijlmer, *Metal Finishing*, 1972, **70**(4), 30-34.

121. "Characterisation of aluminum adherend surfaces", A.Pattnaik and J.D.Meakin, *J.Appl.Polym.Sci.*, 1977, **32**, 145-157.

122. "The durability of some epoxide adhesive-bonded joints on exposure to moist warm air", D.M.Brewis, J.Comyn and J.L.Tegg, *Int.J.Adhesion & Adhesives*, 1980, **1**(1), 35-39.

123. "Pretreatment of aluminium by phosphoric acid anodizing prior to adhesive bonding", P.J.Thompson and H.B.Heaton, *Trans.IMF*, 1980, **58**(3), 81-90.

124. "Failure mechanisms in the boundary zone of polymer-metal compounds", W.Brockmann, O.-D.Hennemann and H.Kollek, *Proc.Org.Coat.Appl.Polym.Sci.*, 1982, **47**, 164-168.

125. "Surface properties and adhesion in bonding aluminium alloys by adhesives", W.Brockmann, O.-D.Hennemann and H.Kollek, *Int.J.Adhesion & Adhesives*, 1982, **2**(1), 33-40.

126. "Aluminium surface pretreatment for adhesive bonding by chromic acid anodizing, CAA, technological and durability aspects", C.W.Matz, *30th Nat.SAMPE Symposium*, 1985, 1088-1097.

127. "Some aspects of chemistry in adhesion on anodized aluminium", H.Kollek, *Int.J.Adhesion & Adhesives*, 1985, **5**(2), 75-80.

128. "Corona discharge treatment of surfaces for bonded joints", A.Njegic and A.Beevers, *Proc.ASE'85 Conf.*, 1985, 349-354.

129. "Durability of aluminium bonded joints in long-term tropical exposure", J.D.Minford, *Int.J.Adhesion & Adhesives*, 1982, **2**(1), 25-32.

130. "Durability of adhesive joints", A.J.Kinloch, W.A.Dukes and R.A.Gledhill, *Am.Chem.Soc.Div.Org.Coat.Plast.Chem.Pap.*, 1975, **35**(1), 546-559.

131. "Bonding metals with acrylic structural adhesives", D.J.Zalucha, *13th Nat.SAMPE Tech.Conf.*, Oct. 13-15 1981, 92-98.

132. "Influence of surface macroroughness on the durability of epoxide-aluminium joints", G.W.Critchlow and D.M.Brewis, *Int.J.Adhesion & Adhesives*, 1995, **5**(3), 173-177.

133. "Influence of chemical pretreatments on surface morphology and bondability of aluminium", P.F.A.Bijlmer, *J.Adhesion*, 1973, **5**(4), 319-331.

134. "Surface analysis and bonding of aluminium - magnesium alloys", A.J.Kinloch, H.E.Bishop and N.R.Smart, *J.Adhesion*, 1982, **14**, 104-119.

135. "The effect of time and type of water pretreatment on the bond strength of epoxy-aluminum joints", W.T.McCarvill and J.P.Bell, *J.Appl.Polym.Sci.*, 1974, **18**(2), 335-342.

136. "Mechanical factors in the adhesion of polyethylene to aluminium", D.E.Packham, K.Bright and B.W.Malpass, *J.Appl.Polym.Sci.*, 1974, **18**, 3237-3247.

137. "Development of oxide films on Al with the phosphoric acid anodization process", J.S.Ahearn, T.S.Sun, J.D.Venables, C.Froede and R.L.Hopping, *Spec.Clean.Finish.Coat.Processes, Proc.Conf. 1980.*, 1981, 125-142.

138. "Application of surface behaviour diagrams to the study of hydration of phosphoric acid-anodised aluminium", G.D.Davis, T.S.Sun, J.S.Ahearn and J.D.Venables, *J.Mater.Sci.*, 1982, **17**, 1807-1818.

139. "The effect of fluoride contamination on the durability of P.A.A. surfaces", D.L.Trawinski, S.P.Kodali, R.C.Curley, D.K.McNamara and J.D.Venables, *14th Nat.SAMPE Tech.Conf.*, Oct. 12-14 1982, 293-301.

140. "Replacement of sulfuric-chromic acid (FPL) etch by 3-dimensional abrasive surface conditioning for pretreatment of aerospace alloys before H_3PO_4 anodization", A.V.Pocius and J.J.Claus, *Proc.SAMPE Meeting*, 2-4 Nov. 1981.

141. "Morphology of anodic oxide for adhesive bonding of aluminium", D.J.Arrowsmith and A.W.Clifford, *Int.J.Adhesion & Adhesives*, 1983, **3**(4), 193-196.

142. "Plasma-sprayed coatings as adherend surface pretreatments", R.A.Pike, V.H.Patarini, R.Zatorski and F.P.Lamm, Int.J.Adhesion & Adhesives, 1992, **12**(4), 227-231.

143. "The influence of metal surface structure on the adhesion of thermosetting resin", E.W.Garnish, *J.Oil Col.Chem.Assoc.*, 1977, **60**(2), 69-74.

144. "Electrochemistry of aluminum alloys in the sulfuric-chromic acid (FPL) etch process", A.V.Pocius, *28th Nat.SAMPE Symp.and Exhib.*, April 1983, 1127-1141.

145. "The effect of an inert atmosphere on the bonding of metals", R.F.Wegman, *Adhesives Age*, 1967, **10**(1), 20-27

146. *Replacement of Hexavalent Chromium in Surface Treatments*, Ed.G.W.Critchlow, ISBN: 0 9517129 3 4.

147. "A chromate-free low-toxicity method of preparing aluminum surfaces for adhesive bonding", W.J.Russell and E.A.Garnis, *SAMPE J.*, 1981, *17*(3), 19-23.

148. "Inhibition of the aluminum + water reaction", D.A.Vermilea and W.Vedder, *Trans.Faraday Soc.*, 1970, **66**(10), 2644-2654.

149. "Durability of adhesive joints", G.D.Davis and D.K.Shaffer in *Handbook of Adhesive Technology*, Eds.A.Pizzi and K.L.Mittal, Marcel Dekker, New York, 1994, 113-128.

150. "The durability of adhesive joints in the presence of water", M.R.Bowditch, *Int.J.Adhesion & Adhesives*, 1996, **16**(2), 73-81.

151. "Cleaning and preparation of metal surfaces", UK Ministry of Defence, *DEF-STAN 03-2, Method O.*

152. "Acid chromate pickling of aluminium alloys", *draft AECMA Standard prEN 2334.*

153. "Chromic acid anodising of aluminium and aluminium alloys", UK Ministry of Defence, *DEF-STAN 03-24.*

154. "Chromic acid anodising - testing of adhesives", *draft AECMA Standard prEN 3002.*

155. "Preparation of metal surfaces for adhesive bonding", *ASTM Standard Practice D-2651-90.*

156. "Preparation of aluminum surfaces for structural adhesives bonding (phosphoric acid anodizing)", *ASTM Standard Practice D-3933-80.*

157. "Polymer-metal(oxide) interfaces", F.J.Boerio, G.D.Davis, J.E.deVries, C.E.Miller, K.L.Mittal, R.L.Opila and H.K.Yasuda, *Critical Reviews in Surface Chemistry*, 1993, 3(1), 81-99.

158. *Boeing Aerospace Corp. BAC5555 (5514) Rev.A*, 1975.

159. "Composition-depth profiling and interface analysis of surface coatings using ball cratering and the scanning Auger microprobe", J.M.Walls, D.D.Hall and D.E.Sykes, *Surf.Interface Anal.*, 1979, 1(6), 204-210.

160. "Characterization of different conversion coatings on aluminium with spectroscopic ellipsometry", J.DeLaet, J.Vanhellemont, H.Terryn and J.Vereeken, *Thin Solid Films*, 1993, **233**, 58-62.

161. "The improvement of adhesion of polymer on titanium surface after treatment with TEA-CO_2 laser irradiation", W.D.Muller, K.Seliger, J.Meyer and J.L.Gilbert, *J.Mater.Sci.: Materials in Medicine*, 1994, **5**, 692-694.

162. A.Buchman, H.Dodiuk, M.Rotel and J.Zahavi, *J.Adhesion Sci.Technol.*, 1994, **8**(10), 1211-1224.

163. W.F.Marwick and J.H.Powell, *A.S.E. 1988*, Brighton 1988.

164. P.A.Fay and G.D.Suthurst, *Proc.S.A.E.11 1989*, University of Bristol, 1989.

165. "Characterization of different conversion coatings on aluminium with spectroscopic ellipsometry", J.DeLaet, J.Vanhellemont, H.Terryn and J.Vereecken, *Thin Solid Films*, 1993, **233**, 58-62.

166. "Pretreatment of aluminium with conversion coatings", D.Wood, *Metals and Materials*, March 1986, 161-163.

167. "Cerium conversion coatings for the corrosion protection of aluminium", B.R.W.Hinton, D.R.Arnott and N.E.Ryan, *Materials Forum*, 1986, **9**(3), 162-173.

168. "Non-chromate conversion coatings", G.M.Sullivan, *Proc.Asia-Pacific Interfinish '94*, Oct.2-6 1994, **Vol.II**, 35.1-35.9.

169. "Review-replacements for chromium pretreatments on aluminum", S.M.Cohen, *Corrosion*, 1995, **51**(1), 71-78.

170. "Study of surface pretreatments for aluminum with reduced environmental impact", P.L.Bonora, *Pitture e Vernici Europe*, May 1995, 33-44.

171. "Characterisation of aluminium pretreatments by SIMS and electrochemical techniques", L.Fedrizzi, R.Canteri, M.Bianchi, M.Gius and P.L.Bonora, *Proc.EAST-AIFM Symp. on Surface Treatment of Aluminium*, May 24-25 1991, 64-76.

172. "The painting of aluminium today-painting techniques: part 4", G.Mura, *Aluminium Finishing*, 1993, **13**(2), 44-48.

173. "The development of chromate-free conversion coatings for aluminium alloys", R.J.Taylor and A.E.Hughes, *Proc.Asia-Pacific Interfinish '94*, Oct.2-6 1994, **Vol.I**, 19.1-19.9.

174. "Influence of the spew fillet and other parameters on the stress distribution in the single lap joint", A.D.Crocombe and R.D.Adams, *J.Adhesion*, 1981, **13**, 141-155.

175. "Stress analysis of adhesive-bonded lap joints", R.D.Adams and N.A.Peppiatt, *J.Strain Analysis*, 1974, **9**(31), 185-196.

176. "Three-dimensional deformations in a single-lap joint", M.Y.Tsai and J.Morton, *J.Strain Analysis*, 1994, **29**(1), 137-145.

177. "Peeling adhesion", A.Hardy in *Aspects of Adhesion - 1*, Ed.D.J.Alner, University of London Press, 1965, 47-65.

178. R.Srinivasan and S.Lazare, *Polymer*, 1985, **26**, 1297.

179. "Surface modification of polymers and ceramics induced by excimer laser radiation", D.W.Thomas, C.Foulkes-Williams, P.T.Rumsby and M.C.Gower in *Laser Ablation of Electronic materials - Basic Mechanisms and Applications*, Eds.E.Fogarassy and S.Lazare, Elsevier Science Publishers, 1992, 221-228.

180. "Improvement of adhesive bonding strength in sealed anodized aluminium through excimer laser prebond treatment", Z.Gendler, A.Rosen, M.Bamberger, M.Rotel, J.Zahavi, A.Buchman and H.Dodiuk, *J.Mater.Sci.*, 1994, **29**, 1521-1526.

181. D.C.Emmony and C.A.Cottam, unpublished work.

182. *Effects of High-power Laser Radiation*, J.F.Ready, Academic Press, 1971, 73.

183. Private communications, A.J.Dowell, Ano-coil UK, Ltd.

184. *Adhesion and Adhesives: Science and Technology*, A.J.Kinloch, Chapman and Hall, London, 1987, 360.

185. "Chapter 3: Kinetics and mechanisms of environmental attack", J.Comyn in *Durability of Structural Adhesives*, Ed.A.J.Kinloch, Applied Science Publishers, London, 1983, 83-131.

186. "Atomic mechanism for the destruction of stressed polymers", S.N.Zhurkov and V.E.Korsukov, *Sov.Phys.Solid State*, 1974, **15**(7), 1379-1384.

187. "Study of the composition of zirconium based chromate free conversion layers on aluminium", T.Schram, G.Goeminne, H.Terryn, W.Vanhoolst and P.VanEspen, *Trans.IMF*, 1995, **73**(3), 91-95.

188. "Aluminum structured vehicle technology - a comprehensive approach to vehicle design and manufacturing in aluminum", M.J.Wheeler, P.G.Sheasby and D.Kewley, *SAE.Tech.Paper 870146*, 1987.

189. U.S. Patent No. 3,964,936, Issued 22 June 1976.

190. "Surface analysis of oxidised aluminium: 1. Hydration of Al_2O_3 and decomposition of $Al(OH)_3$ in a vacuum as studied by ESCA", A.Nylund and I.Olefjord, *Surface and Interface Analysis*, 1994, **21**, 283-289.

191. G.W.Critchlow and K.Bedwell, unpublished data.

192. "Predicting the residual strength of some adhesive joints degraded by moisture", A.D.Crocombe, H.O.H.Hambly and J.Pan, *Proc.Adhesion '96 / Euradh '96 Conf.*, September 1996, Cambridge, UK, 497-502.

193. "Locus of failure of T-peel joints formed between aluminium and various adhesives", D.M.Brewis and G.W.Critchlow, *Int.J.Adhesion & Adhesives*, 1997, **17**, 33-38.

194. "Comparison of the degradation mechanisms of zinc-coated steel, cold rolled steel and aluminium-epoxy bonded joints", M.Brémont and W.Brockmann, *J.Adhesion*, 1996, **58**, 69-99.

APPENDICES

Appendix 1 - Bulk Aluminium Alloy Compositions

Appendix 2 - Abbreviations

Appendix 3 - Stressed Durability Data

APPENDIX 1 - Bulk Aluminium Alloy Compositions

Table A1.1 - Aluminium Association Coding System for Wrought Aluminium Alloy Bulk Compositions

Digit	Principal alloying elements
1xxx	Aluminium 99% minimum purity
2xxx	Copper
3xxx	Manganese
4xxx	Silicon
5xxx	Magnesium
6xxx	Magnesium and silicon
7xxx	Zinc

Table A1.2 - Alloys Commonly Identified in the Literature Survey have the Following Bulk Compositions:

	Composition by weight							
Alloy	Al	Mn	Mg	Cu	Si	Zn	Cr	Fe
2024	93.5	0.6	1.5	4.4	0.0	0.0	0.0	0.0
6061	97.9	0.0	1.0	0.28	0.6	0.0	0.20	0.0
7075	90.0	0.0	2.5	1.6	0.0	5.6	0.23	0.0
5251	Bal	0.1-0.5	1.7-2.4	0.15	0.4	0.0	0.0	0.5

APPENDIX 2 - ABBREVIATIONS

BAC = Boeing Aerospace Corporation
CAA = Chromic Acid Anodise
CAE = Chromic Acid Based Etch
CDP = Climbing Drum Peel
CE = Crack Extension
CIP = Corrosion Inhibiting Primer
CPH = Cycles Per Hour
DCB = Double Cantilever Beam
DGEBA = Diglycidylether of Bisphenol-A
DI = Deionised (water)
ESCA = Electron Spectroscopy for Chemical Analysis
FEM = Finite Element Modelling
FPL = Forest Products Laboratory
FRP = Floating Roller Peel
NTMP = Nitrilotris (Methylene) Phosphonic Acid
MEK = Methyl Ethyl Ketone
PAA = Phosphoric Acid Anodise
PAD = Phosphoric Acid Dip
PLS = Perforated Lap Shear
RH = Relative Humidity
RT = Room Temperature
SCB = Single Cantilever Beam
SEM = Scanning Electron Microscopy
SLS = Single Lap Shear
SSLS = Stressed Single Lap Shear
STAB = Surface Treatment of Aluminum for Bonding
STEM = Scanning Transmission Electron Microscopy
TEM = Transmission Electron Microscopy
UFL = Ultimate Failure Load
XPS = X-ray Photoelectron Spectroscopy

APPENDIX 3 - STRESSED DURABILITY DATA

Table A3.1 - Summary of Stressed Durability Data with Aluminium 5252 Alloy and Araldite AV119 at 60°C, DI water, Full Immersion.

System	Applied Load (kN)	Times-to-failure (h)	Mean time-to-failure (h)
Degrease	0.2	804, 704, 589	699
	0.5	827, 817, 680,	423
	0.75	206, 3, 4	92
	1	35, 0.5, 0.5	12
	1.15	8, 6, <1	5
	1.3	<1, <1, <1	<1
	1.5	<1, <1, <1	<1
80/120 Gb	0.2	1167, 865, 831	954
	0.5	739, 659, 382	593
	1	491, 467, 437	465
	1.3	398, 374, 278	350
	1.5	279, 231, 159	223
Bonderite 705	0.2	1481, 1323, 1288	1364
	0.5	878, 768, 758	801
	0.75	821, 725, 682	743
	1.5	782, 735, 663	727
Bonderite 777	0.2	1416, 1406, 1382	1401
	0.5	998, 974, 878	950
	0.75	735, 687, 638	687
	1.5	600, 576, 566	581
EP2472	0.2	1675, 1549, 1493	1572
	0.5	1092, 1012, 888	998
	0.75	869, 820, 783	824
	1.5	806, 735, 711	751
Optimised CAE	0.2	1498, 1458, 1378	1445
	0.5	1234, 1226, 1209	1223
	0.75	1042, 957, 899	966
	1	774, 731, 659	722
	1.5	693, 661, 503	619
PAA	0.2	2460, 2424, 2388	2424
	0.5	1458, 1378, 1234	1357
	0.75	1154, 1138, 851	1047
	1	1018, 994, 899	970
	1.5	947, 899, 875	907

Table A3.2 - Summary of Stressed Durability Data with Aluminium 5251 Alloy and Araldite AV119 at 60°C, DI water, Full Immersion

System	Mean Stress (MPa)	Mean time (Msecs)	Ln (mean time)
Dg only	1.0	2.51	14.74
	2.5	1.52	14.23
	3.75	0.33	12.71
	5.0	$43x10^{-3}$	10.60
	5.75	$20x10^{-3}$	9.9
	6.5	$3.6x10^{-3}$	8.19
	7.5	-	-
80/120 Gb	1.0	3.43	15.05
	2.5	2.13	14.57
	5.0	1.67	14.32
	6.5	1.26	14.05
	7.5	0.80	13.59
B705	1.0	4.91	15.41
	2.5	2.88	14.87
	3.75	2.67	14.80
	7.5	2.62	14.78
B777	1.0	5.04	15.43
	2.5	3.42	15.05
	3.75	2.47	14.72
	7.5	2.09	14.55
EP 2472	1.0	5.66	15.55
	2.5	3.59	15.09
	3.75	2.97	14.90
	7.5	2.70	14.80
Optimised CAE	1.0	5.20	15.46
	2.5	4.40	15.30
	3.75	3.48	15.06
	5.0	2.60	14.77
	7.5	2.22	14.61
PAA	1.0	8.73	15.98
	2.5	4.89	15.40
	3.75	3.77	15.14
	5.0	3.49	15.07
	7.5	3.27	15.00